

1-1-2009

# Lightning Return-Stroke Transmission Line Modelling Based on the Derivative of Heidler Function and CN Tower Data

Mariusz Milewski  
*Ryerson University*

Follow this and additional works at: <http://digitalcommons.ryerson.ca/dissertations>

 Part of the [Other Electrical and Computer Engineering Commons](#)

---

## Recommended Citation

Milewski, Mariusz, "Lightning Return-Stroke Transmission Line Modelling Based on the Derivative of Heidler Function and CN Tower Data" (2009). *Theses and dissertations*. Paper 337.

This Dissertation is brought to you for free and open access by Digital Commons @ Ryerson. It has been accepted for inclusion in Theses and dissertations by an authorized administrator of Digital Commons @ Ryerson. For more information, please contact [bcameron@ryerson.ca](mailto:bcameron@ryerson.ca).

# LIGHTNING RETURN-STROKE TRANSMISSION LINE MODELLING BASED ON THE DERIVATIVE OF HEIDLER FUNCTION AND CN TOWER DATA

by

Mariusz Milewski  
BEng, Ryerson University (1999)  
M.E.Sc, The University of Western Ontario (2003)

A thesis

presented to Ryerson University

in partial fulfillment of the

requirements for the degree of

Doctor of Philosophy

in the program of

Electrical and Computer Engineering

Toronto, Ontario, Canada, 2009

©Mariusz Milewski 2009



Library and Archives  
Canada

Published Heritage  
Branch

395 Wellington Street  
Ottawa ON K1A 0N4  
Canada

Bibliothèque et  
Archives Canada

Direction du  
Patrimoine de l'édition

395, rue Wellington  
Ottawa ON K1A 0N4  
Canada

*Your file* *Votre référence*  
ISBN: 978-0-494-59000-3  
*Our file* *Notre référence*  
ISBN: 978-0-494-59000-3

#### NOTICE:

The author has granted a non-exclusive license allowing Library and Archives Canada to reproduce, publish, archive, preserve, conserve, communicate to the public by telecommunication or on the Internet, loan, distribute and sell theses worldwide, for commercial or non-commercial purposes, in microform, paper, electronic and/or any other formats.

The author retains copyright ownership and moral rights in this thesis. Neither the thesis nor substantial extracts from it may be printed or otherwise reproduced without the author's permission.

#### AVIS:

L'auteur a accordé une licence non exclusive permettant à la Bibliothèque et Archives Canada de reproduire, publier, archiver, sauvegarder, conserver, transmettre au public par télécommunication ou par l'Internet, prêter, distribuer et vendre des thèses partout dans le monde, à des fins commerciales ou autres, sur support microforme, papier, électronique et/ou autres formats.

L'auteur conserve la propriété du droit d'auteur et des droits moraux qui protègent cette thèse. Ni la thèse ni des extraits substantiels de celle-ci ne doivent être imprimés ou autrement reproduits sans son autorisation.

---

In compliance with the Canadian Privacy Act some supporting forms may have been removed from this thesis.

While these forms may be included in the document page count, their removal does not represent any loss of content from the thesis.

Conformément à la loi canadienne sur la protection de la vie privée, quelques formulaires secondaires ont été enlevés de cette thèse.

Bien que ces formulaires aient inclus dans la pagination, il n'y aura aucun contenu manquant.

  
**Canada**

## Author's Declaration

I hereby declare that I am the sole author of this thesis.

I authorize Ryerson University to lend this thesis to other institutions or individuals for the purpose of scholarly research.

Signature

I further authorize Ryerson University to reproduce this thesis by photocopying or by other means, in total or in part, at the request of other institutions or individuals for the purpose of scholarly research.

Signature



## Abstract

# Lightning Return-Stroke Transmission Line Modelling based on the Derivative of Heidler Function and CN Tower Data

©Mariusz Milewski 2009

Doctor of Philosophy  
Department of Electrical and Computer Engineering  
Ryerson University

One of the most important parameters in a lightning flash that is of interest to researchers is the lightning return-stroke current as it causes most of the destructions and disturbances in electrical and telecommunication networks. In most cases, the lightning return-stroke current can not be directly measured and current characteristics are determined from measured electric and magnetic fields through the use of lightning return-stroke models. The main objective of this work is the development of a lightning return-stroke model for an elevated object. Also, an important objective is the correlation of the wavefront parameters (peak, maximum rate of rise and risetime) of the return-stroke current with the wavefront parameters of its associated lightning electromagnetic pulse (LEMP), measured 2 km north of the tower. The developed field-current parameter relationships for CN Tower lightning return strokes are compared with those obtained from measurements conducted at the Peissenberg Tower in Germany.

A 3-section transmission line (TL) model of the CN Tower, along with the derivative of the modified Heidler function, is used to simulate the measured current derivative signal. Then, the spatial-temporal distribution of the lightning current along the CN Tower and the lightning channel, during the lightning return-stroke phase, is determined. The presented model simulates the measured current derivative signal

instead of the current as has been used by other researchers. The use of the derivative of the modified Heidler function to simulate the lightning current derivative proved to be superior than simulating the lightning current.

For the quantitative assessment of the proposed model, a comparison between the simulated field, obtained through the usage of Maxwell's equations and the simulated current, and the measured field is performed. The developed 3-section TL model based on the measured current derivative and the derivative of the modified Heidler function produced a simulated magnetic field that is much closer to the measured field in comparison with previous models.

The developed field-current parameter relationships as well as the experimentally verified lightning return-stroke model can contribute to solving the inverse-source problem, one of the most challenging problems in lightning research, where the lightning current characteristics are estimated based on the characteristics of the measured LEMP.

**Keywords:** Tall-structure lightning, lightning return-stroke models, Heidler function, lightning electromagnetic pulse (LEMP), lightning detection.

## Acknowledgements

I wish to thank my thesis supervisor Dr. Ali M. Hussein for his help during the course of this work. His continuous guidance, encouragement and financial support are greatly appreciated.

I would also like to thank the Department of Electrical and Computer Engineering and the School of Graduate Studies at Ryerson University for their financial support during the course of this work.

I am also grateful to my fellow graduate student Omid Talakoub for his helpful discussions.

# Contents

<b>1</b>	<b>Introduction</b>	1
<b>2</b>	<b>The Lightning Discharge</b>	
2.1	Physics of Lightning	8
2.2	Negative Cloud-to-Ground Lightning Discharge	11
2.3	Lightning Current Measurements: Past and Present	13
2.4	Lightning to Tall Structures	16
2.5	Summary of Chapter 2	19
<b>3</b>	<b>CN Tower Lightning Measurement Systems</b>	
3.1	Overview of Measurement Systems	20
3.2	Old Rogowski Coil	22
3.3	New Rogowski Coil	24
3.4	Calibration of Rogowski Coils	26
3.5	Optical Fiber Link	26
3.6	Real-Time Digitizers	27
3.7	Electromagnetic Field Measurement System	31
3.8	Video Recording System	32
3.9	CN Tower Lightning Observations	34
3.10	Summary of Chapter 3	40
<b>4</b>	<b>Waveform Parameters</b>	
4.1	Wavefront Parameters of CN Tower Lightning Return-Stroke Current and Current Derivative	41
4.1.1	Lightning Return-Stroke Current Derivative	44
4.1.2	Lightning Return-Stroke Current	45
4.2	Wavefront Parameters of CN Tower Lightning-Generated Electromagnetic Pulse	46
4.3	Denoising the Electric and Magnetic Field Signals	48
4.4	Summary of Chapter 4	53
<b>5</b>	<b>Correlating CN Tower Lightning Return-Stroke Current with its Electromagnetic Pulse</b>	
5.1	Synchronization of Lightning Return-Stroke Currents, Electromagnetic Fields and Video Records	54
5.2	Correlation Analyses	55

5.3	Discussion of Results	64
5.4	Summary of Chapter 5	69
<b>6</b>	<b>Modelling of Lightning Return-Stroke Current</b>	
6.1	Types of Lightning Return-Stroke Current Models	72
6.2	Functions Simulating the Channel Base Current Waveform	77
6.3	Summary of Chapter 6	87
<b>7</b>	<b>Modelling of the Lightning Return-Stroke Current Derivative Using the Derivative of the Modified Heidler function</b>	
7.1	Choice of Channel Base Current Function	89
7.2	The Modified Heidler Function and its Derivative	90
7.3	Matching of the Initial Impulse of the Measured Current Derivative using the Derivative of the Modified Heidler Function	95
7.4	The Lightning Attachment Process and Reflection Coefficients at the Main Structural Discontinuities	103
7.4.1	Calculation of Reflection Coefficients	111
7.4.2	Reflection Coefficients and Location of Reflections	114
7.5	Modelling of the Lightning Current Derivative	121
7.6	Modelling of the Lightning Current Using the Modified Heidler Function	125
7.7	Summary of Chapter 7	128
<b>8</b>	<b>Comparison of Simulated and Measured Electromagnetic Field</b>	
8.1	CN Tower Lightning-Generated Electric and Magnetic Fields	130
8.2	Calculation of the Electric and Magnetic Fields Using a Single Section TL Representation	133
8.2.1	Comparison Between the Simulated Radiated Fields and Those Obtained from Measurements	140
8.2.2	Comparison Between the Simulated Total Electric and Magnetic Fields	142
8.3	Comparison Between the Simulated Total Electric and Magnetic fields (3-Section TL Representation)	145
8.4	Discussion	149
8.5	Summary of Chapter 8	154
<b>9</b>	<b>Conclusions</b>	155
<b>Appendices</b>		
	Appendix A – Calibration of Old and New Rogowski Coils	159
	Appendix B – Matching Heidler Function with Measured Current Derivative	163
	Appendix C – Lightning-Generated Electric and Magnetic Fields	167
	Appendix D – Current and Current Derivative Equations for 3-Section TL Representation	176
	D1. Current Equations in the First TL Section with Length $L_1$	177

D2. Current Equations in the Second TL Section with Length $L_2$	180
D3. Current Equations in the Third TL Section with Length $L_3$	182
D4. Current Equations in the Lightning Return-Stroke Channel $z > h$	184
Appendix E – Publications based on the PhD Thesis	187
<b>References</b>	188
<b>Glossary</b>	199

# List of Tables

4.1	Current and current derivative wavefront parameters obtained from waveforms shown in Figures 4.1 and 4.2.	44
6.1	Expressions for $P(z')$ and $v$ for the engineering lighting-return stroke models	76
6.2	$I(z',t)$ for transmission line type models with $t \geq z'/v_f$ .	76
6.3	$I(z',t)$ for traveling current source type models with $t \geq z'/v_f$ .	76
6.4	Parameters used for plotting of the double exponential current and current derivative waveforms.	78
6.5	Parameters used to plot the Heidler function and its derivative.	81
7.1	Parameters for matching results illustrated in Figure 7.1.	95
7.2	Parameters obtained from matching the measured current derivative with the simulated current derivative using the derivative of the modified Heidler function with $A_2$ eliminated.	99
7.3	Parameters obtained from matching of measured current with the simulated current using the modified Heidler function.	101
7.4	Peaks of impulses corresponding to reflections from main structural discontinuities of the CN Tower (obtained from the measured current derivative signal).	112
7.5	Reflection coefficients calculated from the measured current derivative.	114
7.6	Locations of the current derivative reflections from CN Tower's structural discontinuities.	118
7.7	Reflection coefficients obtained from 47 CN Tower strokes and from the chosen current derivative signal.	121

# List of Figures

1.1	Franklin's electrical kite experiment.	2
2.1	Thunderstorms charging the global battery, earth is generally kept charged negatively while the upper atmosphere is being kept charged positively.	9
2.2	Various sizes of thunderclouds.	10
2.3	Types of lightning dischargers between cloud and ground.	11
2.4	The development of negative cloud-to-ground lightning discharge.	13
2.5	Upward-initiated lightning flash to the CN Tower captured by high-speed camera on March 22, 2007 at 10:31:35.	19
3.1	Location of CN Tower lightning measurement systems.	21
3.2	Old Rogowski coil connection and its placement at the CN Tower.	23
3.3	New Rogowski coil connection and its placement at the CN Tower.	25
3.4	Sony-Tektronix RTD-710A real-time digitizer.	29
3.5	LeCroy LT342L real-time digitizer.	30
3.6	Current derivative signal measured on August 19, 2005 at 14:11:43.	35
3.7	Current, time integral of current derivative signal shown in Figure 3.6.	35
3.8	The electric field generated by the CN Tower lightning stroke, August 19, 2005 at 14:11:43.	36
3.9	The magnetic field generated by the CN Tower lightning stroke, August 19, 2005 at 14:11:43.	36
3.10	Sanyo CCD camera record of August 19, 2005 CN Tower lightning flash, 13:55:56.	37
3.11	High-speed camera record of August 19, 2005 CN Tower lightning flash, 13:55:56.	37
3.12	Current derivative measured by the old Rogowski coil on January 2 <sup>nd</sup> , 1999 at 22:27:02.	38
3.13	Current derivative measured by the new Rogowski coil on January 2 <sup>nd</sup> , 1999 at 22:27:02.	39
3.14	Current waveform (time integral of the current derivative waveform shown in Figure 3.12.	39
3.15	Current waveform (time integral of the current derivative waveform shown In Figure 3.13.	40
4.1	Current derivative wavefront parameters.	43
4.2	Current wavefront parameters.	43

4.3	Electric field wavefront parameters.	47
4.4	Electric field derivative wavefront parameters.	48
4.5	a) Unfiltered electric field signal, b) derivative of unfiltered electric field signal.	49
4.6	FFT magnitude of unfiltered electric field signal shown in Figure 4.5a.	51
4.7	Comparison of filtering results for electric field signal using 5 <sup>th</sup> order elliptic low-pass filter.	52
4.8	a) Filtered electric field signal of Figure 4.5a b) electric field derivative obtained from filtered signal of Figure 4.8a.	52
4.9	FFT magnitude for filtered electric field signal shown in Figure 4.8a.	53
5.1	Electric field peak versus magnetic field peak, CC = 0.988.	58
5.2	Maximum derivative of electric field versus maximum derivative of magnetic field, CC = 0.904.	59
5.3	Electric field 10%-90% risetime ( $T_E$ ) versus magnetic field 10%-90% risetime ( $T_H$ ), CC = 0.962.	59
5.4	Magnetic field peak versus current peak, CC = 0.975.	62
5.5	Maximum magnetic field derivative versus maximum current derivative, CC = 0.78662.	
5.6	Magnetic field risetime ( $T_H$ ) versus current risetime ( $T_i$ ), CC = 0.871.	63
5.7	Magnetic field peak versus maximum current derivative, CC = 0.0822.	63
5.8	Maximum derivative of magnetic field versus current peak, CC = 0.092.	64
6.1	Current waveform for double exponential function.	79
6.2	Current derivative for double exponential function.	79
6.3	Current waveform based on equation (6.4).	83
6.4	Current derivative waveform obtained using the derivative of (6.4).	83
6.5	Current waveform based on (6.6).	84
6.6	Current derivative waveform obtained using the derivative of (6.6).	84
6.7	Heidler current waveform based on (6.7).	85
6.8	Derivative of Heidler current waveform based on the derivative of (6.7).	85
6.9	Pulse function based on (6.8).	86
6.10	Derivative of pulse function shown in Figure 6.9.	86
7.1	Sample comparison for matching of the first impulse of the measured current derivative using three different methods.	94
7.2	Measured current derivative waveform.	97
7.3	Current derivative waveform used for matching.	97
7.4	Measured and simulated first impulse of the lightning return-stroke current derivative.	98
7.5	Measured and simulated current (using the derivative of the modified Heidler function).	99
7.6	Current waveform obtained by the numerical integration of the measured current derivative signal.	101
7.7	Lightning return-stroke current obtained from measurement and simulation.	102

7.8	First impulse of current derivative obtained from measurement and from simulation using the modified Heidler function.	102
7.9	Initiation of the lightning return-stroke current into the strike object and the lightning return-stroke channel.	105
7.10	The CN Tower along with its major structural discontinuities.	106
7.11	Simplified traveling wave model.	107
7.12	Measured current derivative and reflections from CN Tower's main structural discontinuities.	110
7.13	Current waveform and reflections from CN Tower's main structural discontinuities.	110
7.14	Current derivative waveform used to calculate the reflection coefficients.	111
7.15	Calculation of reflection coefficients.	114
7.16	Location of the top of the restaurant vs. the maximum slope of the lightning current derivative.	116
7.17	Location of the bottom of the restaurant vs. the maximum slope of the lightning current derivative.	116
7.18	Location of ground vs. the maximum slope of the lightning current derivative.	117
7.19	Location of the tip of the CN Tower vs. the maximum slope of the lightning current derivative.	117
7.20	Reflection coefficient at the top of the restaurant vs. the maximum slope of the lightning current derivative.	119
7.21	Reflection coefficient at the bottom of the restaurant vs. the maximum slope of the lightning current derivative.	120
7.22	Reflection coefficient at ground vs. the maximum slope of the lightning current derivative.	120
7.23	Reflection coefficient at the tip of the CN Tower vs. the maximum slope of the lightning current derivative.	121
7.24	Lattice diagram showing reflections from major structural discontinuities of the CN Tower.	122
7.25	Simulated and measured current derivative waveforms.	124
7.26	Simulated and measured current waveforms.	124
7.27	Simulated and measured current waveforms.	127
7.28	Simulated and measured current derivative waveforms.	127
8.1	Geometry used for electromagnetic field calculations.	131
8.2	Electric field components due to the CN Tower contribution.	137
8.3	Magnetic field components due to the CN Tower contribution.	138
8.4	Electric field components due to channel contribution.	139
8.5	Magnetic field components due to channel contribution.	139
8.6	Measured electric field versus simulated radiation component of the electric field (CN Tower and channel contributions).	141
8.7	Measured magnetic field versus simulated radiation component of the magnetic field (CN Tower and channel contributions).	142
8.8	Measured electric field versus simulated total electric field (CN Tower and channel contributions).	144

8.9	Measured magnetic field versus simulated total magnetic field (CN Tower and channel contributions).	144
8.10	Measured electric field versus simulated total electric field (3-section TL representation, CN Tower and channel contributions).	148
8.11	Simulated electric field with and without electrostatic component (3-section TL representation).	148
8.12	Measured magnetic field versus simulated total magnetic field (3-section TL representation, CN Tower and channel contributions).	149
A1	Experimental setup for testing of old Rogowski coil.	159
A2	Output of the old Rogowski coil.	160
A3	Time integral of the waveform shown in Figure A2.	160
A4	Setup used for calibration of the new Rogowski coil.	161
A5	Outputs of the scope for Rogowski coil (Figure A5.A.) and Pearson coil (Figure A5.B.), nominal diameter of the Rogowski coil 74”.	162
A6	Outputs of the scope for Rogowski coil (Figure A6.A.) and Pearson coil (Figure A6.B.), nominal diameter of the Rogowski coil 65”.	162
C1	Geometry used for electric and magnetic field derivation due to the lightning return-stroke channel and its image.	168
C2	Geometry used to obtain general solutions for vector magnetic potential $\vec{A}$ .	170
D1.	3-section TL representation of the CN Tower.	177
D2.	Reflections given by equation D1.	178
D3.	Reflections given by equation D2.	178
D4.	Reflections given by equation D3.	178
D5.	Reflections given by equation D4.	179
D6.	Reflections given by equation D5.	179
D7.	Reflections given by equation D6.	179
D8.	Reflections given by equation D7.	180
D9.	Reflections given by equation D8.	181
D10.	Reflections given by equation D9.	181
D11.	Reflections given by equation D10.	181
D12.	Reflections given by equation D11.	182
D13.	Reflections given by equation D12.	183
D14.	Reflections given by equation D13.	183
D15.	Reflections given by equation D14.	183
D16.	Reflections given by equation D16.	184
D17.	Reflections given by equation D17.	185
D18.	Reflections given by equation D18.	185

# Chapter 1

## Introduction

Lightning has been a source of fear and respect among people since beginning of times. In many civilizations lightning was associated with magical powers possessed by gods who in many cases carried lightning bolts. For example, the ancient Vedic books of India describe how Indra, who was thought to be the son of Heaven and Earth, carried thunderbolts on his chariot [1]. With all the interest in lightning throughout the centuries no scientific study was performed until the second half of the 18<sup>th</sup> century when Benjamin Franklin flew his now famous electrical kite to prove that lightning is some form of electrical discharge. The electric kite experiment was carried out during a thunderstorm in 1752. A charged cloud caused the kite to be charged and a spark jumped from a key tied to the bottom of the string to knuckles of Franklin's hand as shown in Figure 1.1 [2]. His body was insulated from the kite's conducting string by silk insulating string (Fig. 1). Franklin also showed that a metallic rod connected to ground can protect a structure from lightning damage and by measuring the charge on the rod he concluded that the lower part of a thundercloud was in most cases negatively charged but there were some instances in which it was positively charged. The first lightning rod used for protective purposes was used in France in 1752 as well as in the United States later in the

same year [1-3]. After the experiments performed by Benjamin Franklin in the 18<sup>th</sup> century, no significant results were obtained from studies of lightning until the late 19<sup>th</sup> century when photography and spectroscopy became available. The early pioneers who first used photographic cameras to observe lightning and to record lightning images were Hoffert (1889), Weber (1889), Walter (1902) and Larsen (1905). Further improvement in photographic equipment was achieved with the invention of the streak camera by Boys in 1926. The streak camera, often referred to as Boys' camera, was used in one of the very first studies of lightning to tall structures in 1935 to record images of lightning strikes to the 449-m high **Empire State Building** (ESB) in New York City [1,4]. History of lightning measurements as well as the physical process associated with the lightning discharge is given in chapter 2.

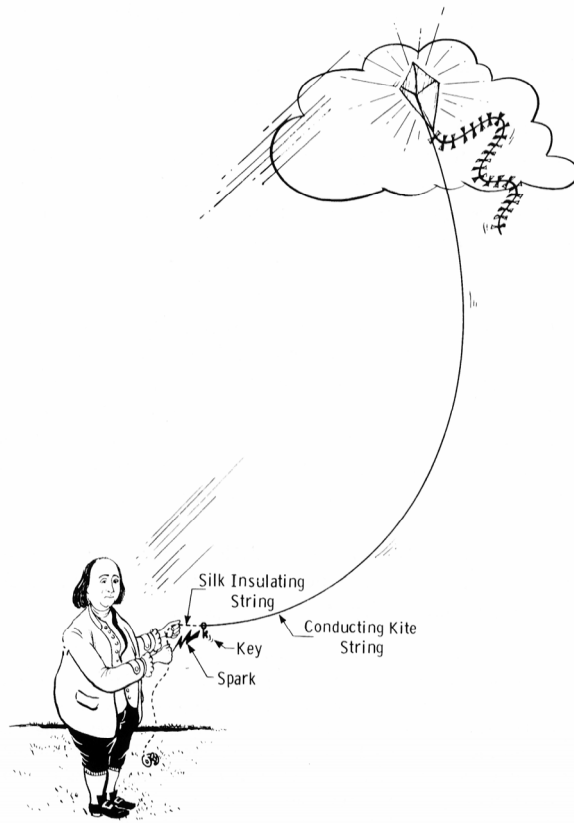


Figure 1.1. Franklin's electrical kite experiment [2].

The main objectives of the work presented in the thesis are:

- The development of field-current characteristic relationships for the CN Tower lightning return-stroke data.
- The development of an experimentally verified lightning return-stroke model using the measured current derivative along with the derivative of the modified Heidler function and a 3-section transmission line (TL) representation of the CN Tower

The first main objective deals with the correlation of the characteristics of the lightning return-stroke current measured at the CN Tower with those of its associated lightning electromagnetic pulse (LEMP), measured 2 km north of the CN Tower. A comparison with Peissenberg Tower field-current characteristic relationships and simplified analytical relationships is carried out.

The second main objective deals with the development of a 3-section TL model, which can be used to describe the current distribution along the CN Tower and the lightning channel when the tower is struck by lightning. This will include the use of the derivative of the modified Heidler function to simulate the lightning current derivative measured at the CN Tower, as well as the computation of the simulated electric and magnetic fields of the LEMP. A quantitative comparison between the simulated and the measured fields is also presented.

The research work presented in the thesis has important application in lightning protection, lightning detection, including the estimation of the lightning current based on the characteristics of the measured LEMP, such as in the case of lightning location and

detection networks. The presented model allows for the estimation of the lightning current in most situations in which the lightning current can not be directly measured.

It is important to study the effects of lightning to the CN Tower on the surrounding area. Beside the fact that the CN Tower is struck by lightning much more often than any building in Toronto (the CN Tower gets hit on average with 40-50 flashes per year while the flash density in the Toronto area is about 2 flashes/km<sup>2</sup>/year), the number of strokes per flash as well as the current wavefront steepness is much higher for lightning flashes hitting the CN Tower. The comparison of the LEMP characteristics resulting from CN Tower lightning strikes and those resulting from non-CN Tower lightning strikes showed that CN Tower flashes produced fields with substantially higher peaks and maximum derivatives [5,6]. Although the CN Tower provides some protection to buildings and installations in its immediate vicinity from direct lightning strikes (due to its extreme height), the presence of the CN Tower greatly increases the electromagnetic field disturbances leading to interruptions to sensitive electronic devices. Simultaneous measurements of the derivative of the lightning return-stroke current at the CN Tower and the corresponding LEMP at a distance of 2 km north of the tower have been accomplished. These simultaneous measurements are necessary for the quantitative assessment of any lightning return-stroke model.

This thesis is divided into nine main chapters:

In chapter 2 the main sources and types of lightning discharges as well as the physical process associated with the lightning discharge are discussed. Methods used in the past as well as at present time for measurement of the lightning return-stroke current

are described. In addition, an overview of lightning strikes to tall structures (such as tall towers) is given.

The CN Tower lightning measurement system is described in chapter 3. Typical records obtained from the lightning return-stroke current measurement system, electric and magnetic field measurement system and video recording systems (VHS as well as high speed camera) are presented.

In chapter 4, the most important lightning return-stroke current and lightning-generated electromagnetic field wavefront parameters, namely initial peak, maximum derivative and 10%-90% risetime to initial peak, are discussed. These parameters are important from point of view of protection and lightning detection. The evaluation of field wavefront parameters (especially the maximum field derivatives) proved to be difficult task due to presence of high frequency noise in the measured field signals. Analysis of the electric and magnetic field records were performed and it was determined that most of the high frequency noise present in the measured field signals is related to broadcasting stations. The denoising process of the CN Tower's lightning-generated electric and magnetic field signals is described. The correlation between field-current wavefront characteristics would not have been possible without first denoising of the measured electric and magnetic field signals.

Chapter 5 focuses on the first major objective of this work, which is the correlation of the CN Tower field-current wavefront characteristics (initial peak, maximum derivative and 10%-90% risetime to initial peak). In addition the electric and magnetic field wavefront characteristics are correlated with each other. The results obtained from the correlation of CN Tower field-current wavefront characteristics are

compared with field-current wavefront characteristics obtained from measurements done at the 160-m Peissenberg Tower in Germany. Detailed discussion of the results is given. One of the biggest challenges in lightning research is to solve the inverse-source problem, in which the lightning current is estimated using the measured LEMP along with a lightning return-stroke model. The developed field-current wavefront characteristics contribute to solving this inverse source problem. The presented analyses are also important for improving the algorithms used in lightning detection and location networks.

In chapter 6, four main types of lightning return-stroke models are discussed with emphasis being placed on the engineering model based on the transmission line representation of the lightning current path. In addition, a literature review related to the use of different simulation functions to represent the lightning return-stroke current at channel base is presented. It is shown that some of the functions used to represent the lightning return-stroke current at channel base are not suitable for modelling since they do not satisfy the two basic requirements, the simulation function as well as its derivative should not have any discontinuity at time  $t = 0$  s. The results presented in this chapter are important for the proper choice of a suitable simulation function that can be used in the proposed model.

Chapter 7 focuses on the second major objective of this thesis, which is the development of lightning return-stroke model based on the measured current derivative and the derivative of the modified Heidler function along with 3-section TL representation of the CN Tower. The expression for the derivative of the modified Heidler function is developed to simulate the initial impulse of the measured current derivative signal before the arrival of any reflections from CN Tower's structural

discontinuities (top and bottom of the restaurant, ground and tip of the tower) as well as from the front of the upward-propagating lightning channel. Reflection coefficients at four main structural discontinuities of the CN Tower are evaluated. The obtained reflection coefficients along with a 3-section TL model are used to simulate the current derivative at every point along the lightning current path, which includes the portion of the lightning channel that is ignited during the return-stroke phase. In addition, the results obtained from matching using the modified Heidler function are also presented. In both cases, the simulated results are compared with the ones obtained from the measurement. The developed model, unlike many models employed in the past, is based on the lightning current derivative, which is being directly measured, rather than the current, which is evaluated by numerical integration. It is shown that the proposed simulation function, which is based on the derivative of the modified Heidler function, is much more suitable for use in the developed lightning return-stroke model.

In chapter 8, the quantitative assessment of the developed lightning return-stroke model is performed. The quantitative assessment is conducted by comparing the simulated electric and magnetic fields with those obtained from measurements. Single section and 3-section TL representations of the CN Tower are used to evaluate the simulated electric and magnetic fields. It is shown that a single section TL model can not accurately represent such a complex structure as the CN Tower. The use of 3-section TL model greatly improves the simulation results. A detailed discussion of the simulation results is included.

The conclusions related to the research work presented in this thesis are given in chapter 9. In addition, suggestions for possible future work are discussed.

# Chapter 2

## The Lightning Discharge

### 2.1 PHYSICS OF LIGHTNING

Lightning is a physical phenomenon, which is often seen as a source of destruction causing millions of dollars in losses annually. Damages to buildings, wind turbine, and aircrafts, as well as forest fires, death and injury to people are few of the lightning hazards [1,3,7]. For example, National Lightning Safety Institute (NLSI) estimated that half of the forest fires in the Western United States are caused by lightning [8]. Although in many cases, lightning strikes cause damage and destruction, lightning is also needed in nature. Fixed nitrogen used by plants in the food making process is produced during lightning discharge. In nitrogen fixation process  $N_2$  is converted to ammonium ( $N_2 \rightarrow NH_4^+$ ) and this process is essential since it is the only way that living organisms can attain nitrogen directly from the atmosphere. Lightning is also needed in order to maintain the earth's fine weather electric field of about 100 V/m. The process of thunderstorms maintains the global battery, which keeps the upper atmosphere charged positively and the earth charged negatively as shown in Figure 2.1 [2]. When thunderstorms occur atmospheric electrical currents flow upward while during fine

weather atmospheric electrical currents flow downward. Charges are transferred to earth from thunderstorms by means of rain, lightning and corona discharge [1,2].

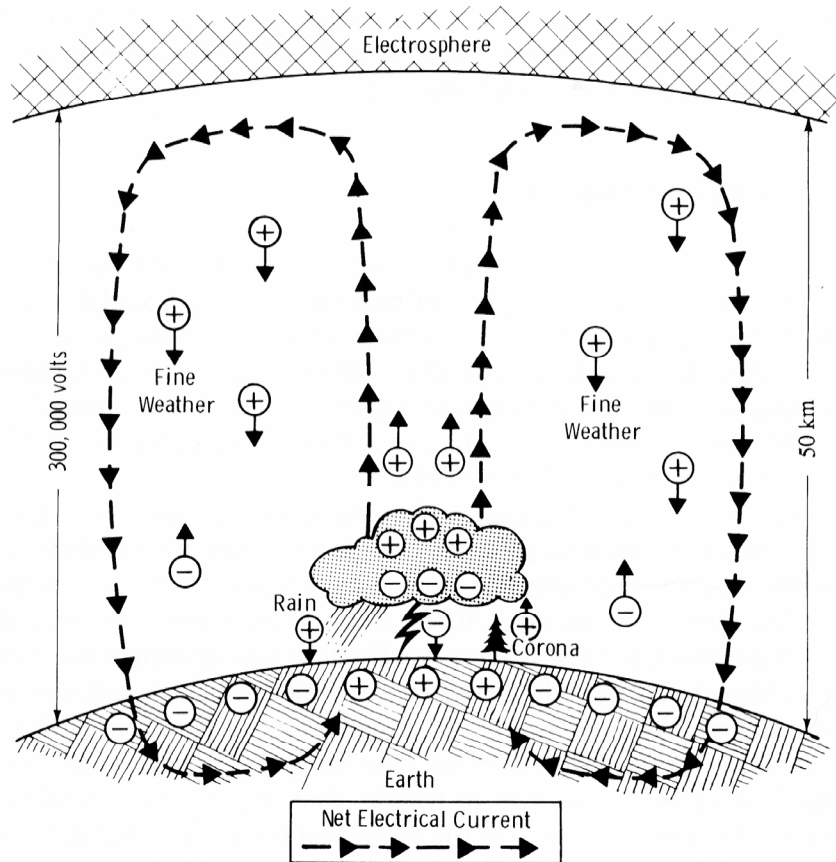


Figure 2.1. Thunderstorms charging the global battery, earth is generally kept charged negatively while the upper atmosphere is being kept charged positively [2].

The most common source of lightning is the thundercloud, also referred to as cumulonimbus; however, it is not the only source. Lightning can occur during sandstorms, snowstorms and volcanic eruptions, and in rare cases during a clear weather [1,2,9,10]. Lightning can be produced by thunderclouds of various sizes starting from very small semitropical cloud to very large thunderstorm cloud; the height of the cloud can be as low as 5 km and as high as 20 km. Different types of thunderclouds that can produce lightning are illustrated in Figure 2.2. A thundercloud is formed in the atmosphere containing cold and dense air; it contains positive charges in the upper part of

the cloud and negative charges in the lower part of the cloud along with a small pocket of positive charges at the base of the cloud [1,2]. The most common definition of lightning is that lightning is a transient, high-current electric discharge, whose path length is measured in kilometres. The electrification of a thundercloud which produces lightning is thought to be due to the charging process in which electrostatic charges are separated in strong air currents by collision between heavy participation particles (hail) and light participation particles (ice crystals) [2,3]. The lightning discharges can be divided into five main categories: intra-cloud discharges which account for more than half of lightning discharges, cloud to cloud, and cloud to air, ground to cloud and cloud to ground discharges. For researchers, the cloud to ground and ground to cloud discharges are of

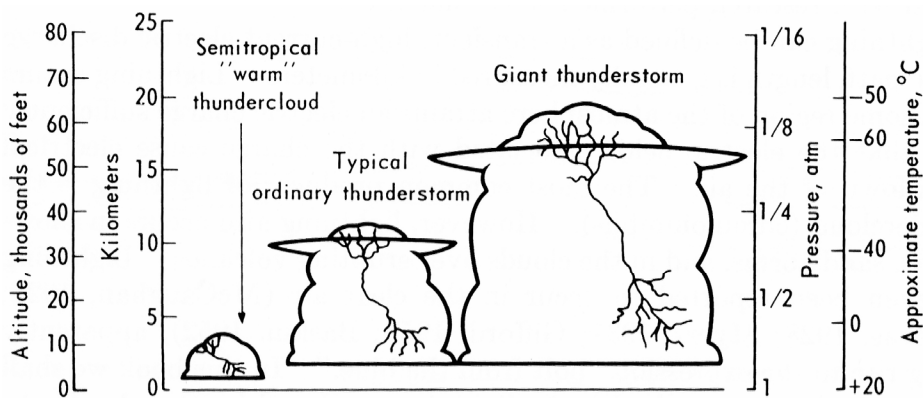


Figure 2.2 Various sizes of thunderclouds [9].

most interest as they are the cause of most damages and disturbances. Based on the polarity of the charge and the direction of propagation, lightning discharges between cloud and ground were classified by Berger into four main categories; downward negative lightning, upward positive lightning, downward positive lightning and upward negative lightning. These four types of lightning discharges that occur between cloud and ground are illustrated in Figure 2.3. Negative cloud to ground lightning accounts for about 90% of the total lightning discharges between cloud and ground, while positive

cloud to ground lightning accounts for less than 10% of lightning discharges between cloud and ground. The upward-initiated positive and negative lightning events generally occur from mountain tops or from tall man-made structures such as tall towers or towers placed on elevated grounds [1,11,12]. Downward discharges, which travel from cloud to ground, are shown in Figure 2.3.1 and 2.3.3 while upward discharges, which travel from ground to cloud are shown in Figure 2.3.2 and 2.3.4. The most common lightning discharge between cloud and ground, the negative cloud-to-ground discharge, is further discussed in the next section.

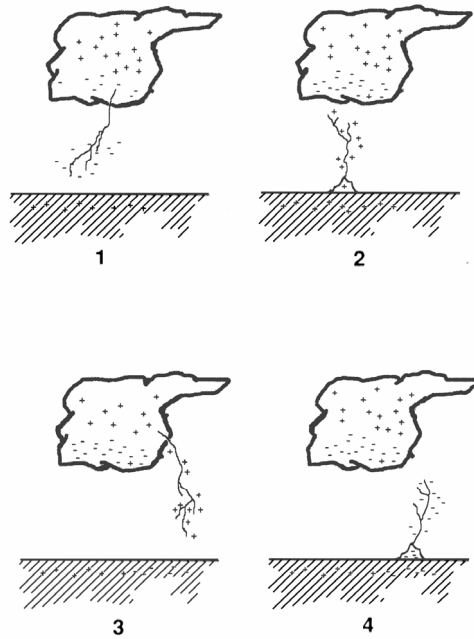


Figure 2.3. Types of lightning discharges between cloud and ground [2].

## 2.2 NEGATIVE CLOUD-TO-GROUND LIGHTNING

The process associated with negative cloud to ground lightning discharge is illustrated in Figure 2.4. It starts with the initiation and propagation of a stepped leader towards the earth. The initiation of the stepped leader is understood to occur by

breakdown in the thundercloud. The stepped leader propagates towards ground in a series of steps. Each step is about 50 m in length; it typically has duration of 1  $\mu$ s with around 50  $\mu$ s pause between each step. A stepped leader propagating with an average velocity of  $2 \times 10^5$  m/s can lower 10 or more coulombs of negative charge towards ground. Electric potential at the bottom of the leader can have a magnitude in excess of  $10^7$  Volts [1-3]. As the stepped leader approaches ground, the electric fields, which are present at sharp objects on the ground or at ground irregularities, become greater than the breakdown value of the air and upward moving streamers are generated. The first lightning return-stroke is initiated by the attachment process of the downward propagating stepped leader and an upward moving streamer. The return-stroke can be easily distinguished by the human eye as it produces high temperature bright light. If there are no additional charges available at the top of the lightning channel after the occurrence of the first return-stroke then the lightning flash (in this case called a single-stroke flash) ends. Any additional charge available at the top of the lightning channel can produce a continuous dart leader propagating down the first return-stroke channel, initiating a second return-stroke. Dart leaders travel much faster towards the ground as opposed to stepped leaders. Dart leaders are usually not branched while stepped leaders can be very heavily branched.

A lightning flash containing two or more lightning return strokes is referred to as a multi-stroke lightning flash. Recent CN Tower lightning studies indicate that more than 64% of CN Tower lightning flashes are multi-stroke flashes [10]. In summary, the lightning discharge between cloud and ground can be classified as positive or negative, it can be upward or downward initiated and a lightning flash can have one or more lightning return strokes.

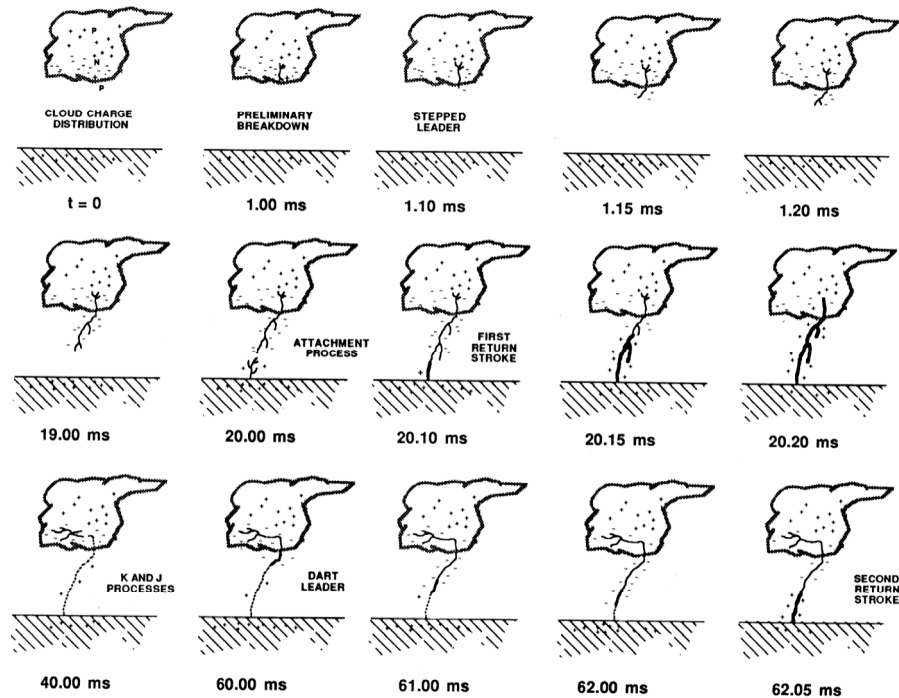


Figure 2.4. The development of negative cloud-to-ground lightning discharge [2].

### 2.3 LIGHTNING CURRENT MEASUREMENTS: PAST AND PRESENT

First successful measurement of the lightning current peak is attributed to Pockles. In 1900 Pockles used a piece of nepheline basalt to measure the peak of the lightning current (nepheline basalt is a common volcanic rock) [13]. The basalt was placed within few centimetres of the lightning rod on the observation tower located on Mount Cimone in the Apennines. By analyzing the magnetic field induced in the basalt by a lightning flash, Pockles was able to estimate the lightning current [2,3]. A step forward in the measurement of the lightning current peak was achieved in the year 1924 when Peters introduced a klydonograph, which measured the voltage using the idea of Lichtenberg figures that are produced by the voltage. Lichtenberg figures are referred to as branching electric discharges that sometimes appear on the surface or interior of

insulating materials [3]. In 1929, a lightning stroke recorder based on Lichtenberg figures was used successfully for the first time to measure the lightning current peak. The size of Lichtenberg figures, produced by a lightning strike, was proportional to the lightning current peak [2,3]. Magnetic links were also used to measure the peak of the lightning current. Measurements done using magnetic links are described next.

The magnetic link is very similar to basalt used by Pockles to estimate the lightning current peak from the induced magnetic field. The main difference between basalt and the magnetic link is that basalt is a product of nature while the magnetic link is man-made in the laboratory. For example, current measurements resulting from lightning strikes to high objects in Czechoslovakia (1959-1985) were carried out using magnetic links [14]. Fulchronographs, magnetic surge recorders and magnetic integrators are three other instruments that are based on the principle of the magnetic link and were used to measure the lightning flash properties. Fulchronograph is similar in operation to the magnetic link in which element of time is introduced. To measure the effective rate of rise of the lightning current, the magnetic surge front recorder was used, while to measure the time integral of the lightning current the magnetic surge integrator was used [3].

Methods and measurement equipment described in previous sections could only be used to determine the peak of the lightning current and not the current waveshape. One of the very first methods used to record the waveshape of the lightning current utilized a precision shunt resistance  $R$ . The potential drop caused by the flow of the lightning current in the resistance could be measured. In early stages, a cathode-ray oscilloscope was used to display the resulting voltage-time characteristics [15,16]. With advancement in equipment, digital recorders such as digitizers replaced cathode-ray oscilloscopes. For

example, lightning current measurements carried out at the 100-m tall radio transmission tower in Gaisberg, Austria, utilized 0.25 mΩ resistor with a bandwidth of 0 Hz to 3.2 MHz. The output signal of the shunt resistor was recorded by 8-bit digitizer board [17]. Another method that has been used in the past and is still being used at present time to record the waveshapes of the lightning current utilizes a long-toroidal coil with many turns, arranged on insulating core. The coil is installed around the current carrying object, like instrumented tower and the induced voltage (*emf* or electromotive force) appearing across the coil terminals is proportional to the rate of change of the current,  $emf = -N * \frac{d\phi}{dt} = -L \frac{di}{dt}$  where N is the number of turns in the coil,  $\frac{d\phi}{dt}$  is the time-rate of change of the magnetic flux  $\phi$ , the negative sign in the *emf* equation is taken from Lenz's Law, which states that the induced current produced by the *emf* is in the direction that would oppose the induced *emf*. In some literature, the long-toroidal coil is called "Rogowski Coil". Two Rogowski coils are used to measure the return-stroke current derivative resulting from lightning strikes to the CN Tower [18]. A variation of the Rogowski coil, which utilizes a small-loop induction coil along with a Pearson current transformer, is used to measure the return-stroke current derivative resulting from lightning strikes to the 160-m Peissenberg Tower in Germany. The principle behind the operation of the small-loop induction coil is similar to that of the Rogowski coils, i.e. the induced voltage in the small-loop coil is proportional to the lightning current derivative [19]. Detailed description of the CN Tower lightning measurement systems, which include the return-stroke current derivative measurement system, the lightning-generated electromagnetic field measurement system and the visual observation system, is given in Chapter 3.

Since mid 1960's there has been a significant increase in lightning studies all over the world. Some of these lightning studies, which have been conducted since mid 1960's, include lightning experiments done by Berger on two towers on Mount San Salvatore near Lugano, Switzerland [3,15,16], Garbagnati using two 40-m television towers, one located on Monte Sasso Di Pale and the second tower located on Monte Rosa (both about 900-m above sea level) [2], studies done by Eriksson using a 60-m tower placed on flat ground in South Africa [2,20], studies of lightning to the CN Tower in Toronto, Canada [11,12], lightning measurements at the Ostankino Television Tower in Moscow, Russia [21], lightning studies using 100-m tall Gaisberg Tower in Austria [22] and the 160-m tall Peissenberg Tower in Germany [23,24], as well as rocket-triggered lightning experiments in Florida and New Mexico [25,26]. The research and studies of lightning play an important role in the development of more sophisticated means to protect structures, equipments, natural resources and people from lightning hazards. With ever increasing use of static sensitive devices, such as computers and other electronic components, there is an increased need for design of protective systems against lightning hazards, including interruptions caused by lightning (e.g., overvoltages on power lines).

## **2.4 LIGHTNING TO TALL STRUCTURES**

The lightning discharge has been studied by many researchers for over a century and one of the most important parameters that is of interest to researchers (especially from the point of view of protection) is the lightning return-stroke current. In order to measure the lightning current one must know the exact location of the lightning strike,

which can be only accomplished using tall-instrumented towers, towers placed on elevated grounds or by rocket triggered lightning [18,24,25]. It is obvious that in most cases the lightning current can not be directly measured and in these cases the lightning-generated electric and magnetic fields are measured to estimate the lightning current characteristics. For example, lightning location and detection networks such as the **North American Lightning Detection Network (NALDN)** and the **Austrian Lightning Detection and Information System (ALDIS)** use the measured electric and magnetic fields of return-strokes along with some models in order to estimate the current peaks and their polarities [27,28]. A tall structure, such as the 553 m CN Tower, presents an ideal location for measurement of the lightning current and for studying the lightning phenomenon. The lightning flash density in Toronto area is only 2 flashes/km<sup>2</sup>/year while the CN Tower is yearly struck on average with 40-50 lightning flashes. Detailed studies of the lightning return-stroke current are important from point of view of protection as strokes with higher current peaks and higher current derivatives increase the probability of damage to the structure being hit. In addition, return-stroke currents with higher peaks produce higher electric and magnetic fields and these increase the electromagnetic interferences and disturbances.

Lightning flashes to tall structures can be upward initiated (flashes branching in the upward direction) or downward initiated (flash branching in the downward direction). The discovery of upward initiated flashes can be attributed to McEachron (1939), who studied lightning flashes to the **Empire State Building (ESB)** in New York City. During his studies, he observed that most of the flashes to ESB were upward-initiated and started at the top of the building [4]. An upward-initiated lightning flash hitting the CN Tower on

December 30, 1998 at 23:32:42 as captured by VHS video camera is shown in Figure 2.5. Upward-initiated lightning can occur at mountain tops, at tall structures or can be triggered artificially. When the height of a structure becomes very large or a structure is placed high above sea level, such as the top of a mountain, an upward-moving stepped leader can be initiated as opposed to downward propagating stepped leader (“normal” cloud to ground lightning). The high object is then capable of initiating the upward-lightning discharge. The probability of upward-initiated lightning increases as the height of the struck object increases. For example, for structures up to 50 m in height 90% of lightning flashes are downward initiated, whereas for structures higher than 400 m only 5% of lightning flashes are downward-initiated [1,20,29]. Studies carried out in 1991 at the 553-m above ground level (AGL) CN Tower showed that only 2.8% of flashes hitting the tower that year were downward-initiated [29]. Another study done at the 540-m tall Ostankino Television Tower in Moscow, Russia, showed that more than 90% of flashes hitting the tower were upward-initiated [21]. Berger, using results obtained from measurements done on two 60 m high towers found that about 85% of recorded lightning strikes were initiated by upward-moving stepped leaders [16]. In upward-initiated lightning, an upward-moving leader is often followed by downward-moving dart leader and upward-moving subsequent return-stroke. Similar to normal cloud to ground discharge (downward lightning), the upward-initiated lightning flash can have one or multiple lightning return-strokes [1-3]. Downward-initiated lightning is rare in case of extremely tall structures. However, in some instances a downward-initiated lightning can strike a tall structure well below its tip as it was shown by studies observed at the CN Tower and Ostankino Tower in Moscow. Recent studies showed that the CN Tower was

hit as low as 70 m below its tip [10]. Ostankino Tower in Moscow on the other hand was hit as low as 200 m below its tip [21]. These findings are important from point of view of protection of tall structures since they illustrate that a tall structure is mostly hit at its tip but on rare occasions it can be hit well below the tip. The probability of a tall structure being hit below the tip must be taken into consideration when designing means of protection against damages caused by lightning.



Figure 2.5. Upward-initiated lightning flash to the CN Tower captured by VHS video camera on December 30, 1998 at 23:32:42.

## 2.5 SUMMARY OF CHAPTER 2

The main sources and types of lightning discharges as well as the physical processes associated with the lightning discharge are discussed. Methods used in the past and at present time for the measurement of the lightning return-stroke current are described. An overview of lightning strikes to tall structures (such as tall towers) is given.

# Chapter 3

## CN Tower Lightning Measurement Systems

### 3.1 OVERVIEW OF MEASUREMENT SYSTEMS

Simultaneous measurements of significant lightning return-stroke parameters resulting from lightning strikes to the CN Tower have been performed since 1991. The current measurement system located at the CN Tower consists of two Rogowski coils, a double channel LeCroy LT342L digitizer with 1 Mpoint memory per channel, Pentium based PC, tri-axial cable connection for one coil (old coil), optical fiber connection for the other coil (new coil) and a TrueTime GPS computer card. The two Rogowski coils are used to measure the derivative of the lightning current. The field measurement system is located at Pratt building at the University of Toronto and it consists of electric and magnetic field sensors, a double channel LeCroy LT342L digitizer, Pentium based PC and a TrueTime GPS computer card. The electric field sensor measures the vertical component of the electric field ( $E_z$ ) and the magnetic field sensor measures the azimuthal component of the magnetic field ( $H_\phi$ ). Two Sanyo CCTV cameras and Vision Research Phantom v5.0 digital high-speed camera (HSC) are used to record the visual

parameters of lightning strikes to the tower. The data collected from lightning strikes to the CN Tower is influenced by the instrumentation used and based on these data the limitations of measurement equipment can be found. The requirements for more appropriate equipment can also be found from the analysis of captured data. The locations of CN Tower measurement systems are shown in Figure 3.1.

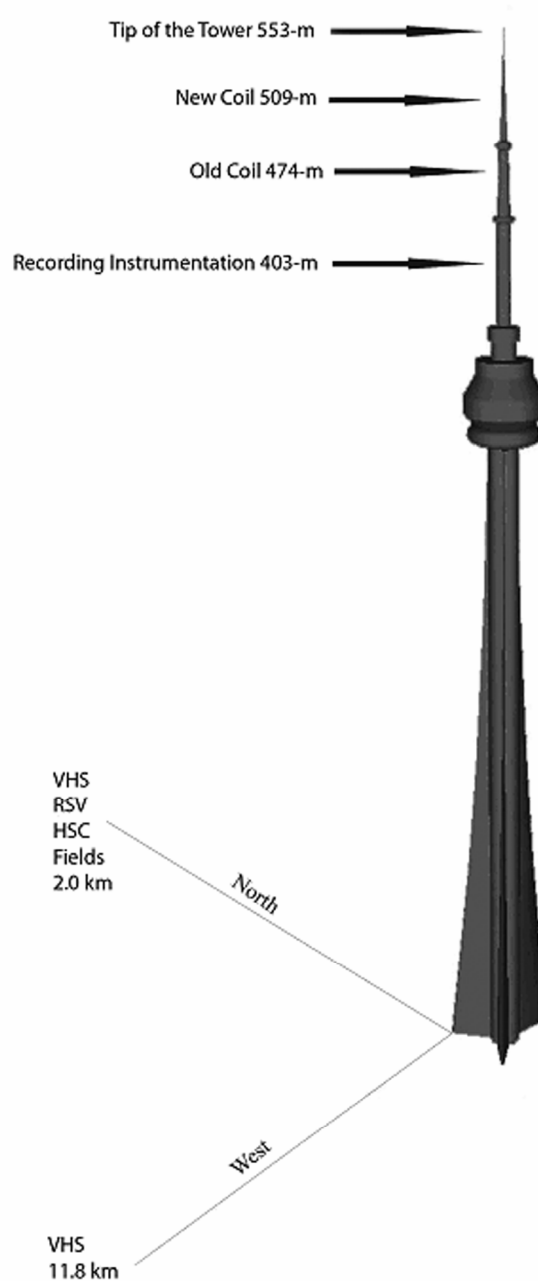


Figure 3.1. Locations of CN Tower lightning measurement systems.

## 3.2 OLD ROGOWSKI COIL

A 40-MHz Rogowski coil was installed at the tower in 1990. The toroidal, non-ferrous Rogowski coil is composed of many turns, which are arranged on an insulating core. This type of coil has a property that its induced voltage is proportional to the time variation of the net current discharged through it independently of where partial currents penetrate the coil. The coil is installed at the 474-m above ground level (AGL) and it encircles one-fifth of the CN Tower's steel structure. Assuming a uniform current distribution along the CN Tower's steel structure, the measured current is estimated to be 20% of the total current. The 3-m long coil consists of two 1.5 m pieces, which are terminated with resistors at one end (resistors are used to absorb reflections and to damp the oscillations in the coil), and connected to an impedance matching box at the other end. The impedance matching box is connected to one channel of the LeCroy LT342L digitizer through a 165-m, 50  $\Omega$  tri-axial cable (Belden RG-8/U) [11]. The impedance of the coil seen through the matching box is made to be 50  $\Omega$ , which is the same as the impedance of the tri-axial cable. Schematics of the coil connection and coil placement at the CN Tower are shown in Figure 3.2 [12,30].

### Technical Specifications of the old Rogowski Coil

- 40 MHz bandwidth
- 8.7 ns risetime
- 0.35 V/(A/ns) sensitivity,  $\pm 6\%$  accuracy
- 50  $\Omega$  impedance
- 3 m length (two 1.5 m long sections)

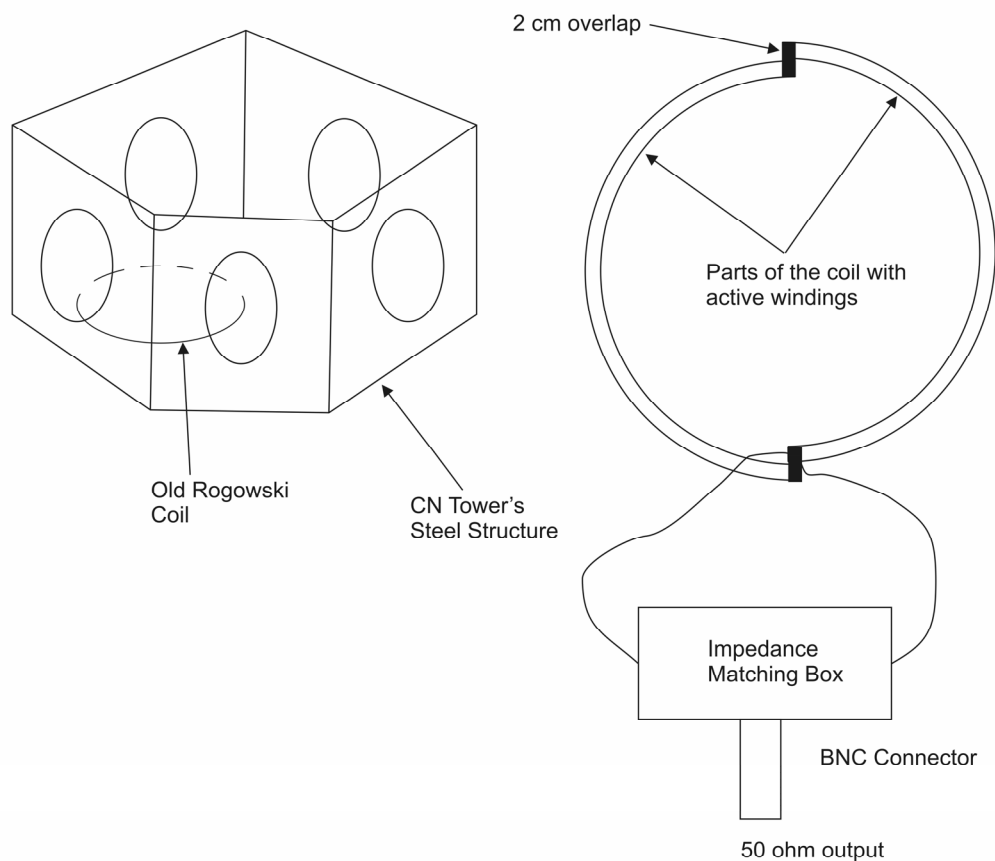


Figure 3.2. Old Rogowski coil connection and its placement at the CN Tower.

One of the main problems associated with data measured using the old Rogowski coil is the large amount of noise being present in the measured signal. The main reasons for the presence of large amount of noise are:

- Since the coil encircles 1/5<sup>th</sup> of the CN Tower's steel structure, only 20% of the total lightning current is measured
- A 165-m tri-axial cable connection to the digitizer
- Different types of noise from communication antennas as well as the LORAN-C signal that is used for radio navigation of ships are picked up by the tower and the old Rogowski coil

### 3.3 NEW ROGOWSKI COIL

A new Rogowski coil was first used for the measurement of the lightning current derivative during the 1997 lightning season. From the observed results during the later part of 1997, it became apparent that the new coil was not working properly and it was sent back to Physics International for repairs and recalibration. The first successful measurements of the lightning current derivative using the new Rogowski coil were performed during the 1999 lightning season. The new Rogowski coil works on the same principle as the old coil but it measures 100% of the total lightning current derivative since it encircles the whole steel structure of the CN Tower at the 509-m AGL. The new Rogowski coil consists of four 1.5-m long segments for a total length of 6 m. To connect the coil to the recording station, an optical fiber link was purchased from NanoFast Inc, Chicago, IL. A schematic of the new Rogowski coil connection and its placement at the CN Tower is shown in Figure 3.3. Two segments of the coil are connected to matching box and the other two segments are connected to another matching box. Both matching boxes are then connected to a third matching box in order to ensure that the impedance seen at the output of the third matching box is  $50 \Omega$ . A 30 dB attenuator was inserted between the third matching box and the fiber optic transmitter to ensure that the output of the new Rogowski coil, which can reach a maximum of 16 volts, will not saturate the optical fiber link [12,30].

#### Technical Specifications of the new Rogowski coil

- 20 MHz bandwidth
- 17.4 ns risetime

- 1.2862 V/(A/ns) sensitivity,  $\pm 6\%$  accuracy
- 50  $\Omega$  impedance
- 6 m length (four 1.5 m long sections)

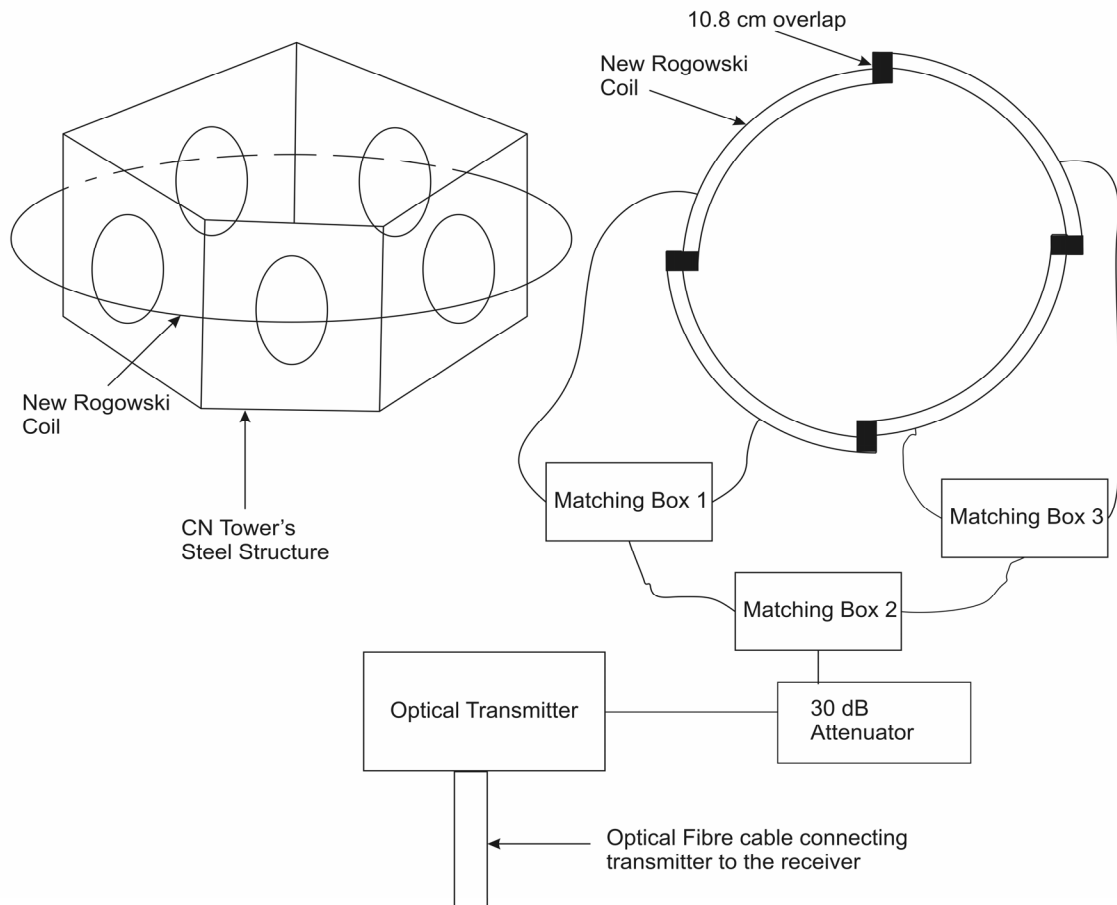


Figure 3.3. New Rogowski coil connection and its placement at the CN Tower.

Current derivative signals measured with the new Rogowski coil have much better signal-to-noise ratio (SNR) than those measured by the old Rogowski coil; this can be especially seen in low current derivative signals. The reasons for the improvement in the SNR of signals measured with the new Rogowski coil are:

- The coil measures 100% of the total lightning current derivative signal

- The connection to the recording station is made through a fiber link as opposed to a tri-axial cable for the old Rogowski coil
- The new coil is also less susceptible to noise due to advanced design

### **3.4 CALIBRATION OF ROGOWSKI COILS**

The old and new Rogowski coils were both calibrated before being installed at the CN Tower. The old Rogowski coil was re-calibrated at the CN Tower in May 1997 and its sensitivity was found to be 0.351 V/(A/ns), which is close to value of 0.350 V/(A/ns) quoted by the manufacturer (see Appendix A) [31]. The new Rogowski coil was tested in May 1997 to find its sensitivity. The sensitivity of the new coil was found to be 1.1985 V/(A/ns), which is quite close to the value quoted by the manufacturer, 1.2862 V/(A/ns). From the lightning current signals measured during the later part of 1997 it was determined that the new Rogowski coil was not functioning properly. The coil was sent back to the manufacturer in early 1998 for repairs and recalibration. The three damaged ground shields of the coil had to be replaced and the coil had to be re-calibrated [12]. Details on re-calibration of the new Rogowski coil are given in Appendix A [31,32].

### **3.5 OPTICAL FIBER LINK**

The NanoFast Optical Transmission System consists of **Radio Frequency Interference (RFI)** protected transmitter chassis with OA-1 Optical Analog plug in board, 10-1/2" RFI protected receiver chassis with one OA-1 Optical Analog Receiver plug in board and a 150 m long fiber optic cable. The chassis of the transmitter and the chassis of

the receiver reduce external electromagnetic noise by more than 120 dB. The system is also designed to attenuate any voltage spikes on the AC line, for example a 5 kV spike creates less than 100 mV signal referred to the input of the transmitter and the receiver [12,33]. The optical fiber link greatly reduces noise, which is the main problem that is seen in the current derivative signals measured by the old Rogowski coil.

#### Technical Specifications of NanoFast OP 2000A Optical Transmission System

- input to the transmitter can range from  $-1\text{ V}$  to  $+1\text{ V}$  full scale into  $50\ \Omega$
- output of the receiver can range from  $-1\text{ V}$  to  $+1\text{ V}$  full scale into  $50\ \Omega$
- the system has 100 MHz bandwidth with 3 dB points located at 35 Hz and 100 MHz

### **3.6 REAL-TIME DIGITIZERS**

The acquisitions of the lightning current derivative and the electromagnetic field resulting from a lightning strike to the CN Tower had been carried out using real-time digitizers. Up to summer of 2002, the acquisition of the CN Tower current and field data was accomplished using two Sony-Tektronix RTD-710A double channel real-time digitizers with 10 bit vertical resolution and 128 Kpoints memory/channel [34]. One of the RTD-710A digitizers was placed at the CN Tower (used for recording the lightning current derivative signals). The second digitizer (used for recording the electromagnetic field signals) was placed at a University of Toronto (Rosebrugh Building). The setup allowed for recording of up to 8 strokes per flash due to memory limitations of the digitizers. In reality some of the CN Tower lightning flashes had more than 8 strokes per

flash, for example, in one occasion the high-speed camera recorded a flash with 19 strokes [10,29]. This memory limitation of the RTD-710A digitizer meant that in many cases not all the strokes in a lightning flash were captured. In 2002, Sony-Tektronix RTD-710A digitizers were replaced with two LeCroy LT342L double channel, 8-bit, 1 Mpoint memory/channel digitizers [35,36]. One of the LeCroy digitizers was placed at the CN Tower to record the lightning current derivative while the second digitizer was placed at the Pratt Building of University of Toronto to measure the electromagnetic field (the vertical component of the electric field and the azimuthal component of the magnetic field). The new digitizers are set to record up to 20 strokes per flash with minimum time resolution of 2 ns. The signals recorded via LeCroy digitizers are stamped with GPS time (1  $\mu$ s resolution) using TrueTime PCI GPS cards. The use of LeCroy digitizers brings improvement in the time resolution of the captured data as well as the number of strokes that can be captured in each flash. In addition, an accurate GPS time is attached to each record. The exact GPS time solves the problem of matching the lightning current data with the corresponding electromagnetic field data, as well as VHS (Video Home System) data. The Sony-Tektronix RTD-710A and LeCroy LT342L digitizers are shown in Figures 3.4 and 3.5, respectively.

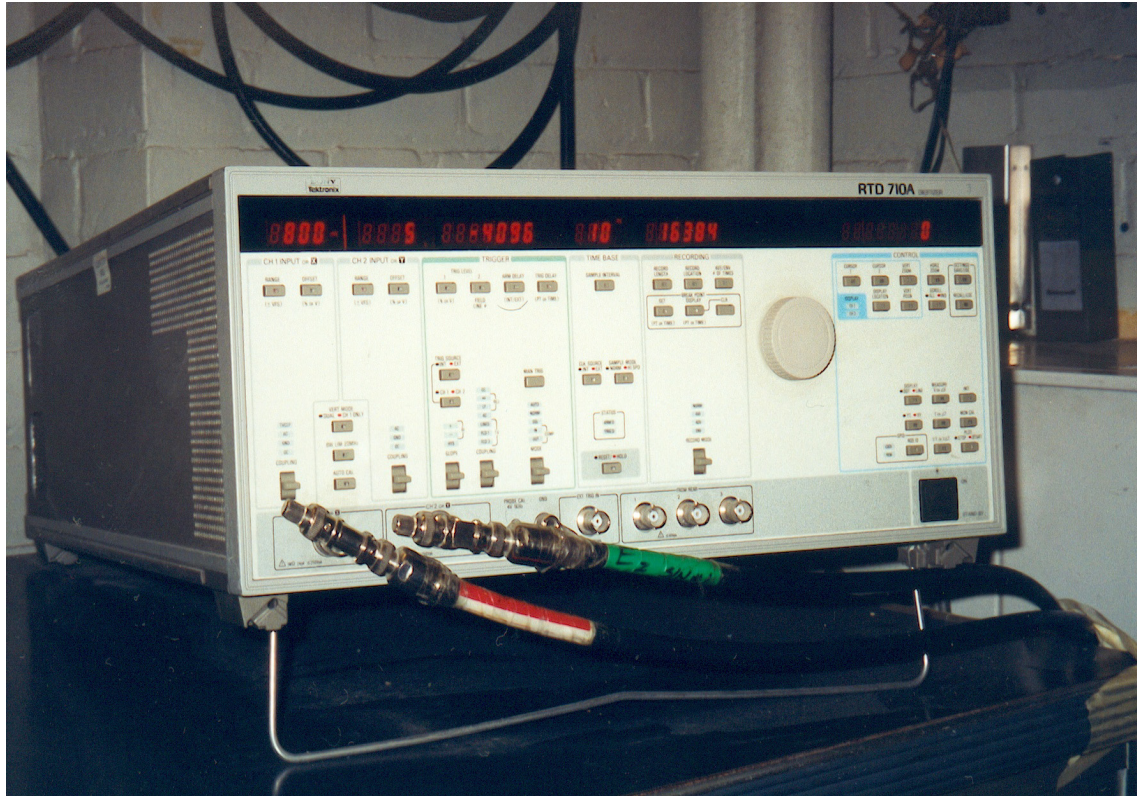


Figure 3.4. Sony-Tektronix RTD-710A real-time digitizer.

Technical specifications of Sony-Tektronix RTD-710A real-time digitizer

- number of channels: 2
- 68000, 16 bit microprocessor is used to control programmable functions of the digitizer
- memory per channel: 128 K points in dual channel mode and 256 K points in single channel mode
- bandwidth: 100 MHz
- vertical resolution: 10 bits
- minimum sampling interval: 10 ns
- trigger mode: single or bi-slope

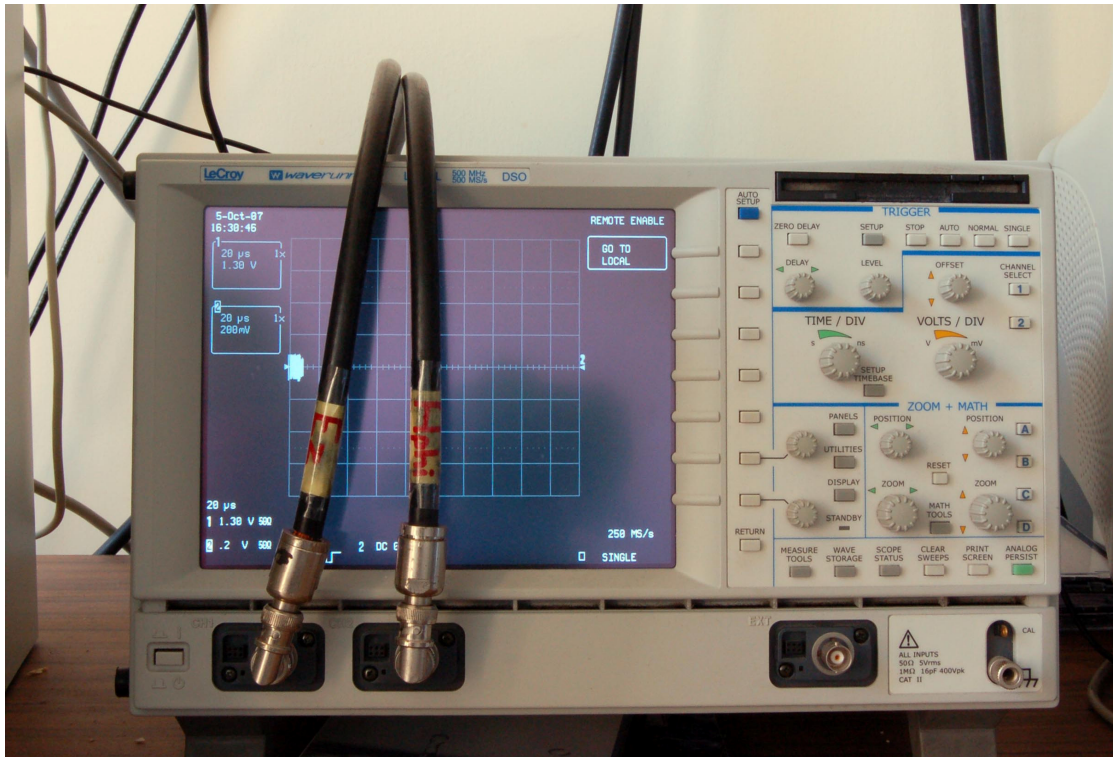


Figure 3.5. LeCroy LT342L real-time digitizer.

Technical specifications of LeCroy LT342L digitizer

- number of channels: 2
- processor: 160 MHz PowerPC
- memory per channel: 1 M points in dual channel mode and 2 M points in single channel mode
- bandwidth: 500 MHz
- vertical resolution: 8 bits
- minimum sampling interval: 2 ns
- trigger: single or bi-slope

### 3.7 ELECTROMAGNETIC FIELD MEASUREMENT SYSTEM

The field measurement system is presently located at the Pratt Building of the University of Toronto (2.0 km north of the CN Tower). It consists of magnetic and electric field sensors, LeCroy LT342L digitizer and a GPS card. The magnetic field sensor measures the azimuthal component of the magnetic field  $H_\phi$  and the electric field sensor measures the vertical component of the electric field  $E_z$ . Each sensor is connected to one channel of the double channel LeCroy digitizer using a coaxial cable. The electric field sensor is an active, hollow, hemispherical-shaped monopole with a sensitivity of 1.44 V/(kV/m). The magnetic field sensor is of the small-loop antenna type with a sensitivity of 0.166 V/(A/m). The circular loop of the magnetic field sensor is oriented in such a way as to capture the azimuthal component of the magnetic field generated by CN Tower lightning strokes. The overall risetime of the field measurement system is estimated to be about 5 ns [5]. It should be mentioned that the magnetic and electric field sensors not only measure the fields resulting from lightning strikes to the CN Tower but also fields created by lightning strikes occurring in the vicinity of the sensors. The technical specifications of the magnetic and electric field sensors are as follows [5,12]:

#### Magnetic Field Sensor:

Type:	active single loop antenna
Sensitivity:	0.166 V/(A/m)
3-dB low roll-off frequency:	697 Hz
3-dB high roll-off frequency	150 MHz
Maximum linear output:	0.62 V (rms)

### Electric Field Sensor:

Type:	Active hemispherical antenna
Sensitivity:	1.44 V/(kV/m)
3-dB low roll-off frequency:	47 Hz
3-dB high roll-off frequency:	100 MHz
Maximum linear output:	0.62 V (rms)

## **3.8 VIDEO RECORDING SYSTEM**

Video monitoring of lightning flashes to the CN Tower has been performed since 1978 [5,11]. The video recording system consists of a Vision Research Phantom v.5.0 1000 pictures-per-second (PPS) high-speed digital camera with 1 gigabyte of internal memory [37] and two B/W Sanyo CCD cameras (model VCB-3424) [38] along with TrueTime XL-DC GPS Time & Frequency receiver [39]. The high-speed camera and one Sanyo CCD camera are located at Pratt Building of University of Toronto (2.0 km north of the CN Tower). Digital data captured by the high-speed Phantom camera is being saved to PC. Accurate GPS timing of video records is provided by the TrueTime XL-DC GPS Time & Frequency receiver. The second Sanyo CCD camera is located at the Kinectrix Inc. building (formerly Ontario Hydro Research Laboratories), 11.8 km west of the CN Tower. The two locations provide almost perpendicular views with an angle of 82.5° between them. The two video recording systems allow for possible reproduction of the 3-D image trajectory of the lightning flash. Detailed specifications of each component of the CN Tower video recording system are next.

### Vision Research Phantom v5.0

Image Sensor:	1024x1024, SR-CMOS colour sensor
Maximum Capture Rate:	1000 picture per second (PPS) recording
Internal Memory:	1024 MB internal memory (1 sec recording at 1000 PPS)
Optional Memory:	4096 MB
Image Control:	Fire Wire or RS422/232 serial interface
Time Code Format:	IRIG-B code, modulated or unmodulated input for timing

### Sanyo B/D VCB-3424 CCD Camera

Image Sensor:	½" CCD Sensor
Picture Elements:	811(horizontal) x 508 (vertical)
Horizontal Resolution:	570 TV lines
Vertical Resolution:	350 TV lines
Signal-to-Noise Ratio:	more than 50 dB
Sensitivity:	0.07 lux with F1.2 lens attached

### True-Time XL-DC GPS Time & Frequency Receiver

Frequency:	1575.42 MHz (L1 signal)
Code:	Coarse Acquisition (C/A code)
Tracking:	Up to six satellites
24 Hr Average Position Accuracy:	< 10 m
Time Accuracy:	< 40 ns rms (150 ns peak)
Video Time Inserter Accuracy	< 1 ms

### 3.9 CN TOWER LIGHTNING OBSERVATIONS

Typical records obtained by the CN Tower lightning measurement systems are presented in this section. The lightning current derivative signals measured by the old Rogowski coil on August 19, 2005 at 14:11:43 Universal Time, Coordinated (UTC) is shown in Figure 3.6 while the current (time integral of current derivative signal of Figure 3.6) is presented in Figure 3.7. The corresponding vertical component of the electric field  $E_z$  and the azimuthal component of the magnetic field  $H_\phi$  are shown in Figures 3.8 and 3.9, respectively. The electric field waveform (Figure 3.8) has a slower decaying portion as compared to the magnetic field waveform (Figure 3.9). The reason for this difference is the presence of the electrostatic component in the electric field. The magnetic field does not contain the electrostatic component. Figures 3.6-3.9 represent the 6<sup>th</sup> stroke of a CN Tower 9-stroke flash. The peak value of the lightning current derivative for this stroke is 23.5 [kA/ $\mu$ s], while the peak values of electric and magnetic fields are 1.39 kV/m and 0.65 A/m, respectively. Video records of lightning return-stroke hitting the CN Tower on August 19, 2005 at 13:5:56 (UTC time) are shown in Figures 3.10 and 3.11. Figure 3.10 represents a video record captured by Sanyo CCD camera while Figure 3.11 represents the same record captured by Phantom high-speed camera. The number 231 in the GPS time (Figure 3.10) indicates the day of the year with day 1 being January 1<sup>st</sup>.

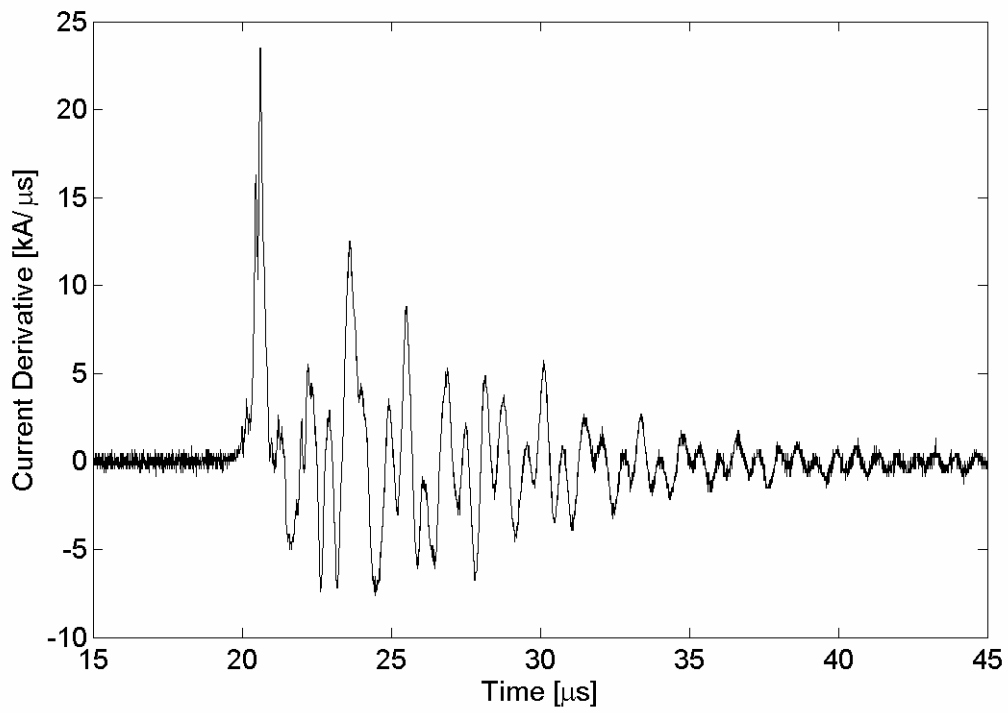


Figure 3.6. Current derivative signal measured on August 19, 2005 at 14:11:43.

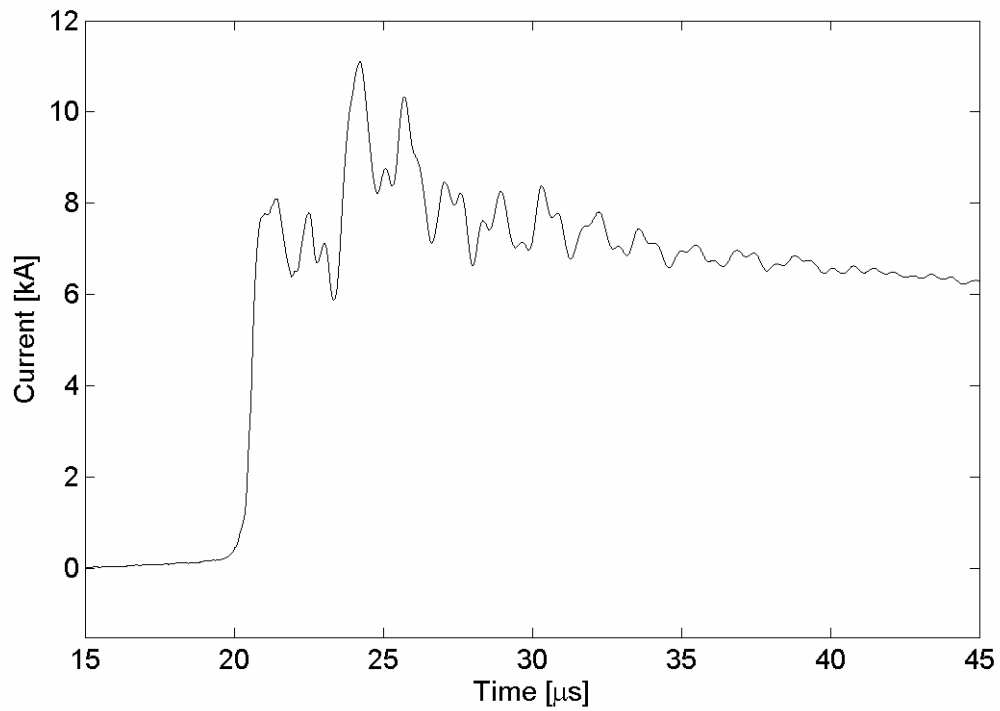


Figure 3.7. Current, time integral of current derivative signal shown in Figure 3.6.

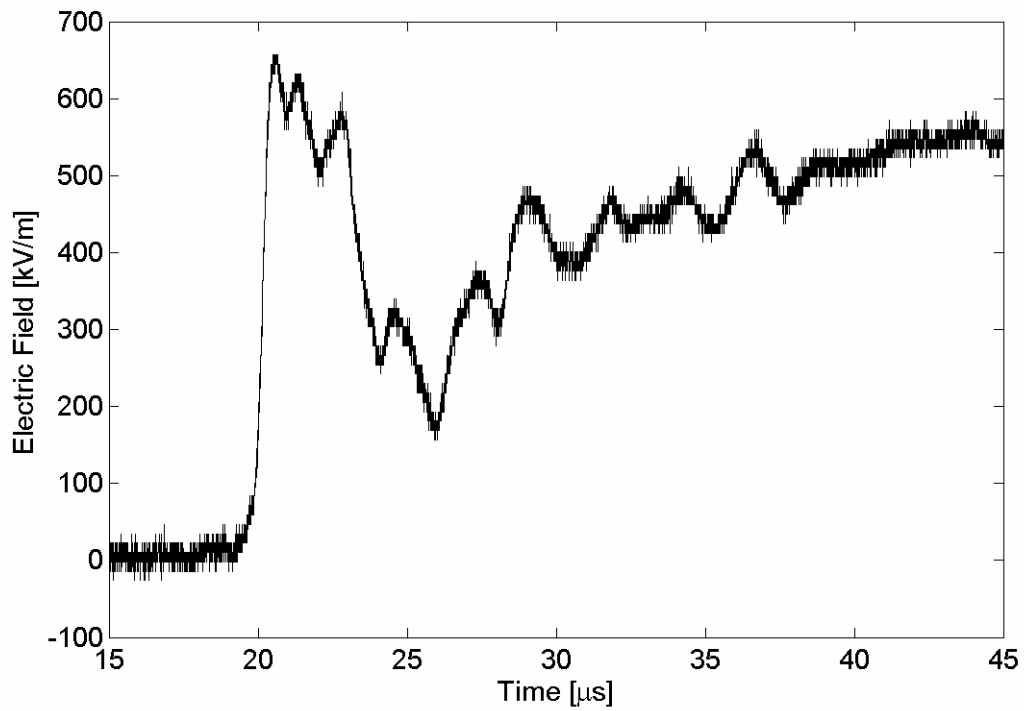


Figure 3.8. The electric field generated by the CN Tower lightning stroke, August 19, 2005 at 14:11:43.

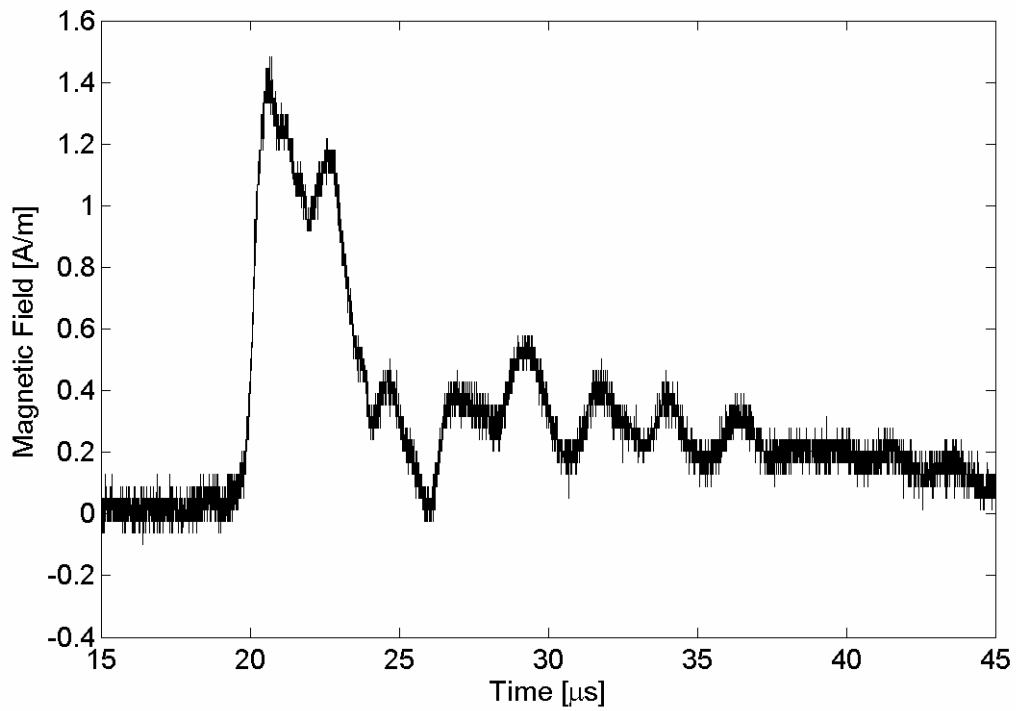


Figure 3.9. The magnetic field generated by the CN Tower lightning stroke, August 19, 2005 at 14:11:43.

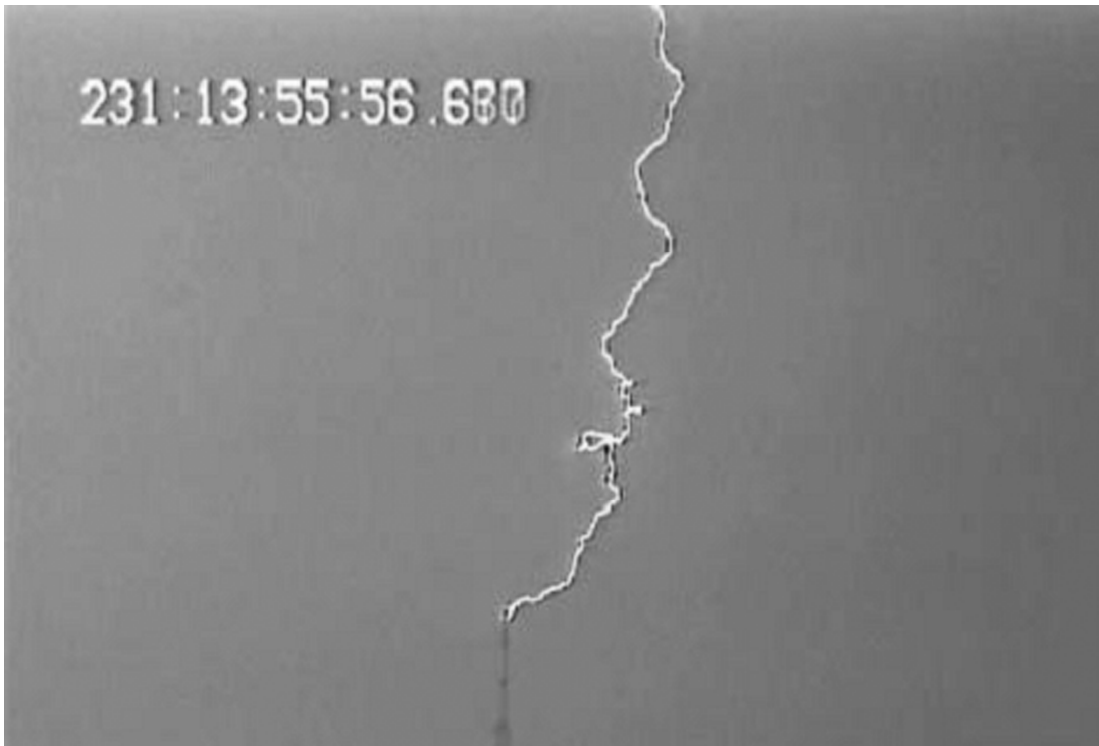


Figure 3.10. Sanyo CCD camera record of August 19, 2005 CN Tower lightning flash, 13:55:56.

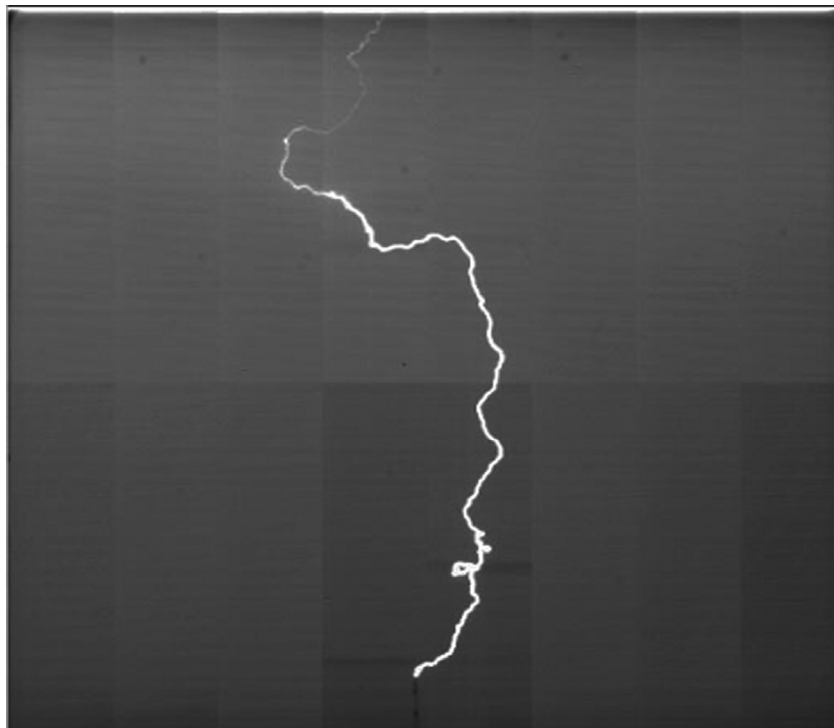


Figure 3.11. High-speed camera record of August 19, 2005 CN Tower lightning flash, 13:55:56.

A comparison between the current derivative signals measured by the old and new Rogowski coil is shown in Figures 3.12 and 3.13, respectively. The comparison of the corresponding current waveforms is shown in Figures 3.14 and 3.15, respectively. The signals represent a 3<sup>rd</sup> stroke of a 4-stroke flash measured at the CN Tower on January 2<sup>nd</sup>, 1999 at 22:27:02. From the waveforms shown in Figures 3.12-3.15 it can be seen that data captured with new Rogowski coil has better signal-to-noise ratio as compared to data captured with the old Rogowski coil. The amount of data captured with the new Rogowski coil is too limited to be used for the analysis and the research work presented in this thesis is based on the data captured with the old Rogowski coil.

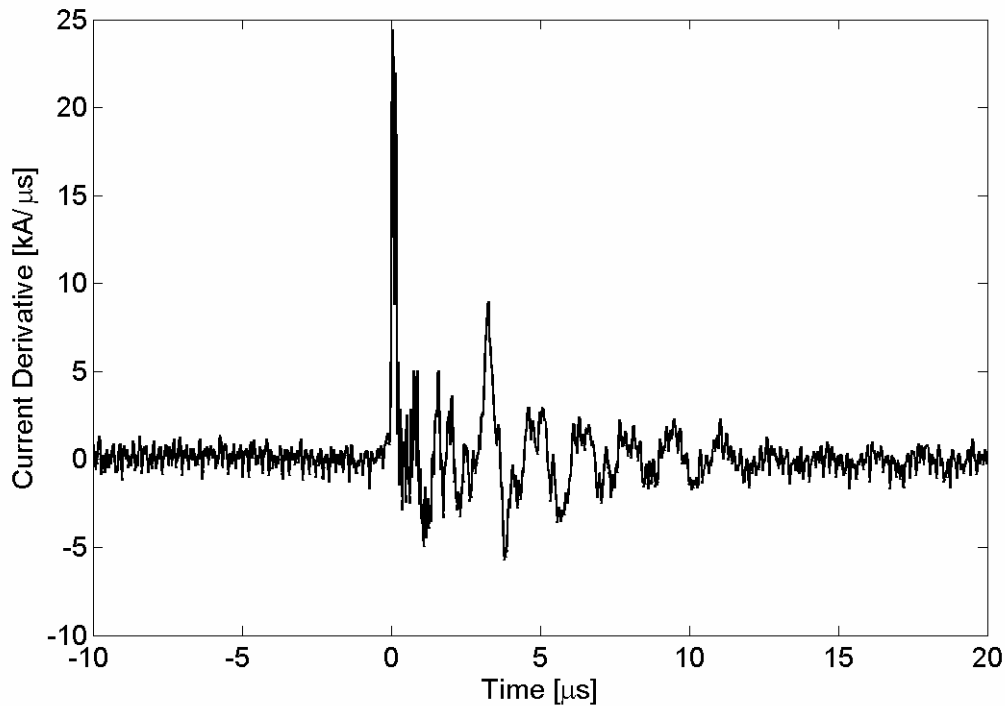


Figure 3.12. Current derivative measured by the old Rogowski coil on January 2<sup>nd</sup>, 1999 at 22:27:02.

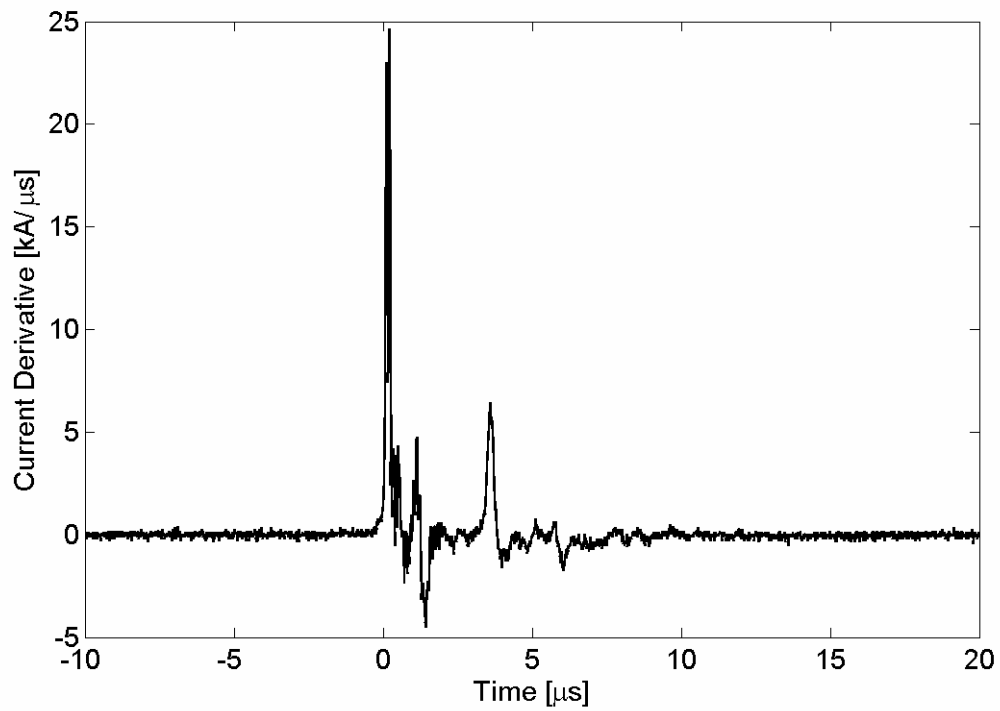


Figure 3.13. Current derivative measured by the new Rogowski coil on January 2<sup>nd</sup>, 1999 at 22:27:02.

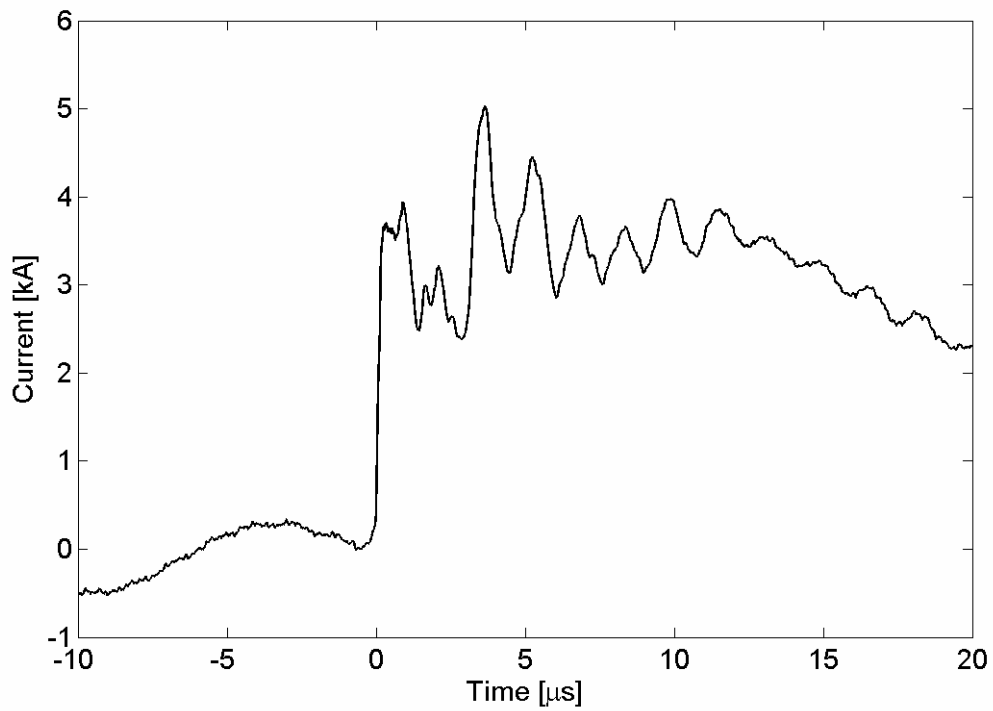


Figure 3.14. Current waveform (time integral of the current derivative waveform shown in Figure 3.12).

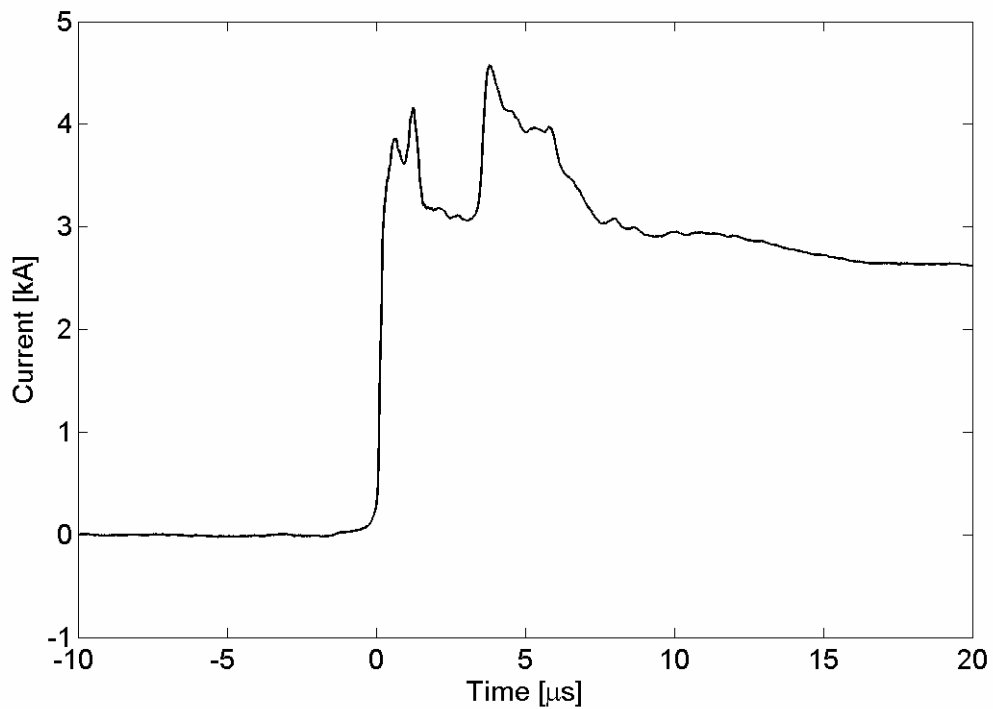


Figure 3.15. Current waveform (time integral of the current derivative waveform shown in Figure 3.13).

### 3.10 SUMMARY OF CHAPTER 3

The description of the CN Tower's lightning measurement systems is given. Typical records obtained from the lightning current measurement system, electric and magnetic field measurement system and video recording system (VHS as well as high-speed camera) are presented.

# Chapter 4

## Waveform Parameters

### **4.1 WAVEFRONT PARAMETERS OF CN TOWER LIGHTNING RETURN-STROKE CURRENT AND CURRENT DERIVATIVE**

The lightning return-stroke current is one of the most important parameters that is of interest to electrical engineers (especially from point of view of protection) since it causes most of the destruction and disturbances in telecommunication networks, it produces overvoltages on power lines and can be a cause of other hazards such as forest fires [8,19,24,40-41]. For example, based on studies done in Germany it was found that about 25% of damages to wind power plants are due to lightning [19]. In order to measure the lightning return-stroke current, the exact location of the lightning strike must be known and this can be only accomplished by using instrumented tall towers, towers placed on elevated grounds or by rocket-triggered lightning. A tall structure such as the CN Tower, with an average number of 40-50 lightning flashes per year, presents an ideal location for measurement of the lightning return-stroke current and studying the lightning phenomenon. Important waveform parameters of the lightning return-stroke current, which are to be evaluated include: the maximum current rate of rise, wavefront initial current peak, absolute current peak and the 10%-90% risetime to initial current

peak. Figure 4.1 shows the definition of the waveform parameters of a current derivative signal measured at the CN Tower. The waveform parameters of the current, obtained by integrating the current derivative signal (Figure 4.1), are shown in Figure 4.2. In order to accurately evaluate these wavefront parameters, a base level for each of the current derivative and current waveforms has to be estimated. The main reasons for the shift observed in the measured data and the need for estimating the base levels include the presence of noise as well as the presence of a DC or low-frequency component in the measured signal. The major source of noise in the CN Tower current waveform was found to be resulting from the low frequency radio navigation Loran-C signal operating in the range of 90 to 100 kHz [18,42-43]. The estimated base level for the current derivative waveform shown in Figure 4.1 is 0.65 kA/ $\mu$ s and the base level for the current waveform shown in Figure 4.2 is 0.34 kA. The determination of the base level is necessary for the calculation of the maximum current derivative, 10%-90% risetime to maximum current derivative, initial current peak, absolute current peak and 10%-90% risetime to initial current peak. In Figures 4.1 and 4.2 the “Not Adjusted Peak” of current derivative and current waveforms indicates the peak in which the base level has not been taken into account. Table 4.1 lists the five waveform parameters obtained from the CN Tower lightning return-stroke current derivative and current waveforms shown in Figures 4.1 and 4.2, respectively. Detailed description of the current derivative and current waveform parameters is given in the next section.

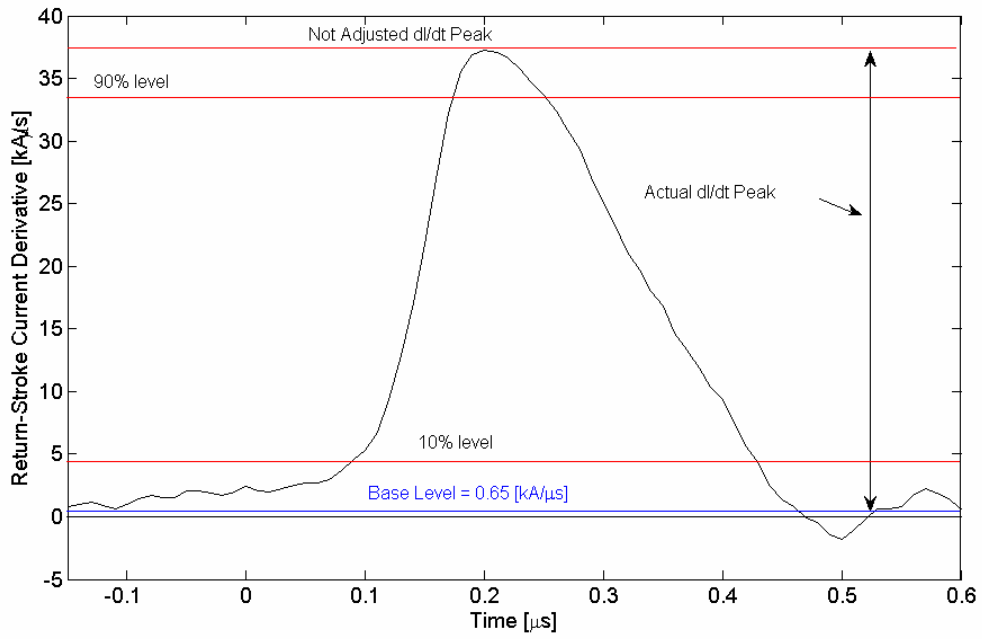


Figure 4.1. Current derivative wavefront parameters, old coil.

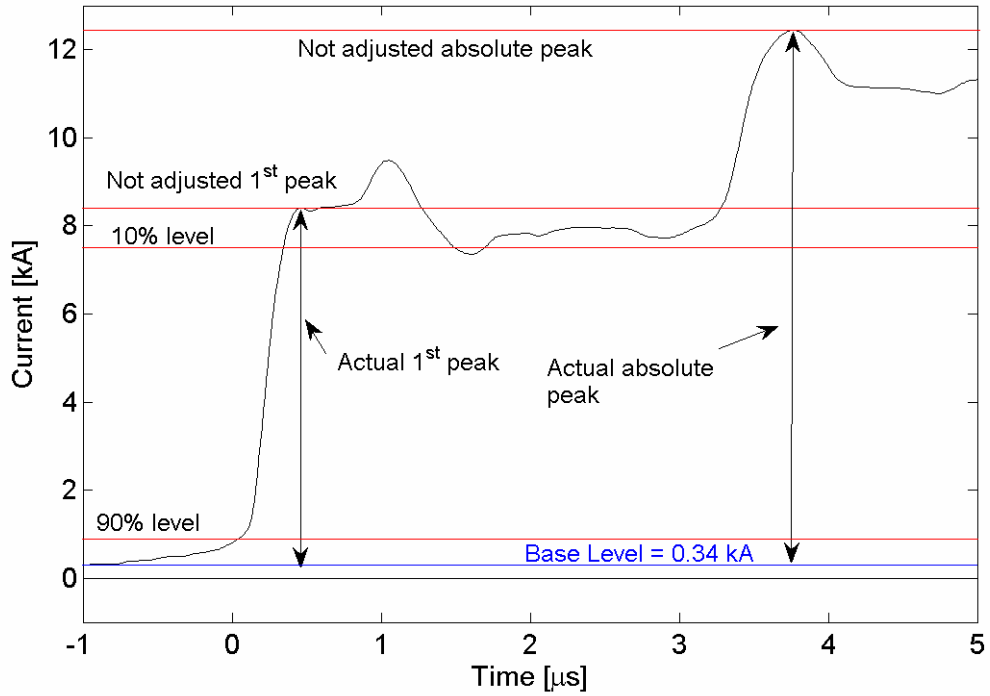


Figure 4.2. Current waveform parameters, old coil.

Table 4.1. Current and current derivative wavefront parameters obtained from waveforms shown in Figures 4.1 and 4.2.

Maximum dI/dt	10%-90% R.T. to Maximum dI/dt	1 <sup>st</sup> Current Peak	10%-90% R.T. to 1 <sup>st</sup> Current Peak	Absolute Current Peak
36.56 [kA/ $\mu$ s]	93.3 ns	8.05 kA	221.6 ns	12.07 kA

#### 4.1.1 LIGHTNING RETURN-STROKE CURRENT DERIVATIVE

The lightning return-stroke current derivative is being directly measured at the CN Tower as described in Chapter 3. Two main wavefront parameters, which are obtained from the measured current derivative signal and are of interest to researchers, are the maximum current derivative and the 10%-90% risetime to maximum current derivative. The maximum lightning current derivative is an important parameter, which has to be known for proper estimation of overvoltages induced in power and telecommunication lines. The increase in maximum current derivative causes an increase in the amplitude of the overvoltage in power and telecommunication lines, which leads to an increase in the currents carried by the lines. The knowledge of the lightning return-stroke current derivative is especially important for protection of tall structures since as the height of the tall structure increases so does the maximum current derivative [44]. The derivative of the lightning current is substantially correlated to the derivative of the electric and magnetic fields and higher electric field derivatives produce more disturbances, damages and interferences to electric and electronic systems [5,6,41]. The knowledge of 10%-90% risetime to maximum current derivative is important for proper calibration and setup of lightning current measurement systems. In order to properly measure the lightning current derivative, the overall risetime of the measurement system

should be significantly smaller than the risetime of the measured return-stroke current derivative.

#### **4.1.2 LIGHTNING RETURN-STROKE CURRENT**

The CN Tower lightning return-stroke current is obtained by numerical integration of the measured lightning current derivative. The three main waveform parameters that are determined from the lightning current data are: initial current peak, absolute current peak and 10%-90% risetime to initial current peak. The initial current peak is the most important waveform parameter from point of view of protection from lightning damages and injuries. As the lightning current increases the possibility of damage to objects being hit by lightning (for example, buildings, airplanes, power lines, trees, etc.) also increases. The initial current peak and electric and magnetic field peaks are greatly correlated. An increase in the initial current peak produces higher electric and magnetic field peaks and this will result in increased electromagnetic disturbances and interferences. The absolute current peak is a parameter, which depends on the structure at which it is measured. The absolute current peak is affected by reflections from structural discontinuities and in case of the CN Tower the absolute current usually corresponds to ground reflection. The absolute current peak is structure dependent, however, it is an important parameter from point of view of protection as it is usually higher than the initial current peak [18,24]. The 10%-90% risetime to the initial current peak is the third parameter that should not be ignored from point of view of protection, especially from overvoltages, as current pulses with faster risetime produce electromagnetic fields with

faster risetime [5]. Very fast lightning current pulses present a greater challenge in the design of means of protection against lightning hazards.

#### **4.2 WAVEFRONT PARAMETERS OF CN TOWER LIGHTNING-GENERATED ELECTROMAGNETIC PULSE**

The electric and magnetic fields generated by lightning return-strokes striking the CN Tower have been measured 2.0 km north of the tower since 1991. The wavefront parameters of the electric and magnetic fields that are of importance are: the initial electric and magnetic field peaks, 10%-90% risetime to initial electric and magnetic field peaks, and maximum derivative of the wavefront of electric and magnetic fields. These parameters are important for protection from the electromagnetic disturbances and interferences caused by lightning return-strokes. In case of lightning to tall structures such as the CN Tower, the presence of a tall structure greatly increases the electric and magnetic field peaks as well as their corresponding derivatives. The increase in the field peak for lightning to a tall structure is mainly caused by the presence of two oppositely propagating current waves (originating at the tip of the structure) as well as by the increased speed of propagation within the structure, which is equal to the speed of light while the speed of propagation in air is only around one-third the speed of light [6,45-47]. Two of the wavefront parameters of the electric field (initial field peak and 10%-90% risetime) resulting from a CN Tower return-stroke are shown in Figure 4.3. As in the case of the current and current derivative waveforms the base level has to be calculated before the electric field waveform parameters can be evaluated. The magnetic field wavefront parameters are not shown since they are evaluated in a similar manner. The derivative of

the electric field waveform of Figure 4.3, showing the maximum electric field derivative, is presented in Figure 4.4. It should be pointed out that a low-pass filtering technique has been applied to all the electric and magnetic field signals before the wavefront parameters were evaluated. The evaluation of the maximum electric and magnetic field derivatives from the measured signals proved to be very difficult task due to presence of high-frequency noise (mostly related to nearby broadcasting stations) that was corrupting the measured signals. When evaluating the maximum electric and magnetic field derivatives, the obtained results would in most-cases correspond to the high-frequency noise rather than the lightning-generated fields [5,46]. Detailed description of the low-pass filtering method used for denoising of the field signals is given later. Waveforms shown in Figures 4.3 and 4.4 represent the measured electric field signal and its derivative after applying a 5<sup>th</sup> order elliptic low pass filter with a cut-off frequency of 5 MHz.

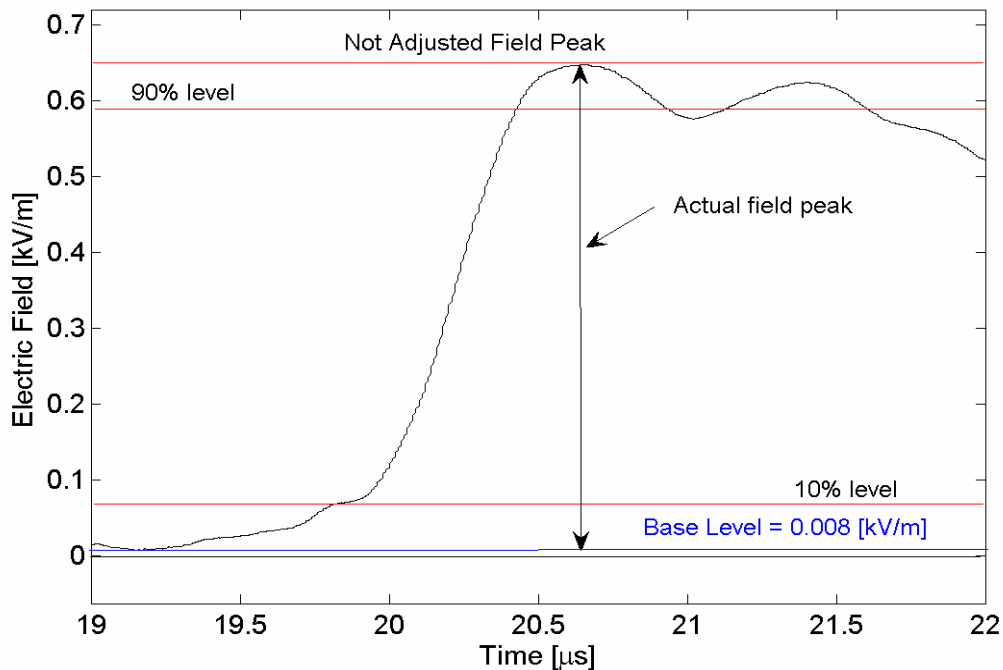


Figure 4.3. Electric field wavefront parameters.

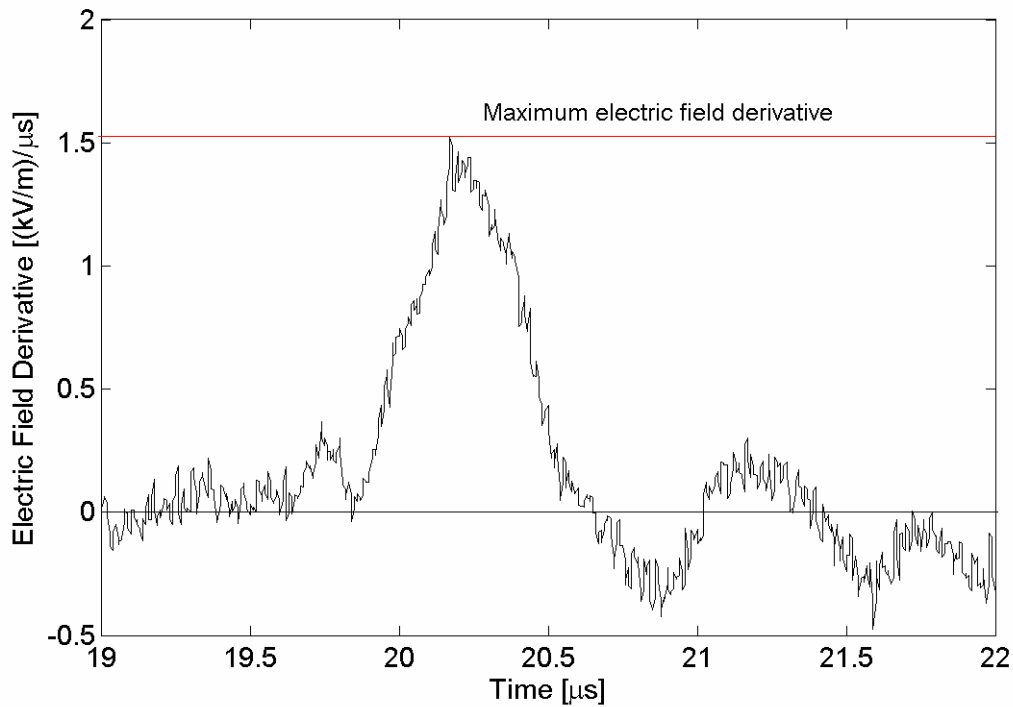


Figure 4.4. Electric field derivative wavefront parameters.

### 4.3 DENOISING THE ELECTRIC AND MAGNETIC FIELD SIGNALS

The evaluation of the electric and magnetic field wavefront parameters presented special difficulty due to the presence of high-frequency noise, mostly related to broadcasting stations. Figure 4.5a shows the measured electric field signal while Figure 4.5b shows the derivative of the measured electric field signal. It can be seen that the noise present in the measured electric field signal (which is also present in the magnetic field signal) causes great difficulties in the evaluation of the wavefront parameters, especially the maximum derivative of the field. Denoising methods described below were applied to both the electric and magnetic field signals generated by lightning return-strokes to the CN Tower. In order to properly filter the electric and magnetic field signals for the calculation of the wavefront parameters, FFT analysis were applied to determine

the frequency range of the noise being present in the measured data. The FFT of the measured electric field signal in the range of 0 to 50 MHz is shown in Figure 4.6. There are significant peaks being present in the FFT magnitude of the electric field signal at 12.0, 14.015, 15.63, 20.01 and 44.0 MHz. Industry Canada provides detailed description of the radio frequency allocations for Canada. Based on the information from 2005 Industry Canada frequency allocation table, it was found that 12 and 15.63 MHz frequencies are related to broadcasting stations, 14.015 MHz frequency is related to amateur satellite, while 15.63 and 44.0 MHz frequencies are related to mobile communications [48]. These high-frequency signals along with other less visible high-frequency signals presented a major difficulty in the proper computation of the electric and magnetic field wavefront parameters.

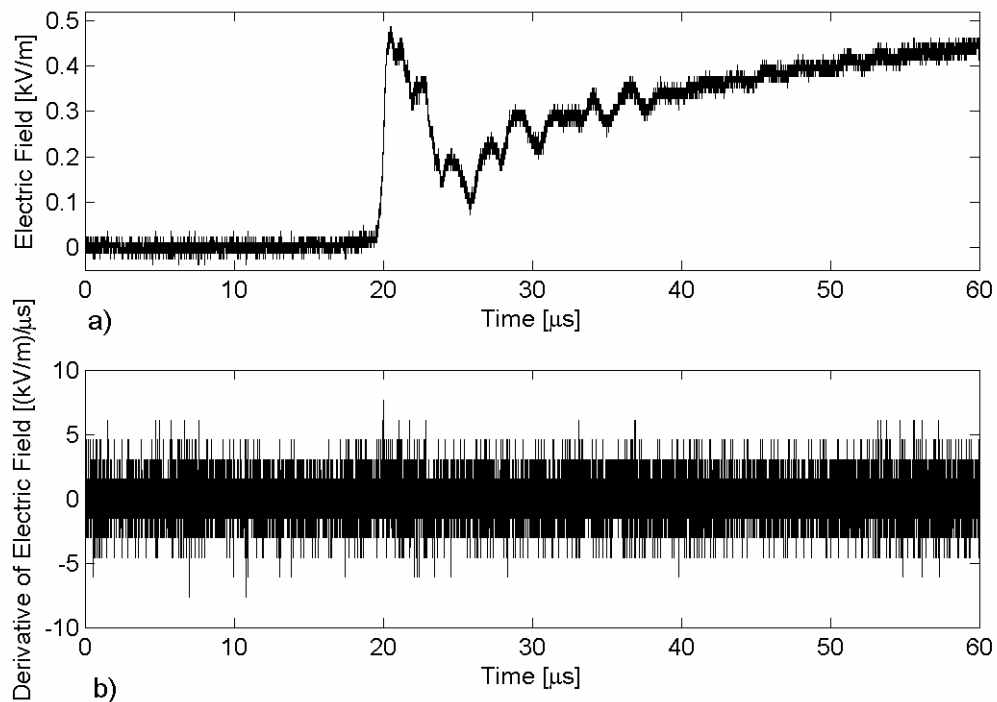


Figure 4.5. a) Measured electric field signal, b) derivative of the measured electric field signal.

Different low-pass filtering (LPF) techniques were applied for denoising the electric and magnetic field signals generated by lightning return-strokes to the CN Tower. Based on the obtained results, it was found that a 5<sup>th</sup> order elliptic low pass filter with cut-off frequency of 5 MHz provided the best fit in terms of improving the signal-to-noise ratio and retaining the lightning-generated electric and magnetic field waveshapes [5]. The 5<sup>th</sup> order elliptic low pass filter was designed using Signal Processing Toolbox from Matlab. The designed filter has a 0.5 dB ripple in the pass band, 20 dB attenuation in the stop band and a cut-off frequency of 5 MHz. The sampling rate for the electric and magnetic field signal is 100 MHz. Comparison of the measured electric field waveform with the denoised field using a 5<sup>th</sup> order elliptic filter with cut-off frequencies of 0.5, 1, 2, 5 and 10 MHz is shown in Figure 4.7. The low cut-off frequencies such as 0.5 and 1 MHz distort the original signal significantly (Figure 4.7). Also, the field signal denoised with lower cut-off frequency elliptic LPF filters is shifted as well as smoothed out (the smoothing would affect the calculation of maximum field derivative) compared to the measured signal. Another reason why filters with low cut-off frequencies were avoided is because they remove a part of the actual lightning signal. It can be seen that 5 MHz and 10 MHz cut-off frequencies provide very good filtering results and since there is no substantial difference in filtering with 10 MHz vs. 5 MHz cut-off frequencies, a filter with 5 MHz cut-off frequency was chosen. The 10 MHz cut-off frequency filter was also not chosen to avoid possibility of unnecessary high-frequency noise being present in the electric or magnetic field waveforms. The waveform of the electric field signal of Figure 4.5a after being denoised with the 5<sup>th</sup> order elliptic low-pass filter is shown in Figure 4.8a, while the derivative obtained from the denoised electric field signal is shown in

Figure 4.8b. A clear improvement in the signal-to-noise ratio can be seen in the denoised electric field waveform in comparison with the measured electric field waveform. FFT magnitude of the denoised electric field signal is shown in Figure 4.9 and it can be seen that the high-frequency noise components that caused problems in the evaluation of the wavefront parameters were removed. Detailed correlation analyses of the lightning electromagnetic pulse measured 2.0 km north of the CN Tower and the lightning current and current derivative measured at the CN Tower is presented in Chapter 5.

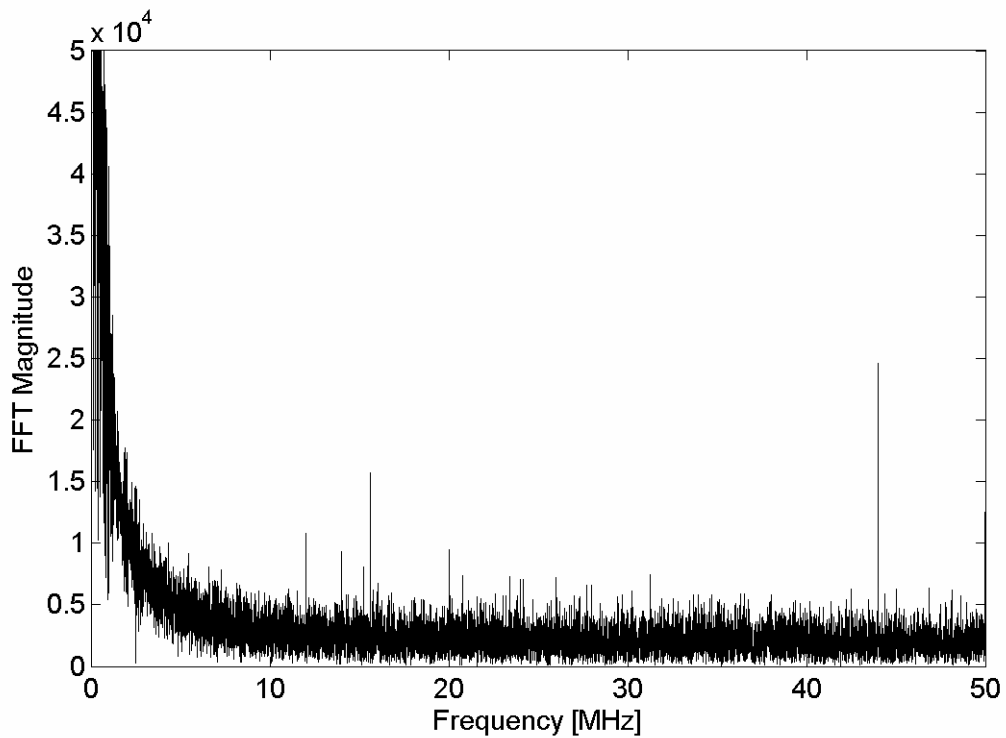


Figure 4.6. FFT magnitude of measured electric field signal shown in Figure 4.5a.

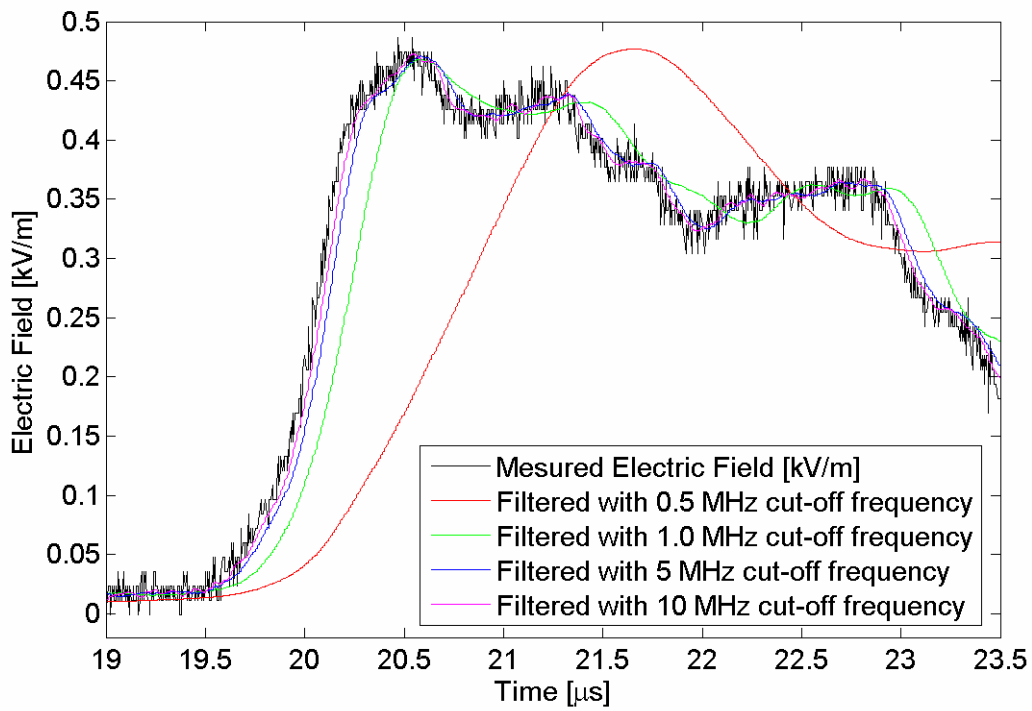


Figure 4.7. Comparison of denoising results of the electric field signal using 5<sup>th</sup> order elliptic low-pass filter.

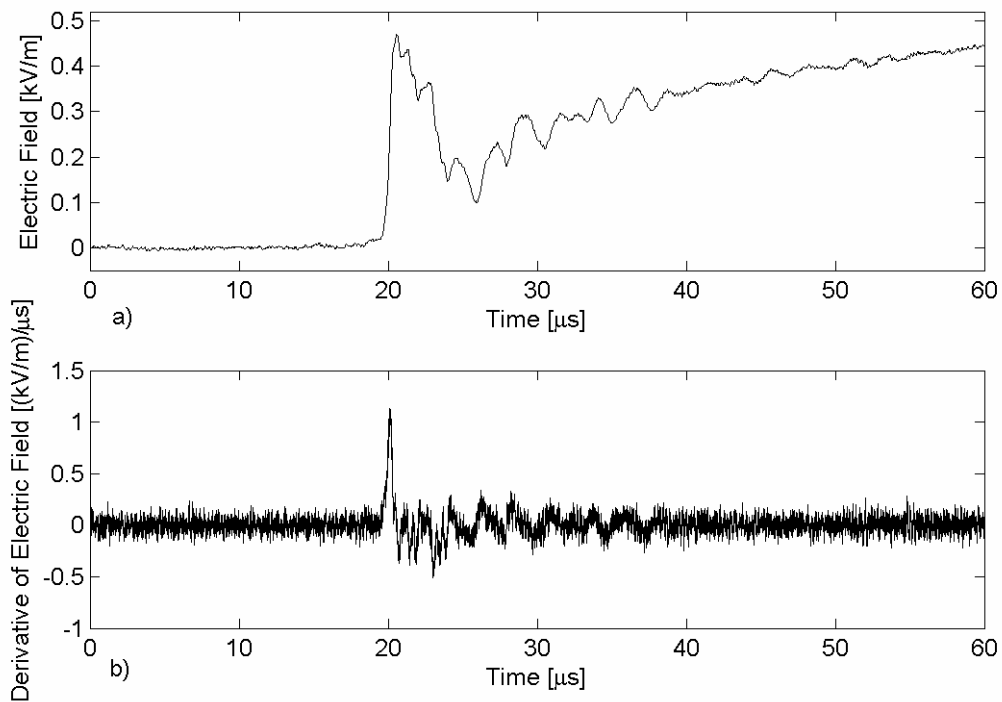


Figure 4.8. a) Denoised electric field signal of Figure 4.5a b) electric field derivative obtained from the denoised signal of Figure 4.8a.

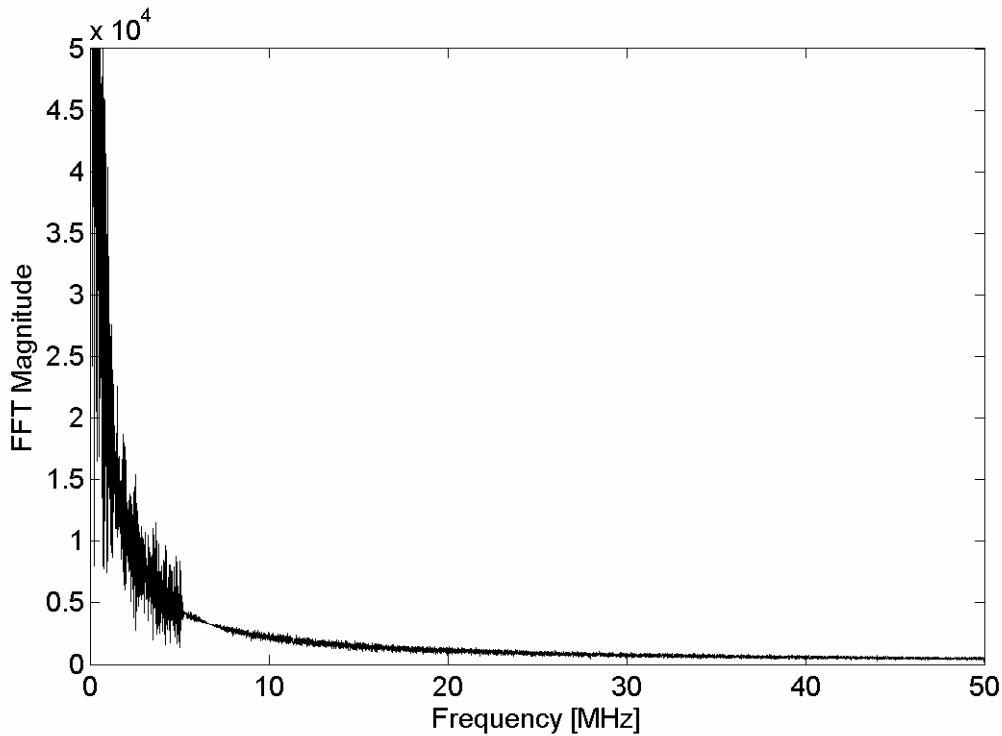


Figure 4.9. FFT magnitude of the denoised electric field signal shown in Figure 4.8a.

#### 4.4 SUMMARY OF CHAPTER 4

The most important lightning return-stroke current and lightning-generated electromagnetic field wavefront parameters are discussed. These parameters are important from point of view of protection and lightning detection. The evaluation of field wavefront parameters (especially the maximum field derivatives) proved to be a difficult task due to presence of high frequency noise in the measured fields. It was determined that most of the high frequency noise present in the measured field signals is related to broadcasting stations. The denoising process of the CN Tower's lightning-generated electric and magnetic field signals is described. The correlation between field-current wavefront characteristics would not have been possible without denoising the measured electric and magnetic field signals.

# Chapter 5

## Correlating CN Tower Lightning Return-Stroke Current with its Electromagnetic Pulse

### 5.1 SYNCHRONIZATION OF LIGHTNING RETURN-STROKE CURRENTS, ELECTROMAGNETIC FIELDS AND VIDEO RECORDS

Simultaneous measurements of the lightning return-stroke current derivative at the CN Tower and the corresponding lightning electromagnetic pulse (LEMP) 2 km north of the Tower have been performed using broadband, high-resolution sensors. Recently installed Global Positioning System (GPS) allowed for time synchronization of the current and its generated electromagnetic field with resolution of 1  $\mu$ s, while VHS video records are synchronized with resolution of 1 ms. The time resolution of stand alone GPS system used for video records is 1 ms as opposed to 1  $\mu$ s time resolution of GPS cards used by current and field measurement systems. The time synchronization of lightning current, electromagnetic field and VHS video records has provided an opportunity for correlating the current wavefront parameters (peak, maximum derivative, 10%-90% risetime) with the corresponding electric and magnetic field wavefront parameters. It should be pointed out that in the absence of GPS timing, the matching of current data

with its corresponding field data was very difficult, especially on stroke by stroke basis since the time between successive strokes is usually in tens of milliseconds. The correlation analysis of the lightning return-stroke current with its lightning generated electromagnetic field is presented in the following section. In addition, the correlation analysis between the electric and magnetic field wavefront parameters will be included. One of the most interesting and challenging areas in lightning studies is related to the solution of the inverse-source problem, where the lightning current characteristics are estimated based on the characteristics of the measured electric and magnetic fields [5,49-50]. Lightning detection networks such as the North American Lightning Detection Network (NALDN) use the measured magnetic field peak in order to estimate the lightning current peak [51,52]. An important step towards reaching the goal of solving the inverse source problem is the establishment of a simple field-current relationship that is based on experimental data [5,24,53-54].

## **5.2 CORRELATION ANALYSES**

The analyses presented here are based on CN Tower lightning data collected during thunderstorms that occurred on August 19<sup>th</sup>, 2005. In total, 6 flashes, containing 36 lightning return-strokes have been measured during that day. The CN Tower lightning return-stroke current data has been perfectly matched with 1  $\mu$ s resolution to its corresponding electric and magnetic field data, measured 2 km north of the tower. The current and field waveform characteristics that are analyzed are the initial wavefront peak, wavefront maximum derivative and 10%-90% risetime to initial wavefront peak. Based on this CN Tower lightning return-stroke data, least square straight line fits

(regression lines) were obtained to correlate the characteristics of electric and magnetic fields to each other as well as to the characteristics of the return-stroke current. In each case, the correlation coefficient (CC) is included in the figure caption to serve as an indicator of the fit quality. It should be also pointed out that the electric and magnetic fields have been filtered with 5<sup>th</sup> order elliptic low pass filter, cut-off frequency 5 MHz, before the field peaks and maximum field derivatives were computed. As mentioned in Chapter 4, it was not possible to determine the maximum derivative of the electric and magnetic fields without filtering as the presence of the high-frequency noise, in many cases, caused the obtained maximum field derivatives to correspond to the noise rather than the field signals.

Figure 5.1 shows a linear correlation of the electric and magnetic field wavefront peaks and it can be seen that the field peaks are strongly correlated with each other (CC = 0.988). The dashed line in Figure 5.1 represents the expected linear relationship in the far-field range for transverse electromagnetic waves, where the ratio of electric field to magnetic field is equal to the intrinsic impedance ( $120\pi$  [ $\Omega$ ] in air). The slope of the regression line in Figure 5.1 is about 32% larger than that of the far-field line. One of the reasons for the difference is that the electric field contains an electrostatic component, which is not present in the magnetic field. The presence of the electrostatic field component might slightly increase the peak of electric field and it also proves that the field sensors are located not far enough from the CN Tower for the measured electromagnetic field to be considered as being in the far-field range. Another reason for the difference between the two regression lines in Figure 5.1 is that since only the azimuthal component of the magnetic field was measured in 2005 (the azimuthal

component is expected to be the dominant component of the magnetic field), the radial component that was not measured may not be completely negligible, especially for non-vertical lightning channels [11]. Also, since the electric field sensor was calibrated in an EMC Cell, the building's electric field enhancement effect may also explain the discrepancy shown in Figure 5.1 [55]

The relationship between the wavefront maximum derivative of the electric field and that for the magnetic field is shown in Figure 5.2. A dashed line representing the expected relationship between the maximum electric and magnetic field derivative in the far-field range is also shown. The slope of the regression line obtained from the measured data is only about 7% larger than the slope of the far-field relationship. The smaller difference between the two lines of Figure 5.2 confirms the fact that the existence of the electrostatic component in the electric field is one of the reasons for the larger difference between two lines of Figure 5.1. The electric field maximum wavefront derivative is almost independent of electrostatic component, and this is why the regression line for the field derivatives obtained from measurement is closer to the theory. On the other hand, the results presented in Figure 5.2 illustrate that the correlation between electric and magnetic field derivatives is not as close as the correlation between electric and magnetic field peaks ( $CC = 0.904$  for the correlation of field derivatives while  $CC = 0.988$  for the correlation of the field peaks). The possible reason for this difference could be attributed to the presence of the high frequency noise that was not fully denoised. The calculation of the electric and magnetic field derivatives has proven to be very sensitive to the high frequency noise that is expected to vary with time. The noise that was still left in the denoised field data would normally be different from one return-stroke to another and

this will affect the degree of accuracy with which the maximum electric and magnetic field derivatives are calculated. This may have contributed to increased scatter in the correlation of electric and magnetic field derivatives of Figure 5.2.

The correlation of the 10%-90% risetime to the electric and magnetic field peaks is shown in Figure 5.3. Figure 5.3 illustrates that the risetime of the electric field is very close to that of the magnetic field. The correlation coefficient in this case was found to be 0.962. It should be pointed out that strong linear correlation between the electric and magnetic field wavefront characteristics (peak, maximum derivative and risetime) serve as good indicator of the proper calibration and similar frequency responses of both the electric and magnetic field sensors. Since reasonably strong linear correlation exists between the corresponding wavefront characteristics of the electric and magnetic fields, only the magnetic field wavefront parameters will be correlated with those of the corresponding lightning return-stroke current.

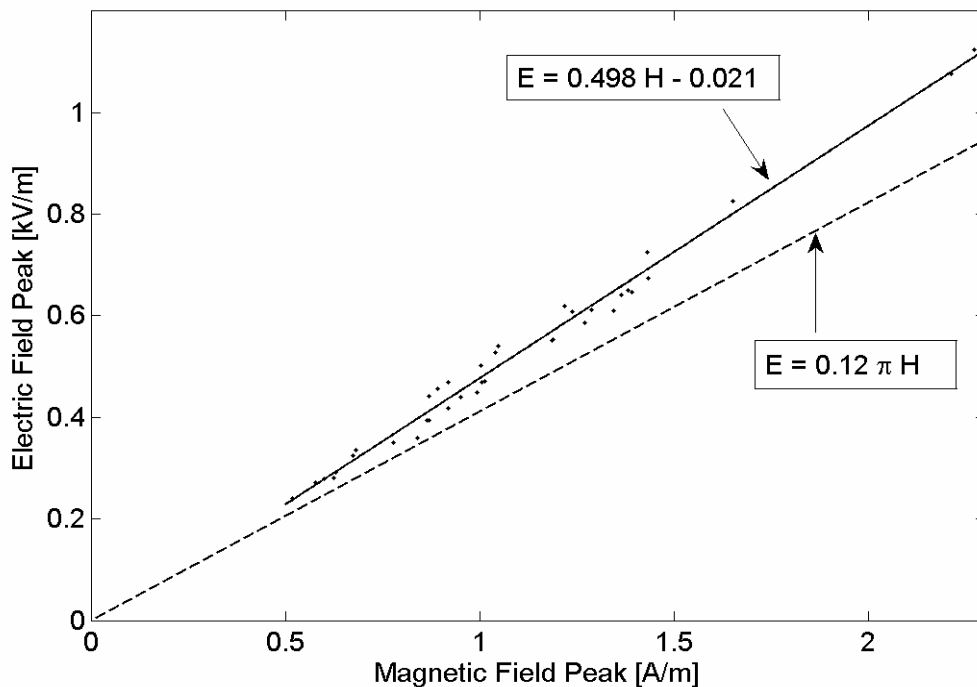


Figure 5.1. Electric field peak versus magnetic field peak, CC = 0.988.

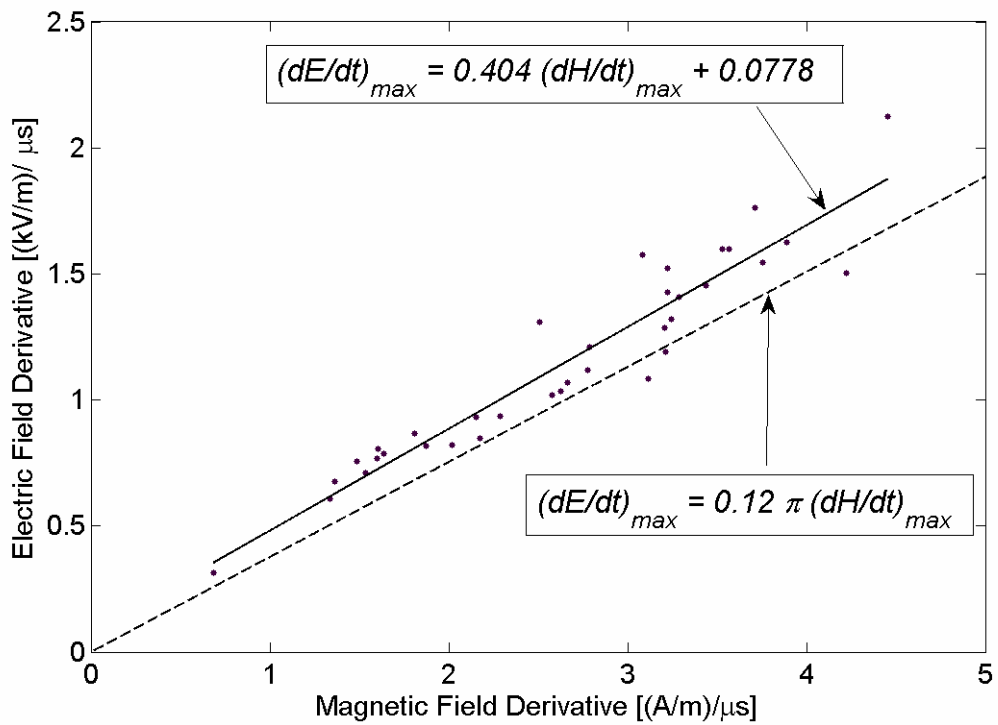


Figure 5.2. Maximum derivative of electric field versus maximum derivative of magnetic field, CC = 0.904.

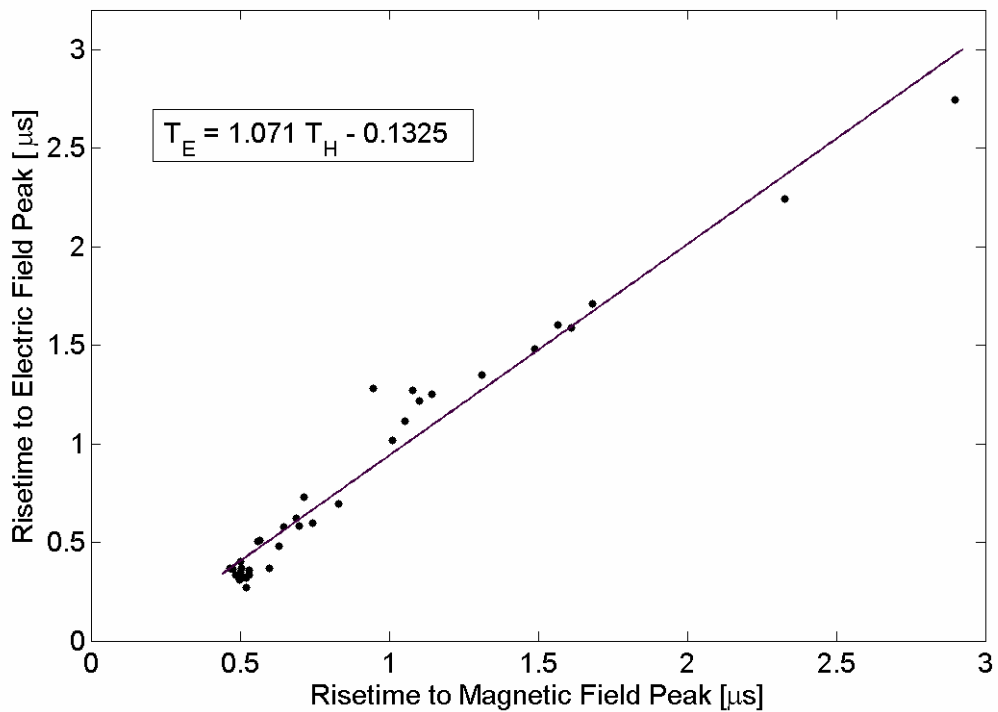


Figure 5.3. Electric field 10%-90% risetime ( $T_E$ ) versus magnetic field 10%-90% risetime ( $T_H$ ), CC = 0.962.

The correlation between the magnetic field wavefront characteristics (peak, maximum derivative and 10%-90% risetime) and the characteristics of the lightning return-stroke current are shown in Figures 5.4-5.8. An important point to mention is that in 2005 the digitizer used to measure the lightning current derivative at the CN Tower was set to record signals up to 2 V, which corresponds to maximum current derivative peak of 27.86 kA/ $\mu$ s. Four current derivative signals out of the 36 measured in 2005 exceeded this maximum level. Although the points representing these four signals are shown in Figures 5.5 and 5.7 (represented by “x’s”), they were not included in the derivation of the regression lines. The results of Figures 5.4-5.6 show that the wavefront peak, maximum derivative and 10%-90% risetime to wavefront peak of the magnetic field are linearly correlated with the corresponding wavefront peak, maximum derivative and 10%-90% risetime of the lightning return-stroke current peak, respectively. Among these three linear correlations, the correlation of the magnetic field peak to the current peak is the strongest,  $CC = 0.975$  (Fig. 5.4).

In studies done with lightning striking the 160-m Peissenberg Tower in Germany, a strong linear correlation between the magnetic field peak and the lightning return-stroke current peak was also found [19,24]. Further discussions regarding the correlation between the magnetic field peak and the lightning return-stroke current peak will be given in the next section.

The linear correlation between the maximum derivative of the magnetic field and that of the CN Tower current is shown in Figure 5.5. Similar relationship between the magnetic field and current maximum wavefront derivatives was developed for lightning to the Peissenberg Tower [19,24]. Since there is a strong linear correlation between field

and current maximum derivatives, the maximum current wavefront derivative can be estimated from the measured magnetic field, after taking into consideration the propagation effects on its derivative. The field maximum steepness can be included in the future lightning detection and peak estimation algorithms to further improve the efficiency of these algorithms. The 10%-90% risetime to initial peak of the magnetic field is strongly correlated to that of the current peak as it can be seen from Figure 5.6. The correlation coefficient for the regression line shown in Figure 5.6 is 0.871.

Although a weak correlation between the magnetic field peak and the corresponding maximum current derivative is found (Fig. 5.7), a general trend of increase in the magnetic field peak is observed as the maximum rate of rise of current increases. Furthermore, a general trend of increase in the magnetic field maximum derivative is observed as the current peak increases (Fig. 5.8). The correlation coefficients for the regression lines presented in Figures 5.7 and 5.8 are  $CC = 0.0822$  and  $CC = 0.092$ , respectively. The general increase in the magnetic field peak and the magnetic field maximum derivative associated with the increase in the current derivative and current peak, respectively, is interesting, but needs further investigations using future or presently available tall-structure and triggered-lightning data.

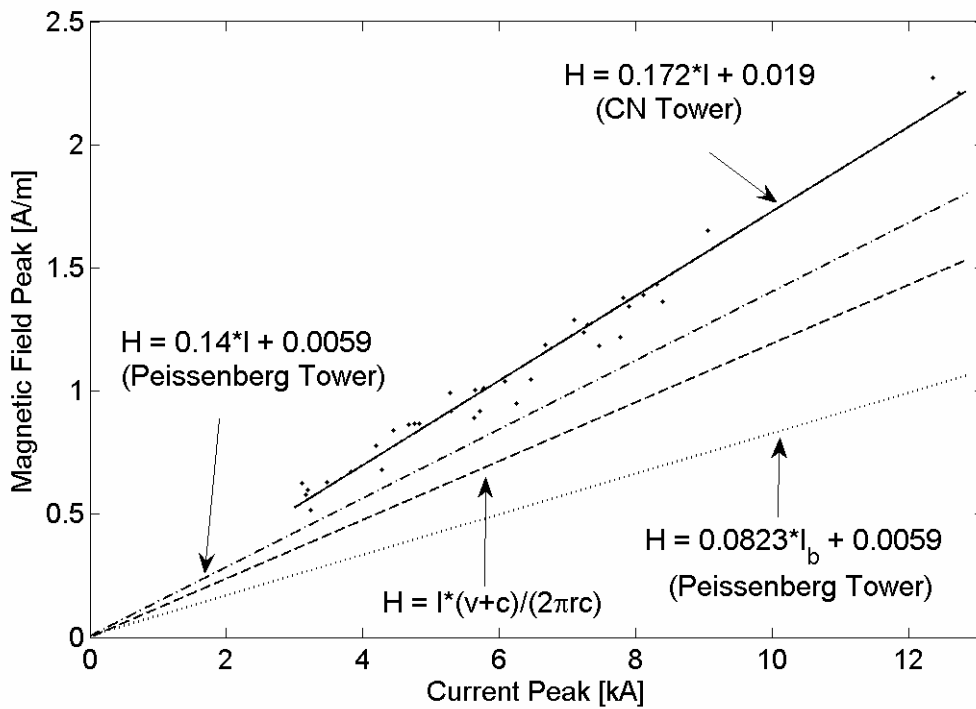


Figure 5.4. Magnetic field peak versus current peak, CC = 0.975.

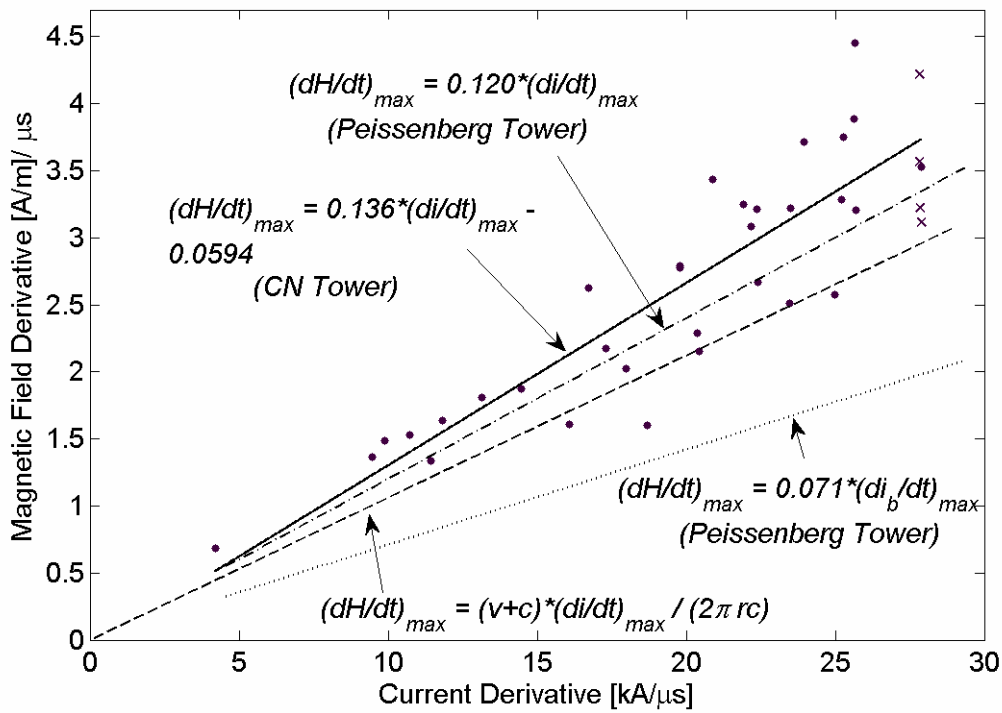


Figure 5.5. Maximum magnetic field derivative versus maximum current derivative, CC = 0.786.

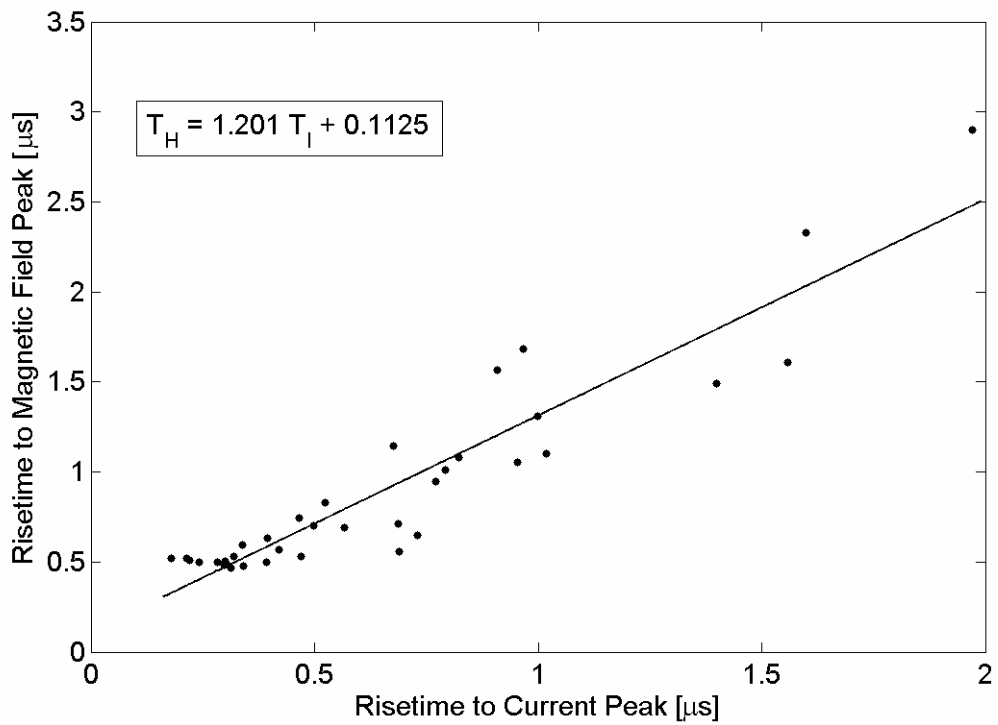


Figure 5.6. Magnetic field risetime ( $T_H$ ) versus current risetime ( $T_i$ ),  $CC = 0.871$ .

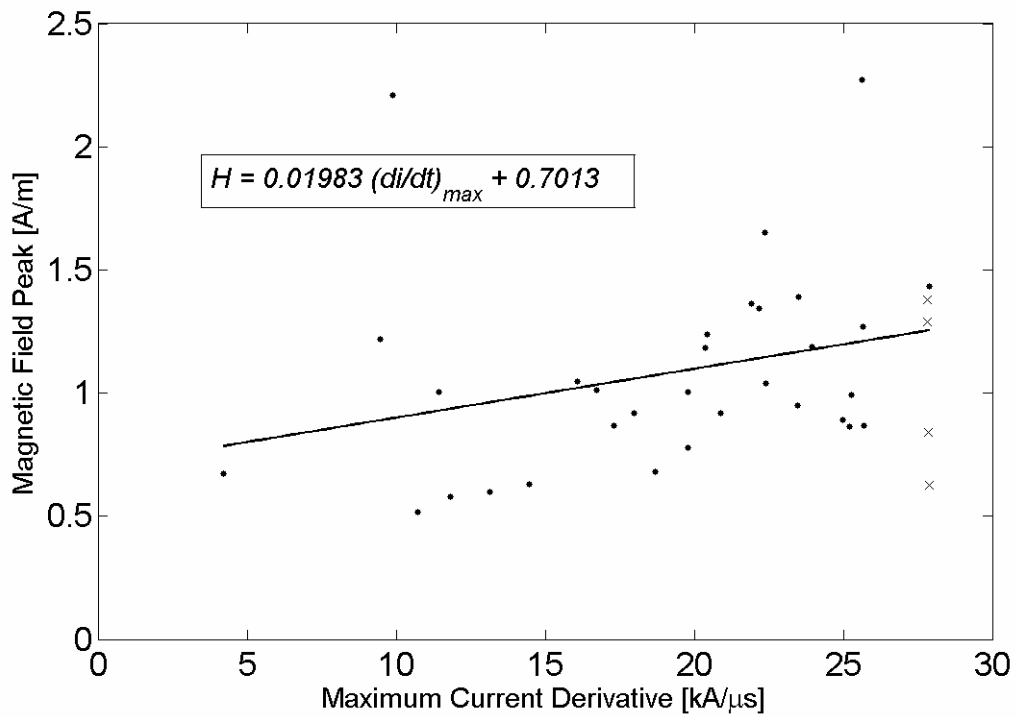


Figure 5.7. Magnetic field peak versus maximum current derivative,  $CC = 0.0822$ .

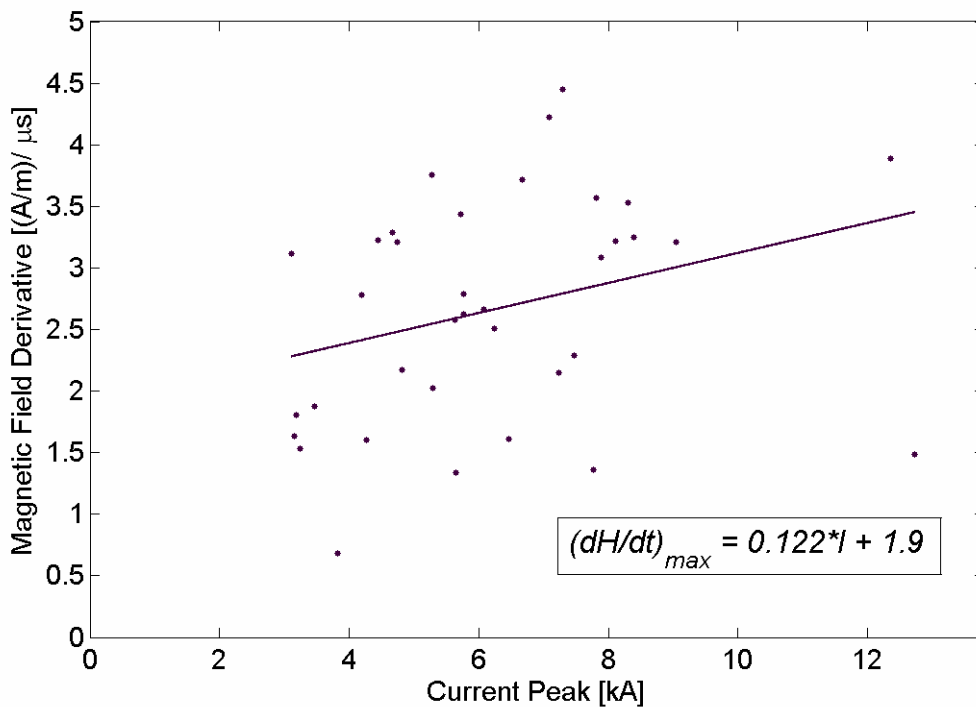


Figure 5.8. Maximum derivative of magnetic field versus current peak, CC = 0.092.

### 5.3 DISCUSSION OF RESULTS

The correlation of the characteristics of the lightning electromagnetic pulse (LEMP) with those of its current is very important when one is dealing with the inverse-source problem of finding the current parameters from the measured electromagnetic field parameters. This inverse-source problem is one of the most challenging problems in the area of lightning research. Of particular interest is the magnetic field peak-current peak (H-I) relationship shown in Figure 5.4. The dependence of the magnetic field maximum rate of rise,  $(\partial H/\partial t)_{max}$ , on that of the current,  $(\partial i/\partial t)_{max}$ , is also of interest (Fig. 5.5).

Using the assumption of constant return-stroke speed ( $v$ ) and a perfectly conducting ground, the transmission line model is normally used to determine the far-

region magnetic field  $H$ , which is entirely in azimuthal direction, is given as follows [56,57]:

$$H(r,t) = \left( \frac{v}{4\pi cr} \right) (1 + \rho_G) i_{sc}(0, t - r/c) \quad (5.1)$$

where  $i_{sc}$  represents the short-circuit current that would be measured at ideally grounded object of negligible height and  $\rho_G$  is the current reflection coefficient at ground for downward propagating waves. In the presence of a tall object with height  $h$ , and assuming that the wavefront risetime of the injected current  $i(h,t)$ , is smaller than  $h/c$  (which is the time required for injected current to reach the ground), the field current relationship given in (5.1) becomes [57]:

$$H(r,t) = \left( \frac{v+c}{4\pi cr} \right) (1 - \rho_T) i_{sc}(h, t - r/c) \quad (5.2)$$

In the two expressions shown above, the ground distance to lightning channel, indicated as  $r$ , is assumed to be much larger than the height of the channel,  $c$  represents the velocity of light in free space. In (5.2),  $\rho_T$  represents the current reflection coefficient at the tower's tip for upward propagating current waves. The propagation of current in the CN Tower is assumed to be at the speed of light in free space. In 35 of the 36 lightning strokes measured during 2005 the current wavefront 10%-90% risetime was lower than  $h/c$  ( $h/c = 1.78 \mu\text{s}$  for CN Tower). The relationship between the current injected at the tip of a tall object  $i(h,t)$  and the short-circuit current at the bottom of the channel  $i_{sc}(h,t)$  in terms of  $\rho_T$  is given by (5.3) [57].

$$i(h,t) = \left( \frac{1 - \rho_T}{2} \right) i_{sc}(h,t) \quad (5.3)$$

Using (5.2) and (5.3), a relationship can be established between far-field range magnetic field and the current injected at the tip of the tall object. This relationship is given by (5.4). Taking the partial derivatives of both sides of (5.4), a new equation (5.5) is obtained.

$$H(r,t) = \left( \frac{v+c}{2\pi cr} \right) i(h,t-r/c) \quad (5.4)$$

$$\frac{\partial H(r,t)}{\partial t} = \left( \frac{v+c}{2\pi cr} \right) \frac{\partial i(h,t-r/c)}{\partial t} \quad (5.5)$$

Based on (5.4) and (5.5) the magnetic field wavefront peak,  $H(r)$ , and its maximum derivative  $(\partial H(r,t)/\partial t)_{\max}$  are related to the current peak,  $I$ , and maximum current derivative  $(\partial i(h,t)/\partial t)_{\max}$ , respectively as:

$$H(r) = \left( \frac{v+c}{2\pi cr} \right) I \quad (5.6)$$

$$\left( \frac{\partial H(r,t)}{\partial t} \right)_{\max} = \left( \frac{v+c}{2\pi cr} \right) \left( \frac{\partial i(h,t-r/c)}{\partial t} \right)_{\max} \quad (5.7)$$

Equations (5.6) and (5.7) are used to determine the linear relationships between the magnetic field wavefront peak and maximum derivative (maximum rate of rise), measured 2 km north of the CN Tower, and the current wavefront peak and maximum current derivative, measured at the CN Tower, respectively. The obtained relationships are shown in Figures 5.4 and 5.5 as dashed lines. When using (5.6) to (5.7), the speed of propagation in the channel is assumed to be 1/3 speed of light [6]. In Figure 5.4, this approximate analytical relationship represented by the dashed line shows that the observed magnetic field wavefront peak is about 62% higher than the calculated one. The main factors that attribute to this discrepancy are:

1. The contribution of the current reflections due to tower's structural discontinuities and reflections within the continuously growing return-stroke channel are ignored.
2. The use of the simplified magnetic field-current peak relationship and the assumption that the field measurement system is located in far-field region in which only the radiated component is present [58-60].

3. The return-stroke speed, on average, could exceed the assumed value of  $v = 1/3c$ . Based on the Peissenberg Tower data, Heidler *et al.* established a relationship between the magnetic field peak, measured 185 m away from the tower and current peak measured near the base of the tower [24]. For proper comparison of Heidler's H-I relationship with the H-I relationship for the CN Tower, the magnetic field peak obtained by Heidler at the Peissenberg Tower was modified to correspond to the field that would have been measured 2 km away from the tower (as is the case for the CN Tower), that is, multiplying the magnetic field peak values obtained by Heidler by a factor of 2000/185. The regression line representing the unmodified Peissenberg Tower data is shown in Figure 5.4 as dotted line. It is apparent from Figure 5.4 that the slopes of the two regression lines, the line based on CN Tower data and the line based on Peissenberg Tower data, are quite different. The fact that the magnetic field sensor for Peissenberg Tower data is very close to the tower (185 m from the tower), as oppose to the magnetic field sensor for the CN Tower measurements which is located 2 km from the tower, this may affect the field-current relationship because of different contributions of the magnetic field induction component in each case. The induction component in case of Peissenberg Tower will be higher as compared to the induction component obtained from the CN Tower lightning-generated fields due to the fact that induction component is

proportional to  $\frac{1}{r^2}$  where  $r$  is the distance from the tower to the observation point (185 m in case of Peissenberg Tower and 2 km in case of CN Tower). The major reason for difference between both regression lines (Figure 5.4) is related to the strong current ground reflection in the case of Peissenberg Tower data because of the proximity of the current sensor to the ground [24,59]. It is worth mentioning that the CN Tower current sensing coil is placed 474-m above ground level, far from the tower's main structural discontinuities, for the purpose of measurement of the lightning current wavefront peak undiluted with reflections. The base current peak  $I_b$  used for correlation of Peissenberg Tower data is substantially larger than the peak of the incident current, as clearly shown in Fig. 11 of Heidler *et al.* [24]. The average current ground reflection for the Peissenberg Tower is 0.7 [59]. In order to eliminate the effect of the large ground reflection at the bottom of the Peissenberg Tower, the magnetic field peak-current peak regression line (dotted line) shown in Figure 5.4 was modified by substituting  $I_b=1.7 I$ , where  $I$  is the peak of the incident current. The modified relationship is included in Figure 5.4 (dash-dot line) for comparison. The modified regression line of the Peissenberg Tower data is much close to the regression line of the CN Tower data. The comparison between two sets of data substantiates the validity and value of each.

The comparison between the analytical results for the far-field relationship of the maximum rate of rise of the magnetic field and that of the current, represented by the dashed line, and the corresponding experimental relationship, represented by solid line, Fig. 5.5, illustrates that the observed maximum rate of rise of the magnetic field is 28% higher than the maximum rate of rise obtained from calculations. Based on the Peissenberg Tower data, Fuchs *et al.* established a relationship between the magnetic

field maximum rate of rise measured at a distance of 189 m from the tower, and that of the current, measured near the tower's base [19]. In order to correctly compare the CN Tower's field data with the data obtained from Peissenberg Tower it was necessary to normalize the Peissenberg Tower field data to represent the magnetic field that would be measured at a distance of 2 km from the tower. The regression line representing normalized Peissenberg Tower magnetic field data is shown in Figure 5.5 as dotted line. Because of the strong ground current reflection ( $\rho_G = 0.7$ ), the Peissenberg Tower regression line has a substantially lower slope as compared to the regression line for the CN Tower data or to the analytical far-field relationship (dashed line). Once the ground reflection was removed from the Peissenberg Tower data (see previous paragraph), the modified regression line (dash-dot line), became much closer to the regression line representing the CN Tower data as well as the one representing the analytical far-field relationship. The close agreements between the CN Tower and Peissenberg Tower regression lines as well as the analytical far-field relationship, shown in Figs. 5.4 and 5.5, substantiate the validity and value of the two data sets [5].

#### **5.4 SUMMARY OF CHAPTER 5**

The focus of this chapter is related to one of the two main objectives of this work, which is the correlation between the field and the current wavefront characteristics (initial peak, maximum derivative and 10%-90% risetime to initial peak) for the CN Tower lightning data. In addition, the electric and magnetic field wavefront characteristics are correlated with each other. The results obtained from the correlation of field-current wavefront characteristics for the CN Tower data are compared with field-current

wavefront characteristics obtained from measurements done at the 160 m Peissenberg Tower in Germany. Detailed discussion of the results is given. The developed field-current wavefront characteristic relationships contribute to solving the inverse source problem in which the lightning current is estimated using the measured LEMP along with lightning return-stroke models. The presented analyses are also important for improving the algorithms used by lightning detection and location networks.

## Chapter 6

# Modelling of Lightning Return-Stroke Current

Modelling of the spatial temporal distribution of lightning return-stroke current along the CN Tower and the lightning channel consists of three main steps. First the analytical function that will represent the simulated current (or current derivative if the derivative is used for modelling) has to be developed. The developed simulation function has to be then matched with the initial pulse of the measured current or current derivative using, for example, curve fitting methods. In the second step of modelling, the simulation function along with the transmission line (TL) model, which accounts for main structural discontinuities of the CN Tower, is used to find the current distribution at any point on the CN Tower and the lightning channel at all times. In a third step, a proper validation and quantitative assessment of the proposed model is performed. For the quantitative assessment of the developed lightning return-stroke current model, the electric and magnetic fields calculated through the use of Maxwell's equations and utilizing the simulated current are compared with measured electric and magnetic fields. The description of different types of lightning return-stroke current models as well as different types of model functions that are used is given next.

## 6.1 TYPES OF LIGHTNING RETURN-STROKE CURRENT MODELS

Lightning return-stroke current models can be divided into four main categories: gas dynamic or “physical” models, electromagnetic models, distributed circuit models and engineering models [61-63].

The gas dynamic models deal with the behaviour of a short segment of a cylindrical plasma column driven by the resistive heating that is caused by the time-varying lightning current. These models usually involve the solution to three gas dynamic equations. The three equations represent the conservation of mass, the conservation of momentum and the conservation of energy. A few of the gas dynamic models were initially developed to describe laboratory discharges in air but were later applied to the lightning discharge process, for example, see Darbakina 1951, and Plooster 1970, 1971 [63-65].

The electromagnetic model is another type of lightning return-stroke models to be discussed here. In this model, the lightning channel is represented by a lossy, vertical thin-wire antenna placed above a perfectly conducting ground. Modelling using the lossy antenna representation of the lightning channel has been proposed by Podgorski and Landt, and later by Moini, Baba and Ishii [63,66]. The solution of the electromagnetic model is obtained by solving Maxwell’s equations using the method of moments (MOM) in order to find the lightning return-stroke current distribution [63,67,68].

The third type of lightning return-stroke model is called the distributed circuit model or the RLC lightning model. In RLC model the lightning discharge is represented as a transient process occurring on a vertical transmission line which is characterised by a series resistance  $R$ , a shunt capacitance  $C$  and a series inductance  $L$  all per unit length

The solutions for the line voltage and line current for the RLC model are obtained by solving telegrapher's equations. The RLC model is an approximation to the engineering model and as in the case of the engineering model it determines the channel current versus time and height. This model can be used for the evaluation of the radiated electric and magnetic fields [1,63,69]. Different variations of distributed circuit models have been proposed for the calculations of the lightning return-stroke current and corresponding radiated electric and magnetic fields. For example, Chia and Liew represented the lightning channel using  $m$  number of circuit sections with each section being composed of capacitance, inductance and resistance. Diodes were used for each circuit section in order to indicate the direction of current flow [68]. Strawe, on the other hand, proposed a RLC model which is a combination of gas dynamic model and distributed circuit model [63].

The fourth type of lightning return-stroke model, which is the most widely used, is the engineering model. In the engineering model, the spatial-temporal current distribution is obtained by taking into account the current at the base of the channel, the speed of propagation and the brightness of the channel (luminosity of the channel). In this type of model, the return-stroke current is simulated by a current pulse driven by a voltage source or a current source placed at the lightning attachment point, usually the top of a tall structure [6,63,67]. For lightning strikes to elevated objects the current pulse propagates along the channel with velocity  $v$  and the same current pulse propagates along the tall structure with velocity of light,  $c$ . The return-stroke velocity  $v$  is less than the speed of light (usually  $1/3$ - $2/3$  the speed of light) due to the fact that during the leader phase the lightning channel is not sufficiently ionized for the current to propagate at the

speed of light in the channel [62,70,71]. These models do not concentrate on the physics of lightning but rather on obtaining a good agreement between the measured electromagnetic field and electromagnetic field obtained from modelling [63,72,73]. The engineering models can be divided into two main subcategories, the transmission line (TL) equivalent models and the travelling current source (TCS) models [63,72]. The model based on the transmission line representation of the lightning return-stroke can be further divided into the transmission line (TL) model, *Uman and McLain* [63,74], the modified transmission line model with linear current decay with height (MTLL), *Rakov and Dulzon* [63,72], the modified transmission line model with exponential current decay with height (MTLE), *Nucci et al* [63,74,75] and recently the transmission line model which incorporates both attenuation and distortion of the current pulse (MTLD), *Baba, Miyazaki and Ishii* [72]. The engineering models based on the travelling current source representation can be divided into original traveling current source model introduced by Heidler [61], Diendorfer-Uman (DU) model [76] and the Bruce-Golde (BG) model, which can be viewed mathematically as special case of TCS or TL model in which the current wave propagates at infinitely large speed while the return-stroke speed (front speed) is still finite [63,77]. The main distinction in terms of current between the two engineering models, TL and TCS, is that in the transmission line model the current wave propagates upward at a finite speed  $v = v_f$  while in the travelling current source model the current wave propagates downward at a speed of light,  $v = -c$ .

The engineering return-stroke model can be defined as an equation relating the channel current  $I(z',t)$  at any height  $z'$  and any time  $t$  to the current  $I(0,t)$  at the channel

origin, i.e. at  $z'=0$ . The current distribution at any time  $t$  and any height  $z'$  for the engineering model can be expressed as follows:

$$I(z',t) = u(t-z'/v_f)P(z')I(0,t-z'/v) \quad (6.1)$$

In (6.1),  $z'$  and  $t$  are, respectively, the height and the time at which current is to be found, and  $P(z')$  is a height dependent current attenuation factor that changes based on the specific engineering model used (see Table 6.1). Parameter  $v_f$  represents the speed of propagation of the return-stroke and  $v$  is the speed of propagation of the current waveform (in case of MTLT,  $P(z')$  is a function of height and time) and  $u$  is the Heaviside function that is equal to unity for values of  $t \geq z'/v_f$  [63,72]. In Table 6.1,  $H$  represents the total channel height while  $\lambda$  is the current decay constant assumed to be 2000 m, Nucci *et al.* [63,75]. The transmission line model representation of the lightning return-stroke uses a current source at channel base (ground), which injects a specific current into the channel. The current wave propagates upward from ground at a speed of  $v$  without distortion or attenuation (TL model), without distortion but with specific attenuation (MTLL and MTLE models) or with attenuation and distortion (MTLT model). On the other hand, in the traveling current source representation of the lightning return-stroke, the return-stroke current can be viewed as being generated at the upward-moving return-stroke front and the propagation of the current waveform is in the downward direction with the speed  $v = -c$  [61,63]. The expressions for the current  $I(z',t)$  and the height  $z' \geq vt$  for the engineering models based on the transmission line model are shown in Table 6.2, while the expressions for the current based on the traveling current source models are shown in Table 6.3. As previously mentioned, the principal distinction between TL engineering models and TCS engineering models in terms of the current is

the direction of the current wave propagation. In the transmission line models, the current propagates upward with a speed of  $v=v_f$ , while in the traveling current source models, the current propagates downward with a speed of  $v=-c$ . Tables 6.1 – 6.3 provide summary of the equations used in transmission line equivalent models as well as models based on traveling current source representation.

Table 6.1. Expressions for  $P(z')$  and  $v$  for the engineering lightning return-stroke models [63,72].

<b>Model</b>	<b><math>P(z')</math></b>	<b><math>v</math></b>
<i>TL</i>	$1$	$v_f$
<i>MTLL</i>	$1-z'/H$	$v_f$
<i>MTLE</i>	$\exp(-z'/\lambda)$	$v_f$
<i>MTLD</i>	$\left[1 - \exp\left(-\frac{t-z'/v}{\tau} \frac{\lambda_p}{z'}\right)\right](1-z'/H)$	$v_f$
<i>BG</i>	$1$	$\infty$
<i>TCS</i>	$1$	$-c$

Table 6.2.  $I(z',t)$  for transmission line type models with  $t \geq z'/v_f$  [50,63,72].

<b>Model (TL Based)</b>	<b><math>I(z',t)</math></b>
<i>TL</i>	$I(z',t) = I(0,t-z'/v)$
<i>MTLL</i>	$I(z',t) = (1-z'/H)I(0,t-z'/v)$
<i>MTLE</i>	$I(z',t) = e^{-z'/\lambda} I(0,t-z'/v)$
<i>MTLD</i>	$I(z',t) = \left[1 - \exp\left(-\frac{t-z'/v}{\tau} \frac{\lambda_p}{z'}\right)\right](1-z'/H)I(0,t-z'/v)$

$v=v_f=\text{constant}$ ,  $H = \text{constant}$ ,  $\lambda = \text{constant}$

Table 6.3.  $I(z',t)$  for traveling current source type models with  $t \geq z'/v_f$  [50,63,76,77].

<b>Model (TCS Based)</b>	<b><math>I(z',t)</math></b>
<i>BG (Bruce and Golde)</i>	$I(z',t) = I(0,t)$
<i>TCS (Heidler)</i>	$I(z',t) = I(0,t+z'/c)$
<i>DU (Diendorfer and Uman)</i>	$I(z',t) = I(0,t+z'/c) - I(0,z'/v^*)e^{-(t-z'/v_f)/\tau_d}$

$v^* = v_f/(1+v_f/c)$ ,  $v_f = \text{constant}$ ,  $\tau_d = \text{constant}$

The model presented in this thesis is an engineering model based on the transmission line representation of the lightning current path. As with every engineering

model there are two parameters that are required for the computation of the electric and magnetic fields:

- 1) the expression for representation of the current waveform at channel base
- 2) the return-stroke speed

In the presented model, the current waveform is assumed to be traveling down the CN Tower at the speed of light  $v = c = 3 \times 10^8$  m/s [6,11,73,78]. Instead of using the representation of the current at channel base as in previous lightning return-stroke models, the modified expression of the derivative of Heidler function is used to represent the lightning return-stroke current derivative at channel base. In the next section, different types of current waveform representations used by researchers to represent a current at channel base and to model the lightning return-stroke process will be discussed.

## **6.2 FUNCTIONS SIMULATING THE CHANNEL BASE CURRENT WAVEFORM**

As mentioned in the previous section, every type of engineering lightning return-stroke model requires an analytical function (simulation function), which represents the channel base current waveform. One of the first functions used to represent the current waveform at channel base was a double exponential function introduced by Bruce and Golde [16,76]. The current waveform representation using the double exponential function is given by (6.2).

$$I(0,t) = I_o [exp(-\alpha t) - exp(-\beta t)] \quad (6.2)$$

$I_o$  represents the current peak, and  $1/\alpha$  and  $1/\beta$  represent the current rise and current decay time constants, respectively. The problem with the double exponential function is

that it assumes  $I_o$  to be the current peak, which is not accurate. The double exponential representation of the current waveform was modified by Uman and McLain to introduce the correction factor for the current peak [74]. The expression for channel base current waveform using the modified double exponential function is given by (6.3) with  $\eta$  being the current peak correction factor.

$$I(0,t) = (I_o/\eta)[\exp(-\alpha t) - \exp(-\beta t)] \quad (6.3)$$

A plot of the current waveform and current derivative waveform based on the double exponential function is shown in Figures 6.1 and 6.2, respectively. Table 6.4 lists the values of the parameters that have been used to plot the waveforms shown in Figures 6.1 and 6.2. The main problem in using the double exponential function, or its modified form, for the calculation of the electric and magnetic fields is that its first derivative has a discontinuity at  $t = 0$  s, i.e. the first derivative is not zero at time  $t = 0$  s.

Table 6.4. Parameters used for plotting of the double exponential current and current derivative waveforms.

Parameter	Value
$I_o$	30 kA
$\eta$	1
$\alpha$	$2 \times 10^4 \text{ s}^{-1}$
$\beta$	$2 \times 10^6 \text{ s}^{-1}$
$t$	0 – 50 $\mu\text{s}$

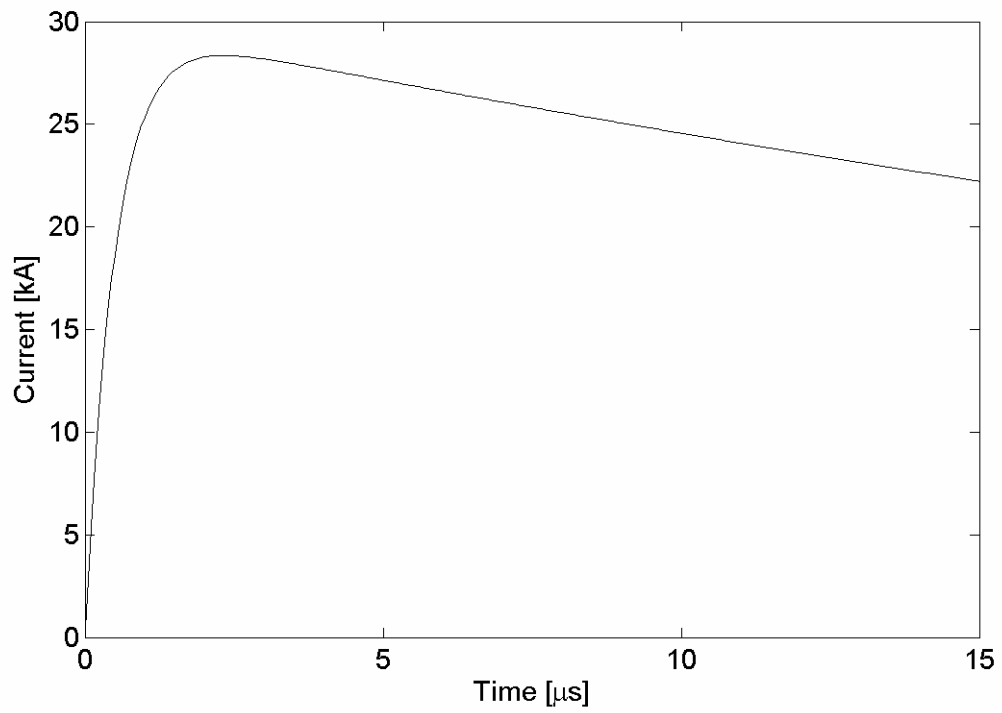


Figure 6.1. Current waveform for double exponential function.

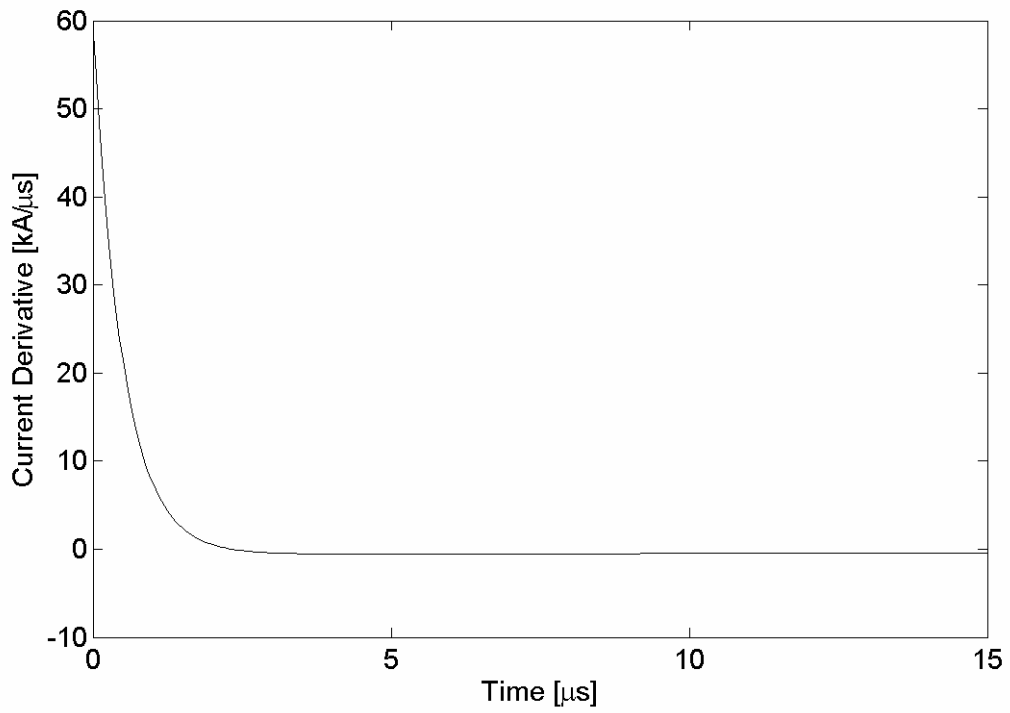


Figure 6.2. Current derivative for double exponential function.

To decrease the discontinuity of the first current derivative at time  $t = 0$  s, a modified double exponential function has been proposed by Jones and it is given by (6.4) [79,80].

To compare (6.4) with (6.2) and (6.3), one can equate  $1/\tau_1 = \alpha$  and  $1/\tau_2 = \beta$ . The variable  $t^*$  shown in (6.4) is given by (6.5).

$$I(0,t) = (I_0/\eta)[\exp(-t^*/\tau_1) - \exp(-t^*/\tau_2)] \quad (6.4)$$

$$t^* = \tau_2^2/\tau_1 + t \quad (6.5)$$

Another channel base current function proposed by Raicic is given by (6.6). The main problem with this function is that at  $t = 0$  s the value of the current is infinite. This function can not be used for current simulation since it is not defined at time  $t = 0$  s [70].

$$I(0,t) = (I_0/\eta) \sqrt{\tau_1/t} [\exp(-\tau_2/2t)] \quad (6.6)$$

The plots of the current function and the corresponding current derivative based on (6.4) are shown in Figures 6.3 and 6.4, respectively, while the plots of the current function and the corresponding derivative based on (6.6) are shown in Figures 6.5 and 6.6, respectively. Using the values of the parameters from Table 6.4, it can be seen that the results obtained using (6.4) are almost identical to the ones obtained from (6.2) and (6.3).

This is due to the fact that  $t^* = \tau_2^2/\tau_1 + t \approx t$  if  $\alpha = 1/\tau_1 = 2 \times 10^4 \text{ s}^{-1}$  and  $\beta = 1/\tau_2 = 2 \times 10^6 \text{ s}^{-1}$ . The function described by (6.6) is not suitable for current simulation as the current waveform and the corresponding current derivative waveform are not defined at  $t = 0$  s, i.e.  $i(t=0) = \infty$  and  $di/dt(t=0) = \infty$ .

A function that overcomes the shortcomings of the channel base current expressions presented in (6.2) – (6.6) was introduced by Heidler [61,79]. The expression

representing the Heidler channel based current is given by (6.7),  $I_o$  is the maximum current peak,  $\eta$  is the current correction factor,  $\tau_1$  is the rise time constant while  $\tau_2$  is the decay time constant,  $k$  is a constant that has a value greater than 1 in order to assure the continuity of the first current derivative at time  $t = 0$  s.

$$I(t) = (I_o / \eta) \frac{(t / \tau_1)^k}{[(t / \tau_1)^k + 1]} e^{-t / \tau_2} \quad (6.7)$$

The equation for channel base current function introduced by Heidler satisfies the two basic requirements needed for the lightning current simulation, i.e. the current does not have discontinuity at  $t = 0$  s and the current derivative also does not have a discontinuity at  $t = 0$  s provided that  $k > 1$ . The waveforms of the Heidler current and the Heidler current derivative in the range of 0-5  $\mu$ s are shown in Figures 6.7 and 6.8, respectively. The values of the parameters  $I_o$ ,  $\tau_1$ ,  $\tau_2$  and  $k$  used for plotting the Heidler current function and its derivative are listed in Table 6.5. From the plots shown in Figures 6.7 and 6.8, it can be seen that the Heidler current function as well as its derivative do not have any discontinuities at the time of onset, i.e. a  $t = 0$  s.

Table 6.5. Parameters used to plot the Heidler function and its derivative.

Parameter	Value
$I_o$	10 kA
$\eta$	1
$\tau_1$	100 ns
$\tau_2$	300 ns
$k$	2
$t$	0 – 5 $\mu$ s

Feizhou and Shanghe introduced a channel base current function called the pulse function which can be used for current simulation as the pulse function and its derivative do not have any discontinuities at time  $t = 0$  s [81]. The proposed pulse function is

described by (6.8). The parameters  $I_o$ ,  $\eta$ ,  $\tau_1$  and  $\tau_2$  represent the maximum current peak, the current peak correction factor, the rise time and decay time constants, respectively. The pulse function representing the channel base current and the derivative of the pulse function are shown in Figures 6.9 and 6.10, respectively. The values of the parameters used to plot the pulse function and its derivative are the same as the ones used to plot Heidler function and its derivative (Table 6.5).

$$I(t) = (I_o/\eta)(1 - e^{-t/\tau_1})^k e^{-t/\tau_2} \quad (6.8)$$

It can be seen from the results shown in Figures 6.9 and 6.10 that the waveshapes of the pulse function and its derivative are very similar to the waveshapes of the Heidler function and its derivative, respectively. Both functions can be used for current simulations as they satisfy the basic two requirements needed for the calculation of the electric and magnetic fields based on the lightning return-stroke current obtained from modelling.

At present time, Heidler representation of the channel base current is one of the most widely used representations for modelling the lightning return-stroke current. In this work, the derivative of the modified Heidler function is used to model the lightning return-stroke current derivative measured at the CN Tower. Modelling of the CN Tower lightning return-stroke current derivative along with the calculation of reflection coefficients at major CN Tower's structural discontinuities is described in Chapter 7, while the evaluation of the proposed model, including the calculation of the electromagnetic field, is described in Chapter 8.

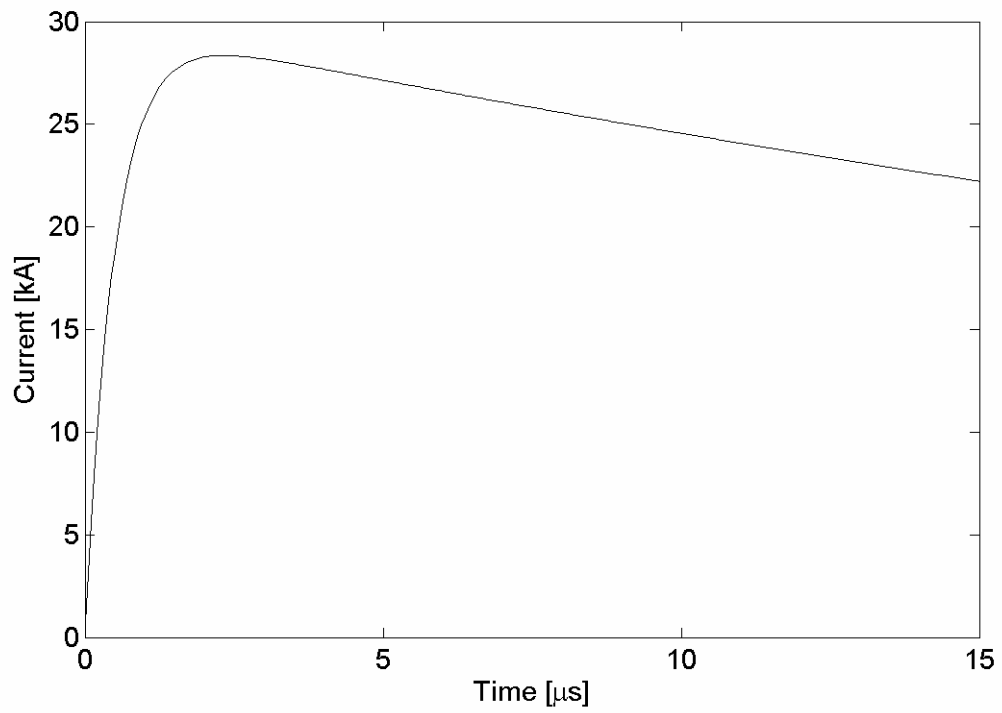


Figure 6.3. Current waveform based on (6.4).

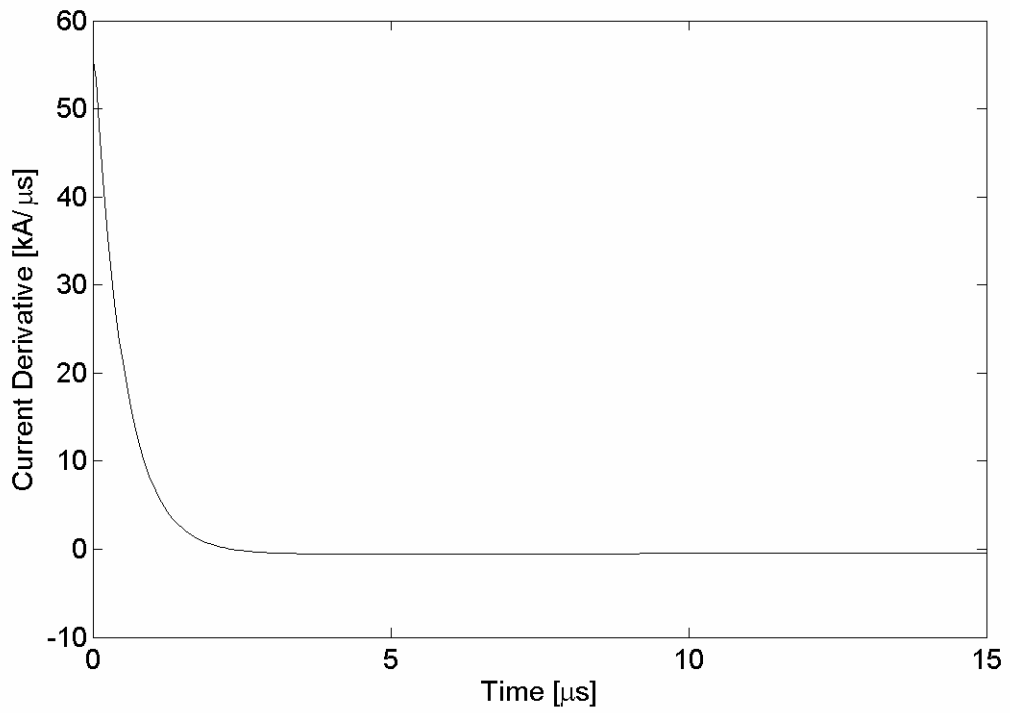


Figure 6.4. Current derivative waveform obtained using the derivative of (6.4).

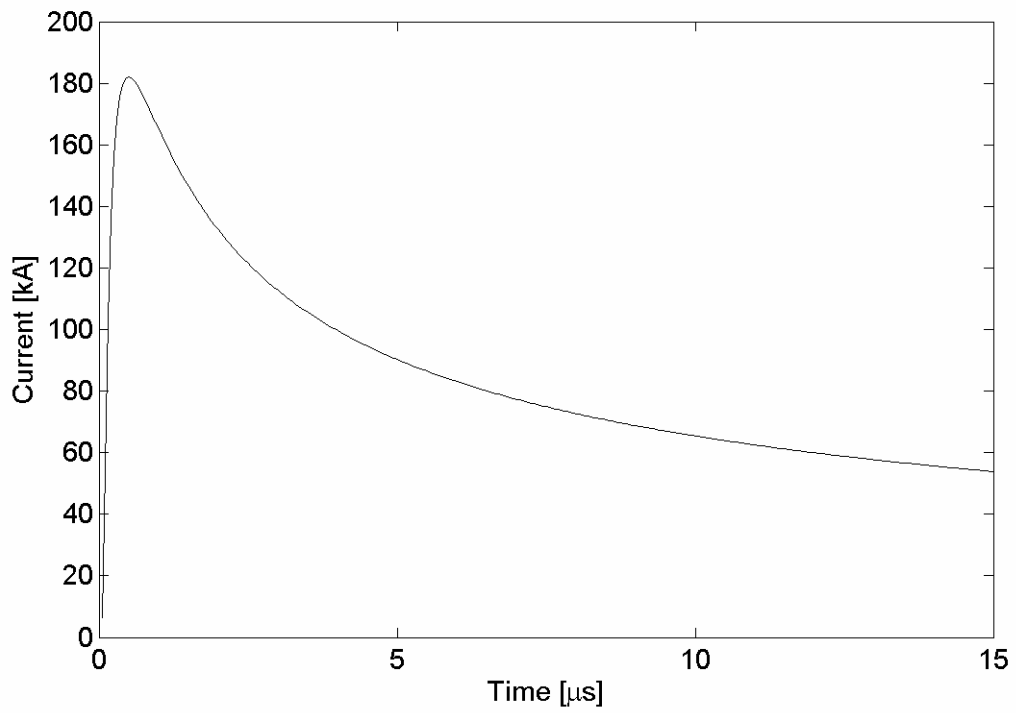


Figure 6.5. Current waveform based on (6.6).

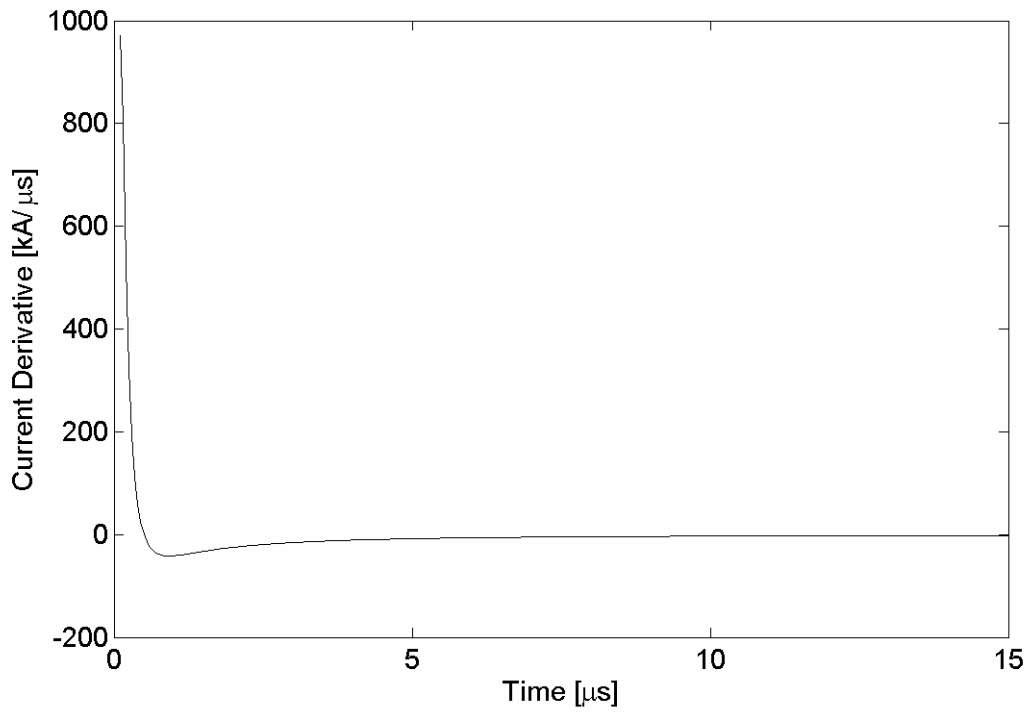


Figure 6.6. Current derivative waveform obtained using the derivative of (6.6).

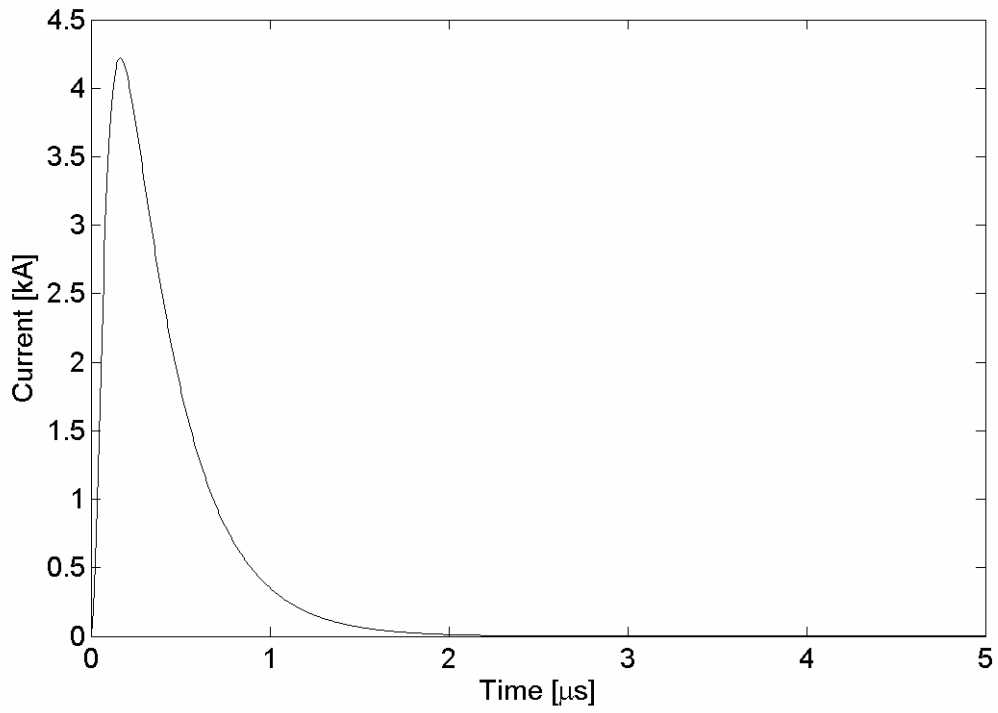


Figure 6.7. Heidler current waveform based on (6.7).

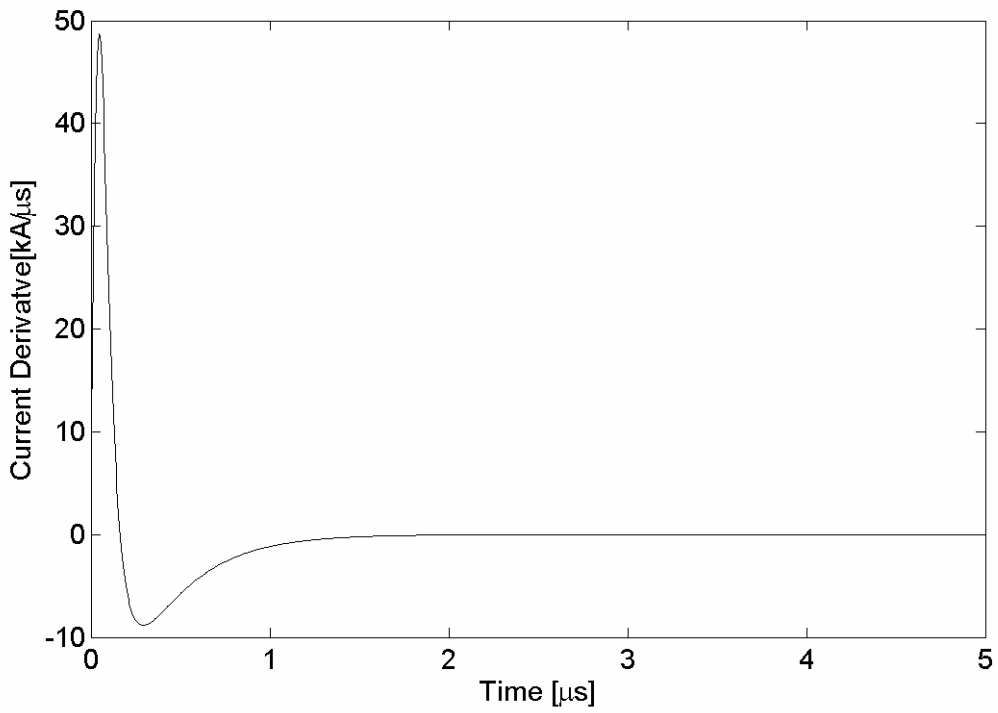


Figure 6.8. Derivative of Heidler current waveform based on the derivative of (6.7).

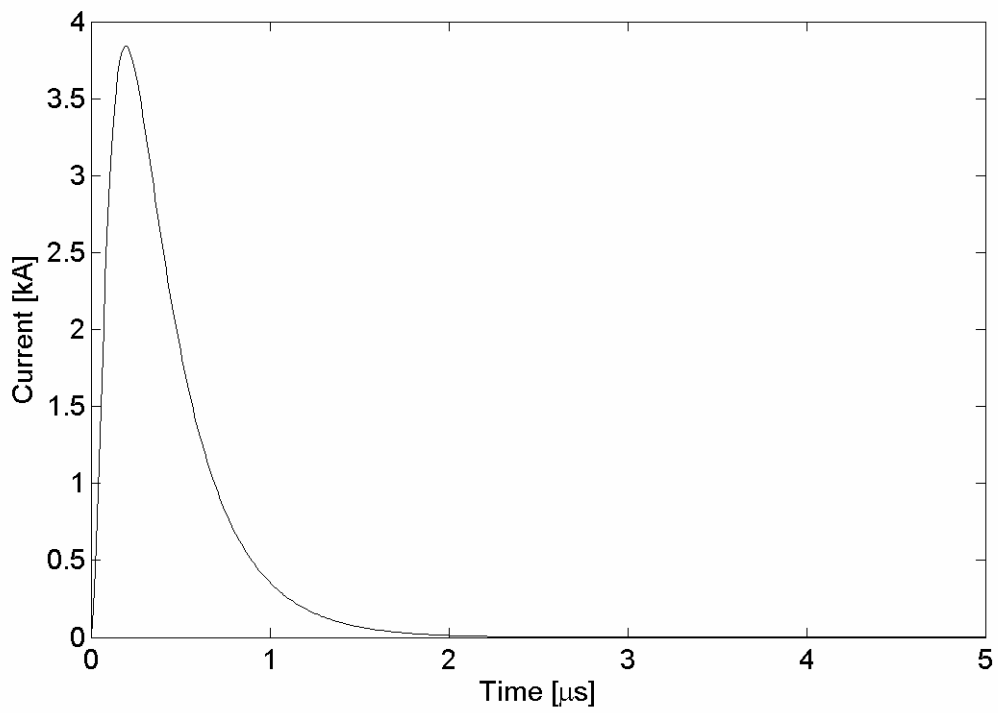


Figure 6.9. Pulse function based on (6.8).

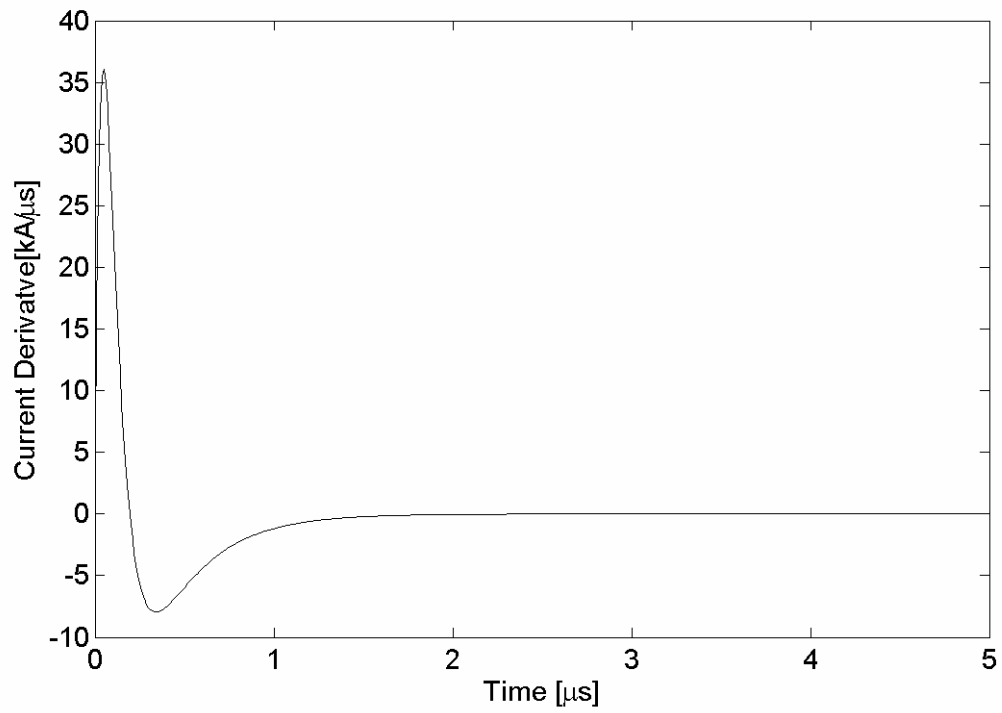


Figure 6.10. Derivative of the pulse function shown in Figure 6.9.

### 6.3 SUMMARY OF CHAPTER 6

Four main types of lightning return-stroke models are discussed with emphasis being placed on the engineering transmission line (TL) model. In addition, literature review related to the use of different current functions for the simulation of the lightning return-stroke current at channel base is presented. It is shown that some of the functions used to represent the lightning return-stroke current at channel base are not suitable for modelling the CN Tower's lightning current derivative since they do not satisfy the two basic requirements, the simulation function as well as its derivative should not have any discontinuity at time  $t = 0$  s. The results presented in this chapter are important for choosing a suitable simulation function that can be used in the proposed model.

## Chapter 7

# Modelling of the Lightning Return-Stroke Current Derivative Using the Derivative of the Modified Heidler Function

Modelling of the spatial temporal distribution of the lightning return-stroke current along the CN Tower and the attached lightning channel consists of three main steps. First step is to find an analytical function representing the current (or current derivative if the current derivative is used for modelling). Once the simulation function is defined, it has to be matched to the first impulse of the measured current or the first impulse of the current derivative (before arrival of reflections) using curve fitting method. In the second step, the simulation function along with the transmission line (TL) model, which accounts for the main structural discontinuities of the CN Tower, is used to find the current distribution at any point on the CN Tower and the lightning channel. As with every model, proper validation (i.e. quantitative assessment) has to be performed. For quantitative assessment of the developed TL lightning return-stroke current model, the electric and magnetic fields obtained from modelling are compared with the measured electric and magnetic fields, respectively.

## 7.1 CHOICE OF CHANNEL BASE CURRENT FUNCTION

The modelling of the lightning return-stroke current requires a function that can be used to simulate the current (or the current derivative) signals obtained from measurements. The choice of the simulation function depends on the nature of the data as well as on other requirements, for example, if one requires to model the lightning current, the simulation function should satisfy at least the basic requirement in which the simulation function is zero at the time of onset and the simulation function should not have discontinuity at time  $t = 0$  s. In modelling of the CN Tower lightning current, the simulation function must satisfy two basic requirements in order to properly simulate the lightning current and current derivative:

- 1] The simulation function should not have a discontinuity at time  $t = 0$  s and it should be zero at time  $t = 0$  s
- 2] The derivative of the simulation function should not have a discontinuity at time  $t = 0$  s

The above conditions must also be satisfied in order to compute the electric and magnetic fields using the simulated function for the purpose of comparing the computed fields with the ones obtained from measurements.

The lightning return-stroke current model presented in this work is based on the derivative of the modified Heidler function, and the transmission line (TL) representation of the CN Tower and the attached lightning channel. Heidler function and the derivative of Heidler function satisfy the above mentioned two basic requirements for proper modelling of the lightning return-stroke current and the calculation of the LEMP. The presented model is based on the lightning current derivative as opposed to the lightning

current used by other researchers [65,78]. Due to the structural complexity of the CN Tower, it is much easier to reproduce the current derivative signal since there is less overlapping between adjacent reflections. In addition, the current derivative waveform is a much faster signal (fast rate of rise) as opposed to the current signal. Also, it is shown that since the current derivative is directly measured this method will provide more accurate match in comparison with the use of the current, which is evaluated by numerically integrating the measured current derivative. Additionally, since the current derivative is a much faster signal, the calculation of reflection coefficients at the main structural discontinuities of the CN Tower is much easier in this case.

## **7.2 THE MODIFIED HEIDLER FUNCTION AND ITS DERIVATIVE**

Heidler function is a mathematical expression that was initially developed to reproduce the lightning return-stroke current for strikes to ground. However, some researchers have started to use Heidler function in order to model the channel base current for lightning strikes to tall structures [6,82-85]. The expression for Heidler function is given by (7.1) [61,79]. The modified Heidler function that is used in this thesis is given by (7.2). Equation (7.2) represents the summation of two Heidler functions and through out this thesis it is referred to as the modified Heidler function. The derivative of the modified Heidler function is given by (7.3). The derivative of the modified Heidler function has been used to match the measured lightning return-stroke current derivative signal. The parameter  $A_2$  was eliminated from the function used for matching by taking the derivative of (7.3) and equating it to zero at  $t = t_a$ , where  $t_a$  is the

time at which the initial impulse of the measured lightning current derivative is maximum. The parameters in (7.3) are:

$A_1$  and  $A_2$  control the channel base current impulse amplitude

$\tau_1$  and  $\tau_3$  are front time constants,

$\tau_2$  and  $\tau_4$  are decay time constants

$k_1$  and  $k_2$  are exponents with values from 1.1 to 20

The minimum values of  $k_1$  and  $k_2$  were chosen to be 1.1, slightly greater than 1, in order to avoid the situation in which the first derivative of the modified Heidler function has a discontinuity at  $t = 0$  s. The first and second derivatives of the modified Heidler function were obtained analytically and they were verified using Symbolic Toolbox in Matlab software. Due to the complexity of the second derivative equation as well as the equation for  $A_2$  they are included in Appendix B. The choice of a parameter or parameters, which can be eliminated from (7.3) in order to reduce the number of variables for curve fitting, was a tedious task. Different scenarios were tried such as the elimination of  $A_1$ , in (7.3), by equating  $di/dt$  at time  $t = t_a$  to the peak of the initial impulse of the measured current derivative signal and then the elimination of the parameter  $A_2$  by equating the second time derivative of (7.2) to zero at  $t = t_a$ . This process gives an expression for the derivative of the modified Heidler function with parameters  $A_1$  and  $A_2$  eliminated. This process was also reversed, i.e.  $A_2$  was found from first derivative while  $A_1$  was found from second derivative of the modified Heidler function. In other trials, any of the six parameters ( $A_1, A_2, \tau_1, \tau_2, \tau_3, \tau_4$ ) were eliminated either by equating the first derivative of Heidler to the measured  $dI/dt_{\max}$ , by equating the second derivative to zero at time  $t = t_a$ , or by using  $i = I_{\max}$  at  $t = t_b$  where  $t_b$  is the time at which the initial peak of the current

occurs. Other combinations such as the elimination of  $A_2$  using the second derivative and the elimination of  $\tau_1$  using the first derivative were also tried. Furthermore, the initial impulse of the measured current derivative was matched using only a single expression for the derivative of Heidler function, as well as single expression for the derivative of Heidler function in which one or two of the parameters were eliminated using  $di/dt = dI/dt_{\max}$  and  $d^2i/dt^2 = 0$  at  $t = t_a$ . From all the work done during this initial stage it was determined that the elimination of  $A_2$  from the derivative of the modified Heidler function by equating the second derivative of the current to zero at  $t = t_a$  provided the closest match between the initial impulse of the measured current derivative and the simulated one. Figure 7.1 illustrates a comparison between the matching of the initial impulse of a measured CN Tower current derivative signal using the single expression for the derivative of Heidler function with four parameters ( $A_1, \tau_1, \tau_2$  and  $k_1$ ), the derivative of the modified Heidler function in which  $A_1$  and  $A_2$  are eliminated ( $A_1$  is eliminated using  $di/dt = dI/dt_{\max}$  and  $d^2i/dt^2 = 0$  at  $t = t_a$ ) and the derivative of the modified Heidler function in which  $A_2$  is eliminated. The matching was done in the range of  $0 - 0.52 \mu\text{s}$  using Curve Fitting Toolbox in Matlab software. The range of  $0 - 0.52 \mu\text{s}$  was chosen so that the used portion of the measured signal is completely free from reflections. In Figure 7.1, blue crosses represent the measured current derivative, the black solid line represents the matched current derivative using the derivative of the modified Heidler function with  $A_1$  eliminated from first derivative and  $A_2$  eliminated from second derivative, the green line represents matching using the derivative of Heidler function (single expression) and the red dashed line represents the matched current derivative using the derivative of the modified Heidler function with  $A_2$  eliminated from second derivative. The results shown

in Figure 7.1 illustrate that matching using the derivative of the modified Heidler function with  $A_2$  eliminated provides the most accurate match between the initial impulse (before the arrival of reflections) of the measured current derivative and the simulated one. The coefficients obtained for each match shown in Figure 7.1 are listed in Table 7.1. The values of R-square are also shown in Table 7.1. The results shown in Table 7.1 confirm that matching using the derivative of the modified Heidler function with the elimination of  $A_2$  from the second derivative, with value of R-square = 0.995, provides the best fit between the measured and the simulated waveforms. The value of the R-square, which is closer to one, indicates a better fit of the measured waveform with the simulated one. In matching of the initial impulse of the measured current derivative with the simulated one it is important that the results are as accurate as possible since any errors introduced in this initial stage will cause more inaccuracies once the reflections from the structural discontinuities are taken into account in the simulation. The results obtained from matching of the initial impulse of the measured current derivative with the derivative of the modified Heidler function in which parameter  $A_2$  is eliminated are presented in the next section.

$$i(t) = A \left[ \frac{(t/\tau_1)^k e^{-t/\tau_2}}{1 + (t/\tau_1)^k} \right] \quad (7.1)$$

$$i(t) = A_1 \left[ \frac{(t/\tau_1)^{k_1} e^{-t/\tau_2}}{1 + (t/\tau_1)^{k_1}} \right] + A_2 \left[ \frac{(t/\tau_3)^{k_2} e^{-t/\tau_4}}{1 + (t/\tau_3)^{k_2}} \right] \quad (7.2)$$

$$\begin{aligned}
\frac{di(t)}{dt} = & A_1 \left( \frac{t}{\tau_1} \right)^{k_1} \exp^{-t/\tau_2} \frac{k_1 \tau_2 - t - t \left( \frac{t}{\tau_1} \right)^{k_1}}{t \left[ 1 + \left( \frac{t}{\tau_1} \right)^{k_1} \right]^2} \\
& + A_2 \left( \frac{t}{\tau_3} \right)^{k_2} \exp^{-t/\tau_4} \frac{k_2 \tau_4 - t - t \left( \frac{t}{\tau_3} \right)^{k_2}}{t \left[ 1 + \left( \frac{t}{\tau_3} \right)^{k_2} \right]^2}
\end{aligned} \tag{7.3}$$

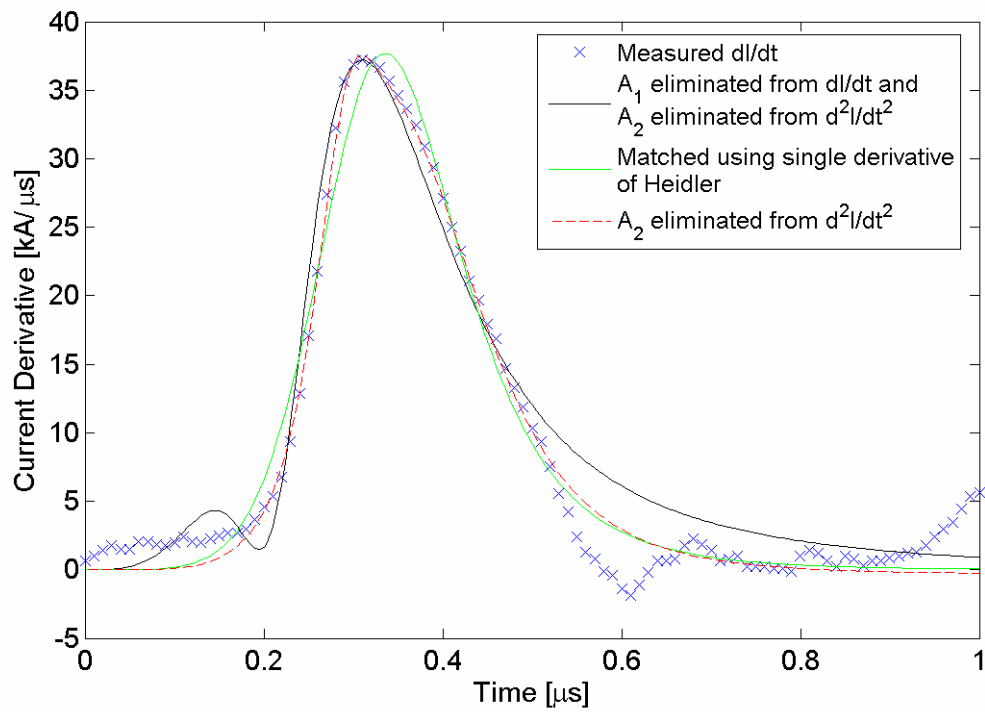


Figure 7.1. Sample comparison for matching of the first impulse of the measured current derivative using three different methods.

Table 7.1. Parameters for matching results illustrated in Figure 7.1.

	Matching using the derivative of the modified Heidler function with $A_2$ eliminated	Matching using the derivative of the modified Heidler function with $A_1$ and $A_2$ eliminated	Matching using single expression for derivative of Heidler function
$A_1$	1.156 kA	-5.729 kA	8.1516 kA
$A_2$	7.130 kA	9.580 kA	N/A
$\tau_1$	0.2962 $\mu$ s	0.2274 $\mu$ s	0.3529 $\mu$ s
$\tau_2$	11.8 ms	0.2980 $\mu$ s	0.978 ms
$\tau_3$	0.3738 $\mu$ s	0.3141 $\mu$ s	N/A
$\tau_4$	21.96 $\mu$ s	9.880 ms	N/A
$k_1$	13.95	8.216	6.368
$k_2$	6.407	4.472	N/A
R-square	0.995	0.9770	0.9817

### 7.3 MATCHING OF THE INITIAL IMPULSE OF THE MEASUREMENT CURRENT DERIVATIVE USING THE DERIVATIVE OF THE MODIFIED HEIDLER FUNCTION

In this section, the results obtained from matching the initial impulse of the measured current derivative with the chosen simulation function (the derivative of the modified Heidler function in which parameter  $A_2$  is eliminated) are presented. The parameters obtained from the matching will be used to plot the simulated current and to compare it with the current obtained from measurement. This comparison is one of the first steps in the quantitative assessment of the proposed model. A measured current derivative signal with fast risetime and high initial impulse peak is used to avoid possibility of overlapping reflection-related peaks and to reduce the influence of noise on the simulation result. The risetime for the chosen current derivative waveform is 93.3 ns (defined as the time between 10% and 90% value of the first impulse peak of the current derivative) and its maximum current derivative is 36.56 kA/ $\mu$ s (the base level of this

current derivative signal is  $0.41 \text{ kA}/\mu\text{s}$ ). The initial peak of the current had a value of  $7.76 \text{ kA}$  (the base level of the current waveform is  $0.45 \text{ kA}$ ). The fast major part of the rising wavefront of the chosen current derivative signal ensures that the initial impulse is free from reflections resulting from CN Tower's structural discontinuities. Also, the large wavefront peak of the chosen signal is important in order to reduce the effect of the noise. As shown in Figure 7.2, the first substantial reflection, which is the reflection from the top of the restaurant (located  $106.09 \text{ m}$  below the sensing coil), arrives at the old Rogowski coil location after  $707.3 \text{ ns}$ . For matching purposes, the starting point of the current derivative waveform had to be determined from the measured signal. Figure 7.2 shows the measured current derivative signal in the range of  $-0.5 - 4 \mu\text{s}$  while Figure 7.3 shows the signal that was used for matching. The starting point at which the slope changes rapidly has been chosen to be at  $t = -0.11 \mu\text{s}$  and the current derivative signal used for matching was shifted by  $0.11 \mu\text{s}$  (Figure 7.3). Figure 7.4 shows the results obtained from matching of the initial impulse of the measured current derivative with the simulated one using the derivative of the modified Heidler function with  $A_2$  eliminated. The non-linear curve fitting was performed using Curve Fitting Toolbox in Matlab software. The parameters obtained from curve fitting are shown in Table 7.2 and the value of R-square for this match is  $0.995$ . The initial impulses of the measured current derivative and the simulated one are well matched with an exception of the initial stage ( $0.175 \mu\text{s}$ ) where the initial impulse of the measured current derivative is slightly lower.

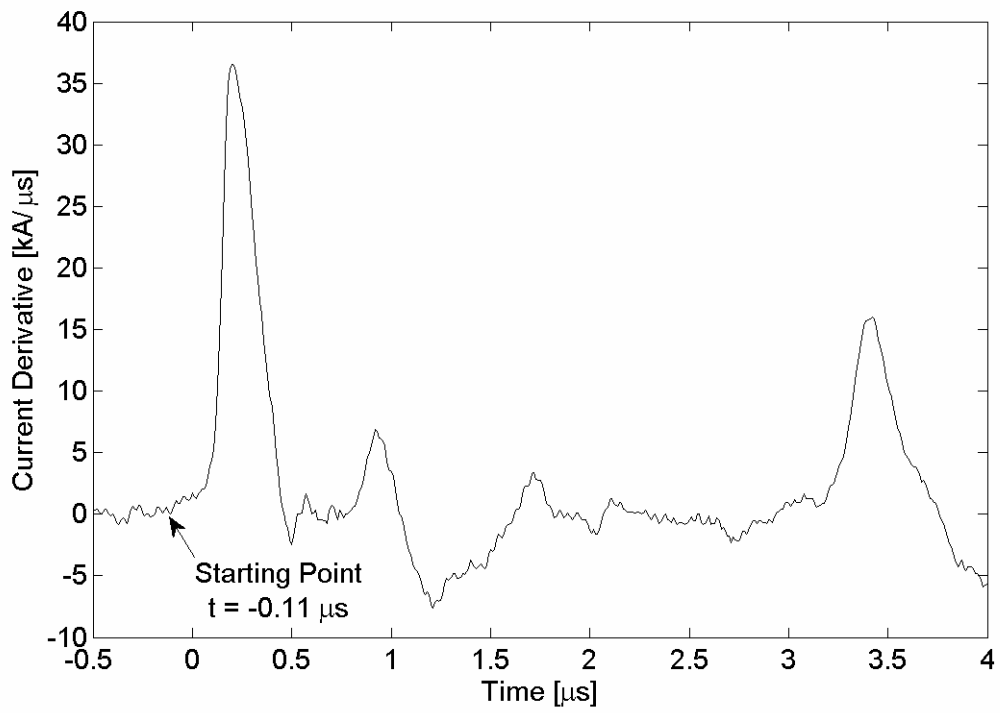


Figure 7.2. Measured current derivative waveform.

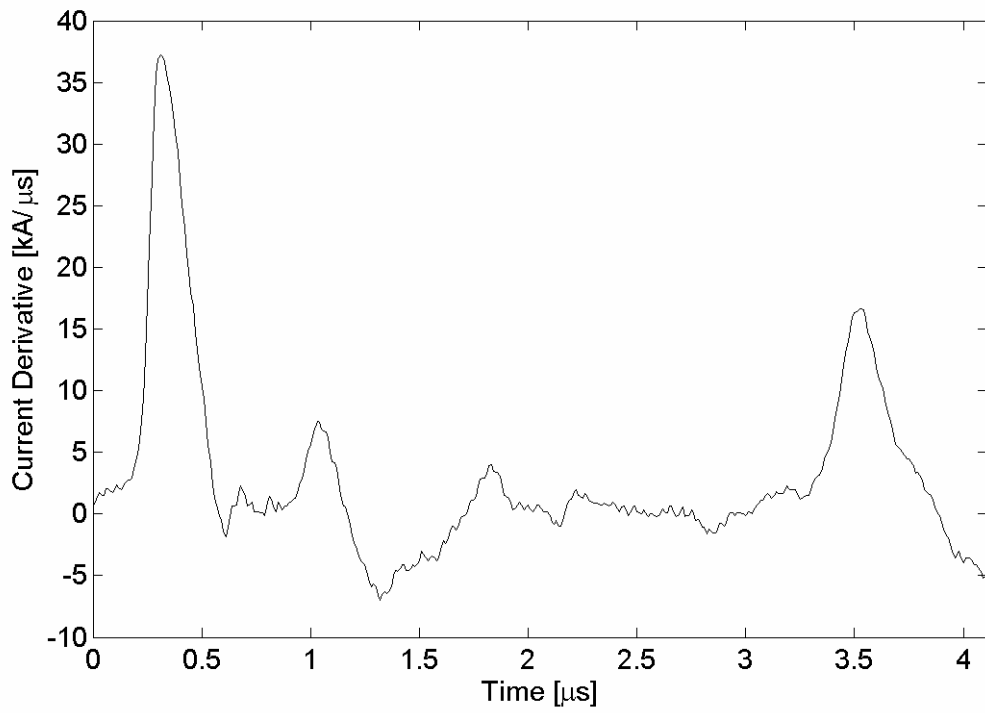


Figure 7.3. Current derivative waveform used for matching.

In future work, the inability of the simulation function to accurately represent the initial impulse of the measured current derivative up to  $0.175 \mu\text{s}$  must be addressed (Figure 7.4).

In order to compare the current obtained by numerical integration of the measured current derivative signal shown in Figure 7.3 and the simulated current obtained from matching using the derivative of the modified Heidler function, Figure 7.5 is constructed. Figure 7.5 shows a slight difference between the measured and the simulated current, with the measured current having higher values up to the initial current peak. The difference can be at least partially attributed to the inability of the chosen simulation function to correctly represent the initial stage of the CN Tower lightning return-stroke current derivative.

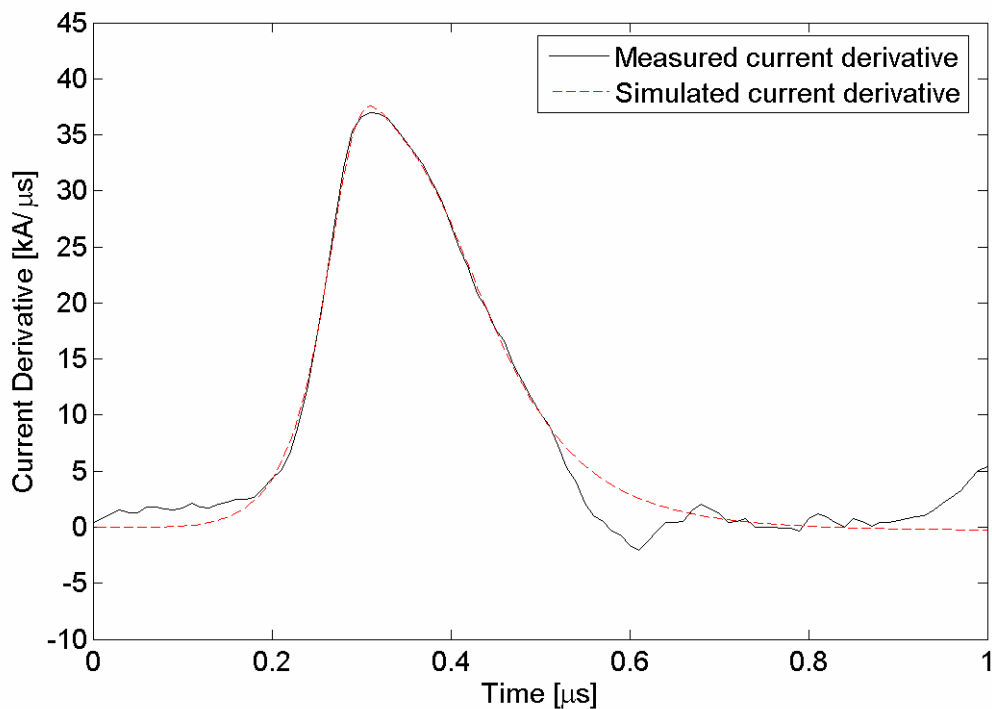


Figure 7.4. Measured and simulated first impulse of the lightning return-stroke current derivative.

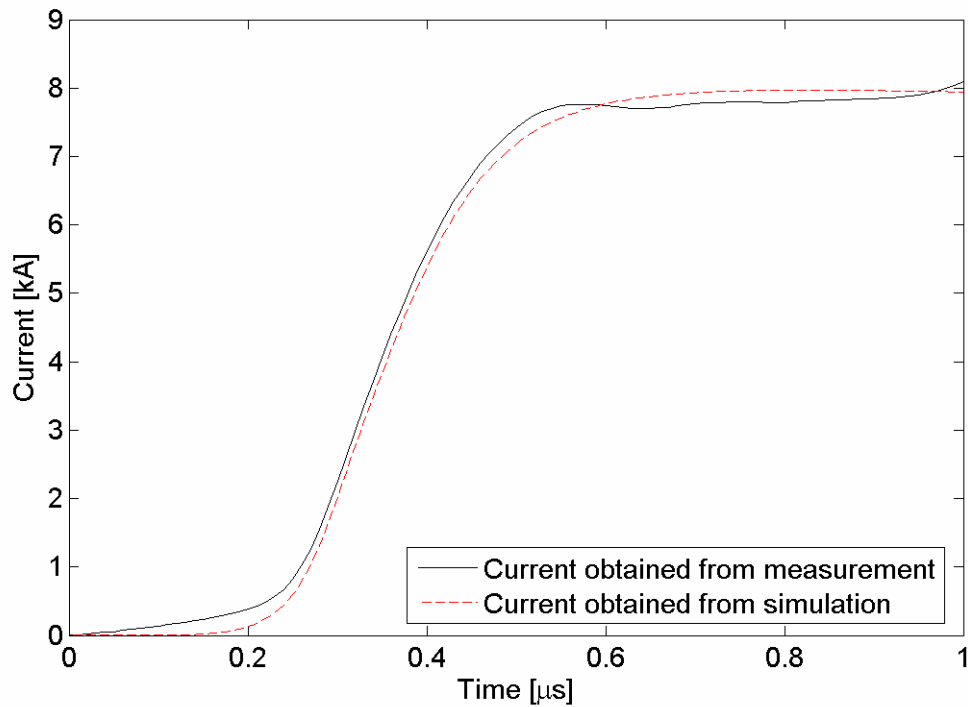


Figure 7.5. Measured and simulated current (using the derivative of the modified Heidler function).

Table 7.2. Parameters obtained from matching the measured current derivative with the simulated current derivative using the derivative of the modified Heidler function with  $A_2$  eliminated.

Parameter	Value
$A_1$	1.156 kA
$A_2$	7.130 kA
$\tau_1$	0.2962 $\mu$ s
$\tau_2$	11.8 ms
$\tau_3$	0.3738 $\mu$ s
$\tau_4$	21.96 $\mu$ s
$k_1$	13.95
$k_2$	6.407

The measured lightning return-stroke current derivative signal shown in Figure 7.3 was integrated numerically in order to obtain the current waveform, which is shown in Figure 7.6. The current waveform obtained from measurement (Fig.7.6) was utilized to simulate the current using the modified Heidler function in the range 0 - 0.63  $\mu$ s. The

parameters of the modified Heidler obtained in this case are shown in Table 7.3 (R-square = 0.997). Figure 7.7 shows the simulated current and the current obtained from measurement. Figure 7.7 shows that the simulated current is slightly closer to measurement in comparison with the case when the derivative of the modified Heidler function is used to model the measured current signal (Fig. 7.5). However, Figure 7.8 shows that the simulated current derivative in this case is quite distant from the measured current derivative signal. This proves that matching of current derivative shown in Figure 7.8 is much less accurate as compared to the matching results shown in Figure 7.4. The initial impulse of the simulated current derivative is shifted to the right as well as there is a small impulse visible at the beginning of the simulated waveform. The presence of small impulse before the main current derivative impulse contributes to deviations between the simulated and measured current derivative. The results presented so far illustrate that the proposed simulation function which is based on the derivative of the modified Heidler function is much more suitable for use in the developed lightning return-stroke model. Although matching the current obtained from measurement with the modified Heidler function (Figure 7.7) gives slightly more accurate results as compared to simulation using the derivative of the modified Heidler function (Figure 7.5), the initial impulse of the measured current derivative is poorly matched when one uses the modified Heidler function for modelling. Further work presented in this thesis is based on the proposed simulation function represented by the derivative of the modified Heidler function with parameter  $A_2$  eliminated.

Table 7.3. Parameters obtained from matching of measured current with the simulated current using the modified Heidler function.

Parameter	Value
$A_1$	6.7610 kA
$A_2$	9.8080 kA
$\tau_1$	0.6549 $\mu\text{s}$
$\tau_2$	0.0943 $\mu\text{s}$
$\tau_3$	0.3563 $\mu\text{s}$
$\tau_4$	3.094 $\mu\text{s}$
$k_1$	1.45
$k_2$	6.138

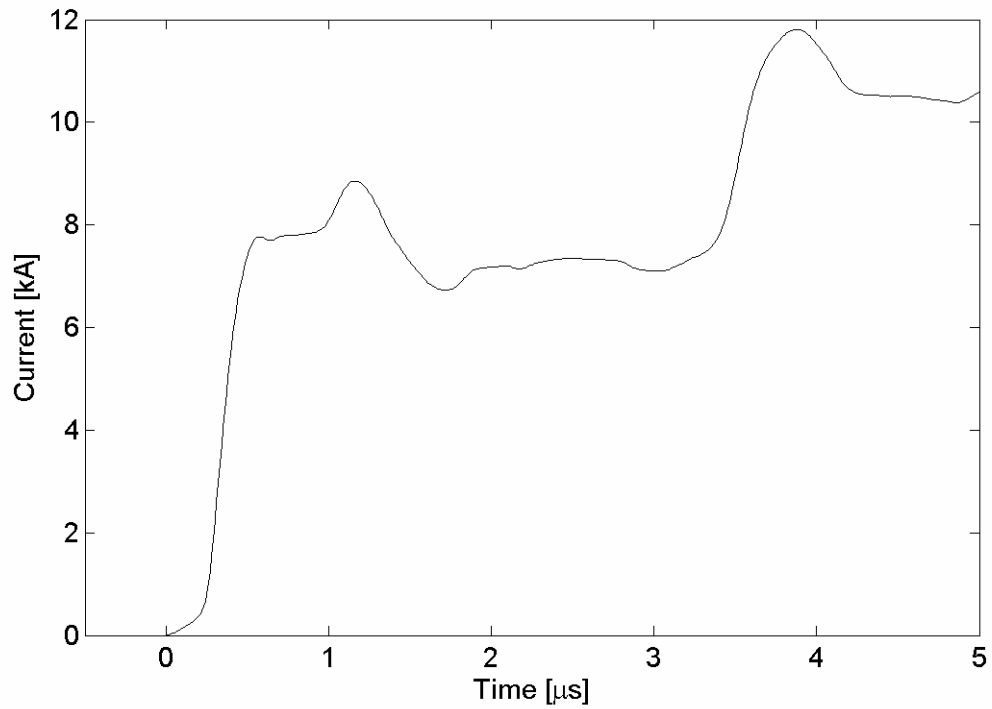


Figure 7.6. Current waveform obtained by numerical integration of the measured current derivative signal.

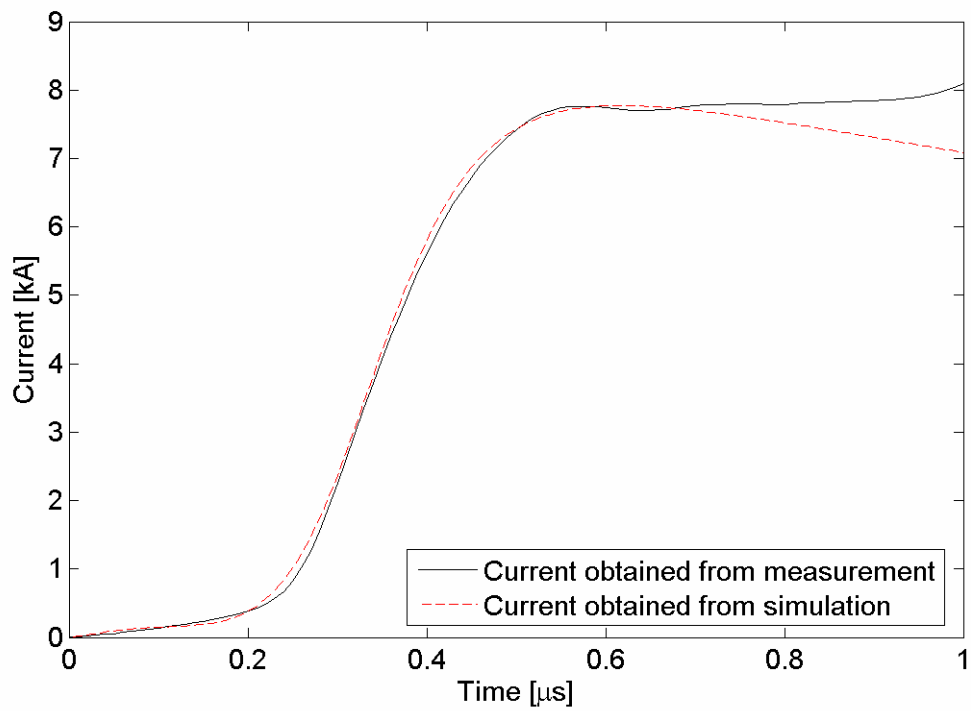


Figure 7.7. Lightning return-stroke current obtained from measurement and simulation.

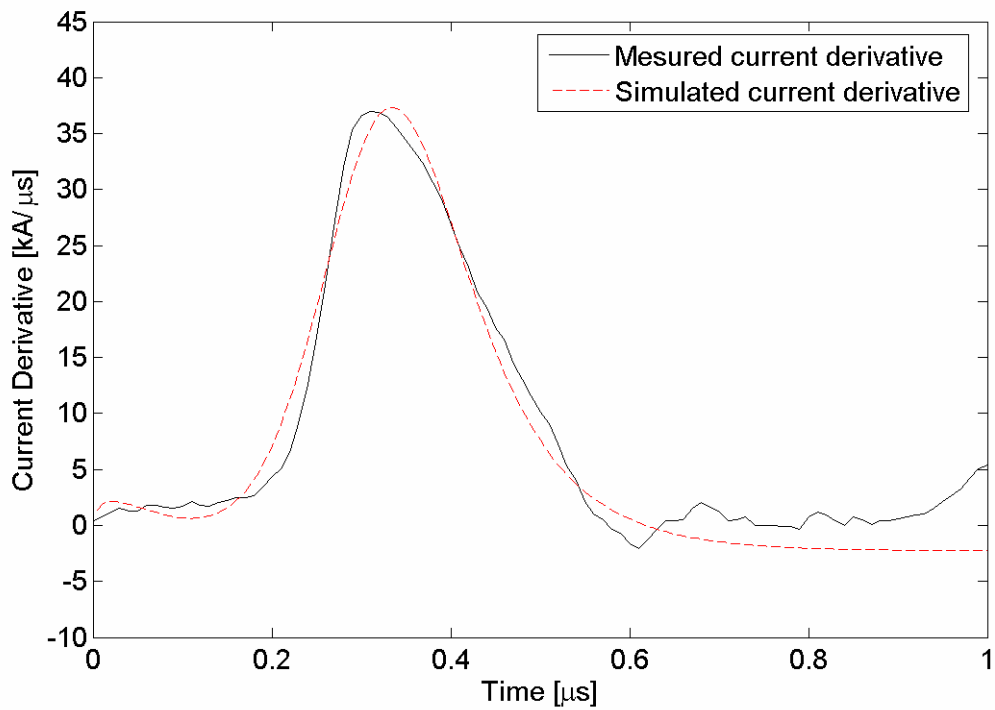


Figure 7.8. First impulse of current derivative obtained from measurement and from simulation using the modified Heidler function.

#### 7.4 THE LIGHTNING ATTACHMENT PROCESS AND REFLECTION COEFFICIENTS AT THE MAIN STRUCTURAL DISCONTINUITIES

A lightning attachment process resulting from a strike to a tall tower and accounting for reflections due to structural discontinuities of the tower can be modeled using lumped voltage source, Rakov *et al.*, or by distributed shunt current source as proposed by Rachidi [6,62]. Both of these methods provide the same end results while taking different approaches. In the method proposed by Rachidi a current is injected at the top of the lightning channel and travels down the channel with a speed of  $v$ . Once the current reaches the tip of the tower, part of it is reflected back from the tip and travels up the channel at a speed of  $v_{ref}$  (Rachidi assumes  $v_{ref} = c$ ) while the other part is transmitted to the tower and travels within the tower with the speed of light,  $c$ . Detailed explanation of distributed current source representation of the lightning channel proposed by Rachidi is given in [6]. Rakov proposes a method based on lossless transmission line representation of the lightning channel and the tower, in which a lumped voltage source,  $V_o(h,t)$ , is inserted between the bottom of the lightning channel and the tip of the tower [57,62]. In the method proposed by Rakov, initially the same current  $V_o(h,t)/(Z_{ch} + Z_{ob})$  is injected into the tall object and the lightning channel.  $Z_{ch}$  is the characteristic impedance of the channel and  $Z_{ob}$  is the characteristic impedance of the object being struck. The current reflection coefficient at the tip for upward propagating waves can be expressed as  $\rho_T = \frac{Z_{ob} - Z_{ch}}{Z_{ob} + Z_{ch}}$  while the current reflection coefficient at ground for downward propagating waves can be expressed as  $\rho_T = \frac{Z_{ob} - Z_{gr}}{Z_{ob} + Z_{gr}}$ ,  $Z_{gr}$  is a

lumped grounding impedance. Rakov assumes that the speed of propagation in the channel as well as speed of ground reflections that are transmitted to the channel is equal to  $v$ , while the speed of propagation in the tower is assumed to be equal to the speed of light,  $c$  [57,62].

In this work the struck object (the CN Tower) is represented as a 3-section uniform lossless transmission line with constant reflection coefficients at the tip of the tower, top and bottom of the restaurant and the ground. The initial current pulse  $i_o(t)$  injected into the CN Tower at its tip will be referred to as “non-contaminated” current and this is the simulated current pulse that has been matched to the measured initial current pulse [86]. It should be pointed out that the model presented in this work is based on the current derivative and the simulated current is obtained using numerical integration of the current derivative. The “non-contaminated” current pulse represents a current waveform that is not diluted with any reflections. This injected “non-contaminated” current will produce two similar current pulses with one pulse travelling down the tower and second pulse travelling up into the channel [63,82,87]. The magnitude of the “non-contaminated” current pulse injected at the tip of the CN Tower is the same for the current travelling up into the lightning channel and down the CN Tower but their vector directions are opposite as show in Figure 7.9. In Figure 7.9 the height of the CN Tower is denoted as  $h$  while the height of the channel plus the height of the tower is denoted as  $H$  (height of channel  $h_c = H - h$ ), the speed of propagation in the channel is denoted as  $v$  and the speed of propagation in the tower is denoted as  $c$ .

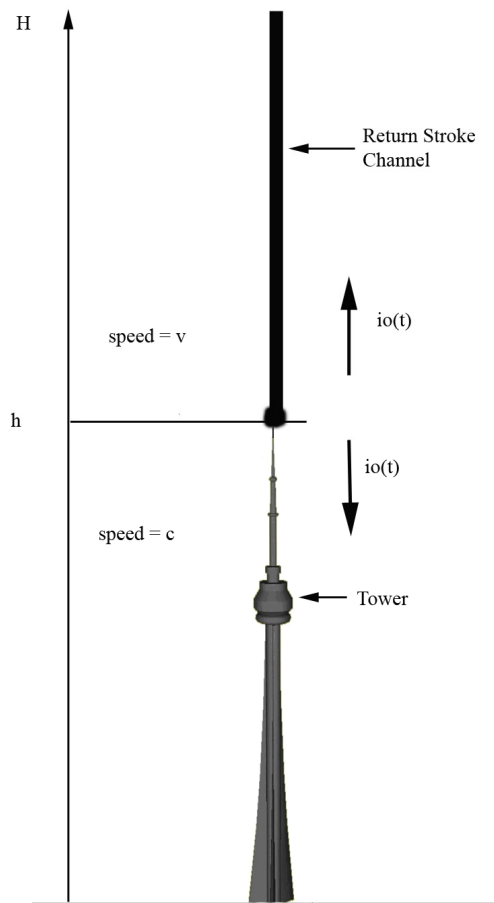


Figure 7.9. Initiation of the lightning return-stroke current into the strike object and the lightning return-stroke channel.

A current waveform resulting from lightning strike to a tall object such as CN Tower will be reflected from main structural discontinuities of the struck object. A diagram of the CN Tower along with four major structural discontinuities which include; the tip of the tower, top and bottom of the restaurant and the ground, is shown in Figure 7.9. Each structural discontinuity of the CN Tower will introduce reflections that have to be taken into account during the simulation of the current and current derivative. In order to account for reflections from structural discontinuities of the CN Tower, a 3-section TL model is used for the simulation of the lightning return-stroke current and current

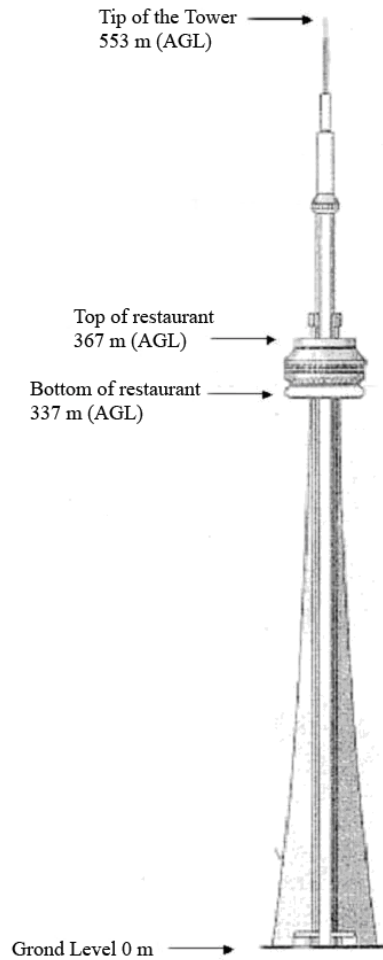


Figure 7.10. The CN Tower along with its major structural discontinuities.

derivative. The first section of the TL model is between the tip of the tower and the top of the restaurant, the second section is between the top and bottom of the restaurant while the third section is between the bottom of the restaurant and the ground. The reflection coefficients for lightning strikes to tall structures are usually evaluated from the lightning return-stroke current waveforms [88-90]. For example, Bierl used simplified traveling wave model to estimate the current reflection coefficients. In his model the tower was represented by an ideal transmission line with wave impedance  $Z_T$ , the ground impedance

of the tower was modeled using resistor  $R_E$  and the current waveform was modeled by an ideal current source  $i_B$  with its constant parallel resistance  $R_B$ . The model proposed by Bierl is illustrated in Figure 7.11. Using this simple model the current reflection coefficient at the bottom of the tower  $\rho_{TE}$  for downward propagating waves and current reflection coefficient at top of the tower  $\rho_{TB}$  for upward propagating waves are given by the following two equations [90]:

$$\rho_{TE} = \frac{Z_T - R_E}{Z_T + R_E} \qquad \rho_{TB} = \frac{Z_T - R_B}{Z_T + R_B} \qquad (7.4)$$

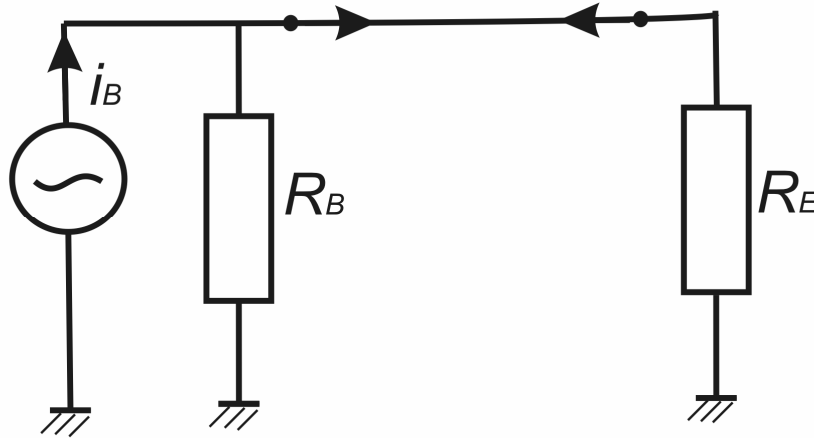


Figure 7.11. Simplified traveling wave model [90].

Willet, on the other hand used electric field waveforms with sharp initial peaks to estimate the ground reflection coefficients for triggered lightning experiments done at Kennedy Space Centre in Florida [91]. To estimate the current reflection coefficients a fast current waveform which has no overlapping peaks has to be used. This type of current waveform can be only obtained for strikes to tall structures as shorter structures will introduce overlapping reflection peaks in the measured current waveform. For example, in case of short structures, the accurate calculation of reflection coefficient from

the tip of the structure is not possible due overlapping of the reflection peaks as the time to travel down the tower and back to the top is much smaller in comparison to tall towers such as the CN Tower. For a 60-m tower the time to travel from tip of the tower to ground and than back to the tip is  $0.4 \mu\text{s}$  (speed of propagation in the tower is equal to speed of light) while the same time for a 553-m CN Tower is  $3.68 \mu\text{s}$ . Even with a tall structure such as the CN Tower, the calculation of some current reflection coefficients can present a problem due to the complexity of the tower and the presence of multiple reflections as well as due to the fact that many current waveforms are not fast enough. Another method used to obtain the reflection coefficients for a tall structure utilizes the measured current derivative waveform [89,92,93]. The current derivative waveform is much faster as opposed to the current waveform and it has much sharper and more distinguishable peaks (the peaks of the current derivative decay to zero much faster allowing for more reliable identification of them). For example, from the analysis of 1992-2001 CN Tower lightning data, it was found that the average 10%-90% risetime to the initial impulse of current derivative was 311 ns while the average 10%-90% risetime to initial current peak was 861 ns [18,94]. For calculation of reflection coefficients to be used in the proposed model, a fast current derivative waveform, with no overlapping peaks and large maximum  $di/dt$  was used. Figure 7.12 shows a current derivative signal measured at the CN Tower while Figure 7.13 shows the corresponding current waveform. The initial impulse peak (initial peak in case of the current) along with impulses (peaks), which correspond to reflections from main structural discontinuities of the CN Tower are indicated on both waveforms. It is very difficult to determine the two points that correspond to (5) and (6) in the lightning current waveform due to overlapping of

reflections. For example, the location of point (5) in Figure 7.13 is estimated based on the travel time within the CN Tower. In the next section the calculation of reflection coefficients using the measured CN Tower current derivative waveform will be presented. To confirm the validity of calculation of reflection coefficients from the current derivative waveform, a comparison will be made between the current waveform obtained from the measurement and the current waveform simulated by the derivative of the modified Heidler function.

As previously mentioned, the main structural discontinuities of the CN Tower will introduce reflections in the lightning current derivative and current waveforms. The reflections corresponding to structural discontinuities of the CN Tower are shown in Figures 7.12 and 7.13. The initial impulse of the measured current derivative is denoted by (1). The reflections from top and bottom of the restaurant are denoted by (2) and (3), respectively. The reflection from ground is denoted by (4) while the reflection from ground that is reflected from tip of the CN Tower and goes back to the coil location is denoted by (5). The origin of the sixth reflection (6) is unknown but it is thought to be a reflection from the lightning channel itself. The first three reflections along with the main peak can be also seen in the current waveform; however the reflections denoted by (5) and (6) are not distinguishable (Fig. 7.13). Also it is very difficult to determine the reflection coefficients based on the current waveform due to the fact that current waveform is much slower as compared to the current derivative and it does not have zero crossings. For example, if one wants to determine the reflection from the top of the restaurant using current signal obtained from measurements, a starting point at which the reflection begins has to be estimated in order to estimate the peak of that reflection.

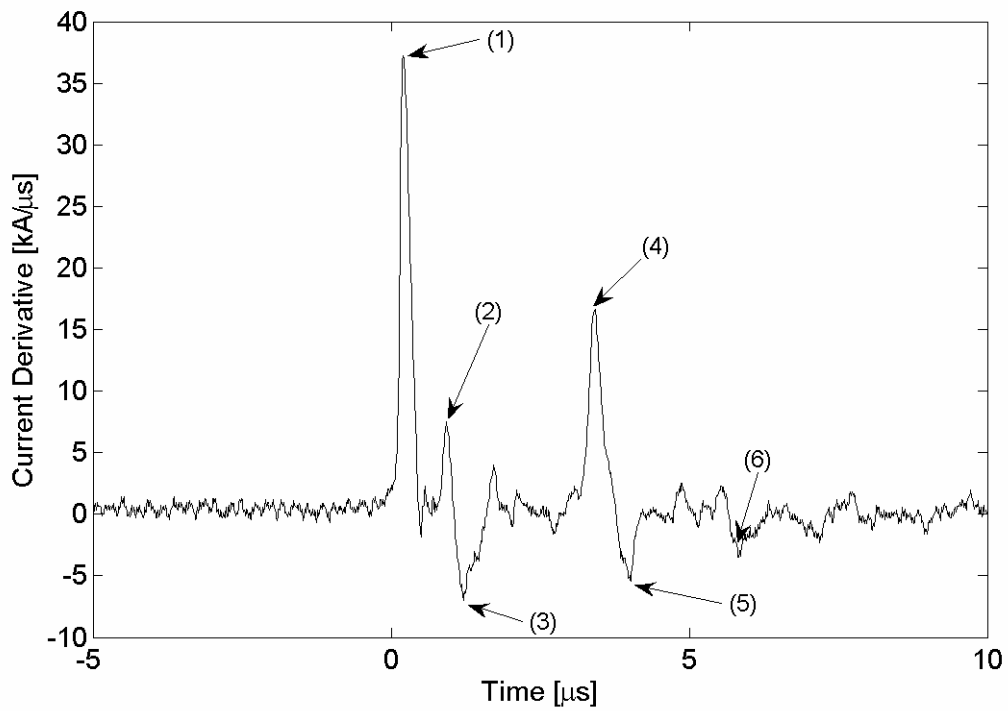


Figure 7.12. Measured current derivative and reflections from CN Tower's main structural discontinuities.

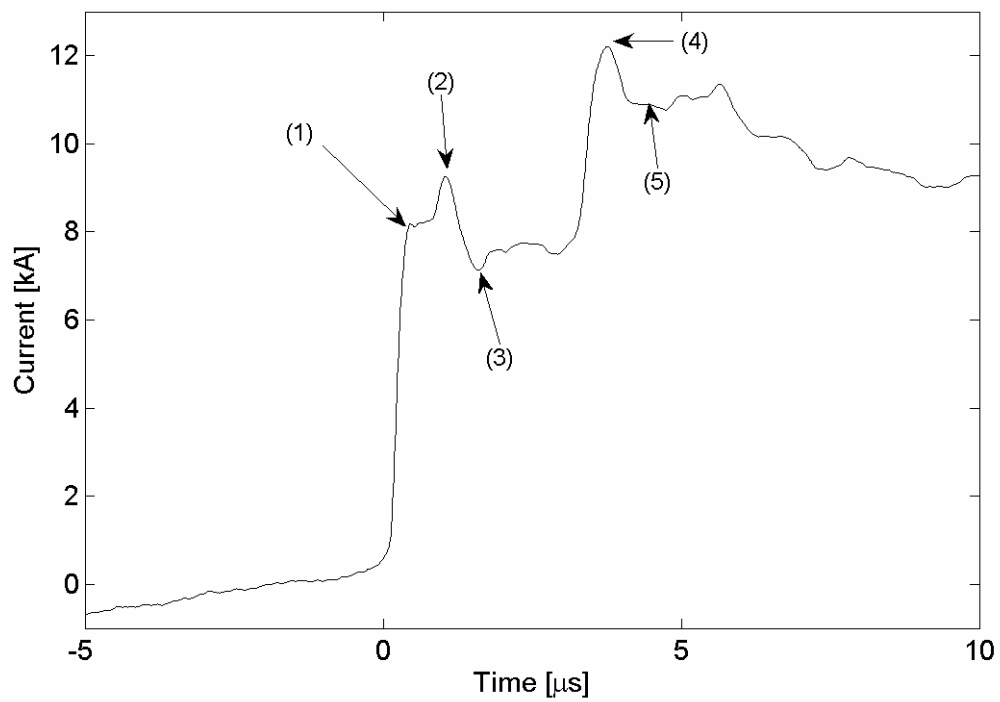


Figure 7.13. Current waveform and reflections from CN Tower's main structural discontinuities.

### 7.4.1 CALCULATION OF REFLECTION COEFFICIENTS

An example of a measured current derivative signal, representing a CN Tower lightning return-stroke, which is used to calculate the main reflection coefficients, is shown in Figure 7.14. The maximum value of the lightning current derivative for this stroke is 36.56 kA/ $\mu$ s. The four main reflection coefficients have been determined from the current derivative signal and they include: the reflection coefficient at the top of the restaurant, the reflection coefficient at the bottom of the restaurant, the reflection coefficient at the ground and the reflection coefficient at the tip of the CN Tower. The values of the current derivative impulses corresponding to the reflections at main structural discontinuities of the CN Tower have been obtained and are shown in Table 7.4.

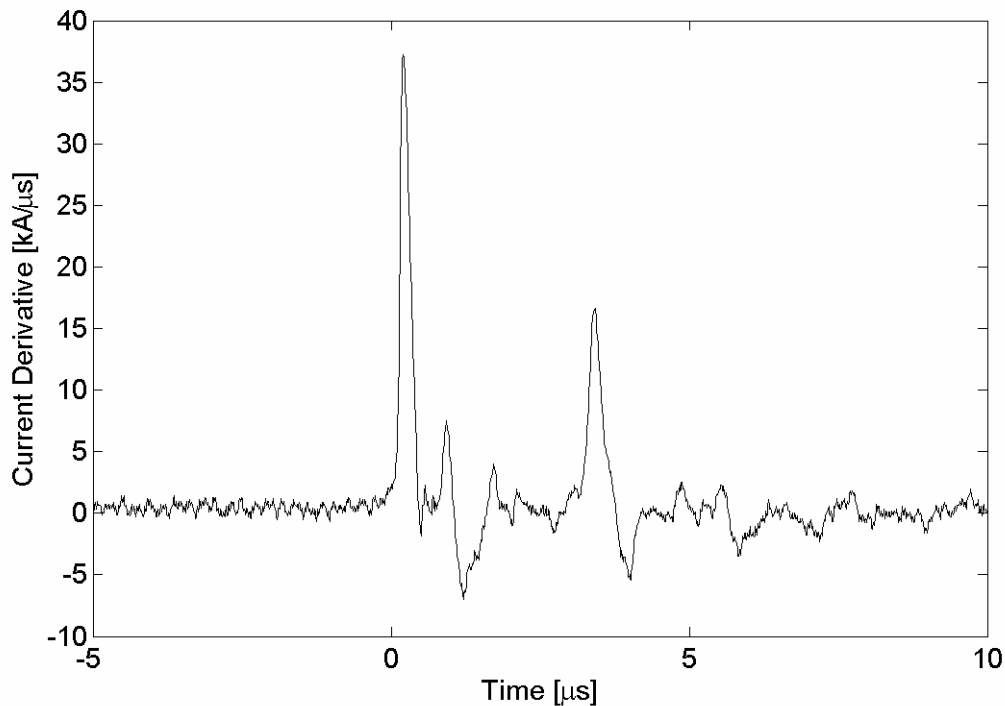


Figure 7.14. Current derivative waveform used to calculate the reflection coefficients.

Table 7.4. Peaks of impulses corresponding to reflections from main structural discontinuities of the CN Tower (obtained from the measured current derivative signal).

Reflection	Impulse Peak [kA/ $\mu$ s]
Top of the restaurant	7.51
Bottom of the restaurant	-6.96
Ground	16.65
Tip of the CN Tower	-5.44

In order to calculate the values of reflection coefficients a simple diagram shown in Figure 7.15, has been developed. The main current derivative impulse is denoted as  $f_1$ , impulse corresponding to reflection from the top of the restaurant is  $f_2$ , the bottom of the restaurant  $f_3$ , ground  $f_4$  and the tip of the CN Tower is  $f_5$ . The reflection coefficient at the top of the restaurant is  $\rho_1$ , bottom of the restaurant  $\rho_2$ , ground  $\rho_G$  and at the tip of the tower  $\rho_T$ . The reflection coefficients at four main structural discontinuities have been obtained using the peaks of the current derivative impulses corresponding to the respective reflections along with diagram shown in Figure 7.15. For example, the reflection coefficient at the top of the restaurant  $\rho_1$  was obtained using the following

formula:  $\rho_1 = \frac{f_2}{f_1}$ . This formula represents a ratio of the measured current derivative

impulse corresponding to reflection from top of the restaurant divided by the initial impulse of the measured current derivative. Formulas used to obtain the values of the reflection coefficients at four main structural discontinuities of the CN Tower are given in Table 7.5. The reflection coefficients at the bottom of the restaurant and the tip of the CN Tower are negative. This means that the characteristic impedance of the restaurant is lower than the characteristic impedance of the tower below the restaurant and that the characteristic impedance of the channel is greater than the impedance at the tip of the CN Tower. For example, the current reflection coefficient at the tip of the CN Tower for

upward propagating current waves can be evaluated using the following simple expression:  $\rho_T = \frac{Z_T - Z_{ch}}{Z_T + Z_{ch}}$ , where  $Z_T$  is the characteristic impedance at the tip of the CN Tower and  $Z_{ch}$  is the characteristic impedance of the channel [62,89,95]. To confirm the validity of the reflection coefficients used for modelling as well as the locations of these reflections, a detailed analysis of 1996 CN Tower data were made. In the analysis a total of 47 lightning return-strokes measured during 1996 lightning season were used and the reflection coefficients at the top and the bottom of the restaurant, ground and at the tip of the CN Tower as well as the location of these reflections have been determined for each stroke. In some cases the reflections at the top and bottom of the restaurant could not be found. In most of these cases either the noise was too high and was corrupting the signal or the measured current derivative signals were not sharp or fast enough and the impulses corresponding to these reflections could not be distinguished. The denoising of the CN Tower current derivative signal is a very difficult process due to presence of many types of noise that are corrupting the measured signal. For example, one of the noise signals that corrupts the current derivative signal measured at the CN Tower is the Loran-C signal (radio-navigation signal used for ship navigation), which uses a frequency band from 90 kHz – 110 kHz [43]. Denoising of the current derivative signal measured at the CN Tower is beyond scope of this work and for further information reader can refer to already published work, *et al. Jahir, et al. Ourda* [96,97]. Furthermore, to confirm that the reflection coefficients calculated from the current derivative signal are valid, the current obtained from the measurement is compared with the simulated current that has been obtained by matching of the derivative of the modified Heidler function with the measured current derivative.

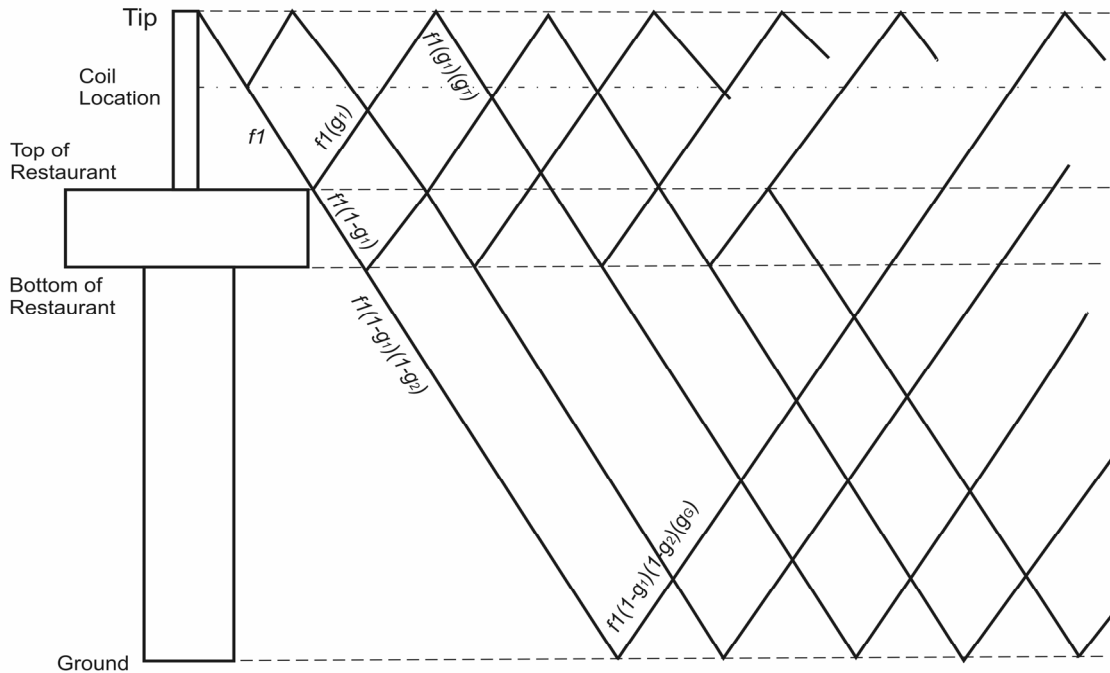


Figure 7.15. Calculation of reflection coefficients.

Table 7.5. Reflection coefficients calculated from the measured current derivative.

Reflection	Equation for Calculation	Value
Top of the restaurant	$\rho_1 = \frac{f_2}{f_1}$	0.20175438
Bottom of the restaurant	$\rho_2 = \frac{f_3}{f_1} \frac{1}{(1 - \rho_1^2)}$	-0.19507499
Ground	$\rho_G = \frac{f_4}{f_1} \frac{1}{(1 - \rho_1^2)(1 - \rho_2^2)}$	0.48479986
Tip of the CN Tower	$\rho_T = \frac{f_5}{f_1} \frac{1}{(1 - \rho_1^2)(1 - \rho_2^2)\rho_G}$	-0.32679738

## 7.4.2 REFLECTION COEFFICIENTS AND LOCATION OF REFLECTIONS

The measured current derivative data used in this section is composed of 12 CN Tower flashes containing 47 strokes. The location of each reflection with reference to the ground level, which was assumed to be at 0 m, has been calculated for the 47 strokes along with peak of each reflection. In some cases, the current derivative impulses

corresponding to reflections from the top and bottom of the restaurant as well as the tip of the CN Tower could not be determined and they were not included in the final plots. Figures 7.16 and 7.17 show the locations of the top and bottom of the restaurant where reflections occur. Similarly, the locations of ground and the tip of the CN Tower where reflections occur are shown in Figures 7.18 and 7.19, respectively. In Figures 7.16 – 7.19 the horizontal axes represents the maximum wavefront rate of rise of the measured current derivative signal. Each figure also shows a horizontal line that represents the location which would be approached by the asymptote with the asymptotic value given in rectangular box. As that as the maximum wavefront slope of the current derivative increases, the location for each of the reflections approaches asymptotically a steady value (Fig. 7.16-7.19). This illustrates the importance of choosing fast waveforms, with large initial impulse peaks of the current derivative and no overlapping peaks in order to calculate the location of reflections as well as the reflection coefficients [67,86,93]. The obtained location of the ground level indicates that the current actually propagates a few meters below the level which was originally assumed to be the ground. The asymptotic values for the locations of the top and bottom of the restaurant, the ground and the tip of the CN Tower obtained from the plots shown in Figure 7.16 – 7.19 are summarized in Table 7.7.

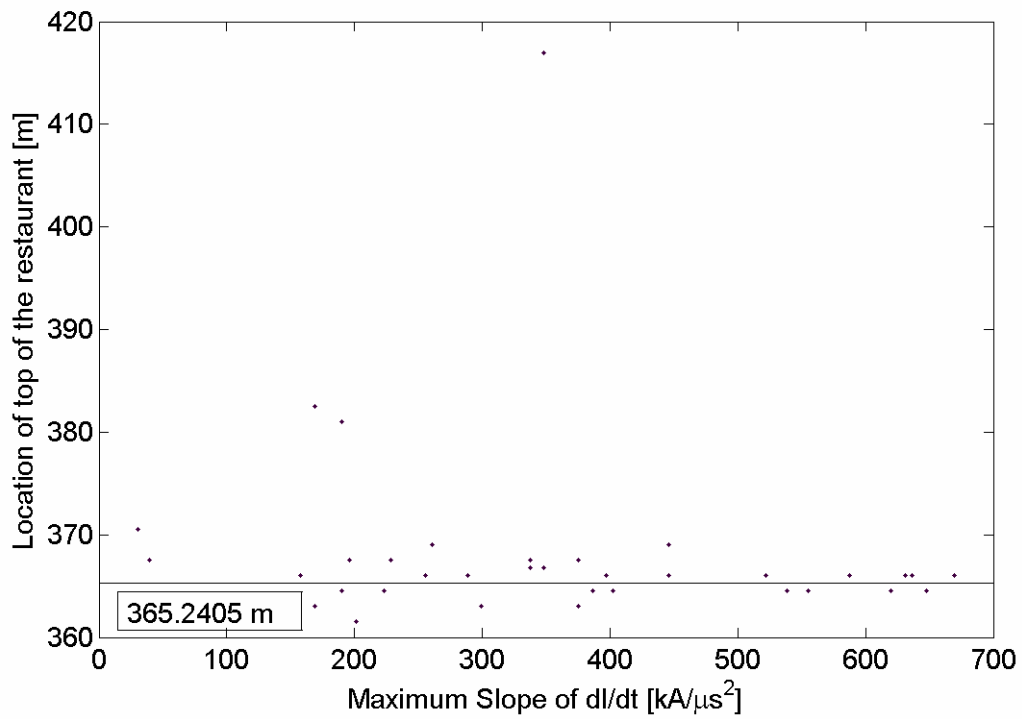


Figure 7.16. Location of the top of the restaurant vs. the maximum slope of the lightning current derivative.

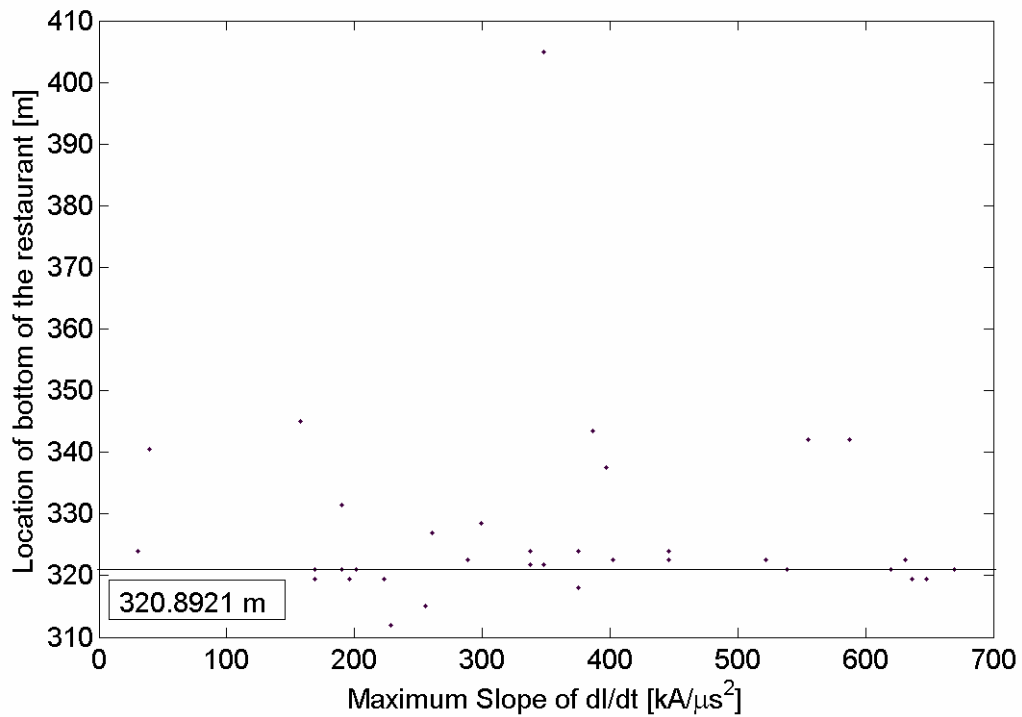


Figure 7.17. Location of the bottom of the restaurant vs. the maximum slope of the lightning current derivative.

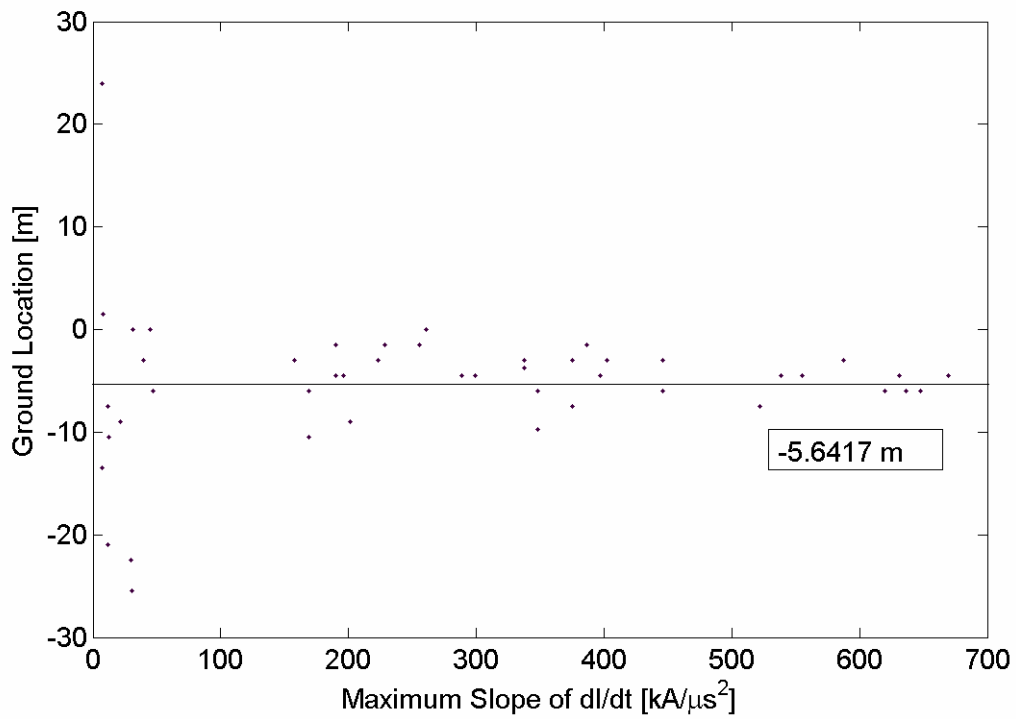


Figure 7.18. Location of ground vs. the maximum slope of the lightning current derivative.

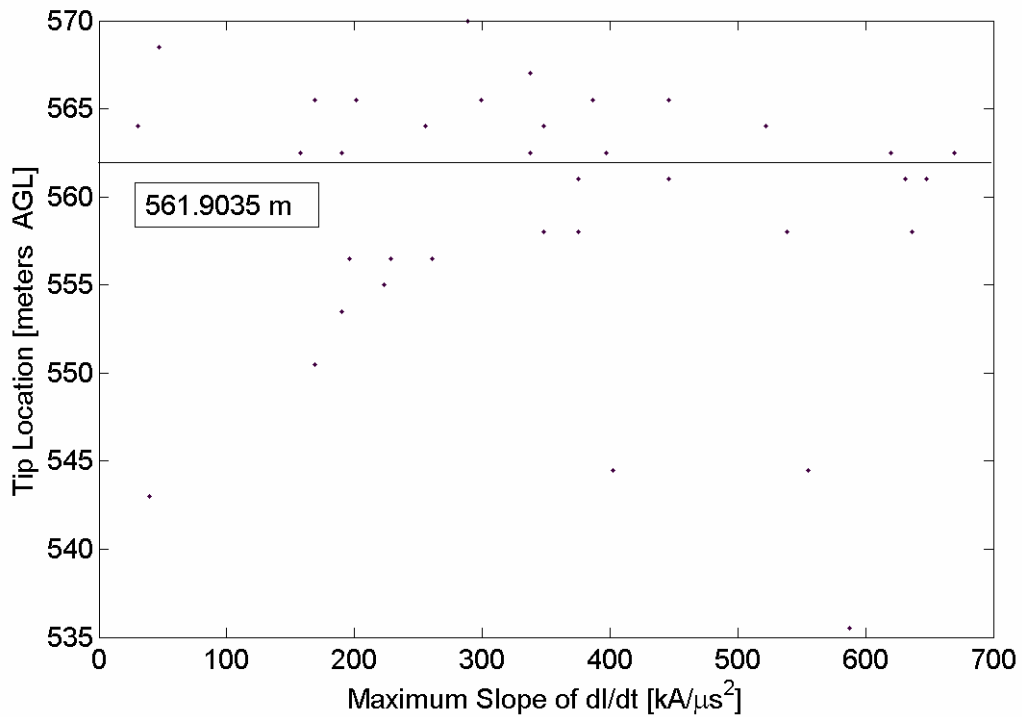


Figure 7.19. Location of the tip of the CN Tower vs. the maximum slope of the lightning current derivative.

Table 7.6. Locations of the current derivative reflections from CN Tower's structural discontinuities.

<b>Location</b>	<b>Value obtained from 1996 Data [m]</b>	<b>Value obtained from dI/dt waveform used for matching [m]</b>
Top of the Restaurant	365.3905	366.0
Bottom of the Restaurant	320.8921	322.5
Ground	-5.6417	-7.5
Tip of CN Tower	561.9035	564.0

The 47 measured strokes used to determine the locations where the reflections occur are also used to compute the reflection coefficients at the top and bottom of the restaurant, the ground and the tip of the CN Tower. Figures 7.20-7.23 show the plots of the reflection coefficients versus the maximum slope of current derivative for the 47 strokes used. As mentioned before, in some cases the reflection coefficients at the top and bottom of the restaurant as well as at the tip of CN Tower could not be determined. In two cases the measured current derivative signal was saturated, i.e. the maximum value that could be measured by the digitizer was exceeded. The saturated points are marked as 'x' in Figures 7.20-7.23. As in the case of the location of the reflections, a horizontal line which represents the value that would be approached by an asymptote is shown in each of Figures 7.20-7.23. The numbers in the rectangular boxes in these figures indicate the asymptotic values of the reflection coefficients. The reflection coefficients obtained from Figures 7.20-7.23 are in close agreement with the reflection coefficients obtained from the current derivative signal used in the proposed model. The ground and tip reflection coefficients obtained from the 47 strokes are very close to the ones obtained from the current derivative chosen for simulation. The reflection coefficients at the top and bottom of the restaurant have larger differences. One of the reasons for the larger differences is that impulses corresponding to ground and tip reflections are much higher and can be

distinguished more easily as opposed to impulses corresponding to reflections from top and bottom of the restaurant. The results presented validate the use of a sharp current derivative waveform with high initial impulse, low risetime and high maximum slope of  $dI/dt$  for determination of the reflection coefficients. The results also illustrate that a current derivative waveform that has low initial impulse and is not fast enough (i.e. reflections are overlapping) will not produce accurate results. Table 7.7 gives a summary of the reflection coefficients obtained using asymptotic values from 1996 data and the ones obtained from the current derivative signal used for modelling.

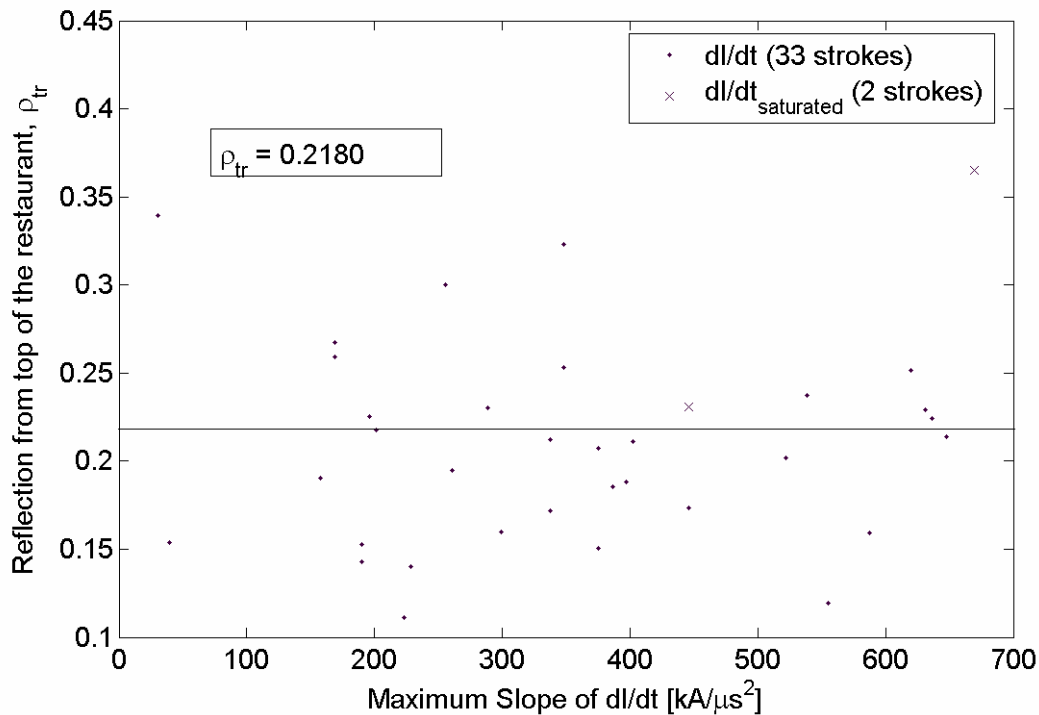


Figure 7.20. Reflection coefficient at the top of the restaurant vs. the maximum slope of the lightning current derivative.

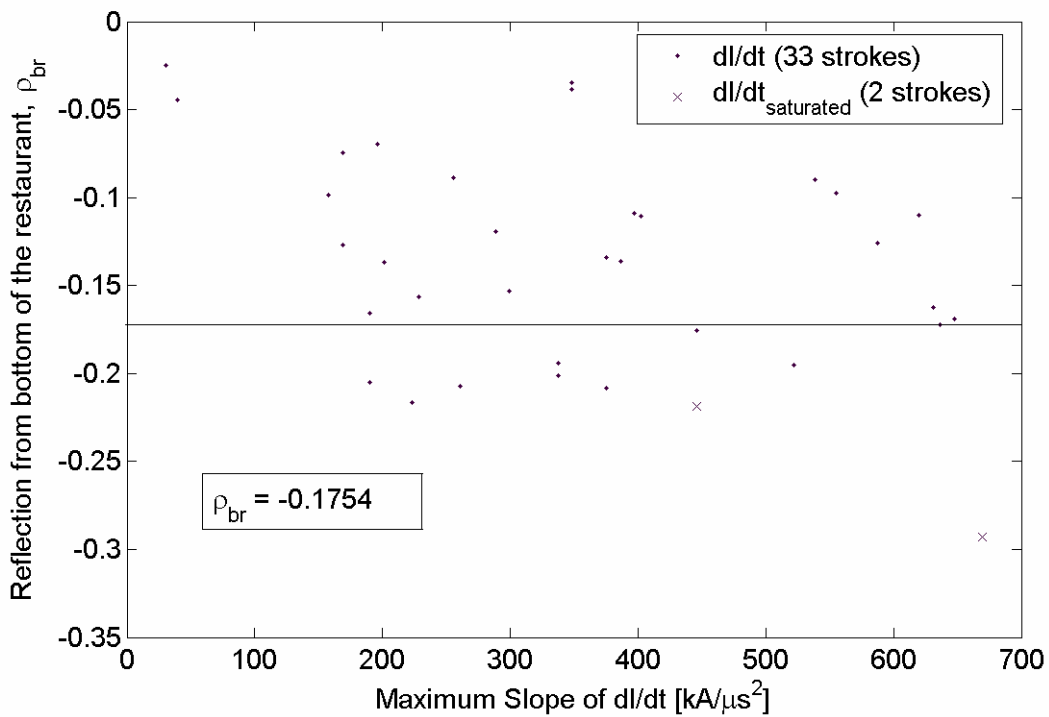


Figure 7.21. Reflection coefficient at the bottom of the restaurant vs. the maximum slope of the lightning current derivative.

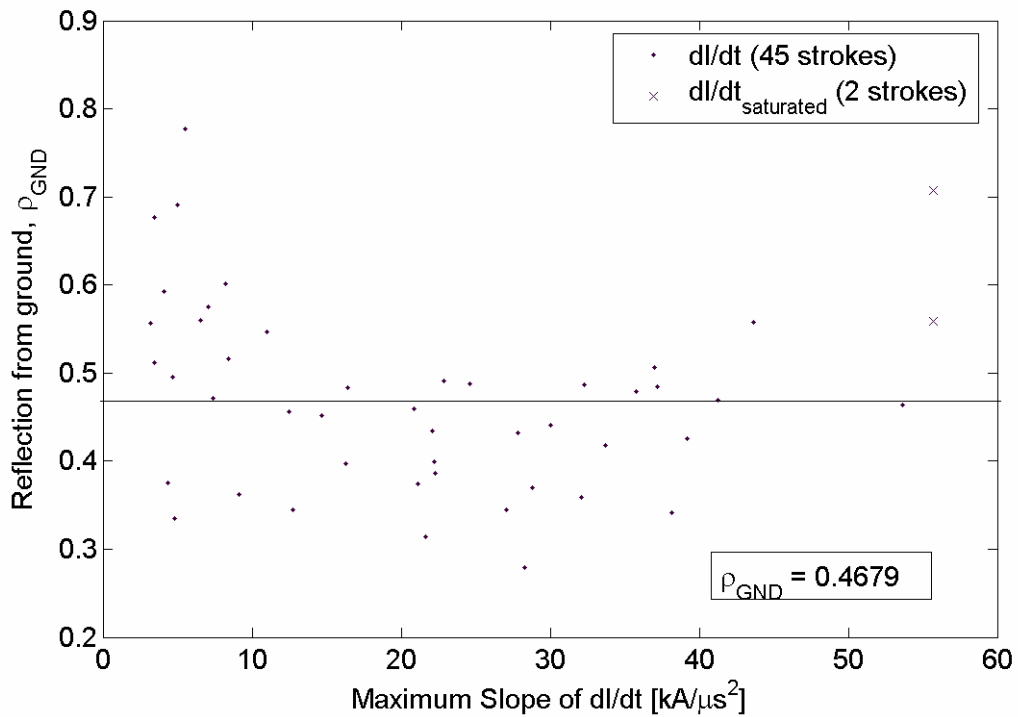


Figure 7.22. Reflection coefficient at ground vs. the maximum slope of the lightning current derivative.

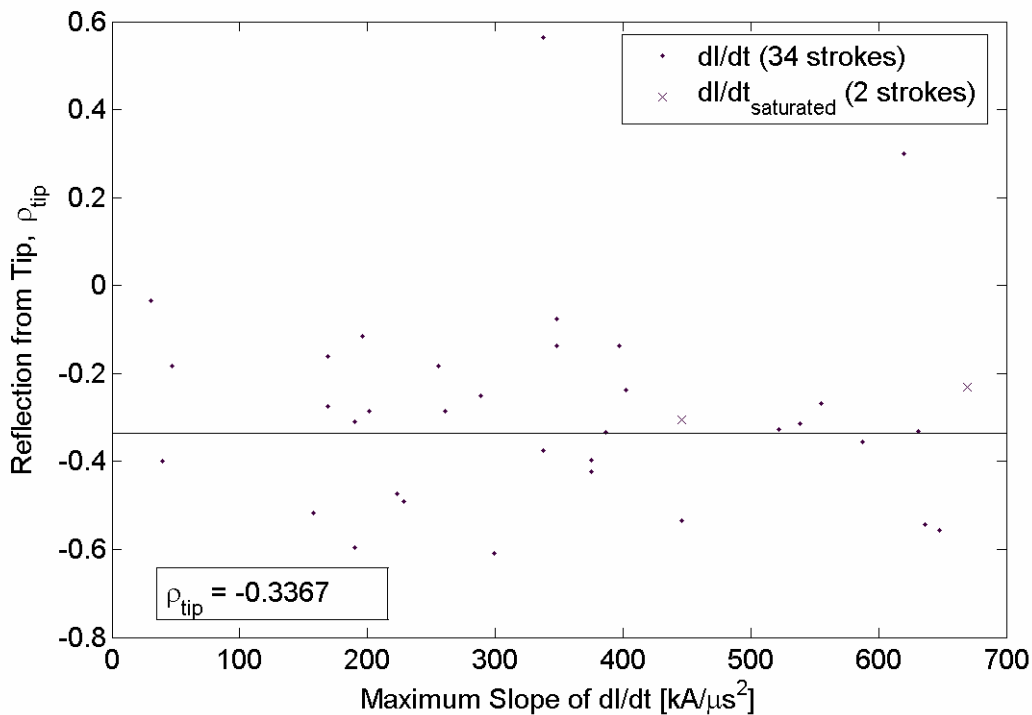


Figure 7.23. Reflection coefficient at the tip of the CN Tower vs. the maximum slope of the lightning current derivative.

Table 7.7. Reflection coefficients obtained from 47 CN Tower strokes and from the chosen current derivative signal.

Reflection	Asymptotic value from Figs. 7.21 – 7.23	Value obtained from $di/dt$ signal used for matching
Top of the Restaurant	0.2180	0.2018
Bottom of the Restaurant	-0.1754	-0.1951
Ground	0.4679	0.4848
Tip of CN Tower	-0.3367	0.3268

## 7.5 MODELLING OF THE LIGHTNING CURRENT DERIVATIVE

The simulation of the measured current derivative signal is presented in this section. The parameters of the modified Heidler function obtained from curve fitting of the initial impulse of the measured current derivative signal and the derivative of the modified Heidler function are described in section 7.3. Multiple reflections from the four main CN Tower's discontinuities namely the top and bottom of the restaurant, the ground

and the tip of the CN Tower are taken into consideration in modelling. These reflections greatly affect the wave shapes of the current derivative and current waveforms. A lattice diagram illustrating the main CN Tower's structural discontinuities and multiple reflections is shown in Figure 7.24. The reflection coefficients used for matching are determined from the chosen measured current derivative signal and are listed in Table 7.7. Figure 7.25 shows the measured current derivative signal and the simulated current derivative waveform obtained when the derivative of the modified Heidler function was used for matching. The corresponding current waveform obtained by numerically integrating the measured current derivative and the current obtained using the integration of the simulated current derivative are shown in Figure 7.26. All multiple reflections are included in the simulation unless peaks of reflected pulses are smaller than 1% of the initial impulse peak of the measured current derivative. In the simulation it was assumed that no reflection comes back from the progressing lightning channel front.

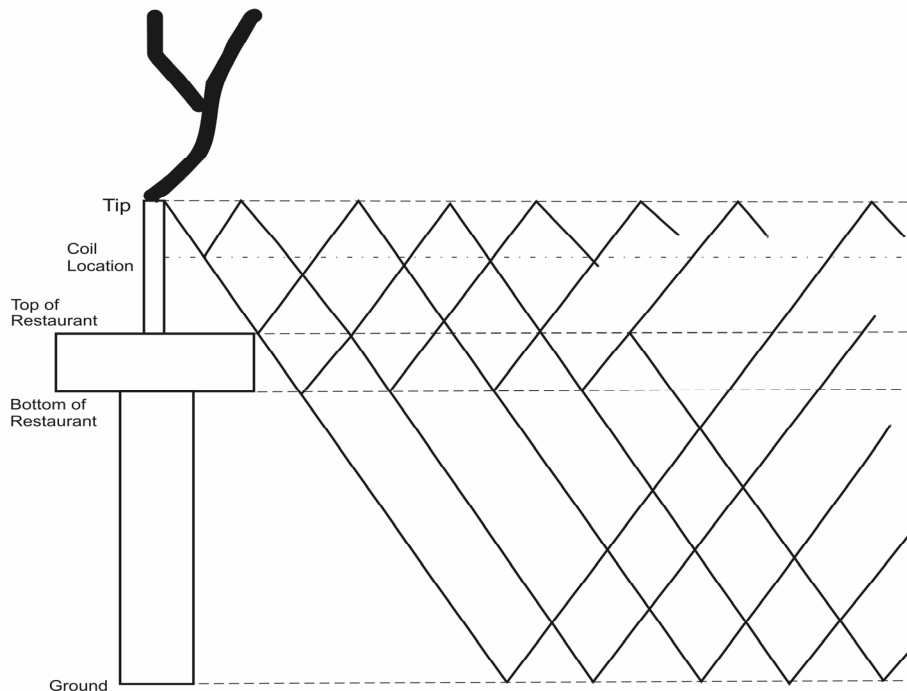


Figure 7.24. Lattice diagram showing reflections from major structural discontinuities of the CN Tower.

Figure 7.25 shows that the simulated current derivative waveform is well matched with the measured one. One of the problems with use of the Heidler function is the inability of the function to correctly simulate the initial stage of the lightning current (Figure 7.26) or the lightning current derivative (Figure 7.25). This inability may cause inaccuracy in matching during and after the initial stage. In addition, reflections from other discontinuities of the CN Tower are visible in the measured current derivative signal; for example, there is a clear reflection visible at  $0.68 \mu\text{s}$ , which corresponds to location of 418.5 m above ground level assuming the speed of propagation in the CN Tower is equal to speed of light. The origin of this reflection is unknown. Additional reflections that are unaccounted for are seen in the range of  $2.2 - 3.2 \mu\text{s}$ , some of these reflections may be due to reflection at  $0.68 \mu\text{s}$  that is reflected again from main structural discontinuities. The simulated and measured current waveforms shown in Figure 7.26 were obtained by time integration of the corresponding current derivative waveforms shown in Figure 7.25. The simulated current includes all multiple reflections that were used to plot the simulated current derivative.

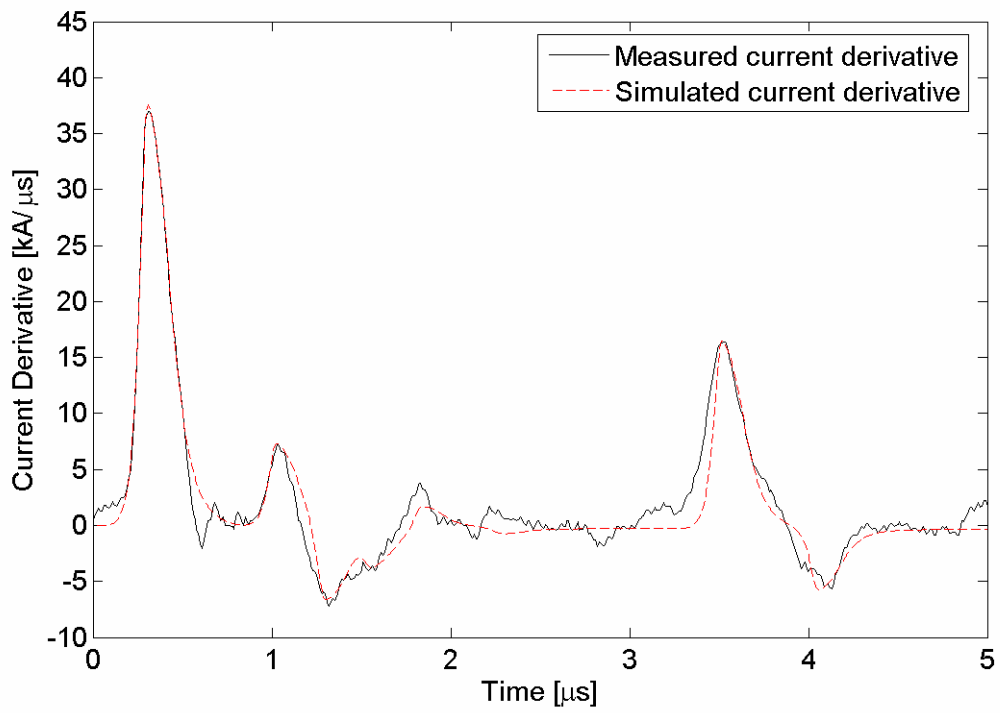


Figure 7.25. Simulated and measured current derivative waveforms.

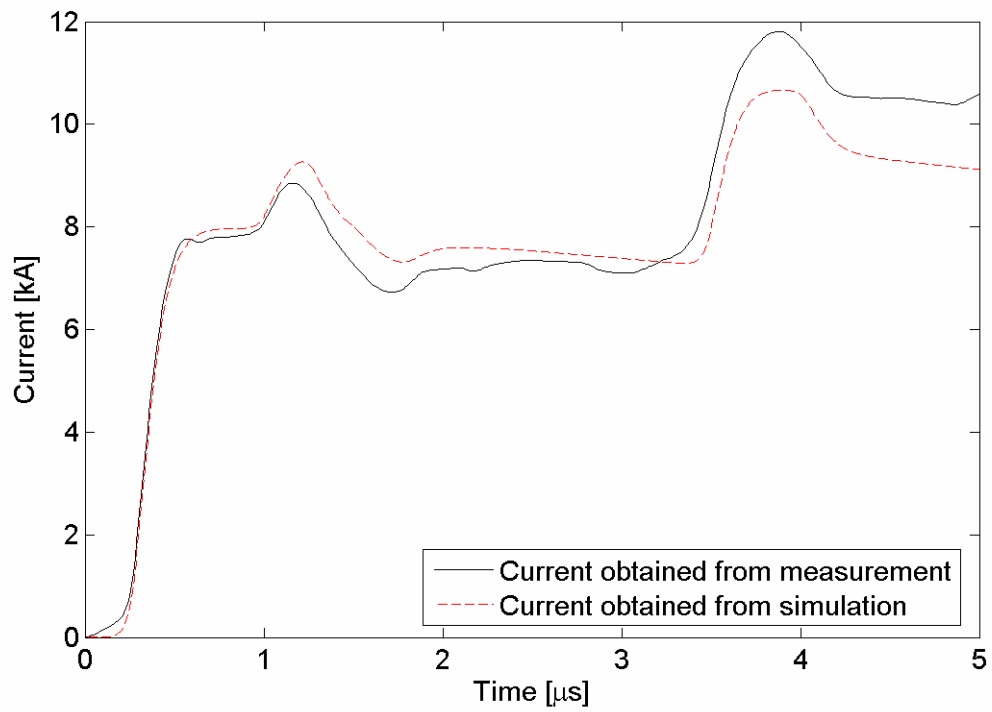


Figure 7.26. Simulated and measured current waveforms.

The current obtained from the simulated current derivative is well matched with the current waveform obtained from the measured current derivative signal (Figure 7.26). The results shown in Figure 7.26 again illustrate the inability of the Heidler function to simulate the initial stage of the current and current derivative waveforms. Furthermore, the simulated current peak corresponding to ground reflection is lower when compared to the measured one. This discrepancy can be caused by some neglected reflections. In future work, one of the possible improvements that could result in better matching between the simulated and experimental results during initial stage is the addition of a function that would only affect the results during initial stage of the simulation. Such a function could be represented by the decaying exponential with a constant term. The results presented in this section illustrate that proposed simulation function based on the derivative of the modified Heidler function matches well the experimental data.

## **7.6 MODELLING OF THE LIGHTNING CURRENT USING THE MODIFIED HEIDLER FUNCTION**

In this section, the lightning return-stroke current modeled using the modified Heidler function is compared with the current obtained from measurements. In addition the simulated current derivative (obtained from the simulated current) is compared with the measured one. The presented results further confirm that modelling the measured current derivative provides much better match between the simulated and measured waveforms. The values of the parameters obtained from modelling of the measured current (in the range from 0 - 0.63  $\mu$ s) with the modified Heidler function are given in Table 7.3. The reflections from four major structural discontinuities of the CN Tower are

taken into account. The values of the reflection coefficients are given in Table 7.5. The lightning return-stroke current obtained from measurements and the simulated current obtained from matching using the modified Heidler function are shown in Figure 7.27. The measured current derivative and the simulated current derivative obtained from matching using the modified Heidler function are shown in Figure 7.28. The simulated waveforms shown in Figures 7.27 and 7.28 include the contributions due to the CN Tower as well due to the lightning return-stroke channel. As it can be seen from the results shown in Figure 7.27, beyond the initial peak, the simulated current is poorly matched with the current obtained from measurements. Up to the first current peak the matching is quiet good but once the reflections from structural discontinuities are taken into account the quality of fit deteriorates rapidly. The decaying portion of the simulated current is much faster as opposed to the decaying portion of the current obtained from measurement (Fig. 7.27). In addition the peaks corresponding to the reflections from main structural discontinuities are shifted down in case of the simulated current. The absolute peak of the simulated current corresponding to ground reflection is reduced to 53% of the measured one. On the other hand, using the results obtained from matching the derivative of the modified Heidler function (Figure 7.26), the simulated current peak corresponding to ground reflection is only reduced to 90% of the measured one.

In conclusion, it has been shown that the simulation function represented by the modified Heidler function did not match well the current obtained from measurement (Figure 7.27). Also, the derivative of this simulation function did not match well the measured current derivative signal (Figure 7.28).

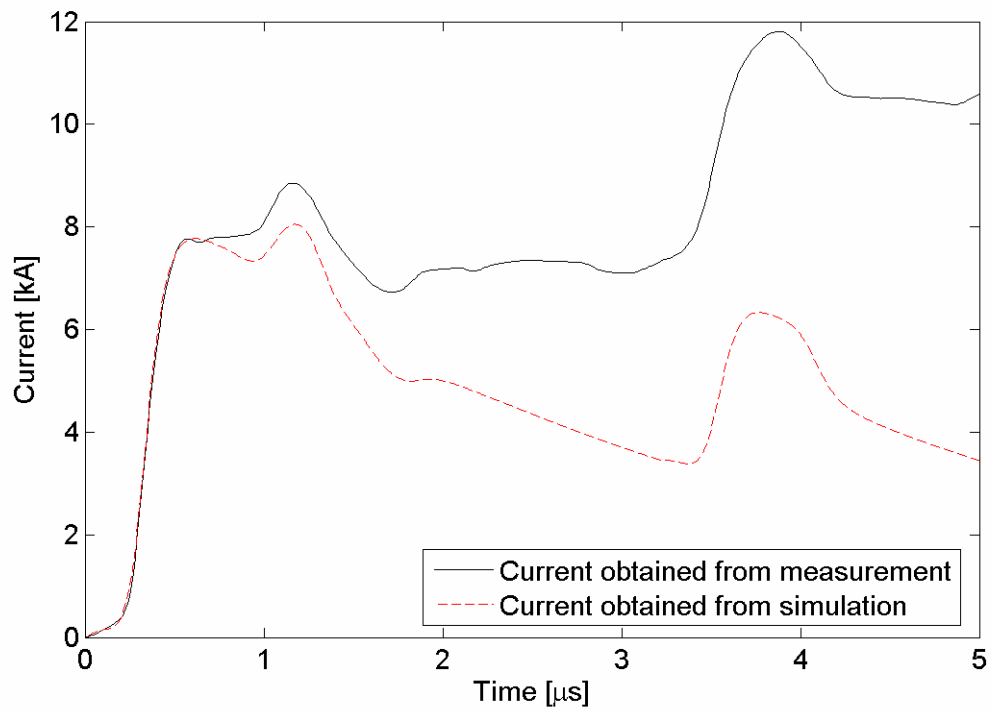


Figure 7.27. Simulated and measured current waveforms.

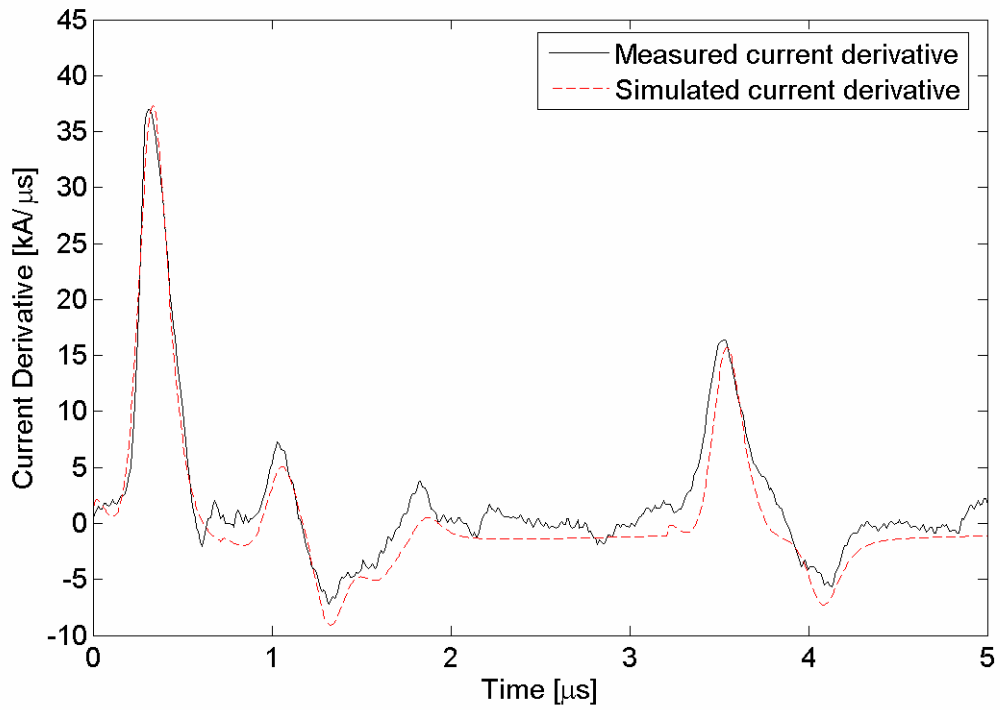


Figure 7.28. Simulated and measured current derivative waveforms.

## 7.7 SUMMARY OF CHAPTER 7

The main focus of this chapter is related to the second major objective of this thesis, which is the development of lightning return-stroke model based on the measured current derivative and the derivative of the modified Heidler function along with 3-section TL representation of the CN Tower. The expression for the derivative of the modified Heidler function is developed and using non-linear curve fitting it is matched with the initial impulse of the measured current derivative. Reflection coefficients at four main structural discontinuities of the CN Tower (the tip of the Tower, the top and bottom of the restaurant and the ground) are evaluated and they are used to simulate the current derivative and current signals. In addition the results obtained from matching using the modified Heidler function with the current obtained from measurements are shown. In both cases the results of simulations are compared with the ones obtained from measurements. It is shown that the proposed simulation function, which is based on the derivative of the modified Heidler function, is much more suitable for use in the developed lightning return-stroke model. The comparison of the simulated current and current derivative with the ones obtained from measurements represents a first step in the quantitative assessment of the proposed model.

## Chapter 8

# Comparison of Simulated and Measured Electromagnetic Field

In lightning return-stroke modelling, one of the most important steps is the evaluation (assessment) of the developed model. The evaluation is achieved by comparing the simulated electric and magnetic fields, and the measured electric and magnetic fields. No model is complete without being validated. In the work presented in this thesis a lightning return-stroke model based on the derivative of the modified Heidler function is developed. The simulated current and current derivative waveforms are compared with the return-stroke current and current derivative signals obtained from measurements done at the CN Tower. In order to properly validate the proposed lightning return-stroke model, a comparison between the simulated electromagnetic field and the electromagnetic field measured at 2 km north of the CN Tower is made. The vertical component of the electric field and the azimuthal component of the magnetic field resulting from CN Tower return-strokes have been measured since 1991.

## 8.1 CN TOWER LIGHTNING-GENERATED ELECTRIC AND MAGNETIC FIELDS

In this section, time-domain expressions for electric and magnetic fields due to a vertical antenna (CN Tower) placed above a perfectly conducting ground will be presented. The presented field equations along with the simulated current and current derivative are used to determine the simulated electric and magnetic fields. A comparison is made between the simulated and measured electric and magnetic fields. In the simulation of the electric and magnetic fields using a 3-section TL representation of the CN Tower, reflections from the tip of the CN Tower, the top and bottom of the restaurant and ground will be included. For comparison, the simulated electric and magnetic fields, obtained using a single section TL model representing the CN Tower's extremities (tip and ground) are computed. The field contributions from the CN Tower and the lightning channel are included in the simulation. In the simulation of the electric and magnetic fields it is assumed that no reflection is coming back to the sensing coil location from the lightning channel front.

The lightning return-stroke channel and the tower are considered as a vertical antenna placed above a perfectly conducting ground. The geometry used to derive the electric and magnetic field expressions is shown in Figure 8.1. To satisfy the boundary conditions an image of the antenna is assumed below the conducting plane (Figure 8.1). The current at any height  $z'$  and time  $t$ ,  $i(z',t)$ , is assumed to be a continuous function.

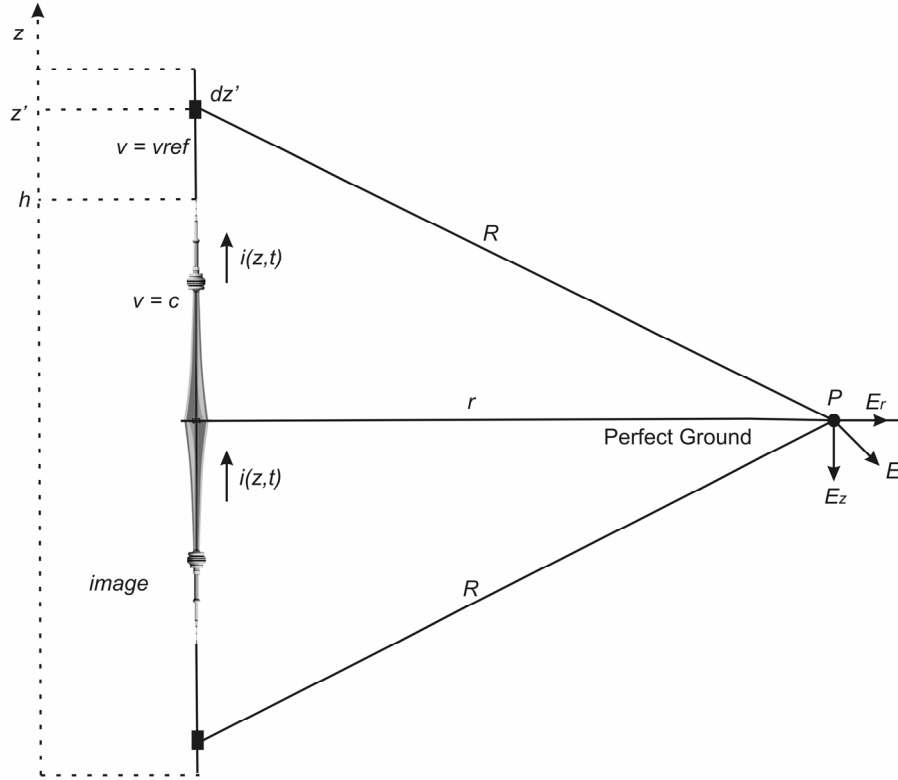


Figure 8.1. Geometry used for electromagnetic field calculations.

The expressions for the vertical electric field ( $E_z$ ) and the azimuthal magnetic field ( $H_\phi$ ) at any ground point  $P(r, \phi, 0)$  in free space due to a vertical dipole antenna of infinitesimal length  $dz'$  (placed above perfectly conducting plane), located along the  $z$  axis at a height of  $z'$  meters are given by (8.1) and (8.2), respectively (see appendix C for derivation) [56,98]:

$$\begin{aligned}
 dE_z(r, \phi, z, z', t) = & \\
 & \frac{dz'}{2\pi\epsilon_0} \left[ \frac{2(-z')^2 - r^2}{R^5} \int_{R/c}^t i(z', \tau - R/c) d\tau \right. \\
 & + \frac{2(-z')^2 - r^2}{cR^4} i(z', t - R/c) \\
 & \left. - \frac{r^2}{c^2 R^3} \frac{\partial i(z', t - R/c)}{\partial t} \right] \quad (8.1)
 \end{aligned}$$

$$dH_{\phi}(r, \phi, z, z', t) = \frac{dz'}{2\pi} \left[ \frac{r}{R^3} i(z', t - R/c) + \frac{r}{cR^2} \frac{\partial i(z', t - R/c)}{\partial t} \right] \quad (8.2)$$

The variables in (8.1) and (8.2) represent the following:

- $r, \phi$  are the cylindrical horizontal coordinates of the point of observation
- $R$  is the distance from the source (the infinitesimal current element) to the observation point,  $R$  is given by:  $R = \sqrt{r^2 + (z' - z)^2}$
- $z$  is the height of observation point above ground level (in this case  $z = 0$  m) and  $z'$  is the height at which the elemental dipole is placed above ground level
- $c$  is the speed of light ( $3 \times 10^8$  m/s) while  $\epsilon_0$  is the permittivity of free space  $8.854 \times 10^{-12}$  F/m
- $i(z', t)$  is the current distribution in the channel and the CN Tower at height  $z'$  and time  $t$ .

The first term in (8.1) for the vertical electric field (proportional to  $1/R^5$ ) is the electrostatic field term, the second term (proportional to  $1/R^4$ ) is the induction field term and the third term (proportional to  $1/R^3$ ) is the radiation field term. In equation (8.2), which represents the azimuthal magnetic field, the first term (proportional to  $1/R^3$ ) is the induction field term while the second term (proportional to  $1/R^2$ ) is the radiation field term. In the far-field region (i.e. when the height of the antenna is much less than the distance from the antenna to the observation point) only the radiation terms of the electric and magnetic fields are significant. In case of the CN Tower, which is located 2.0 km

from the electromagnetic field sensors, all three terms of the electric field and both terms of the magnetic field will be taken into account, as the distance from the Tower to the field sensors is not quite large enough. For comparison purposes, fields due to CN Tower lightning evaluated using only the radiation components of the magnetic and electric fields will be also presented. Equations (8.1) and (8.2) take into consideration the electric and magnetic fields due to the antenna as well as its image. The comparison between the vertical electric field and azimuthal magnetic field, measured 2.0 km north of the CN Tower, and the simulated electric and magnetic fields using the derivative of the modified Heidler function is presented in the next sections of this chapter.

## **8.2 CALCULATION OF THE ELECTRIC AND MAGNETIC FIELDS USING A SINGLE SECTION TL REPRESENTATION**

As with every model a proper validation of the model is required. In case of lightning return-stroke current model the first step in the validation is the comparison between the lightning current and current derivative obtained from the measurements with those obtained from simulation. The second step in the proper validation is to compare the measured electric and magnetic fields with those obtained from modelling. In this part of the thesis, the electric and magnetic fields measured at 2.0 km north of the CN Tower will be compared with the electric and magnetic fields obtained using the proposed simulation function (the derivative of the modified Heidler function) and single section transmission line representation of the CN Tower. First, only the radiation component of the vertical electric field ( $E_z$ ) and the azimuthal magnetic field ( $H_\phi$ ) are used for the comparison. Next, a more detailed comparison (all three terms of the electric

field and both terms of the magnetic field are used) is carried out. To simulate the radiated electric and magnetic fields, the contributions from both the CN Tower and the lightning channel are taken into account. In the simulation, for the current propagation in the CN Tower, the speed of propagation is equal to the speed of light  $c$ , while for the propagation of the initial current wave in the lightning return-stroke channel, where the speeds of the return-stroke range between  $1/3$  and  $2/3$  speed of light, the speed of  $0.5c$  is used, where  $c$  is the speed of light in vacuum,  $3 \times 10^8$  m/s. The reflections from the tower's structural discontinuities, which are passed through the tip to the channel in the upward direction, are assumed to travel in the channel at the speed of light [57,58,71,78]. In order to evaluate the electric and magnetic fields, the expressions for  $di(z,t)/dt$  and  $i(z,t)$  in the CN Tower and along the lightning channel are determined. Taking into account only the reflections from the ground and the tip of the CN Tower in the evaluation of the electric and magnetic fields, the expressions for the current distribution along the CN Tower and along the lightning return-stroke channel are given by (8.3) and (8.4), respectively. Similarly the expressions for the distribution of lightning current derivative along the CN Tower and along the lightning return-stroke channel are given by (8.5) and (8.6), respectively [6,56,63,99]. The speed of propagation in the CN Tower is taken to be the speed of light in vacuum while the speed of propagation of the initial current wave in the channel is taken to be  $v$  ( $0.5c$ ) [62,70,71]. The variable  $v_{ref}$  represents the speed of upward propagating current wave that is reflected from the ground and then transmitted to the channel. This speed will be taken to be the same as  $c$ . In (8.3)-(8.6),  $\rho_g$  is the ground reflection coefficient while  $\rho_t$  is the reflection coefficient at the tip of the CN Tower,  $i_o(t)$  is the return-stroke current pulse that is injected at the tip of the CN Tower

and is not contaminated with any reflections, similarly  $di_o(t)/dt$  is the return-stroke current derivative pulse injected at the tip of the CN Tower and is not contaminated with any reflections. The current  $i_o(t)$  and the current derivative  $di_o(t)/dt$  in (8.3) to (8.6) represent the simulated waveforms that have been matched to the actual waveforms obtained from measurements.

$$i(z,t) = \sum_{n=0}^{\infty} \left[ \rho_g^n \rho_t^n i_o \left( t - \frac{h-z}{c} - \frac{2nh}{c} \right) + \rho_g^{n+1} \rho_t^n i_o \left( t - \frac{h+z}{c} - \frac{2nh}{c} \right) \right] \quad (8.3)$$

$$i(z,t) = i_o \left( t - \frac{z-h}{v} \right) + \sum_{n=1}^{\infty} \left[ \rho_g^n \rho_t^{n-1} (1 + \rho_t) i_o \left( t - \frac{z-h}{v_{ref}} - \frac{2nh}{c} \right) \right] \quad (8.4)$$

$$\partial i(z,t) / \partial t = \sum_{n=0}^{\infty} \left[ \begin{aligned} & \rho_g^n \rho_t^n \partial i_o \left( t - \frac{h-z}{c} - \frac{2nh}{c} \right) / \partial t \\ & + \rho_g^{n+1} \rho_t^n \partial i_o \left( t - \frac{h+z}{c} - \frac{2nh}{c} \right) / \partial t \end{aligned} \right] \quad (8.5)$$

$$\partial i(z,t) / \partial t = \partial i_o \left( t - \frac{z-h}{v} \right) / \partial t + \sum_{n=1}^{\infty} \left[ \rho_g^n \rho_t^{n-1} (1 + \rho_t) \partial i_o \left( t - \frac{z-h}{v_{ref}} - \frac{2nh}{c} \right) / \partial t \right] \quad (8.6)$$

It should be pointed out that the simulated current used to evaluate the electric and magnetic fields has to be shifted to the tip of the CN Tower as the original simulated current is referenced to the Rogowski coil location (474 m above ground level). The shift is necessary since (8.1) to (8.6) have been derived based on the assumption that the current is injected at the tip of the tall structure.

The three components of the electric field due to contribution from the CN Tower (electrostatic, induction and radiation) simulated using the proposed simulation function

based on the derivative of the modified Heidler function are shown in Figure 8.2. The results shown in Figure 8.2 do not include any reflections from structural discontinuities of the CN Tower. Similarly the two components of the magnetic field (induction and radiation) due to the contribution from the CN Tower are shown in Figure 8.3. The following values of the parameters have been used to simulate the waveforms shown in Figures 8.2 and 8.3:  $r = 2000$  m,  $t = 0 - 15$   $\mu$ s, speed of propagation in the CN Tower is equal to speed of light in vacuum,  $v = c$ . From Figures 8.2 and 8.3, it can be seen that the radiation components of the simulated electric and magnetic fields are the dominant components. For example, the initial peak of the radiation component of the simulated electric field is 283.5 V/m at 7.6  $\mu$ s while the electrostatic and induction components of the simulated electric field are 11.93 V/m and 0.31 V/m, respectively, at the same time instant. In percentages, the induction component of the simulated electric field is only 4.21% of the radiation component. The electrostatic term of the simulated electric field is only 0.11% of the radiated term. The electrostatic and induction components of the simulated fields may not have large effect on the initial field peak; however, their contribution becomes more visible during later part of the waveform. For example, at a time instant of 8.6  $\mu$ s the electrostatic, induction and radiation components of the simulated electric field are 4.97 V/m, 49.43 V/m and 237.61 V/m, respectively. At 8.6  $\mu$ s the induction component of the simulated electric field is 20.80% of the radiation component while the electrostatic component is 2.1% of the radiation component. As one can see, the induction and radiation components of the electric field and induction component of the magnetic field become more significant during the decaying portion of the field waveforms (after the initial field peak). For CN Tower fields, measured 2 km

away from the tower, the electrostatic and induction components could be neglected if only the approximated field waveform is needed. However, in the modelling process there is a need to get results that are as close as possible to the experimental ones, and thus in the presented simulation all components of the electric and magnetic fields are considered.

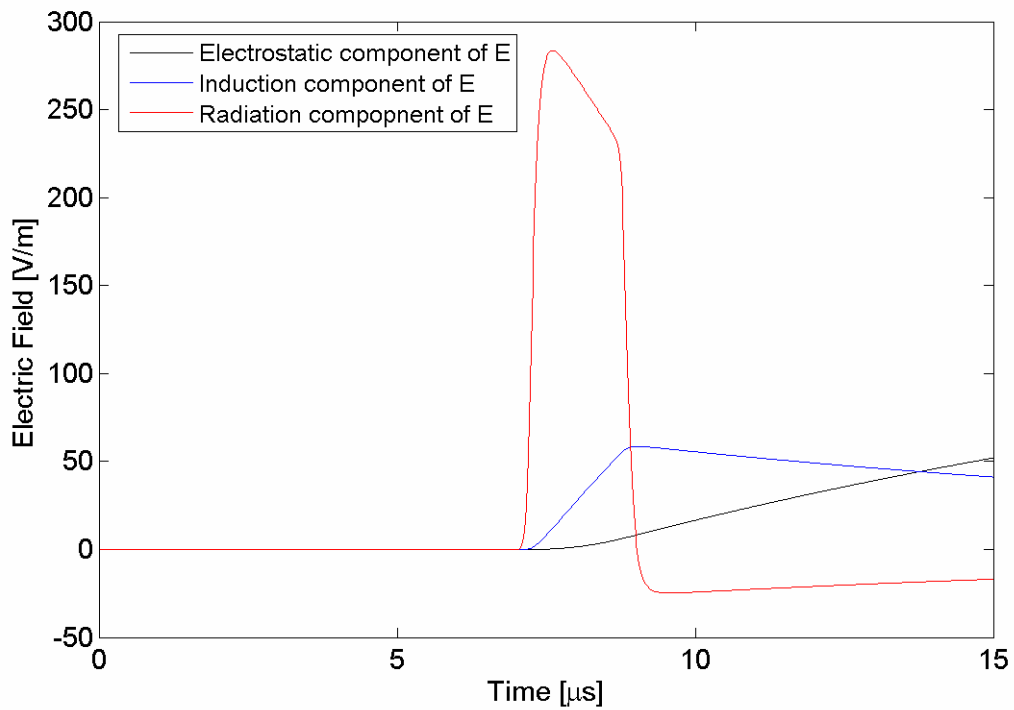


Figure 8.2. Electric field components due to the CN Tower contribution.

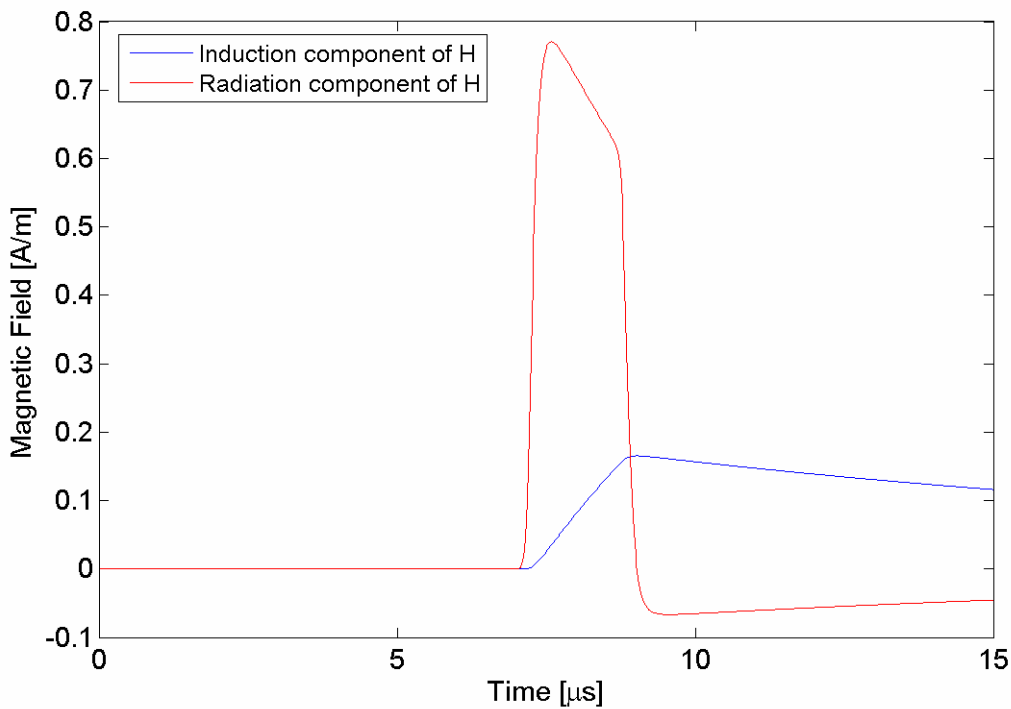


Figure 8.3. Magnetic field components due to the CN Tower contribution.

Similarly the electric and magnetic fields due to the channel contribution have been evaluated using the developed field expressions given by (8.1) and (8.2), along with expressions for the current and current derivative given by (8.4) and (8.6). The channel is assumed to be 2000 m high and the speed of propagation in the channel for the initial pulse is taken to be  $0.5c$ . The electrostatic, induction and radiation components of the simulated electric field due to the channel are shown in Figure 8.4, while the induction and radiation components of the simulated magnetic field are shown in Figure 8.5. The results shown in Figures 8.4 and 8.5 confirm again that the radiation components of both the electric and magnetic fields are dominant, while the electrostatic and induction terms have more significant effect on the later part of the electric and magnetic field waveforms.

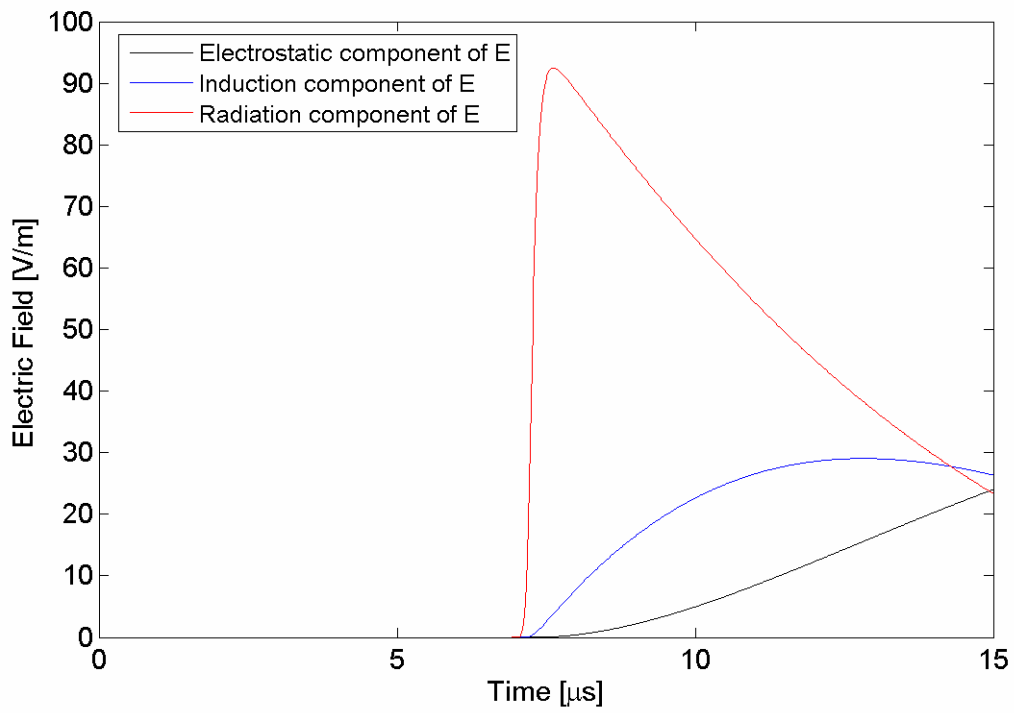


Figure 8.4. Electric field components due to channel contribution.

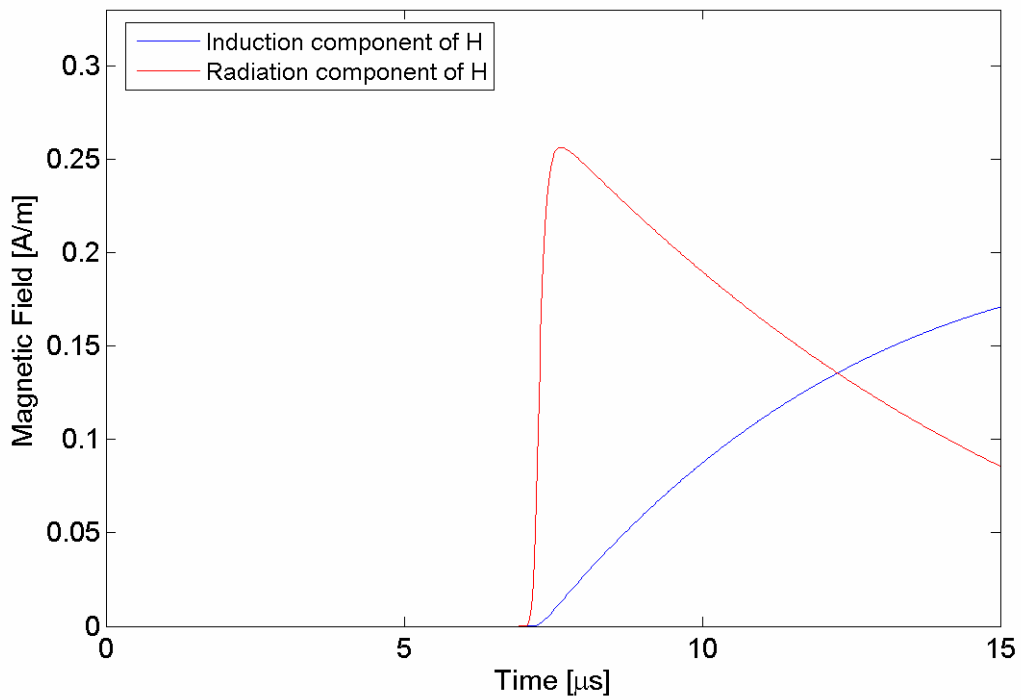


Figure 8.5. Magnetic field components due to channel contribution.

### 8.2.1 COMPARISON BETWEEN THE SIMULATED RADIATED FIELDS AND THOSE OBTAINED FROM MEASUREMENTS

In this section, the radiation components of the simulated electric and magnetic fields are compared with the actual electric and magnetic fields obtained from measurement. If we consider that the distance from the CN Tower to the point of measurement is much larger than the length of the lightning current path (antenna), the electrostatic and induction components of the electric field and induction component of the magnetic field become negligible in comparison to the radiation component, i.e. we are in the field in far-field region. The CN Tower with a height of 553 m is about 4 times smaller than the distance from the CN Tower to the measurement equipment (2000 m). It is shown that contribution of the electrostatic and induction components is not very significant at a distance of 2.0 km from the CN Tower; however it should not be ignored as it may not have a significant effect on the initial peak of the electric or magnetic field but it has a significant effect on the later portion of the electric and magnetic field waveforms. The radiated component of the simulated electric field due to the CN Tower and 2 km long lightning channel contributions and accounting for reflections from the ground and the tip of the CN Tower is shown in Figure 8.6. For calculations the lightning channel was assumed to be uniform, 2 km long and the speed of the propagation in the channel was assumed to be  $0.5c$  for the initial current wave. The speed of propagation for reflections passed through the tip of the tower to the channel was assumed to be  $c$ . The reflection coefficients at the tip of the CN Tower and at the ground were assumed to be constant, and not dependent on frequency, their values were found to be  $\rho_t = -0.3268$  and  $\rho_g = 0.4848$ , respectively. For comparison, the measured electric field is also shown

in Figure 8.6. The radiated component of the simulated magnetic field (CN Tower and channel contributions) is shown in Figure 8.7. The measured electric field is also shown in Figure 8.7. The simulated fields shown in Figures 8.6 and 8.7 are shifted in order to align the initial peaks of the simulated and measured fields. The initial peak of the simulated radiation component of electric field is about 5.74 times lower than the measured initial peak of the electric field, 376.01 V/m and 2158.0 V/m, respectively. Similarly, the initial peak of the simulated radiation component of the magnetic field is about 2.73 times lower as compared to the measured one, 1.0266 A/m versus 2.0874 A/m, respectively (Fig. 8.7). The measured magnetic field waveform has a double peak (Fig. 8.7), which could be possibly related to unknown reflection that is unaccounted for in the simulation. A comparison of the total simulated lightning electric and magnetic field using the single section TL representation of the CN Tower is presented next.

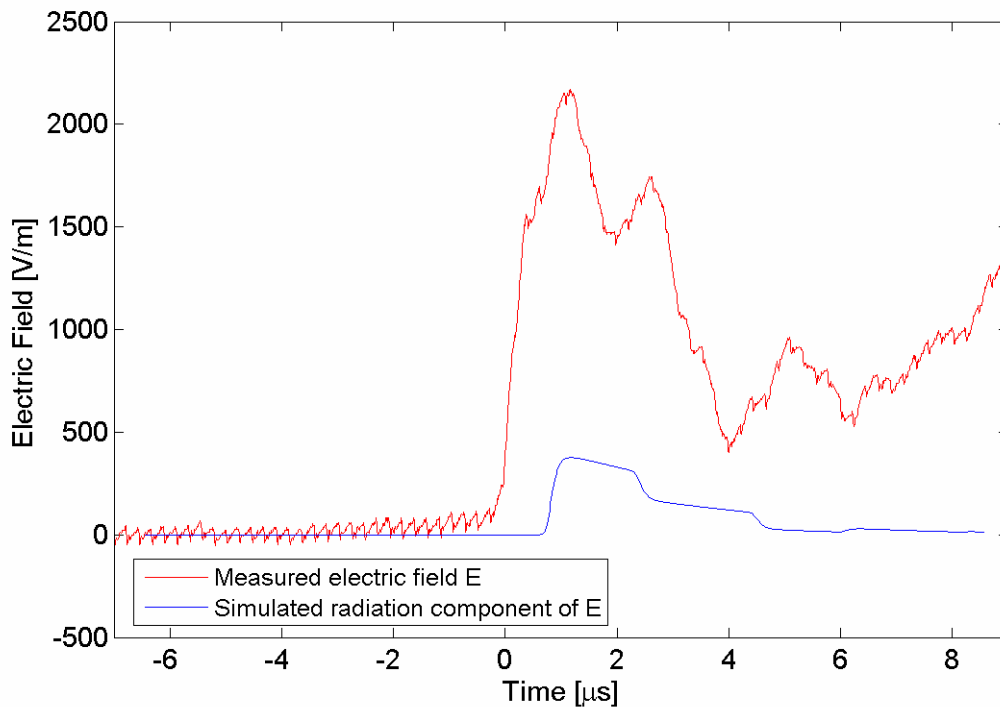


Figure 8.6. Measured electric field versus simulated radiation component of the electric field (CN Tower and channel contributions).

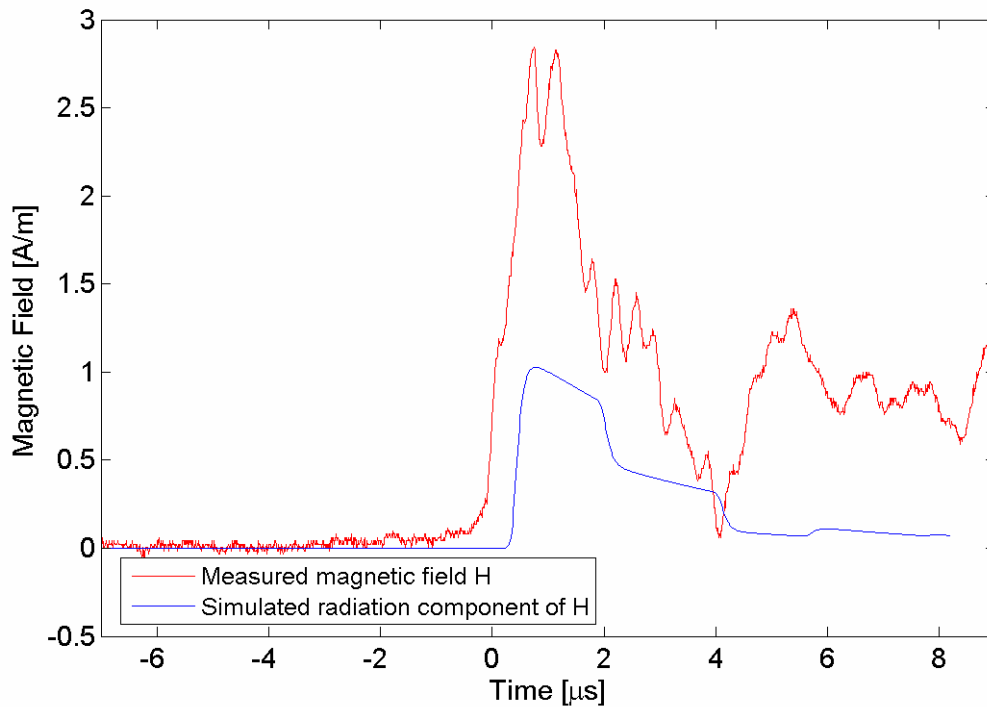


Figure 8.7. Measured magnetic field versus simulated radiation component of the magnetic field (CN Tower and channel contributions).

## 8.2.2 COMPARISON BETWEEN THE SIMULATED TOTAL ELECTRIC AND MAGNETIC FIELDS

In order to improve the accuracy of the results for the simulated LEMP the electrostatic, induction and radiation components in case of the electric field and induction and radiation components in case of the magnetic field should be included regardless of the distance from the vertical antenna to the point of observation. Figure 8.8 shows the simulated electric field (including electrostatic, induction and radiation components) versus the measured electric field. Similarly the simulated magnetic field (including induction and radiation components) and the measured magnetic field waveforms are shown in Figure 8.9. The initial peak of the simulated electric field is

about 5.46 times lower than the actual initial peak of the electric field obtained from measurements, 395.4 [V/m] versus 2158.0 [V/m]. It can be also noticed that the simulated electric field shown in Figure 8.8 has much flatter decaying portion of the waveform as opposed to the simulated electric field shown in Figure 8.6. This difference is mainly due to presence of the electrostatic component, which has been included in the waveform shown in Figure 8.8. The initial peak of the simulated magnetic field (Fig. 8.9) is about 2.59 times lower than the initial peak of the measured magnetic field, 1.0825 A/m versus 2.8074 A/m. In addition the simulated magnetic field shown in Figure 8.9 also has a flatter decaying part of the waveform but not as pronounced as in the case of the electric field. Slight fluttering of the magnetic field after the initial peak is due to the presence of the induction component. The electrostatic and induction field components do not have very significant effect on the initial field peaks but they should be not ignored as they have significant contribution to the decaying part of the electric and magnetic field waveforms. The presented simulation results illustrate that a single section TL representation is not sufficient to model such a complex structure as the CN Tower. The simulated field peaks are much lower (approximately 5.5 times lower in case of electric field and 2.6 times lower in case of magnetic field) in comparison to the ones obtained from the measurements.

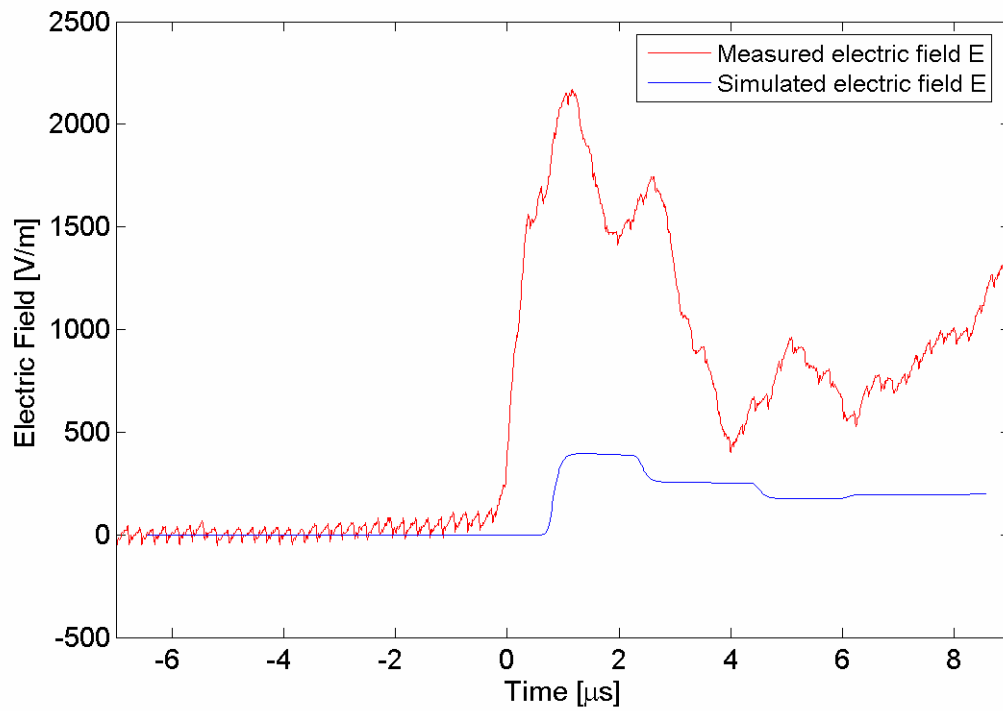


Figure 8.8. Measured electric field versus simulated total electric field (CN Tower and channel contributions).

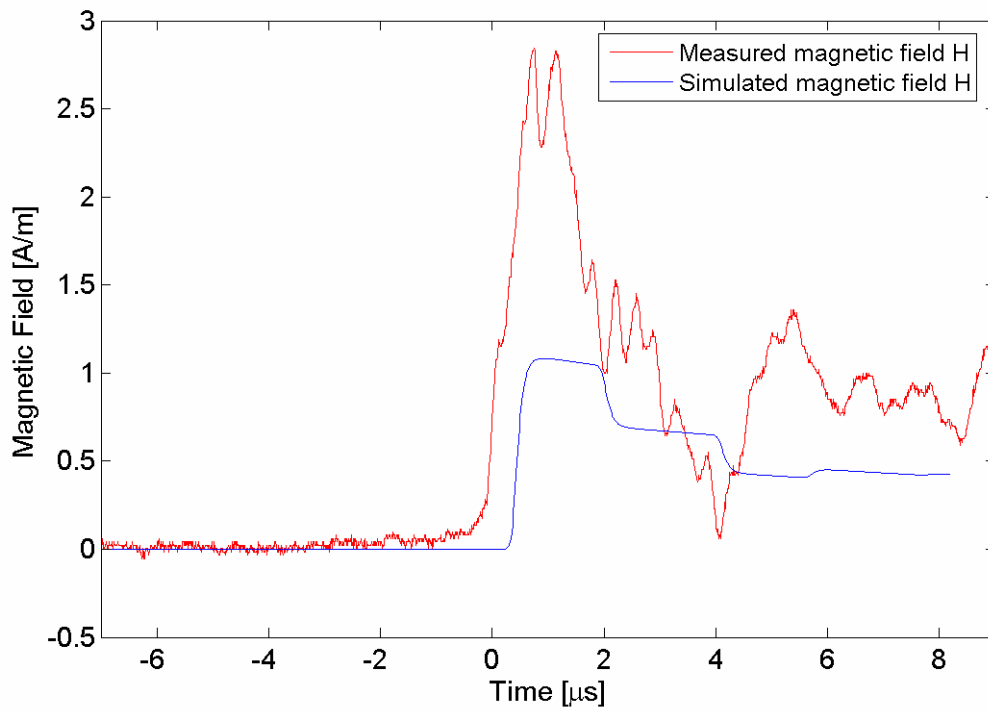


Figure 8.9. Measured magnetic field versus simulated total magnetic field (CN Tower and channel contributions).

### **8.3 COMPARISON BETWEEN THE SIMULATED TOTAL ELECTRIC AND MAGNETIC FIELDS (3-SECTION TL REPRESENTATION)**

The simulation results presented in previous sections for electric and magnetic fields using single section TL representation of the CN Tower show that the single section model does not accurately represent the CN Tower. The initial peak of the simulated electric field is only 18.3 % of the one obtained from measurements. Similarly the initial peak of the simulated magnetic field is only 38.6 % of the measured one. In order to improve the field simulation results, a 3-section TL model of the CN Tower is used to find the simulated electric and magnetic fields. In a 3-section TL model of CN Tower the first section of the transmission line is inserted between tip of the CN Tower and the top of the restaurant, the second section of the transmission line is inserted between the top and bottom of the restaurant and the third section of the transmission line is inserted between the bottom of the restaurant and ground. As in a single section TL representation of the CN Tower the speed of propagation in the Tower is assumed to be equal to speed of light,  $c$ , the channel is assumed to be uniform and 2 km long, the speed of propagation of the initial wave in the channel is assumed to be equal to  $0.5c$  while the speed of propagation of the reflections passed to the channel is assumed to be equal to  $c$ . The developed current equations that are used to represent the lightning current in the CN Tower and the lightning channel for a 3-section TL representation of the Tower are given in Appendix D. The reflections from four main structural CN Tower's discontinuities (tip of the Tower, top and bottom of the restaurant and ground) are included in the simulation and their values are given in Table 7.6.

The comparison between the simulated electric field using 3-section TL representation of the CN Tower and the measured vertical component of the electric field ( $E_z$ ) is shown in Figure 8.10. Figure 8.11 shows the comparison between the simulated electric field with and without electrostatic component included. The results shown in Figure 8.10 illustrate a significant improvement in the electric field obtained from simulation using 3-section TL representation of the CN Tower as oppose to using just a single section TL representation. The initial peak of the simulated electric field shown in Figure 8.10 is 886.9 [V/m] while the initial peak of the electric field obtained from measurements is 2158.0 [V/m]. The initial peak of the simulated electric field is 41% of the measured one. Also, the contribution of the electrostatic component is visible in the later part of the simulated electric field (after 5  $\mu$ s). The contribution of electrostatic component can be clearly seen in Figure 8.11. Figure 8.12 shows the comparison between the simulated magnetic field (3-section TL model) and the actual azimuthal magnetic field ( $H_\phi$ ) obtained from measurements. A significant improvement is also seen in the simulated magnetic field when using a 3-section TL representation of the CN Tower as opposed to just a single section TL representation. The initial peaks of the simulated and measured magnetic fields are 2.4105 [A/m] and 2.8074 [A/m], respectively. The initial peak of the simulated magnetic field is 86% of the one obtained from measurements. The simulation results obtained for the magnetic field are much closer to the actual results obtained from measurements as opposed to the simulation results obtained for the electric field. Simulation could not reproduce the double peak that is seen in the measured magnetic field waveform. This peak is thought to be a result of some kind of reflection that occurs before the current wave arrives at top of the restaurant [100]. In other studies

done with CN Tower data as well as data from other structures and rocket-triggered lightning it was also found that the simulated electric field is much smaller as compared to electric field obtained from measurements. The simulated magnetic field on the other hand was closer to the actual field obtained from measurements [67,82,101-102]. The larger discrepancy between the simulated and measured electric field as oppose to the simulated and measured magnetic field can be attributed in part to field enhancement factor due to the presence of the building on which the field sensors are installed. The field enhancement factor has a very significant effect on the measured electric field and it also affects the measured magnetic field but to a lesser degree [55, 82, 101-102]. The developed lightning return-stroke model based on the derivative of the modified Heidler function and 3-section TL representation of the CN Tower greatly improves the simulation results for the magnetic field in comparison to lightning return-stroke current models used in the past. The results obtained for the simulated electric field, which is very much influenced by the building's field enhancement factor, are slightly improved in comparison to the ones obtained from the models developed in the past. The correct estimation of the magnetic field peak is very important if one wants to correctly estimate the current peak. Lightning detection networks such as NALDN use magnetic field peaks in their algorithms in order to estimate lightning return-stroke current peaks. The electric field peaks are used to determine the polarity of the stroke. Further discussion of the simulation results for the electric and magnetic field is presented next.

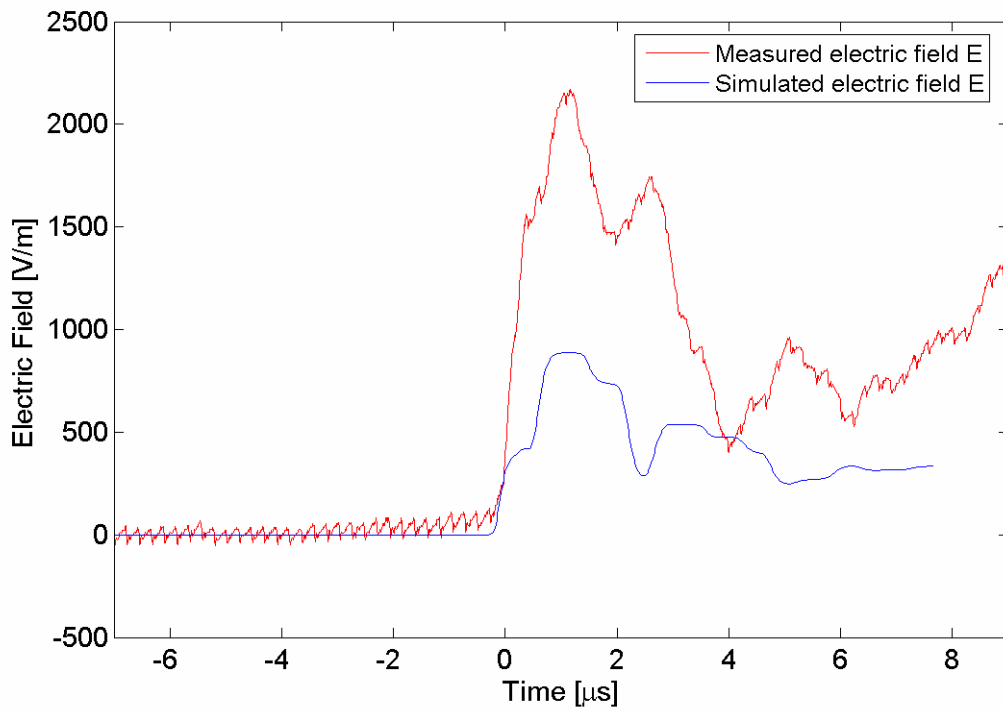


Figure 8.10. Measured electric field versus simulated total electric field (3-section TL representation, CN Tower and channel contributions).

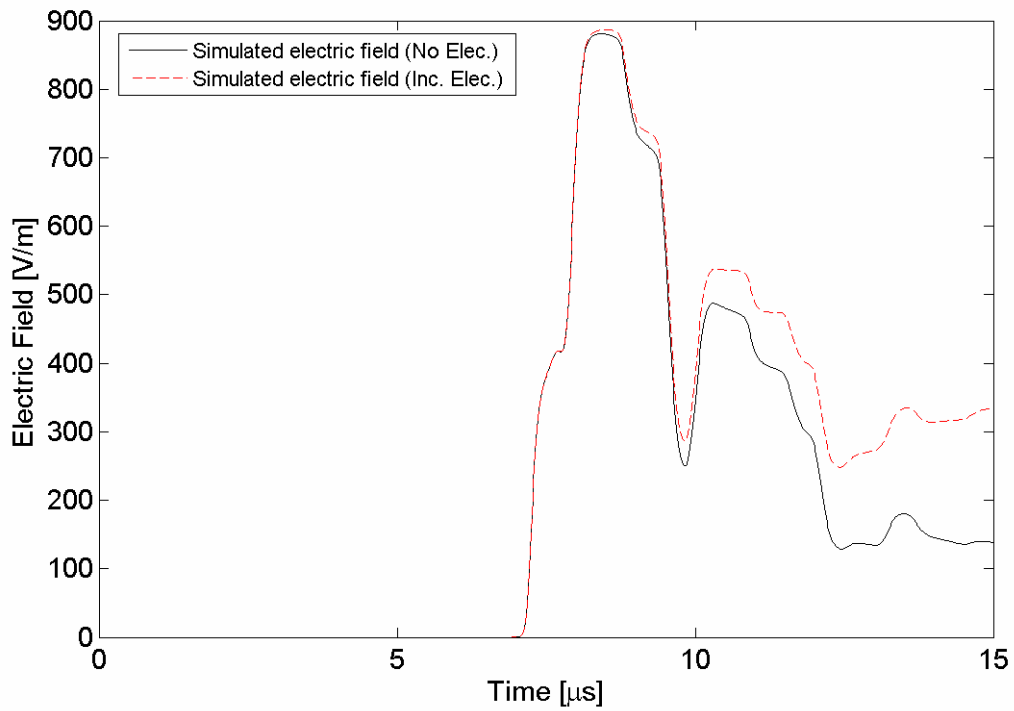


Figure 8.11. Simulated electric field with and without electrostatic component (3-section TL representation).

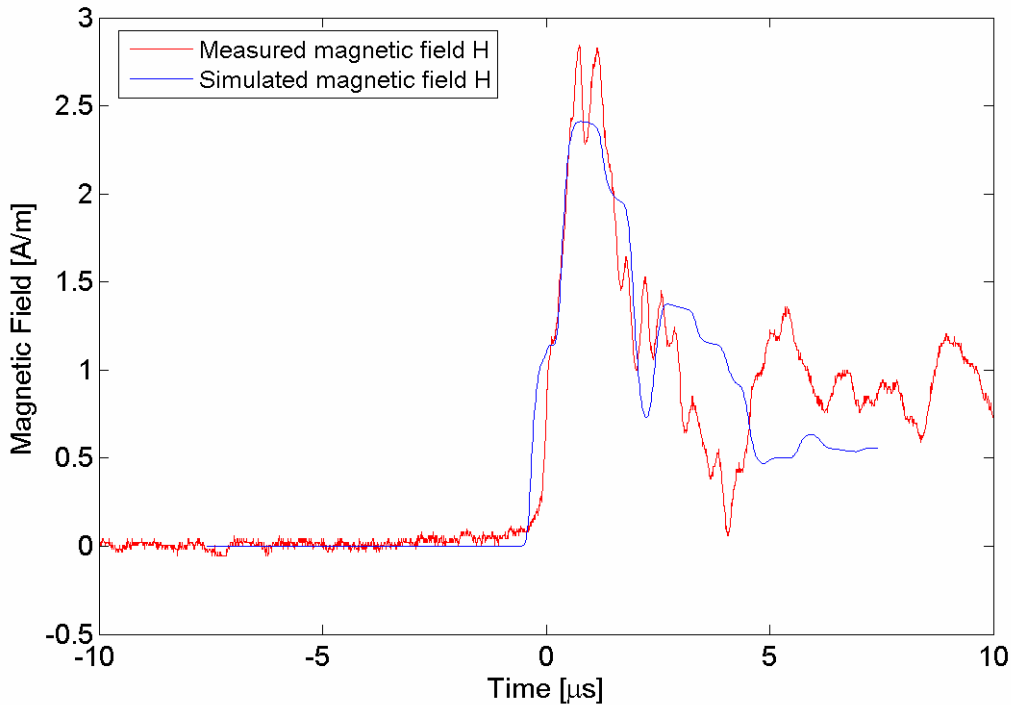


Figure 8.12. Measured magnetic field versus simulated total magnetic field (3-section TL representation, CN Tower and channel contributions).

#### 8.4 DISCUSSION

The field simulation results based on 3-section TL representation of the CN Tower show that the initial peak of the simulated electric field is about 41% of the initial peak of the measured electric field. On the other hand, the simulated magnetic field has an initial peak, which is 86 % of the initial peak obtained from measurements. It was also shown that a single section TL representation of the CN Tower is not sufficient to accurately simulate the measured LEMP. The reflections from the top and bottom of the restaurant have a significant effect on the simulated electric and magnetic fields and should not be ignored. For example, initial peaks of the simulated electric and magnetic fields obtained using a single section TL representation are 18.3% and 38.6% of the

measured ones. A 3-section TL representation of the CN Tower significantly improves the comparison between the results obtained from simulation and measurement.

In other research involving the modelling of the CN Tower it was also found that the initial peaks of the modeled electric fields are much lower in comparison to the initial peaks of the measured electric fields. In the case of the magnetic field the differences were not as pronounced. Kordi *et al.* used antenna theory model to simulate the lightning return-stroke current for the strikes to the CN Tower. In his research he found that his predicted initial electric field peaks were about 40% of the measured initial electric field peaks, while his predicted initial magnetic field peaks were about 67% of the initial magnetic field peaks obtained from measurements [67]. Rusan *et al.* using a uniform and lossless transmission line (TL) representation of the CN Tower found that the simulated magnetic fields peaks are about 25% lower than the measured magnetic field peaks [93]. In another study with CN Tower lightning data Pavanello, Bermudez *et al.* also found discrepancies between the measured and simulated electric and magnetic field peaks [87,101-102]. Pavanello, using 2005 CN Tower data along with different lightning return-stroke models, including transmission line (TL) Bruce-Golde (BG) and travelling current source model (TCS), found that the simulated initial magnetic field peaks were 75% of the measured initial magnetic field peaks [82,101-102]. In comparison, the developed 3-section TL model based on the measured current derivative and the derivative of the modified Heidler function produced the magnetic field that is much closer to the measured field. The initial peak of the simulated magnetic field is 86% of the measured one. A study of rocket triggered lightning data carried out by Thottappillil and Uman using 18 sets of simultaneously measured currents and electric fields at a

distance of 5.16 km from the lightning return-stroke channel also found that the measured electric field peaks are higher in comparison to the modeled electric field peaks [103]. In their study they used different models, including the transmission line (TL), Diendorfer-Uman (DU), travelling current source (TCS) models to predict the electric field peaks based on the measured currents. They found that the predicted electric field peaks were within an error whose mean absolute value was from 20%-40% [63,103]. The presented lightning return-stroke model as well as models, which were developed in the past underestimate the measured electric and magnetic field peaks. The main reasons for the discrepancies between the measured and simulated magnetic and electric fields are described next.

There are many reasons, which cause that the simulated electric and magnetic fields are different from the electric and magnetic fields measured 2 km north of the CN Tower. First of all, the measured current derivative may be smaller than the actual current derivative; Kordi *et al.* indicated that the measured current derivative may be in fact 10%-25% smaller than the actual current derivative [67]. The current that travels from the tip of the CN Tower could be reflected at some points above the coil location and not all the current arrives at the location of the coil. The proposed model based on the derivative of the modified Heidler function did not accurately simulate the initial stage of the measured lightning current derivative (during the first 0.175  $\mu$ s) and any errors in the estimation of the simulated current derivative will have an effect on the simulated electric and magnetic fields. The reflection coefficients were assumed to be constant and frequency independent but according to the study done by Bermudez the reflection coefficient at the tip of the tower may be frequency dependent [89,91]. Also, since the

electric and magnetic field sensors have been placed on the roof of a building, the electric and magnetic fields are enhanced by the presence of the building [5,55,87,102]. The enhancement factor of the building can be quite significant in case of the electric field. On the other hand the presence of a tall building does not have significant effect on the azimuthal component of the magnetic field [87,102,104]. For example, Rubenstein used electric field measured at ground level and on the top of 17-floor building in order to determine the enhancement factor for the measured electric field [87,104-105]. In his studies he found that the electric field measured at the top of the building could be enhanced by a factor of about 1.5 when compared to the same electric field measured at ground level [104-105]. Bermudez *et al.*, using 2005 CN Tower electromagnetic field data, which was measured on top of a 20 m high building, estimated the enhancement factor for the electric field to be about 1.4 [87]. Baba and Rakov *et al.*, using finite difference time domain method to solve Maxwell's equations, calculated the azimuthal magnetic field on the roof (flat roof, sensor placed in the middle of the roof) of the building and they found that the magnetic field is enhanced by about 10% due to the presence of a 100 m high building [55,106]. Similarly Baba and Rakov *et al.* found that the electric field due to strike to a 500 m tall tower and measured at 500 m from the tower, with sensors placed on the roof of 100 m high building, can be enhanced by a factor of about 3.3 as compared to the electric field measured at the ground level in the absence of the building [55]. In addition, they also determined that the enhancement factor for the electric field increases as the height of the building on which the sensors are placed increases. They also found a weak dependence of the enhancement of the electric field on the distance between object being struck and the building on which the sensors

are placed. For example, if one assumes 20 m high building as a reference, then electric field enhancement factors for buildings of height 50 m and 100 m will be increased by a factor of about 1.4 and 2.1, respectively [55]. Bonyadi-Ram *et al.* used theoretical methods to study the effects of tall building on the measured electric fields [107]. Bonyadi-Ram *et al.* modeled the building as a grid of conductive wires and they assumed a perfect ground. They compared the theoretical results with the measurements using field sensors placed on a roof of 25 m high building. They determined that as the height of the building (on which the sensors are placed) increases the measured electric field also increases due to building enhancement factor. In their study, Bonyadi-Ram *et al.* showed that for a 20 m, 30 m and 40 m high buildings the electric field enhancement factors can be as high as 3.46, 4.5 and 5.3, respectively. Mosaddeghi *et al.*, using electromagnetic field sensors placed on the roof of a 9 m high building as well as on the ground, 2 m from the building, found that the vertical component of the electric field and the azimuthal component of the magnetic field are enhanced by the presence of the building while the radial component of the magnetic field was nearly identical for both the roof and the ground measurements [108]. The results obtained by Mosaddeghi showed that the vertical component of the electric field measured on the roof of 9 m high building can be enhanced by a factor of 1.7-1.9. During the reporting time, the electric and magnetic field sensors were placed on the roof of the Rosebrugh building at the University of Toronto, at a height of about 20 m above ground level. The sensors have been installed on top of a rectangular box that was placed near the edge of the building. The placement of the field sensors above the ground level as well as their close proximity to the edge of the building likely contributed to the enhancement of the measured electric

field and the slight enhancement of the measured magnetic field. Using the results obtained by Baba and Rakov *et al.*, it was estimated that the enhancement factor for the CN Tower's electric fields measured on the roof of the 20 m high Roseburgh building is at least 1.6 times. In conclusion, the differences between the simulated and measured magnetic fields can be, in part, attributed to the slight enhancement of the magnetic field due to presence of the building on which the sensors are installed. For the electric field the difference between the simulation and measurement can be mainly attributed to the enhancement factor of the electric field, which can be very significant.

## **8.5 SUMMARY OF CHAPTER 8**

Quantitative assessment of any developed lightning return-stroke model is required and this assessment is conducted by comparing the simulated electromagnetic fields with the electromagnetic fields obtained from measurements. The comparison between the simulated electric and magnetic fields obtained using the developed lightning return-stroke model and the ones obtained from measurement done at 2 km north of the CN Tower is presented. Single section and 3-section TL representations of the CN Tower are used to evaluate the simulated electric and magnetic fields. A detailed discussion of the simulation results is included.

# Chapter 9

## Conclusions

The first objective of the work presented in this thesis was to experimentally correlate the wavefront parameters of CN Tower lightning return-stroke current with those of their generated electromagnetic pulse (LEMP). The second objective was to simulate the lightning return-stroke current using the derivative of the modified Heidler function. The third objective was to use a 3-section transmission line representation of the CN Tower to determine the return-stroke current along the current path in order to compute the electric and magnetic fields of LEMP. The current-field characteristic relationships as well as the developed engineering model of the lightning return-stroke current will assist in solving one of the most challenging problems in lightning research, the inverse-source problem, in which the lightning current is estimated based on the measured LEMP. The correlation between the characteristics of the lightning return-stroke current and those of its LEMP is also important in the development of lightning detection network algorithms.

The CN Tower lightning return-stroke current and its generated LEMP have been time synchronized using GPS systems with resolution of 1  $\mu$ s. A total of 6 flashes containing 36 return-strokes have been used for the correlation analyses. Least square

straight line fits (regression lines) were obtained to correlate the wavefront characteristics (peak, maximum derivative and 10%-90% risetime) of the electric and magnetic fields to each other as well as to the wavefront characteristics of the return-stroke currents. Strong linear correlations were found between the wavefront characteristics of the measured CN Tower lightning-generated electric and magnetic fields. These strong linear correlations are good indicators of the proper sensor calibrations and similar frequency responses, and thus field-current characteristic relationships concentrated on the magnetic field. The magnetic field wavefront characteristics were also found to linearly correlate to the corresponding characteristics of the current. Among these, the correlation between the magnetic field peak and current peak was found to be the strongest. Furthermore, the strong linear correlation between the magnetic field maximum derivative and the current maximum derivative indicates that there is a possibility of estimating the maximum current derivative based on the measured maximum field derivative. The high degree of correlation between wavefront characteristics of fields and currents allows for estimation of lightning return-stroke current from measured LEMP.

The developed field-current characteristic relationships were compared with those obtained from Peissenberg tower lightning data. It was shown that the results obtained from both studies were close to each other, substantiating the validity of both data sets.

To determine the spatial-temporal distribution of the lightning return-stroke current along the lightning channel and the CN Tower, the derivative of the modified Heidler function is used along with a 3-section transmission line model of the CN Tower. The measured lightning current derivative signal was simulated using the derivative of Heidler function as oppose to simulating the lightning current in earlier return-stroke

models. The simulation of the current derivative produced better matching with the measurement in comparison with the simulation of the current.

Quantitative assessment of any lightning return-stroke model requires the comparison between the computed and measured electric and magnetic fields. It was shown that the single transmission line representation of the CN Tower proved inadequate to represent the complex structure of the CN Tower. Representing the CN Tower as a 3-section transmission line greatly improved the matching between the computed and measured LEMP. In this case the computed magnetic field peak was found to be 86% of the measured peak, a substantial improvement over earlier investigations.

In future work, the simulation of the measured current derivative using the derivative of the modified Heidler function could be improved by modifying Heidler function. Taking into consideration additional reflections such as the reflection from the lightning channel front may result in closer match between the computed and measured fields. Furthermore, the use of non-uniform transmission line sections to represent the tower is expected to produce a closer resemblance between computed and measured fields.

The major research accomplishments of this work are:

1. The development of detailed field-current characteristic relationships for CN Tower lightning return-strokes.
2. CN Tower lightning field-current characteristic relationships were compared with those obtained from measurements conducted at the Peissenberg Tower in Germany.
3. Correction of the Peissenberg Tower field-current characteristic relationships.

4. The use of the derivative of the modified Heidler function to simulate the measured lightning current derivative proved to be superior than simulating the lightning current.
5. The developed 3-section transmission line model based on the measured current derivative and the derivative of the modified Heidler function produced a simulated magnetic field that is substantially closer to the measured field in comparison with previous investigations.

# Appendix A

## Calibration of Old and New Rogowski Coils

The experimental setup used for testing of the old Rogowski coil is shown in Figure A1. The current derivative and current waveforms obtained from experimental setup (Figure A1) are shown in Figures A2 and A3 respectively [31]. The old Rogowski coil was calibrated at the CN Tower on May 27, 1997 and its sensitivity was found to be  $0.351 \text{ V}/(\text{A}/\text{ns})$ . The sensitivity quoted by the manufacturer was  $0.350 \text{ V}/(\text{A}/\text{ns})$  and this indicates that the coil did not deteriorate over the years during which it was placed at the CN Tower [31].

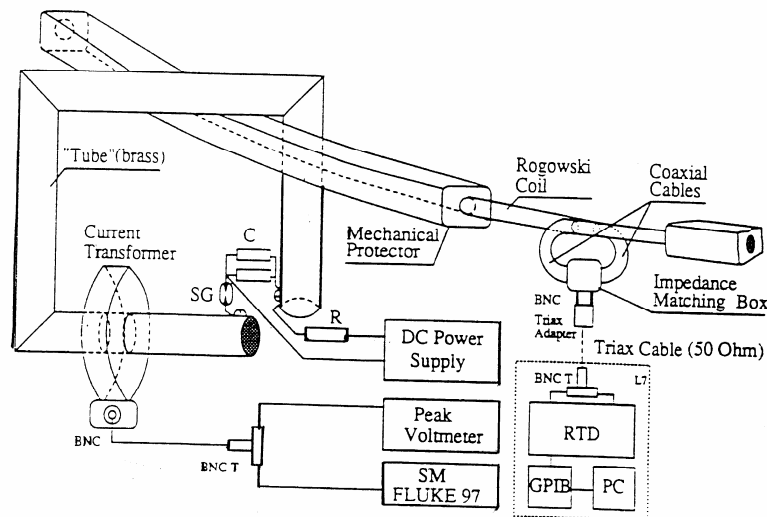


Figure A1. Experimental setup for testing of old Rogowski Coil.

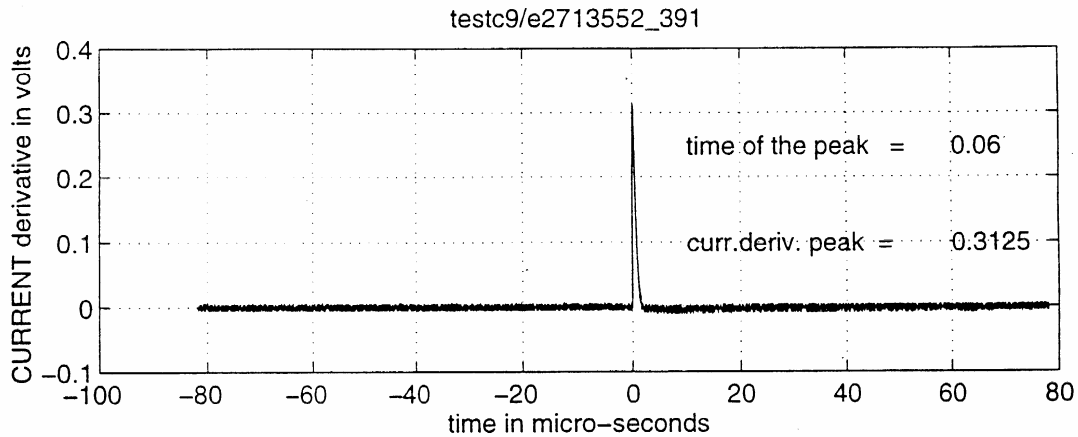


Figure A2. Output of the old Rogowski Coil.

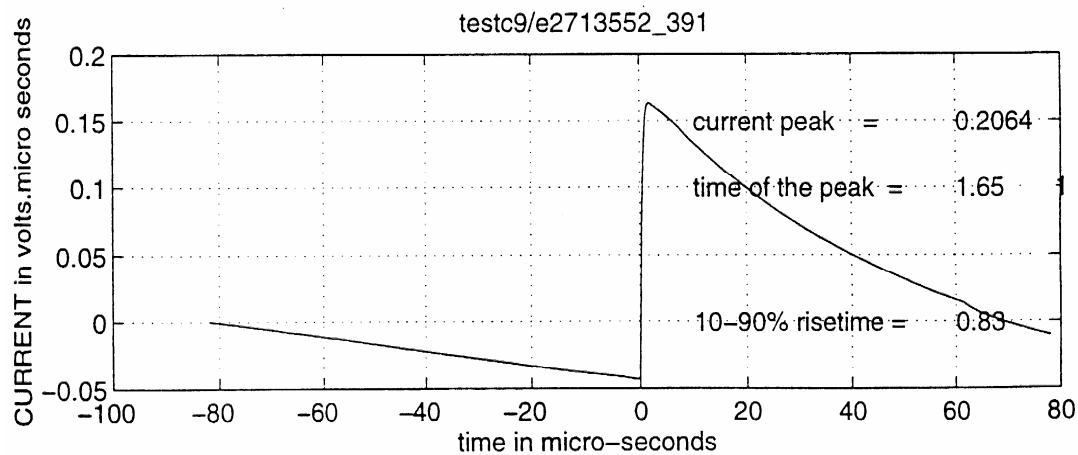


Figure A3. Time integral of the waveform shown in Figure A2.

The calibration of new Rogowski coil was performed on April 13, 1998 at Physics International, San Leandro, CA. For the calibration the coil was separated into four segments (A, B, C, D), which are normally arranged in a clockwise manner (Figure A4). The outputs from segments A+B and C+D are combined in their respective impedance matching networks (blue boxes) and then summed in a power tee. For the Rogowski coil configuration, the plastic ties marking the ends of the active regions are aligned to give a nominal major diameter of 74". The coil output is then proportional to  $dI/dt$  regardless of the location of the current threading the major loop; the output polarity is the same as the  $dI/dt$  threading the loop from behind. Other configuration of the coil that could be used is

with the segments being overlapped. The coil was calibrated using both 74" and 65" "overlapped" configurations. In the 65" configuration the B/C and A/D junctions were overlapped by an additional 14" each. The drive current was threaded through a Pearson 110 coil for reference and then fed to a pair of radial discs (aluminium foil) that enclosed the Rogowski coil. A square pulse with a risetime of few ns represented the drive current. The AB and CD matching boxes were connected to the power tee using 10-ns, 50  $\Omega$  cables. The summed signal was sent through a fast passive integrator with time constants  $RC = 4.95 \mu\text{sec}$  and the output has been displayed on a 250 MHz scope. The outputs from the scope for 74" and 65" nominal diameters of the coil are shown in Figures A5 and A6 respectively. The outputs of the Pearson 110 coil are also shown for comparison. The calibration waveforms show that the Rogowski coil has a risetime longer than that of the Pearson coil, which is specified at 20 ns [32].

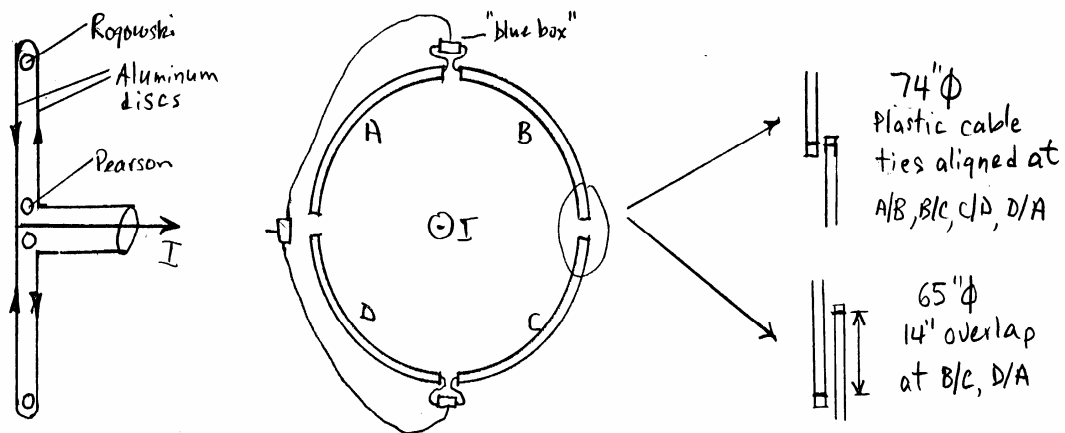


Figure A4. Setup used for calibration of the new Rogowski coil.

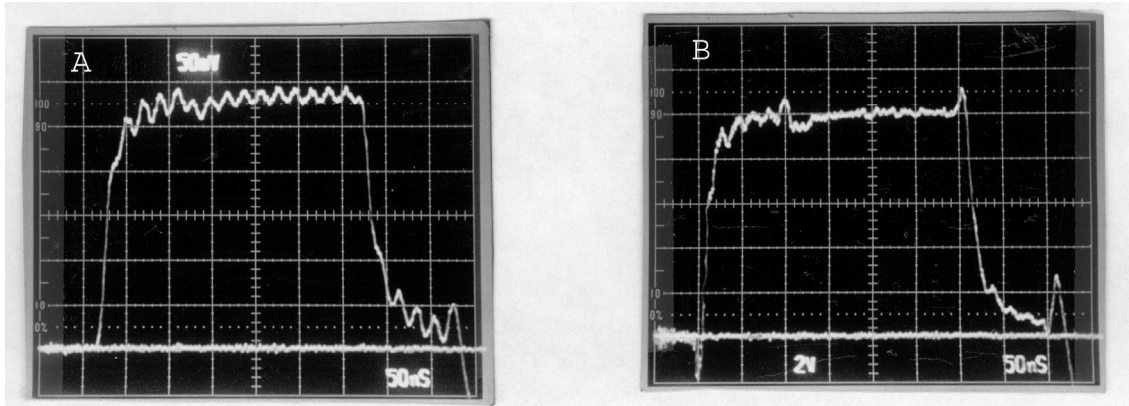


Figure A5. Outputs of the scope for Rogowski coil (Figure A5.A.) and Pearson coil (Figure A5.B.), nominal diameter of the Rogowski coil 74".

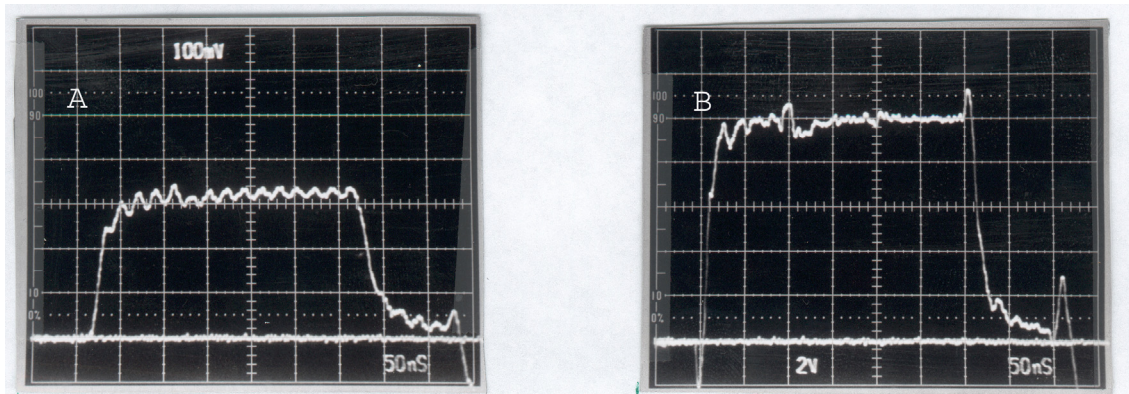


Figure A6. Outputs of the scope for Rogowski coil (Figure A6.A.) and Pearson coil (Figure A6.B.), nominal diameter of the Rogowski coil 65".

## Appendix B

### Matching Heidler Function with Measured Current Derivative

The function proposed by Heidler for a lightning current for a strike to ground is given by (B1). The derivative of Heidler function is given by (B2). In this work a summation of two Heidler functions and two Heidler derivative functions were used for modeling, these functions are shown in (B3) and (B4). Parameters  $A_1$  and  $A_2$  in (B3) and (B4) control the channel base current and current derivative amplitudes,  $\tau_1$  and  $\tau_3$  are front time constants,  $\tau_2$  and  $\tau_4$  are decay time constants while  $k_1$  and  $k_2$  are exponents with values from 1.1 to 20.

$$i(t) = A \left[ \frac{(t/\tau_1)^k e^{-t/\tau_2}}{1 + (t/\tau_1)^k} \right] \quad (\text{B1})$$

$$\frac{di(t)}{dt} = A \left( \frac{t}{\tau_1} \right)^k \exp^{-t/\tau_2} \frac{k \tau_2 - t - t \left( \frac{t}{\tau_1} \right)^k}{t \left[ 1 + \left( \frac{t}{\tau_1} \right)^k \right]^2} \quad (\text{B2})$$

$$i(t) = A_1 \left[ \frac{(t/\tau_1)^{k_1} e^{-t/\tau_2}}{1 + (t/\tau_1)^{k_1}} \right] + A_2 \left[ \frac{(t/\tau_3)^{k_2} e^{-t/\tau_4}}{1 + (t/\tau_3)^{k_2}} \right] \quad (\text{B3})$$

$$\begin{aligned}
\frac{di(t)}{dt} &= A_1 \left( \frac{t}{\tau_1} \right)^{k_1} \exp^{-t/\tau_2} \frac{k_1 \tau_2 - t - t \left( \frac{t}{\tau_1} \right)^{k_1}}{t \left[ 1 + \left( \frac{t}{\tau_1} \right)^{k_1} \right]^2} \\
&+ A_2 \left( \frac{t}{\tau_3} \right)^{k_2} \exp^{-t/\tau_4} \frac{k_2 \tau_4 - t - t \left( \frac{t}{\tau_3} \right)^{k_2}}{t \left[ 1 + \left( \frac{t}{\tau_3} \right)^{k_2} \right]^2}
\end{aligned} \tag{B4}$$

In order to reduce the number of unknown variables from eight to seven in (B4), a derivative of (B4) was taken and it was equated to zero at time  $t = t_a$ , where  $t_a$  is the time at which the maximum value of the first impulse of the measured current derivative occurs. A tedious work of eliminating one of the parameters and then matching the derivative of Heidler function to the actual measured current derivative was done, it was found that the closest results between the simulated and the measured current derivative are obtained when the parameter  $A_2$  is eliminated using second derivative of Heidler function. The derivative of (B4), which is the second derivative of (B3), is given by (B5), while the solution to  $A_2$  obtained from second derivative is given by (B6).

$$\begin{aligned}
\frac{d^2i(t)}{dt^2} &= A_1 \left\langle e^{-t/\tau_2} \right\rangle \frac{\left[ -\frac{1}{\tau_2} \left[ 1 + \left( \frac{t}{\tau_1} \right)^{k_1} \right] - \left( 2 \frac{k_1}{\tau_1} \right) \left( \frac{t}{\tau_1} \right)^{k_1-1} \right]}{1} \\
&* \frac{\left[ \left( \frac{k_1}{\tau_1} \right) \left( \frac{t}{\tau_1} \right)^{k_1-1} - \left( \frac{1}{\tau_2} \right) \left[ \left( \frac{t}{\tau_1} \right)^{k_1} + \left( \frac{t}{\tau_1} \right)^{2k_1} \right] \right]}{\left[ 1 + \left( \frac{t}{\tau_1} \right)^{k_1} \right]^3}
\end{aligned} \tag{B5}$$

$$\begin{aligned}
& + A_1 \left\langle e^{-t/\tau_2} \right\rangle \frac{\left[ \left( k_1 k_1 - 1 / \tau_1^2 \right) \left( t / \tau_1 \right)^{k_1 - 2} - \left( k_1 / \tau_1 \tau_2 \right) \left[ \left( t / \tau_1 \right)^{k_1} + 2 \left( t / \tau_1 \right)^{2k_1 - 1} \right] \right]}{\left[ 1 + \left( t / \tau_1 \right)^{k_1} \right]^2} \\
& + A_2 \left\langle e^{-t/\tau_4} \right\rangle \frac{\left[ -1 / \tau_4 \left[ 1 + \left( t / \tau_3 \right)^{k_2} \right] - \left( 2k_2 / \tau_3 \right) \left( t / \tau_3 \right)^{k_2 - 1} \right]}{1} \\
& * \frac{\left[ \left( k_2 / \tau_3 \right) \left( t / \tau_3 \right)^{k_2 - 1} - \left( 1 / \tau_4 \right) \left[ \left( t / \tau_3 \right)^{k_2} + \left( t / \tau_3 \right)^{2k_2} \right] \right]}{\left[ 1 + \left( t / \tau_3 \right)^{k_2} \right]^3} \\
& + A_2 \left\langle e^{-t/\tau_4} \right\rangle \frac{\left[ \left( k_2 k_2 - 1 / \tau_3^2 \right) \left( t / \tau_3 \right)^{k_2 - 2} - \left( k_2 / \tau_3 \tau_4 \right) \left[ \left( t / \tau_3 \right)^{k_2} + 2 \left( t / \tau_3 \right)^{2k_2 - 1} \right] \right]}{\left[ 1 + \left( t / \tau_3 \right)^{k_2} \right]^2} \\
A_2 = & \left\{ A_1 \left\langle e^{-t/\tau_2} \right\rangle \frac{\left[ -1 / \tau_2 \left[ 1 + \left( t / \tau_1 \right)^{k_1} \right] - \left( 2k_1 / \tau_1 \right) \left( t / \tau_1 \right)^{k_1 - 1} \right]}{1} \right. \\
& * \frac{\left[ \left( k_1 / \tau_1 \right) \left( t / \tau_1 \right)^{k_1 - 1} - \left( 1 / \tau_2 \right) \left[ \left( t / \tau_1 \right)^{k_1} + \left( t / \tau_1 \right)^{2k_1} \right] \right]}{\left[ 1 + \left( t / \tau_1 \right)^{k_1} \right]^3} \\
& + A_1 \left\langle e^{-t/\tau_2} \right\rangle \frac{\left[ \left( k_1 k_1 - 1 / \tau_1^2 \right) \left( t / \tau_1 \right)^{k_1 - 2} - \left( k_1 / \tau_1 \tau_2 \right) \left[ \left( t / \tau_1 \right)^{k_1} + 2 \left( t / \tau_1 \right)^{2k_1 - 1} \right] \right]}{\left[ 1 + \left( t / \tau_1 \right)^{k_1} \right]^2} \left. \right\} \\
& * \left\{ \frac{1}{\left\langle e^{-t/\tau_4} \right\rangle} \frac{\left[ 1 + \left( t / \tau_3 \right)^{k_2} \right]^3}{\left[ -1 / \tau_4 \left[ 1 + \left( t / \tau_3 \right)^{k_2} \right] - \left( 2k_2 / \tau_3 \right) \left( t / \tau_3 \right)^{k_2 - 1} \right]} \right\}
\end{aligned} \tag{B6}$$

$$\begin{aligned}
& * \left[ \frac{1}{\left(\frac{k_2}{\tau_3}\right)\left(\frac{t}{\tau_3}\right)^{k_2-1} - \left(\frac{1}{\tau_4}\right)\left[\left(\frac{t}{\tau_3}\right)^{k_2} + \left(\frac{t}{\tau_3}\right)^{2k_2}\right]} \right] \\
& + \left[ \frac{\left[1 + \left(\frac{t}{\tau_3}\right)^{k_2}\right]^3}{\left[1 + \left(\frac{t}{\tau_3}\right)^{k_2}\right]} \right] \left[ \frac{1}{\left(k_2 \frac{k_2-1}{\tau_3^2}\right)\left(\frac{t}{\tau_3}\right)^{k_2-2} - \left(\frac{k_2}{\tau_3 \tau_4}\right)\left[\left(\frac{t}{\tau_3}\right)^{k_2} + 2\left(\frac{t}{\tau_3}\right)^{2k_2-1}\right]} \right] \}
\end{aligned}$$

The solution to  $A_2$  obtained from second derivative of Heidler function given by (B5) was substituted into (B4) in order obtained the final equation of the modified derivative of Heidler function with seven unknown parameters that was used for modeling.

# Appendix C

## Lightning-Generated Electric and Magnetic Fields

Equations for the electric and magnetic fields due to a vertical lightning return-stroke channel placed above perfectly conduction ground and in free space will be derived. The symmetry of the problem is shown in Figure C1, where  $P(\rho, \varphi, z)$  is the point of observation that is located at ground level with  $(\rho, \varphi, z)$  being cylindrical coordinates of the point of observation,  $R$  is the distance from the point of observation to the differential current element,  $\rho$  is the horizontal distance from point of observation to the lightning return-stroke channel,  $H$  is the height of the channel,  $dz'$  is the length of the differential current element located at a height of  $z'$  and having a current  $i(z', t)$ . Since a perfect ground is assumed to satisfy the boundary conditions an image of lightning return-stroke channel is added below the perfectly conducting ground [56,98]. For the observer at the ground level the image current flowing in the image of the lightning return-stroke channel has the same magnitude and direction as the current flowing in the lightning return-stroke channel [56].

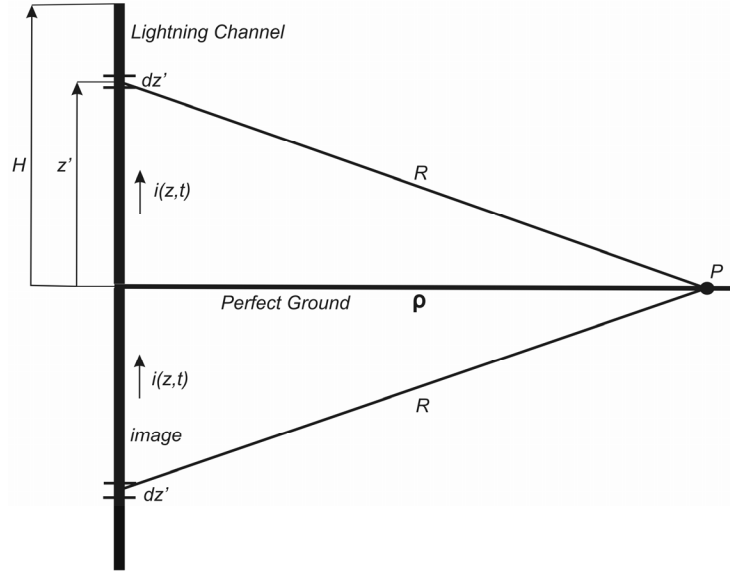


Figure C1. Geometry used for electric and magnetic field derivation due to the lightning return-stroke channel and its image.

In order to obtain the equations for radiated electric and magnetic fields due to a vertical lightning channel placed above perfectly conduction ground one must first start with Maxwell's equations [56,98]. The Maxwell's equations for time varying fields in free space are given by (C1)-(C4).

$$\nabla \times \vec{E} = -\frac{\partial \vec{B}}{\partial t} \quad (C1)$$

$$\nabla \times \vec{H} = \vec{J} + \frac{\partial \vec{D}}{\partial t} \quad (C2)$$

$$\nabla \cdot \vec{D} = \rho_v \quad (C3)$$

$$\nabla \cdot \vec{B} = 0 \quad (C4)$$

Magnetic flux density  $\vec{B}$  can be expressed in terms of vector magnetic potential  $\vec{A}$  (equation C5). Substituting magnetic flux density  $\vec{B}$  into (C2) a new equation C6 for curl of  $\vec{B}$  is obtained. Equations (C1)-(C6) will be used to derive the expression for the vector magnetic potential  $\vec{A}$ .

$$\vec{B} = \nabla \times \vec{A} \quad (C5)$$

$$\nabla \times \vec{B} = \mu \vec{J} + \mu \epsilon \frac{\partial \vec{E}}{\partial t} \quad (C6)$$

$$\nabla \times \vec{E} = -\frac{\partial \vec{B}}{\partial t} = -\frac{\partial (\nabla \times \vec{A})}{\partial t} \quad (C7)$$

$$\nabla \times \left( \vec{E} + \frac{\partial \vec{A}}{\partial t} \right) = 0 \quad (C8)$$

$$\vec{E} + \frac{\partial \vec{A}}{\partial t} = -\nabla V \quad (C9)$$

Substituting (C5) into (C6) a following equation is obtained:

$$\nabla \times \nabla \times \vec{A} = \mu \vec{J} + \mu \epsilon \frac{\partial \vec{E}}{\partial t} \quad (C10)$$

Using vector identity  $\nabla \times \nabla \times \vec{A} = \nabla(\nabla \cdot \vec{A}) - \nabla^2 \vec{A}$  and solving (C9) for  $\vec{E}$  and then substituting the result into (C10), an expression for vector magnetic potential  $\vec{A}$  can be obtained (equation C12).

$$\nabla(\nabla \cdot \vec{A}) - \nabla^2 \vec{A} = \mu \vec{J} - \mu \epsilon \frac{\partial}{\partial t} \nabla V - \mu \epsilon \frac{\partial^2 \vec{A}}{\partial t^2} \quad (C11)$$

$$\nabla^2 \vec{A} - \mu \epsilon \frac{\partial^2 \vec{A}}{\partial t^2} = -\mu \vec{J} + \nabla \left( \nabla \cdot \vec{A} + \mu \epsilon \frac{\partial V}{\partial t} \right) \quad (C12)$$

The expression for vector magnetic potential given by (C12) can be simplified using

Lorentz's condition which states that  $\nabla \cdot \vec{A} = -\mu \epsilon \frac{\partial V}{\partial t}$  and the simplified expression for

vector magnetic potential is given by (C13).

$$\nabla^2 \vec{A} - \mu \epsilon \frac{\partial^2 \vec{A}}{\partial t^2} = -\mu \vec{J} \quad (C13)$$

$\vec{J}$  represents the current density due to sum of conduction current, convection current and impressed current sources. Assuming a free space region where  $\mu = \mu_o$  and  $\varepsilon = \varepsilon_o$  equation (C13) can be rewritten as follows:

$$\nabla^2 \vec{A} - \mu_o \varepsilon \frac{\partial^2 \vec{A}}{\partial t^2} = -\mu \vec{J}_i \quad (\text{C14})$$

where  $\vec{J}_i$  represents the impressed current density. The simplest solution to (C14) can be obtained by considering infinitesimal current element with location specified by position vector  $\vec{r}'$ . The geometry of the solution for (C14) is shown in Figure C2.  $\vec{r}'$  represents a vector from origin to the location of the infinitesimal current element,  $\vec{r}$  represents a vector from the origin to the point of observations (point at which  $\vec{A}$  is to be evaluated),  $\vec{R} = \vec{r} - \vec{r}'$  is the vector from the current source to the point of observation.

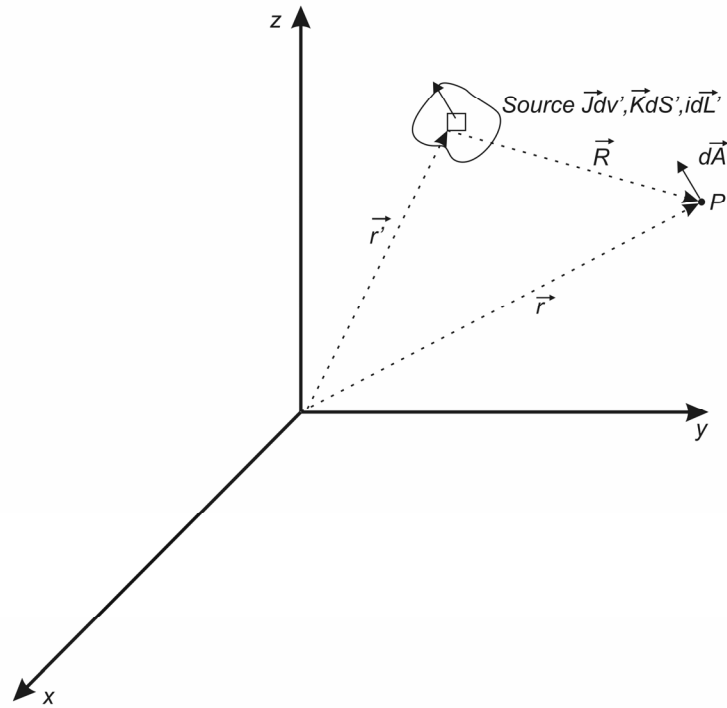


Figure C2. Geometry used to obtain general solutions for vector magnetic potential  $\vec{A}$ .

The infinitesimal current element can be considered to be a volume current element,  $\vec{J}_i dv'$ , surface current element  $\vec{K} dS'$  or a line current element  $I d\vec{L}$  where  $\vec{J}$  is the volume current density,  $\vec{K}$  is the surface current density and  $I$  is the line current density. The solutions to (C14) using different current element (volume, surface and line) are given by (C15)-(C17).

$$d\vec{A} = \frac{\mu_o [\vec{J}] dv'}{4\pi |\vec{r} - \vec{r}'|} \quad (C15)$$

$$d\vec{A} = \frac{\mu_o [\vec{K}] dS'}{4\pi |\vec{r} - \vec{r}'|} \quad (C16)$$

$$d\vec{A} = \frac{\mu_o [i] d\vec{L}}{4\pi |\vec{r} - \vec{r}'|} \quad (C17)$$

To obtain expression for lightning generated electromagnetic fields at point of observation located at ground level and at a horizontal distance of  $\rho$  from the lightning return-stroke channel a geometry shown in Figure C1 will be used along with (C17). For a geometry shown in Figure C1 parameters  $\vec{r}$ ,  $\vec{r}'$  and  $d\vec{L}$  can be expressed as follows:

$$\vec{r}' = \rho \vec{a}_\rho, \quad \vec{r}' = z' \vec{a}_z, \quad d\vec{L} = dz' \vec{a}_z,$$

$$\vec{R} = \vec{r} - \vec{r}' = \rho \vec{a}_\rho - z' \vec{a}_z, \quad R = |\vec{r} - \vec{r}'| = \sqrt{(\rho^2 + z'^2)}$$

The derivative of vector magnetic potential in a direction of  $z$  is obtained using (C17) and it is given by (C18) while the derivative of magnetic field is given by (C19).

$$dA_z = \frac{\mu_o}{4\pi R} i \left( z', t - \frac{R}{c} \right) dz' \quad (C18)$$

$$d\vec{H} = \frac{1}{\mu_o} \nabla \times d\vec{A} = \frac{-dz'}{4\pi} \left[ \frac{1}{R} \frac{\partial i}{\partial \rho} - \frac{i}{R^2} \frac{\partial R}{\partial \rho} \right] \vec{a}_\phi \quad (C19)$$

$$R^2 = \rho^2 + z'^2, \quad 2R \frac{\partial R}{\partial \rho} = 2\rho, \quad \frac{\partial R}{\partial \rho} = \frac{\rho}{R}, \quad \frac{\partial i}{\partial \rho} = \frac{\partial i}{\partial R} \frac{\partial R}{\partial \rho} = \frac{\rho}{R} \frac{\partial i}{\partial R}$$

$$\frac{\partial i}{\partial R} = \frac{\partial i}{\partial(t-R/c)} \frac{\partial(t-R/c)}{\partial R} = -\frac{1}{c} \frac{\partial i}{\partial(t-R/c)} \quad (\text{C20})$$

Since “ $i$ ” is always a function of  $(t-R/c)$  than  $\frac{\partial i}{\partial t} = \frac{\partial i}{\partial(t-R/c)}$  and  $\frac{\partial i}{\partial \rho} = -\frac{\rho}{Rc} \frac{\partial i}{\partial t}$ ,

substituting these into (C19), gives a new equation for the derivative of magnetic field in the azimuthal direction:

$$d\vec{H} = \frac{dz'}{4\pi} \left[ \frac{\rho i(z', t-R/c)}{R^3} + \frac{\rho}{R^2 c} \frac{\partial i(z', t-R/c)}{\partial t} \right] \vec{a}_\phi \quad (\text{C21})$$

Considering the contribution of the image of the lightning return-stroke channel on the derivative of the magnetic field the final equation due to lightning return-stroke channel placed above perfectly conduction ground becomes:

$$d\vec{H} = \frac{dz'}{2\pi} \left[ \frac{\rho i(z', t-R/c)}{R^3} + \frac{\rho}{R^2 c} \frac{\partial i(z', t-R/c)}{\partial t} \right] \vec{a}_\phi \quad (\text{C22})$$

Integrating (C22) from 0 to  $H$  gives an expression for the azimuthal magnetic field at point  $P$  located at ground level at horizontal distance  $\rho$  m from the lightning channel and due to lightning return-stroke channel and its image.

$$\vec{H} = \int_0^H \frac{dz'}{2\pi} \left[ \frac{\rho i(z', t-R/c)}{R^3} + \frac{\rho}{R^2 c} \frac{\partial i(z', t-R/c)}{\partial t} \right] \vec{a}_\phi \quad (\text{C23})$$

The first component of  $\vec{H}$  that is dependent on  $\frac{1}{R^3}$  is the induction component while the second component of  $\vec{H}$  that is dependent on  $\frac{1}{R^2}$  is the radiation component of the magnetic field.

The equation of the electric field due to vertical lightning return-stroke channel placed above perfectly conducting ground can be obtained in similar manner. Everywhere except at  $\rho = 0$  the following expression is valid  $\nabla \times d\vec{H} = \epsilon_o \frac{\partial d\vec{E}}{\partial t}$ . For a perfectly conducting ground the electric field will only have the vertical component at the point of observation located at ground level  $P(r, \phi, 0)$ . Taking the curl of  $d\vec{H}$  in the  $\vec{a}_z$  direction only the following expression results:

$$\begin{aligned} (\nabla \times d\vec{H}) \cdot \vec{a}_z = \\ \frac{-dz'}{4\pi\rho} \left[ \frac{\rho^3}{R^3 c^2} \frac{\partial^2 i}{\partial t^2} + \left( \frac{\rho^3}{cR^4} - \frac{2\rho(R^2 - \rho^2)}{cR^4} \right) \frac{\partial i}{\partial t} - \frac{\rho}{R^5} (2R^2 - 3\rho^2) i \right] \end{aligned} \quad (C24)$$

$$(\nabla \times d\vec{H}) \cdot \vec{a}_z = \epsilon_o \frac{\partial d\vec{E}}{\partial t} \cdot \vec{a}_z \quad (C25)$$

Substituting (C25) into (C24) the following equation for the derivative of the vertical component of the electric field is obtained:

$$\frac{\partial \vec{E}}{\partial t} = \frac{dz'}{4\pi\epsilon_o} \left[ \frac{2R^2 - 3\rho^2}{R^5} i + \frac{2R^2 - 3\rho^2}{cR^4} \frac{\partial i}{\partial t} - \frac{\rho^2}{R^3 c^2} \frac{\partial^2 i}{\partial t^2} \right] \vec{a}_z \quad (C26)$$

Replacing  $i$  in (C26) by  $i(z', t-R/c)$  and modifying (C26) in order to get rid off second derivative of  $i$  a new equation given by (C27) is obtained.

$$\frac{\partial \vec{E}}{\partial t} = \frac{dz'}{4\pi\epsilon_0} \left[ \frac{2R^2 - 3\rho^2}{R^5} \int_0^t i(z', t - R/c) + \frac{2R^2 - 3\rho^2}{cR^4} i(z', t - R/c) - \frac{\rho^2}{R^3 c^2} \frac{\partial i(z', t - R/c)}{\partial t} \right] \vec{a}_z \quad (C27)$$

Considering the image of the lightning return-stroke channel and replacing  $R^2$  in (C27) by  $R^2 = \rho^2 + z'^2$  a new equation for the derivative of the vertical component of the electric field at point  $P$  located at ground level, due to lightning return-stroke channel and its image is obtained.

$$\frac{\partial \vec{E}}{\partial t} = \frac{dz'}{2\pi\epsilon_0} \left[ \frac{2z'^2 - \rho^2}{R^5} \int_{R/c}^t i(z', t - R/c) + \frac{2z'^2 - \rho^2}{cR^4} i(z', t - R/c) - \frac{\rho^2}{R^3 c^2} \frac{\partial i(z', t - R/c)}{\partial t} \right] \vec{a}_z \quad (C28)$$

Integrating (C28) from 0 to  $H$  a final equation for the vertical electric field at point  $P$  located at ground level at a horizontal distance  $\rho$  m from the channel and due to lightning return-stroke channel and its image is given by (C29).

$$\vec{E} = \int_0^H \frac{dz'}{2\pi\epsilon_0} \left[ \frac{2z'^2 - \rho^2}{R^5} \int_{R/c}^t i(z', t - R/c) + \frac{2z'^2 - \rho^2}{cR^4} i(z', t - R/c) - \frac{\rho^2}{R^3 c^2} \frac{\partial i(z', t - R/c)}{\partial t} \right] \vec{a}_z \quad (29)$$

The first term in (C29) that is dependent on  $1/R^5$  is the electrostatic term; the second term that is dependent on  $1/R^4$  is the induction term while the third term that is dependent on  $1/R^3$  is the radiation term of the vertical electric field. In the far field region i.e. when the distance to the lightning return-stroke channel is much larger than the height of the channel only the radiation components of the magnetic and electric field could be

considered as they will be the dominant components. In far-field region the equations for the azimuthal magnetic field and vertical electric field are given by (C30) and (C31) respectively.

$$\vec{H}_{far-field} = \int_0^H \frac{dz'}{2\pi} \left[ \frac{\rho}{R^2 c} \frac{\partial i(z', t - R/c)}{\partial t} \right] \vec{a}_\phi \quad (C30)$$

$$\vec{E}_{far-field} = \int_0^H \frac{dz'}{2\pi\epsilon_o} \left[ -\frac{\rho^2}{R^3 c^2} \frac{\partial i(z', t - R/c)}{\partial t} \right] \vec{a}_z \quad (C31)$$

Equations (C30) and (C31) can be further simplified considering very far distance from the lightning return-stroke channel by assuming that  $\rho \cong R$ . Using this assumption (C30) and (C31) can be rewritten as follows:

$$\vec{H}_{far-field} \cong \int_0^H \frac{dz'}{2\pi R c} \left[ \frac{\partial i(z', t - R/c)}{\partial t} \right] \vec{a}_\phi \quad (C32)$$

$$\vec{E}_{far-field} \cong \int_0^H -\frac{dz'}{2\pi\epsilon_o R c^2} \left[ \frac{\partial i(z', t - R/c)}{\partial t} \right] \vec{a}_z \quad (C33)$$

## Appendix D

### Current and Current Derivative for 3-Section TL Representation

The equations for the lightning return-stroke current along the CN Tower and the lightning channel for 3-section TL representation of the CN Tower are presented. A 3-section TL representation of the CN Tower is shown in Figure D1. The first section of transmission line is inserted between the tip of the Tower and the top of the restaurant; the second section is inserted between top and bottom of the restaurant while the third section is inserted between the bottom of the restaurant and the ground [86,100]. In Figure D1,  $h$  is the height of the CN Tower taken from the ground level,  $H$  is the height of the channel taken from the tip of the CN Tower,  $L_1$  is the length of the first TL section (tip to top of the restaurant),  $L_2$  is the length of second TL section (top of the restaurant to bottom of the restaurant),  $L_3$  is the length of third TL section (bottom of the restaurant to the ground),  $L_{12}$  is the length of  $L_1+L_2$  and  $L_{23}$  is the length of  $L_2 +L_3$ . The current equations in each of the three sections were derived for the reflections that occur in that particular section. For each equation a diagram is shown to illustrate the reflection for which the equation is derived.

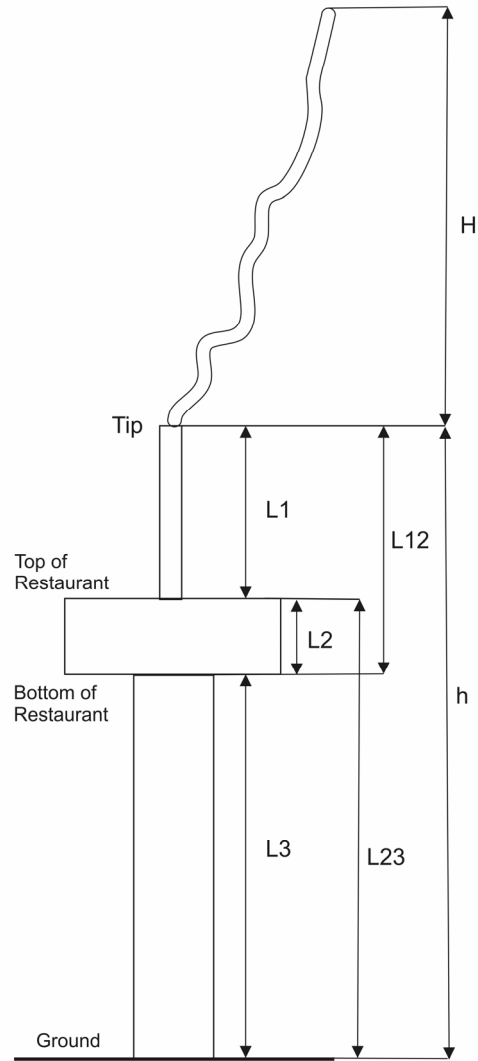


Figure D1. 3-section TL representation of the CN Tower.

### D.1 Current equations in the first TL section with length $L_1$ .

The reflections occurring between tip of the CN Tower and top of the restaurant and which have been taken into account are shown in Figures D2-D7. The current equations corresponding to the reflections shown in Figures D2-D7 are given by (D1)-(D6) respectively. In the equations the reflection coefficient for tip of the CN Tower is

denoted as  $\rho_T$ , the reflection coefficients for top and bottom of the restaurant are  $\rho_1$  and  $\rho_2$ , respectively, while the reflection coefficient for ground is  $\rho_G$ ,  $c$  is the speed of light.

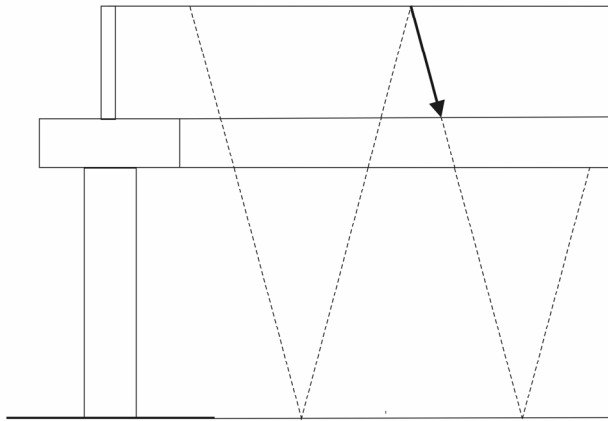


Figure D2. Reflections given by equation (D1).

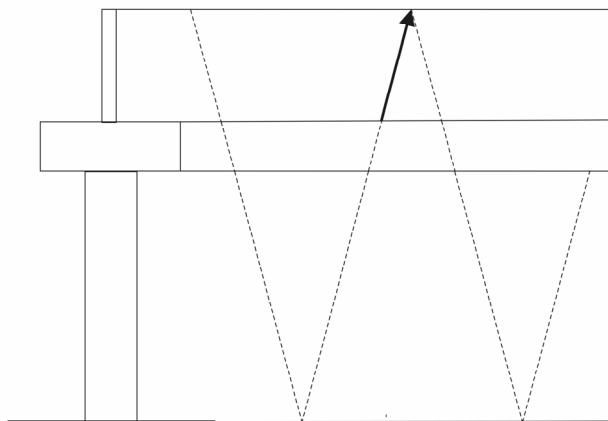


Figure D3. Reflections given by equation (D2).

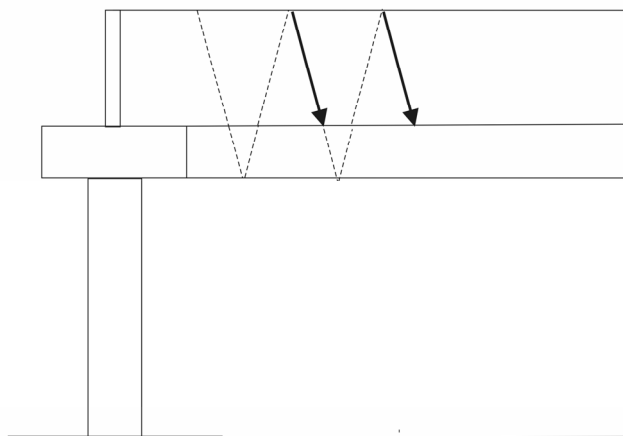


Figure D4. Reflections given by equation (D3).

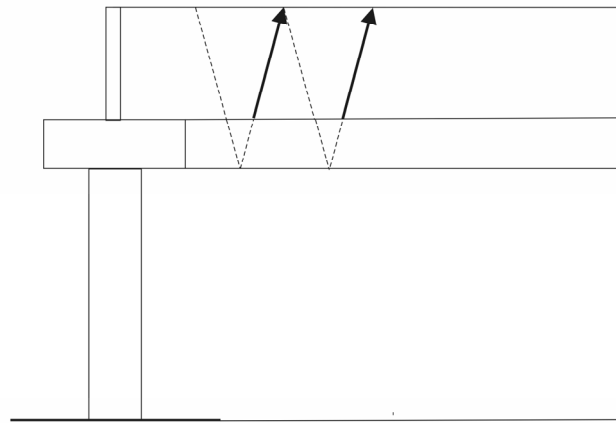


Figure D5. Reflections given by equation (D4).

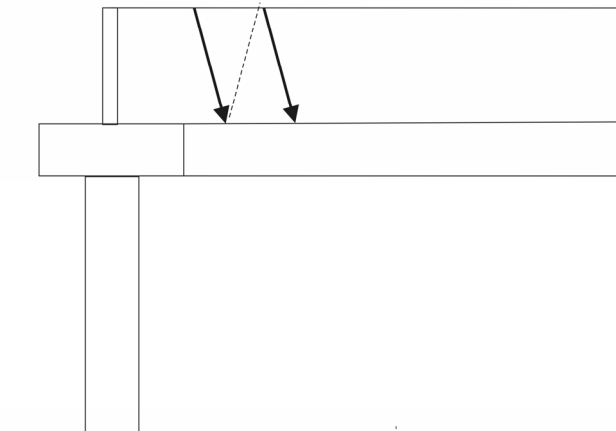


Figure D6. Reflections given by equation (D5).

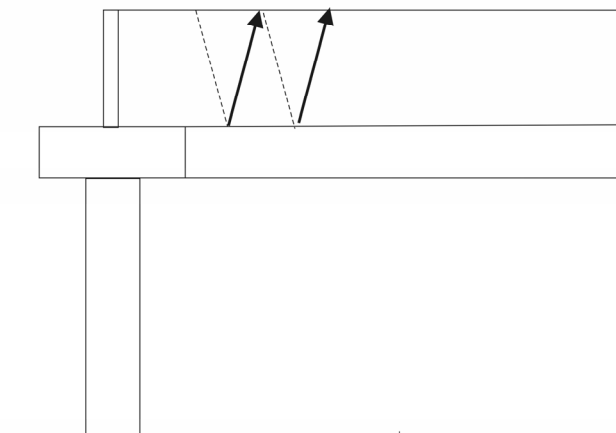


Figure D7. Reflections given by equation (D6).

$$i_{D1}(z,t) = \sum_{j=0}^{\infty} \rho_T^{j+1} (1+\rho_1)^{j+1} (1+\rho_2)^{j+1} \rho_G^{j+1} (1-\rho_2)^{j+1} (1-\rho_1)^{j+1} i_o \left( t - \frac{h-z}{c} - \frac{2h(j+1)}{c} \right) \quad (D1)$$

$$i_{D2}(z,t) = \sum_{j=0}^{\infty} \rho_T^j (1+\rho_1)^{j+1} (1+\rho_2)^{j+1} \rho_G^{j+1} (1-\rho_2)^{j+1} (1-\rho_1)^{j+1} i_o \left( t - \frac{h+L_{23}+z}{c} - \frac{2hj}{c} \right) \quad (D2)$$

$$i_{D3}(z,t) = \sum_{j=0}^{\infty} \rho_T^{j+1} (1+\rho_1)^{j+1} \rho_2^{j+1} (1-\rho_1)^{j+1} i_o \left( t - \frac{h-z}{c} - \frac{2L_{12}(j+1)}{c} \right) \quad (D3)$$

$$i_{D4}(z,t) = \sum_{j=0}^{\infty} \rho_T^j (1+\rho_1)^{j+1} \rho_2^{j+1} (1-\rho_1)^{j+1} i_o \left( t - \frac{L_{12}+L_2+z}{c} - \frac{2L_{12}j}{c} \right) \quad (D4)$$

$$i_{D5}(z,t) = \sum_{j=0}^{\infty} \rho_T^j \rho_1^j i_o \left( t - \frac{h-z}{c} - \frac{2L_1j}{c} \right) \quad (D5)$$

$$i_{D6}(z,t) = \sum_{j=0}^{\infty} \rho_T^j \rho_1^{j+1} i_o \left( t - \frac{L_1+z}{c} - \frac{2L_1j}{c} \right) \quad (D6)$$

## D.2 Current equations in the second TL section with length $L_2$ .

In this section current equations for the second TL section, which is placed between top and bottom of the restaurant are given. The reflections that occur in the second section are shown in Figures D8-D11 while the equations for the corresponding reflections are given by (D7)-(D10).

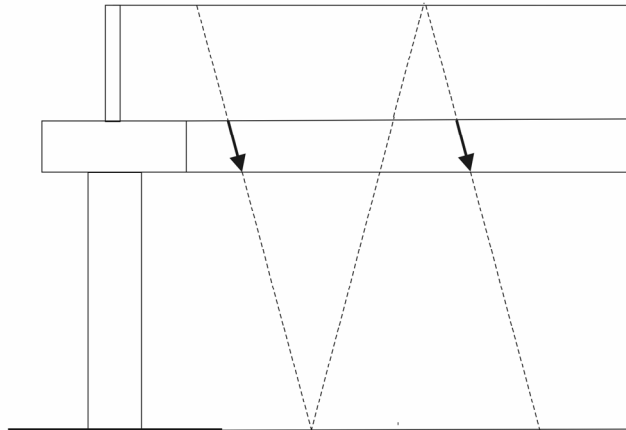


Figure D8. Reflections given by equation (D7).

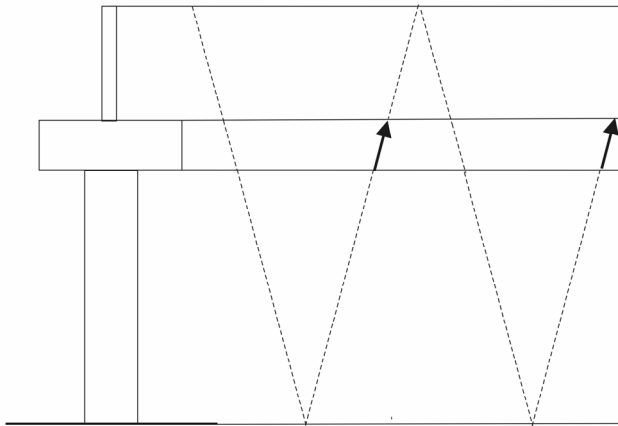


Figure D9. Reflections given by equation (D8).

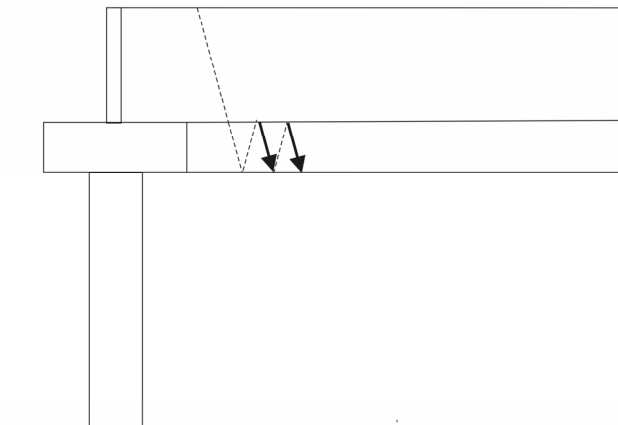


Figure D10. Reflections given by equation (D9).

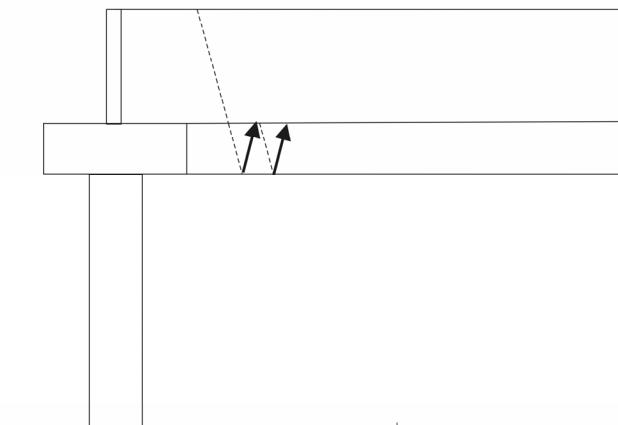


Figure D11. Reflections given by equation (D10).

$$i_{D7}(z,t) = \sum_{j=0}^{\infty} \rho_T^j (1-\rho_1)^{j+1} (1-\rho_2)^j \rho_G^j (1+\rho_2)^j (1+\rho_1)^j i_o \left( t - \frac{h-z-L_1}{c} - \frac{2hj}{c} \right) \quad (D7)$$

$$i_{D8}(z,t) = \sum_{j=0}^{\infty} \rho_T^j (1-\rho_1)^{j+1} (1-\rho_2)^{j+1} \rho_G^{j+1} (1+\rho_2)^{j+1} (1+\rho_1)^j i_o \left( t - \frac{h+L_3+z}{c} - \frac{2hj}{c} \right) \quad (D8)$$

$$i_{D9}(z,t) = \sum_{j=1}^{\infty} (-\rho_1)^j (1-\rho_1)(\rho_2)^j i_o \left( t - \frac{h-L_{12}+L_2-z}{c} - \frac{2L_2(j-1)}{c} \right) \quad (D9)$$

$$i_{D10}(z,t) = \sum_{j=0}^{\infty} (-\rho_1)^j (1-\rho_1)(\rho_2)^{j+1} i_o \left( t - \frac{L_{12}}{c} + \frac{z}{c} - \frac{2L_2j}{c} \right) \quad (D10)$$

### D.3 Current equations in the third TL section with length $L_3$

In this section current equations for the third TL section, which is placed between bottom of the restaurant and the ground are presented. The reflections that occur in the third section are shown in Figures D12-D15 while the equations for the corresponding reflections are given by (D11) and (D14).

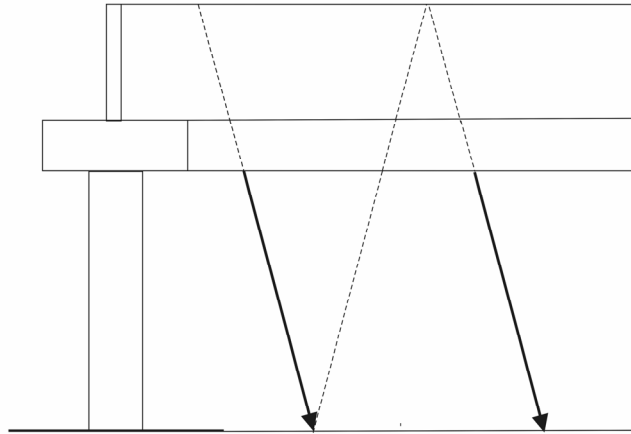


Figure D12. Reflections given by equation (D11).

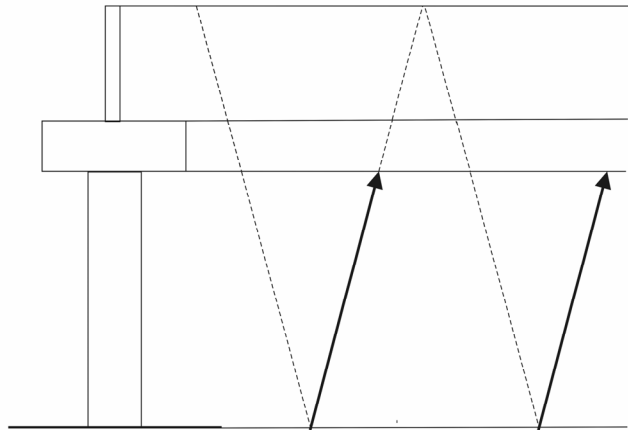


Figure D13. Reflections given by equation (D12).

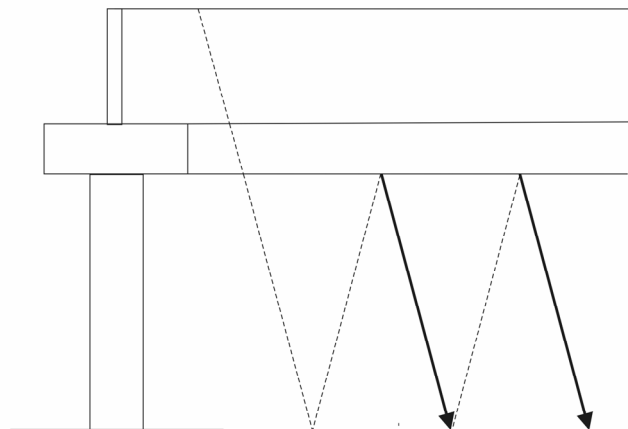


Figure D14. Reflections given by equation (D13).

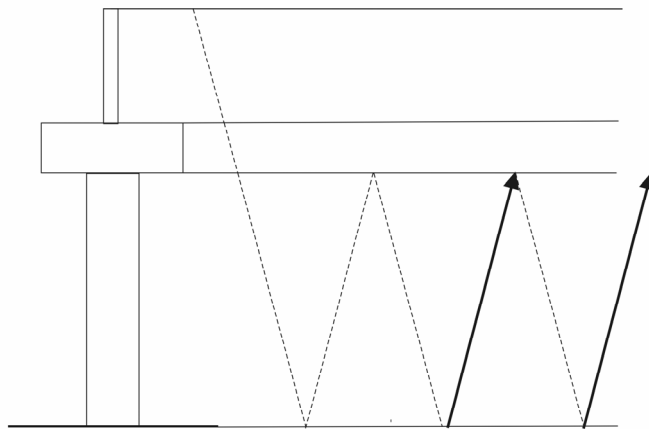


Figure D15. Reflections given by equation (D14).

$$i_{D11}(z,t) = \sum_{j=0}^{\infty} \rho_T^j (1-\rho_1)^{j+1} (1-\rho_2)^{j+1} \rho_G^j (1+\rho_2)^j (1+\rho_1)^j i_o \left( t - \frac{h-z-L_{12}}{c} - \frac{2hj}{c} \right) \quad (D11)$$

$$i_{D12}(z,t) = \sum_{j=0}^{\infty} \rho_T^j (1-\rho_1)^{j+1} (1-\rho_2)^{j+1} \rho_G^{j+1} (1+\rho_2)^j (1+\rho_1)^j i_o \left( t - \frac{h+z}{c} - \frac{2hj}{c} \right) \quad (D12)$$

$$i_{D13}(z,t) = \sum_{j=1}^{\infty} (-\rho_2)^j (1-\rho_1)(1-\rho_2) \rho_G^j i_o \left( t - \frac{h+L_3}{c} - \frac{z}{c} - \frac{2L_3(j-1)}{c} \right) \quad (D13)$$

$$i_{D14}(z,t) = \sum_{j=1}^{\infty} (-\rho_2)^j (1-\rho_1)(1-\rho_2) \rho_G^{j+1} i_o \left( t - \frac{h+L_3}{c} - \frac{L_3+z}{c} - \frac{2L_3(j-1)}{c} \right) \quad (D14)$$

#### D.4 Current equations in the lightning return-stroke channel, $z > h$ .

In this section current equations due to lightning channel are presented. The initial current wave propagates in the channel with a speed of  $v = 0.5c$ , the reflections passed through the tip to the channel propagate in the channel at a speed of  $c$ . The equation for the current of the initial wave is given by (D15). The reflections that are passed to the channel and have been taken into account are shown in Figures D16-D18 while the equations for the corresponding reflections are given by (D16)-(D18).

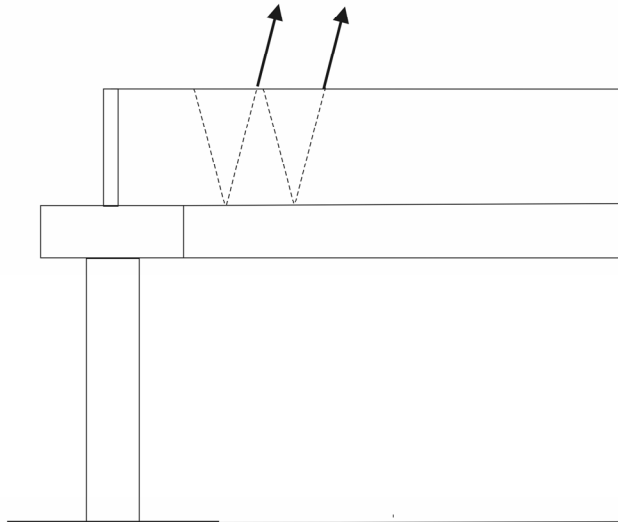


Figure D16. Reflections given by equation D16.

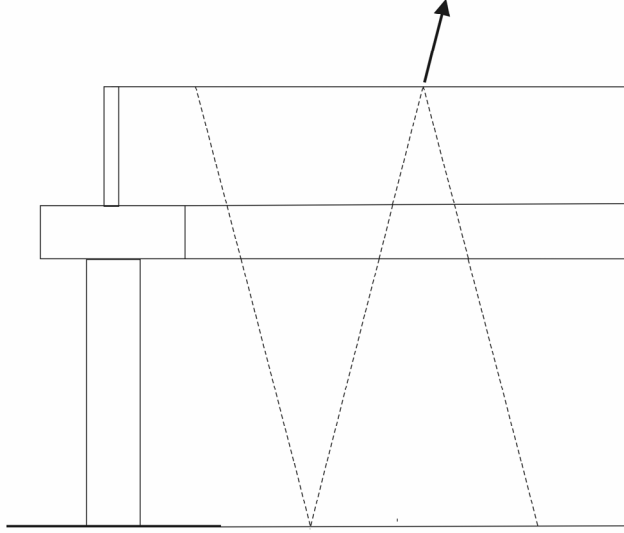


Figure D17. Reflections given by equation D17.

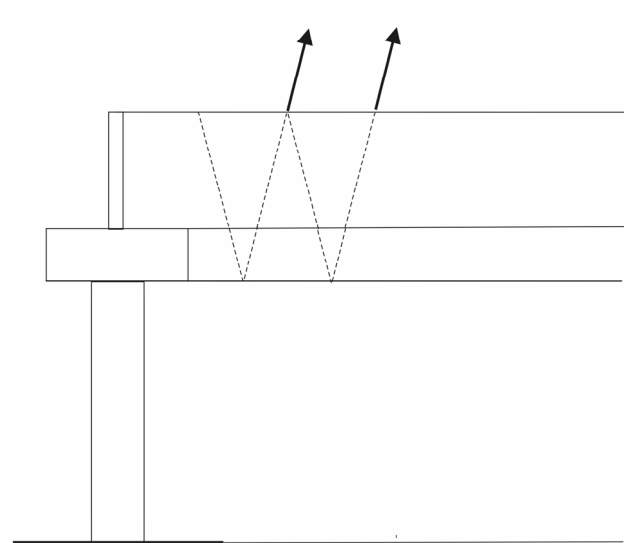


Figure D18. Reflections given by equation D18.

$$i_{D15}(z_{ch}, t) = i_o \left( t - \frac{z_{ch} - h}{v} \right) \quad (D15)$$

$$i_{D16}(z_{ch}, t) = \sum_{j=1}^{\infty} (1 + \rho_T) \rho_T^{j-1} \rho_1^j i_o \left( t - \frac{z_{ch} - h}{c} - \frac{2jL_1}{c} \right) \quad (D16)$$

$$i_{D17}(z_{ch}, t) = \sum_{j=1}^{\infty} (1 - \rho_1)^j (1 - \rho_2)^j \rho_G^j (1 + \rho_2)^j (1 + \rho_1)^j (1 + \rho_T) \rho_T^{j-1} i_o \left( t - \frac{z_{ch} - h}{c} - \frac{2jh}{c} \right) \quad (D17)$$

$$i_{D18}(z_{ch}, t) = \sum_{j=1}^{\infty} (1 - \rho_1)^j \rho_2^j (1 + \rho_1)^j (1 + \rho_T) \rho_T^{j-1} i_o \left( t - \frac{z_{ch} - h}{c} - \frac{2jL_{12}}{c} \right) \quad (D18)$$

The total current within the CN Tower and the lightning channel is represented by a summation of currents given by (D1)-(D18). This total current was used to calculate the simulated electric and magnetic fields at a distance of 2.0 km from the Tower.

# Appendix E

## Publications based on the PhD Thesis

**M. Milewski** and A. M. Hussein, "Evaluation of tall-structure lightning return-stroke model using CN Tower data," *19<sup>th</sup> International Conference on Electromagnetic Disturbances*, Sept. 23-25, Bialystok, Poland, 2009, pp. 180-185.

**M. Milewski** and A. Hussein, "Lightning return-stroke transmission line model based on CN Tower lightning data and derivative of Heidler function," in *Proc. 21<sup>st</sup> IEEE Canadian Conference on Computer and Electrical Engineering*, May 4-7, Niagara Falls, ON, Canada, 2008, pp. 1861-1866.

A.M. Hussein, **M. Milewski**, W. Janischewskyj, "Correlating the characteristics of the CN Tower lightning return-strokes current with those of its generated electromagnetic pulse," *IEEE Transactions on Electromagnetic Compatibility*, vol. 50, no. 3, pp. 642-650, August 2008.

# References

- [1] Vladimir A. Rakov and Martin A. Uman, “*Lightning – Physics and Effects*,” New York, N.Y: Cambridge University Press, 2003.
- [2] Martin A. Uman, “*The Lightning Discharge*,” Orlando, FL: Academic Press Inc., 1987.
- [3] Martin A. Uman, “*Lightning*,” Pittsburgh PA: McGraw Hill, 1969.
- [4] K.B. McEachron, “Lightning to the Empire State building,” *AIEE Transactions*, vol. 60, pp. 885-889, September 1941.
- [5] A. Hussein, M. Milewski and W. Janischewskyj, “Correlating the characteristics of the CN Tower lightning return-strokes with those of its generated electromagnetic pulse,” *IEEE Transactions on Electromagnetic Compatibility*, vol. 50, no. 3, pp. 642-650, August 2008.
- [6] F. Rachidi, W. Janischewskyj, A. M. Hussein, C.A. Nucci, S. Guerrieri, B. Kordi and J.-S. Chang, “Current and electromagnetic field associated with lightning-return strokes to tall towers,” *IEEE Transactions on Electromagnetic Compatibility*, vol. 43, no. 3, pp. 356-367, August 2001.
- [7] A. Williams, “Lightning causes \$25,000 damage to the CN Tower,” *Toronto Star* (Canada), May 6, 1976.
- [8] R. Kithil, “Annual USA lightning costs and losses,” [www.lightningsafety.com](http://www.lightningsafety.com), April 22, 2007. [Online]. Available: [http://www.lightningsafety.com/nlsi\\_lls/nlsi\\_annual\\_usa\\_losses.htm](http://www.lightningsafety.com/nlsi_lls/nlsi_annual_usa_losses.htm), [Accessed June 29, 2008].
- [9] C. Magono, “*Thunderstorms*,” New York, N.Y: Elsevier Scientific Publishing Company, 1980.
- [10] A.M. Hussein, M. Milewski, A. Abdelraziq, W. Janischewskyj and F. Jabbar, “Visual characteristics of CN Tower lightning flashes,” in *Proc. 28<sup>th</sup> International Conference on Lightning Protection*, September 18-22, Kanazawa, Japan, 2006, pp. 89-94.

- [11] Ali M. Hussein, W. Janischewskyj, J.-S. Chang, V. Shostak, W.A. Chisholm, P. Dzurevych and Z.-I. Kawasaki, "Simultaneous measurements of lightning parameters for strokes to the Toronto Canadian National Tower," *Journal of Geophysical Research*, vol. 100, no. D5, pp. 8853-8861, May 1995.
- [12] M. Milewski, "Statistical analysis of CN Tower lightning current parameters (1992-2001)," M.E.Sc thesis, University of Western Ontario, London, ON, Canada, 2003.
- [13] Wikipedia – The Free Encyclopaedia ,” Basalt,” [Online]. Available: <http://en.wikipedia.org/wiki/Basalt>, [Accessed: July 2, 2008].
- [14] F. Popolansky, "Lightning Current Measurement on High Objects in Czechoslovakia," in *Proc. 20<sup>th</sup> International Conference on Lightning Protection*, September 24-28, Interlaken Switzerland, 1990, paper 1.3, pp. 1-7.
- [15] K. Berger, R.B. Anderson and H. Kroninger, "Parameters of lightning flashes," *Electra*, no. 41, pp. 23-37, July 1975.
- [16] R.H. Golde, "*Lightning – Physics of Lightning*," New York, N.Y: Academic Press Inc., 1977.
- [17] G. Diendorfer, M. Mair, W. Schulz, W. Hadrian, "Lightning current measurements in Austria – experimental setup and first results," in *Proc. 25<sup>th</sup> International Conference on Lightning Protection*, September 18-22, Rhodes, Greece, 2000, pp. 44-47.
- [18] A. Hussein, W. Janischewskyj, M. Milewski, V. Shostak, J.-S. Chang and W. Chisholm, "Current waveform parameters of CN Tower lightning return strokes," *Journal of Electrostatics*, vol. 60, no. 2-4, pp. 149-162, March 2004.
- [19] F. Fuchs, E.U. Landers, R. Schid and J. Wiesinger, "Lightning current and magnetic field parameters caused by lightning strikes to tall structures relating to interference of electronic systems," *IEEE Transactions on Electromagnetic Compatibility*, vol. 40, no. 4, pp. 444-451, November 1998.
- [20] R.B. Anderson and A.J. Eriksson, "Lightning parameters for engineering applications," *Electra*, no. 69, pp. 65-105, 1980.
- [21] Eduard M. Bazelyan and Yuri P. Raizer, edited by William L. Donn, "*Lightning Physics and Lightning Protection*," Bristol, U.K: J.W. Arrowsmith Ltd., 2000.
- [22] G. Diendorfer, M. Mair and W. Schulz, "Detailed brightness versus lightning current amplitude correlation of flashes to the Gaisberg Tower," in *Proc. 26<sup>th</sup> International Conference on Lightning Protection*, September 2-6, Cracow, Poland, 2002, pp. 8-13.

- [23] F. Fuchs, "Lightning current and LEMP parameters of upward dischargers measured at the Peissenberg Tower," in *Proc. 24<sup>th</sup> International Conference on Lightning Protection*, September 14-18, Birmingham, U.K., 1998.
- [24] F. Heidler, W. Zischank and J. Wiesinger, "Statistics of lightning current parameters and related nearby magnetic fields measured at the Peissenberg Tower," in *Proc. 25<sup>th</sup> International Conference on Lightning Protection*, September 18-22, Rhodes, Greece, 2000, pp. 78-83.
- [25] V. Kodali, V.A. Rakov, M.A. Uman, K.J. Rambo, G.H. Schnetzer, J. Schone and J. Heralld, "Triggered-lightning properties inferred from measured current and very close electric fields," *Atmospheric Research*, vol. 76, no. 1-4, pp. 355-376, 2005.
- [26] P. Hubert, P. Laroche, A.Eybert-Berard and L. Barret, "Triggered lightning in New Mexico," *Journal of Geophysical Research*, vol. 89, no. D2, pp. 2511-2521, April 1984.
- [27] A. Lafkovici, "A performance analysis of the North American Lightning Detection Network using CN Tower lightning data," M.E.Sc thesis, Ryerson University, Toronto, ON, Canada, 2005.
- [28] V.A. Rakov, M.A. Uman and K.J. Rambo, "A review of ten years of triggered-lightning experiments at Camp Blanding, Florida," *Atmospheric Research*, vol. 76, no. 1-4, pp. 503-517, 2005.
- [29] W. Janischewskyj, A.M. Hussein, V. Shostak and P. Dzurevych, "Characterization of the Current Wavefront Parameters of Lightning Strikes to the CN Tower in Toronto," *8<sup>th</sup> International Symposium on High Voltage Engineering*, August 23-27, Yokohama, Japan, 1993.
- [30] V. Shostak, M. Wiacek and D. Tam, "Report on new Rogowski coil calibration," University of Toronto, Toronto, ON, Canada, May 29, 1998.
- [31] Mohamed Abdel-Rahman, "Currents and fields of CN Tower multi-stroke flashes," M.E.Sc thesis, University of Toronto, Toronto, ON, Canada, 1998.
- [32] John Riordan, "New Rogowski coil calibration," Physics International, San Leandro, CA, USA, Rep. 910A, 1998.
- [33] Instruction Manual, "*OP 2000A Optical Transmission System*," NANOFAST Inc., Chicago, IL, USA, 1996.
- [34] TEK Instruction Manual, "*RTD-710A Digitizer*," Tektronix, Beaverton, OR, USA, 1988.

- [35] Operator's Manual, "*LeCroy Waverunner*," LeCroy Corporation, Chestnut Ridge, NY, USA, January 2001
- [36] LeCroy Corporation, "Products Archive," [www.lecroy.com](http://www.lecroy.com), [Online]. Available: <http://www.lecroy.com/tm/products/discontinuedproducts.asp?propcatid=1>, [Accessed July 1, 2008].
- [37] Phantom Technical Specifications, "*Phantom v 5.0*," Vision Research Inc., Wayne, NJ, USA, 2000.
- [38] Instructions Manual, "*Sanyo B/W CCD Camera VCB-3524*," Sanyo, Chatsworth, CA, USA, 2003.
- [39] Instructions Manual, "*TrueTime Model XL-DC GPS Receiver*," TrueTime Inc., Santa Rosa, CA, USA, September 15, 1997.
- [40] A.M. Hussein, M. Milewski, W. Janischewskyj, F. Noor and F. Jabbar, "Characteristics of lightning flashes striking the CN Tower below its tip," *Journal of Electrostatics*, vol. 56, no. 5-6, pp. 307-315, May 2007.
- [41] J.C. Willet and J.C. Bailey, "Submicrosecond intercomparison of radiation fields and currents in triggered lightning return strokes based on the transmission-line model," *Journal of Geophysical Research*, vol. 94, no. D11, pp. 13,275-13,286, September 1989.
- [42] P. Depasse, "Statistics on artificially triggered lightning," *Journal of Geophysical Research*, vol. 99, no. D9, pp. 18,515-18,522, September 1994.
- [43] P. Liatos and A.M. Hussein, "Characterization of 100-kHz noise in the lightning current derivative signals measured at the CN Tower," *IEEE Transactions on Electromagnetic Compatibility*, vol. 47, no. 4, pp. 986-997, November 2005.
- [44] A.M. Hussein, W. Janischewskyj, M. Milewski, V. Shostak, F. Rachidi and J.-S. Chang, "Comparison of current characteristics of lightning strokes measured at the CN Tower and other elevated objects," in *Proc. IEEE Symposium on Electromagnetic Compatibility*, August 18-22, Boston, MA, USA, 2003, pp. 495-500.
- [45] A.M. Hussein, W. Janischewskyj, M. Milewski, V. Shostak and J.-S. Chang, "Waveform parameters of fields generated by lightning strokes to the CN Tower and objects in its vicinity," in *Proc. IEEE PowerTech*, June 23-26, Bologna, Italy, 2003, pp. 1-8.

- [46] A.M. Hussein, M. Milewski and W. Janischewskyj, "Correlation of characteristics of currents and electromagnetic fields generated by lightning return strokes to the CN Tower," in *Proc. 18<sup>th</sup> International Wroclaw Symposium and Exhibition on Electromagnetic compatibility*, June 28-30, Wroclaw, Poland, 2006, pp. 296-301.
- [47] W. Schulz and G. Diendorfer, "Lightning field peaks radiated by lightning to tall towers," presented at 2004 International Conference on Grounding and Earthing, Belo Horizonte, Brazil, 2004.
- [48] Industry Canada, "Canadian table of frequency allocations, 2005 edition," <http://www.ic.gc.ca>, [Online]. Available: <http://www.ic.gc.ca/epic/site/smt-gst.nsf/en/sf08531e.html>, [Accessed July 17, 2008].
- [49] V. Corray and C. Gomes, "Estimation of peak return stroke currents, current time derivatives and return stroke velocities from measured fields," *Journal of Electrostatics*, vol. 43, no. 3, pp. 163-172, May 1998.
- [50] F. Rachidi, J. L. Bermudez, M. Rubinstein and V. A. Rakov, "On the estimation of lightning peak currents from measured fields using lightning location systems," *Journal of Electrostatics*, vol. 60, no. 2-4, pp. 121-129, March 2004.
- [51] A. Lafkovici, A. M. Hussein, W. Janischewskyj and K. Cummins, "Performance analysis of the North American Lightning Detection Network using CN Tower lightning data," in *Proc. 19<sup>th</sup> International Lightning Detection Conference*, April 24-25, Tuscon, Arizona, 2006, pp. 1-32.
- [52] G. Diendorfer, W. Schulz and V. A. Rakov, "Lightning characteristics based on data from the Austrian lightning location system," *IEEE Transactions on Electromagnetic Compatibility*, vol. 40, no. 2, pp. 452-464, November 1998.
- [53] C. Leteinturier, C. Weidman and J. Hamelin, "Current and electric field derivatives in triggered lightning return strokes," *Journal of Geophysical Research*, vol. 95, no. D1, pp. 811-828, January 1990.
- [54] V. A. Rakov, R. Thottappillil and M. A. Uman, "On the empirical formula of Willet et al. relating lightning return-stroke current and peak electric field," *Journal of Geophysical Research*, vol. 97, no. D11, pp. 11,527-11,533, May 1992.
- [55] Y. Baba and V. A. Rakov, "Electromagnetic fields at the top of a tall building associated with nearby lightning return stroke," *IEEE Transactions on Electromagnetic Compatibility*, vol. 49, no. 3, pp. 632-643, August 2007.
- [56] R. Thottappillil, "Computation of electromagnetic fields from lightning discharge," in *The Lightning Flash*, Ed. V. Corray, London, U.K., IEE, 2003, pp. 241-279.

- [57] Y. Baba and V. A. Rakov, "Lightning electromagnetic environment in the presence of tall grounded strike object," *Journal of Geophysical Research*, vol. 110, no. D09108, doi: 10.1029/2004JD005505, 2005.
- [58] V. Shostak, W. Janischewskyj and A. M. Hussein, "Expanding the modified transmission line model to account for reflections within the continuously growing lightning return-stroke channel," in *Proc. IEEE Power Engineering Society Summer Meeting*, July 16-20, Seattle, Washington, 2000, no. 4, pp. 2589-2602.
- [59] F. Heidler, J. Wiesinger and W. Zischank, "Lightning currents measured at the telecommunication tower from 1992-1998," in *Proc. 14<sup>th</sup> International Symposium and Technical Exhibition on Electromagnetic Compatibility*, February 20-22, Zurich, Switzerland, 2001, pp. 325-330.
- [60] G. Lupo, C. Petrarca, V. Tucci and M. Vitelli, "EM fields generated by lightning channels with arbitrary location and slope," *IEEE Transactions on Electromagnetic Compatibility*, vol. 42, no.1, pp 39-53, February 2000.
- [61] F. Heidler, "Travelling current source model for LEMP calculation," in *Proc. 6<sup>th</sup> International Symposium on Electromagnetic Compatibility*, March 5-7, Zurich, Switzerland, 1985, pp. 157-162.
- [62] Y. Baba and V. A. Rakov, "On the use of lumped sources in lightning return stroke models," *Journal of Geophysical Research*, vol. 110, no. D03101, doi: 10.1029/2004JD005202, February 2005.
- [63] V. A. Rakov and M. A. Uman, "Review and evaluation of lightning return stroke models including some aspects of their application," *IEEE Transactions on Electromagnetic Compatibility*, vol. 40, no. 4, pp. 403-426, November 1998.
- [64] S.I. Drabkina, "The theory of the development of the spark channel," *Journal of Experimental and Theoretical Physics*, vol. 21, pp. 473-483, 1951.
- [65] M. N. Polster, "Numerical simulation of spark discharges in air," *Physics of Fluids*, vol. 14, pp. 2111-2123, 1971.
- [66] Y. Baba and M. Ishii, "Numerical electromagnetic field analysis of lightning current in tall structures," *IEEE Transactions on Power Delivery*, vol. 16, no. 2, pp. 324-328, April 2001.
- [67] B. Kordi, R. Moini, W. Janischewskyj, A. M. Hussein, V. Shostak and V. A. Rakov, "Application of antenna theory model to a tall tower struck by lightning," *Journal of Geophysical Research*, vol. 108, no. D17, doi: 10.1029/2003JD003398, September 2003.

- [68] M. N. O. Sadiku, “*Elements of Electromagnetics*,” Philadelphia, PA: Oxford University Press, 1995.
- [69] K. A. Chia and A. C. Liew, “Modeling of lightning return stroke current with inclusion of distributed channel resistance and inductance,” *IEEE Transactions on Power Delivery*, vol. 19, no. 3, pp. 1342-1347, July 2004.
- [70] D. M. Mach and W. D. Rust, “Photoelectric return-stroke velocity and peak current estimates in natural and triggered lightning,” *Journal of Geophysical Research*, vol. 94, no. D11, pp. 13,237-13,247, September 1989.
- [71] D. Wang, Z. I. Kawasaki, K. Yamamoto, K. Matsuura, J.-S. Chang and W. Janischewskyj, “Luminous propagation of lightning attachment to CN Tower,” *Journal of Geophysical Research*, vol. 100, no. D6, pp. 11,661-11,667, June 1995.
- [72] Y. Baba, S. Miyazaki and M. Ishii, “Reproduction of lightning electromagnetic field waveforms by engineering model of return stroke,” *IEEE Transactions on Electromagnetic Compatibility*, vol. 46, no. 1, pp. 130-133, February 2004.
- [73] K. Bitner and A. M. Hussein, “Modeling of the CN Tower lightning return-stroke current derivative,” in *Proc. 28<sup>th</sup> International Conference on Lightning Protection*, September 18-22, Kanazawa, Japan, 2006, pp. 261-266.
- [74] M. Uman and D. K. McLain, “Magnetic field of lightning return stroke,” *Journal of Geophysical Research*, vol. 74, no. 28, pp. 6899-6910, December 1969.
- [75] C. A. Nucci, C. Mazzetti, F. Rachidi and M. Ianoz, “On lightning return stroke models for LEMP calculations,” in *Proc. 19<sup>th</sup> International Conference on Lightning Protection*, April 25-29, Graz, Austria, 1988, pp. 463-469.
- [76] G. Diendorfer and M. A. Uman, “An improved return-stroke model with specified channel-based current,” *Journal of Geophysical Research*, vol. 95, no. D9, pp. 13,621-13,644, August 1990.
- [77] C. E. R. Bruce and R. H. Golde, “The lightning discharge,” *Journal of Institute of Electrical Engineers*, vol. 88, no. 2, pp. 487-520, 1941.
- [78] H. Motoyama, W. Janischewskyj, A. M. Hussein, R. Rusan, W. A. Chisholm and J.-S. Chang, “Electromagnetic field radiation model for lightning strokes to tall structures,” *IEEE Transactions on Power Delivery*, vol. 11, no. 3, pp. 1624-1632, July 1996.
- [79] F. Heidler, J. M. Cvetic and B. V. Statnic, “Calculation of lightning current parameters,” *IEEE Transaction on Power Delivery*, vol. 14, no. 2, pp. 399-404, April 1999.

- [80] R. D. Jones, "On the use of tailored return-stroke current representations to simplify the analysis of lightning effects on systems," *IEEE Transactions on Electromagnetic Compatibility*, vol. 19, no. 2, pp. 95-96, May 1977.
- [81] Z. Feizhou and L. Shanghe, "A new function to represent lightning return-stroke currents," *IEEE Transactions on Electromagnetic Compatibility*, vol. 44, no. 4, pp. 595-597, November 2002.
- [82] D. Pavanello, F. Rachidi, M. Rubinstein, W. Janischewskyj, V. Shostak, A. M. Hussein and J.-S. Chang, "On return-stroke currents and remote electromagnetic fields associated with lightning strikes to tall structures: 1. Computational models," *Journal of Geophysical Research*, vol. 112, no. D13101, doi: 10.1029/2006JD007958, July 2007.
- [83] C. Gomes and V. Cooray, "Concepts of lightning return stroke models," *IEEE Transactions on Electromagnetic Compatibility*, vol. 42, no. 1, pp. 82-96, February 2000.
- [84] I. Boev, "Development of five-section model for computing lightning current in the CN Tower," M.E.Sc Thesis, University of Toronto, Toronto, ON, Canada, 2006.
- [85] J. L. Bermudez, "Lightning currents and electromagnetic fields associated with return strokes to elevated strike objects," PhD. thesis, Ecole Polytechnique Federale de Lausanne, Lausanne, Switzerland, 2003.
- [86] M. Milewski and A. Hussein, "Lightning return-stroke transmission line model based on CN Tower lightning data and derivative of Heidler function," in *Proc. 21<sup>st</sup> IEEE Canadian Conference on Computer and Electrical Engineering*, May 4-7, Niagara Falls, ON, Canada, 2008, pp. 1861-1866.
- [87] J. L. Bermudez, F. Rachidi, M. Rubinstein, W. Janischewskyj, V. Shostak, D. Pavanello, J.-S. Chang, A. M. Hussein, C. A. Nucci and M. Paolone, "Far-field-current relationship based on the TL model for lightning return strokes to elevated strike objects," *IEEE Transactions on Electromagnetic Compatibility*, vol. 47, no. 1, pp. 146-159, February 2005.
- [88] W. Janischewskyj, V. Shostak, J. Barrat, A. M. Hussein, I. Rusan and J.-S. Chang, "Collection and use of lightning return stroke parameters taking into account characteristics of the struck object," in *Proc. 23<sup>rd</sup> International Conference on Lightning Protection*, September 23-27, Florence, Italy, 1996, pp. 16-23.
- [89] J. L. Bermudez, M. Rubinstein, F. Rachdi, F. Heidler and M. Paolone, "Determination of reflection coefficients at top and bottom of elevated strike objects struck by lightning," *Journal of Geophysical Research*, vol. 108, no. D14, doi: 10.1029/2002JD002973, July 2003.

- [90] O. Beirel, "Front shape parameters of negative subsequent strokes measured at the Peissenberg Tower," in *Proc. 21<sup>st</sup> International Conference on Lightning Protection*, September 21-25, Berlin, Germany, 1992, pp. 1.4/1-1.4/6.
- [91] F. Fuchs, "On transient behavior of the telecommunication tower at mountain Hoher Peissenberg," in *Proc. 24<sup>th</sup> International Conference on Lightning Protection*, September 14-18, Birmingham, U.K., 1998, pp. 36-41.
- [92] S. Guerrieri, C. A. Nucci, F. Rachidi and M. Rubinstein "On the influence of elevated strike objects on directly measured and indirectly lightning currents," *IEEE Transactions on Power Delivery*, vol. 13, no. 4, pp. 1543-1555, October 1998.
- [93] R. Rusan, W. Janischewskyj, A. M. Hussein and J.-S. Chang, "Comparison of measured and computed electromagnetic fields radiated from the lightning strikes to the Toronto CN Tower," in *Proc. 23<sup>rd</sup> International Conference on Lightning Protection*, September 23-27, Florence, Italy, 1996, pp. 297-303.
- [94] A. M. Hussein, W. Janischewskyj, M. Milewski, V. Shostak, J.-S. Chang and W. A. Chisholm, "Return-stroke current waveform characteristics of lightning to the CN Tower (1992-2001)," in *Proc. 26<sup>th</sup> International Conference on Lightning Protection*, September 2-6, Krakow, Poland, 2002, pp. 161-166.
- [95] Y. Baba and V. A. Rakov, "Transmission line model of lightning return strokes generalized to include a tall strike object and upward connecting leader," in *Proc. 17<sup>th</sup> International Symposium on Electromagnetic Compatibility*, February 27 – March 3, Zurich, Switzerland, 2006, pp. 120-123.
- [96] M. J. Islam and A. M. Hussein, "De-noising the CN Tower lightning current derivative signal using short-term Fourier-transform based spectral subtraction," in *Proc. 17<sup>th</sup> International Wroclaw Symposium and Exhibition on Electromagnetic Compatibility*, June 29 – July 1, Wroclaw, Poland, 2004, pp. 400-406.
- [97] O. Nedjah, A. M. Hussein, R. Sotudeh and W. Janischewskyj, "Wavelet noise removal from CN Tower lightning current waveforms," in *Proc. International Signal Processing Conference*, March 31 – April 3, Dallas, Texas, 2003, pp. 1-6.
- [98] M. A. Uman, D. K. McLain and E. P. Krider, "The electromagnetic radiation from finite antenna," *American Journal of Physics*, vol. 43, pp. 33-38, January 1975.

- [99] J. L. Bermudez, F. Rachidi, W. Janischewskyj, V. Shostak, M. Rubinstein, D. Pavanello, A. M. Hussein, J.-S. Chang and M. Paolone, "Determination of lightning currents from far electromagnetic fields: Effect of a strike object," *Journal of Electrostatics*, vol. 65, no. 5-6, pp. 289-295, May 2007.
- [100] M. Milewski and A. M. Hussein, "Evaluation of tall-structure lightning return-stroke model using CN Tower data," paper submitted to *19<sup>th</sup> International Conference on Electromagnetic Disturbances*, September 23-25, Bialystok, Poland, 2009, pp. 180-185.
- [101] D. Pavanello, A. Mosaddeghi, F. Rachidi, M. Rubinstein, W. Janischewskyj, V. Shostak, A. M. Hussein, C. A. Nucci and J.-S. Chang, "Ability of engineering models to reproduce electromagnetic fields from lightning return strokes to tall towers," in *Proc. 29<sup>th</sup> International Conference on Lightning Protection*, June 23-26, Uppsala, Sweden, 2008, pp. 3b-4.1 – 3b-4.8
- [102] D. Pavanello, F. Rachidi, W. Janischewskyj, M. Rubinstein, A. M. Hussein, E. Petrache, V. Shostak, I. Boev, C. A. Nucci, W. A. Chisholm, M. Nyffeler, J.-S. Chang and A. Jaquier, "On return stroke currents and remote electromagnetic fields associated with lightning strikes to tall structures: 2. Experiment and model validation," *Journal of Geophysical Research*, vol. 112, no. D13122, doi: 10.1029/2006JD007959, July 2007.
- [103] R. Thottappillil and M. A. Uman, "Comparison of lightning return-stroke models," *Journal of Geophysical Research*, vol. 98, no. D12, pp. 22,903-22,914, December 1993.
- [104] M. Rubinstein, "Effect of 17-floor building in lightning electric field measurements," Private Communication, Berne, Switzerland, 2001, pp. 4.
- [105] M. Rubinstein, E. Montandon and M. Ianoz, "Analysis of multi-station cloud lightning electric field pulses recorded with the Swiss LPATS-network," presented at 22<sup>nd</sup> International Conference on Lightning Protection, September 19-23, Budapest, Hungary, 1994.
- [106] Y. Baba and V. A. Rakov, "Evaluation of lightning return stroke electromagnetic models," in *Proc. 29<sup>th</sup> International Conference on Lightning Protection*, June 23-26, Uppsala, Sweden, 2008, pp. 1a-1.1 – 1a.1.8.
- [107] S. Bnyadi-Ram, R. Moini, S. H. H. Sadeghi and A. Mahanfar, "The effects of tall buildings on the measurement of electromagnetic fields due to lightning return-strokes," in *Proc. IEEE EMC International Symposium*, August 13-17, Montreal, Quebec, Canada, 2001, pp. 1001-1004.

- [108] A. Mosaddeghi, D. Pavanello, F. Rachidi, M. Rubinstein and P. Zwiackner, “An experimental analysis of the effect of nearby buildings on electromagnetic fields from lightning,” in *Proc. 29<sup>th</sup> International Conference on Lightning Protection*, June 23-26, Uppsala, Sweden, 2008, pp. 3b-3.1 - 3b-3.7.

# Glossary

AGL	Above Ground Level
ALDIS	Austrian Lightning Detection and Information System
BG	Bruce-Golde
CC	Correlation Coefficient
CCD	Charge-Coupled Device
CCTV	Closed Circuit Television
DU	Diendorfer-Uman
ESB	Empire State Building
EMC Cell	Electromagnetic Cell
GPS	Global Positioning System
HSC	High-Speed Camera
IRIG	Inter-Range Instrumentation Group Time Codes
LEMP	Lightning Electromagnetic Pulse
LPF	Low Pass Filter
MOM	Method of Moments
MTLD	Modified Transmission Line Model Incorporating Current Attenuation and Distortion
MTLE	Modified Transmission Line Model with Exponential Current Decay
MTLL	Modified Transmission Line Model with Linear Current Decay
NALDN	North American Lightning Detection Network
NLSI	National Lightning Safety Institute
RFI	Radio Frequency Interference
R.T.	Risetime
SNR	Signal-to-Noise Ratio

TL	Transmission Line
TCS	Travelling Current Source
UTC	Coordinated Universal Time
VHS	Video Home System